Self-Organising Heterogeneous Cellular Networks

Robert Michael Joyce

Submitted in accordance with the requirements for the degree of

Doctor of Philosophy

The University of Leeds
School of Electronic and Electrical Engineering

September 2013

The candidate confirms that the work submitted is his own, except where work which has formed part of jointly-authored publications has been included. The contribution of the candidate and the other authors to this work has been explicitly indicated below. The candidate confirms that appropriate credit has been given within the thesis where reference has been made to the work of others.

Within this thesis Chapters 3 through 7, have been based on work from jointly authored publications.

Chapter 3 contains work from the following publications:

- R. M. Joyce, L. Zhang, D. Barker, "HSPA Performance Improvement through Coordinated Dynamic Antenna Tilt & Scheduling", *Proc. IEEE Wireless Communications and Networking Conference*, Shanghai, 2013, pp. 3953 - 3957.
- R. M. Joyce, L. Zhang, D. Barker, "Coordinated Dynamic Antenna Tilt & Scheduling in a Central London LTE Network", *Proc. European Wireless Conference*, Guildford, 2013.
- R. M. Joyce, L. Zhang, D. Barker, "Coordinated Dynamic Antenna Tilt & Scheduling in a Central London LTE Network", presented at the LTE 2013 World Summit, Amsterdam, 2013.
- R. M. Joyce, L. Zhang, D. Barker, "Rapid Dynamic Antenna Tilting in 3G/WCDMA and 4G/LTE Networks", *IEEE Trans. Antennas & Propagation, submitted, under review*.

Chapter 4 contains work from the following publications:

- R. M. Joyce, D. Morris, S. Brown, L. Zhang, "Higher Order Horizontal Sectorisation Gains For a Real 3GPP/HSPA+ Network", *Proc. European Wireless Conference*, Guildford, 2013.
- R. M. Joyce, D. Morris, S. Brown, D. Vyas, L. Zhang, "Higher Order Horizontal Sectorisation Gains for 6, 9, 12 and 15 Sectored Cell Sites in a 3GPP/HSPA+ Network", *IEEE Trans. Antennas & Propagation, submitted, under review*.

Chapter 5 contains work from the following publication:

- R. M. Joyce, L. Zhang, "Locating Small Cells Using Geo-located UE Measurement Reports & RF Fingerprinting", *IEEE International Conference on Communication*, Sydney, 2014 *, submitted, under review.*

Chapter 6 contains work from the following publication:

- R. M. Joyce, L. Zhang, "The Effectiveness of Low Power Co-channel Lamppost Mounted 3G/WCDMA Microcells", *IEEE Wireless Communications and Networking Conference*, Istanbul, 2014, *submitted, under review.*

Chapter 7 contains work from the following publications:

- R. M. Joyce, "Automatic Optimisation of Macro and Micro Cells to Maximise Traffic Offload onto a Central London Small Cell Network", presented at the Small Cell World Summit 2013, London, 2013.
- R. M. Joyce, "Small Cells and Heterogeneous Networks", *IEEE spectrum magazine, submitted, under review*.
- R. M. Joyce, L. Zhang, "Self Organising Network Techniques to Maximise Traffic Offload onto a 3G/WCDMA Small Cell Network using MDT UE Measurements", *IEEE International Conference on Communication*, Sydney, 2014 *, submitted, under review.*

For all of the publications listed above the author of this thesis has been the lead author and has carried out all of the work. The other authors have acted as either supervisors of the research or have contributed data upon which the research was based.

Acknowledgements

This thesis is based on research funded in part by the Engineering and Physical Sciences Research Council (EPSRC) to whom I am very grateful.

I would like to thank Professor Timothy O'Farrell for his help, guidance and encouragement throughout my research. Tim was my primary supervisor before he relocated to Swansea University mid-way through my first year at Leeds.

I would also like to thank Dr. Hal Strangeways who took over as my primary supervisor after Tim's departure and was my supervisor for the second year of my studies.

However, my greatest thanks must go to Dr. Li Zhang who took over as my primary supervisor following Hal's departure and has been instrumental in helping me focus and complete this thesis after my many years in the twilight zone between industry, academia and parenthood.

I would also like to thank my colleagues at Telefonica UK, in particular Steve Brown, David Morris, Andrew Stead and Deven Vyas for their help in providing Telefonica UK network data that has been used in some of the research undertaken in this thesis. Special thanks must also go to my manager Andy Conway and Telefonica as a whole for encouraging me to complete my PhD and for granting me a twelve month sabbatical in order to do so.

Thanks also must be given to David Barker and Quintel Technology Inc. for allowing me to collaborate with them on the development of the Quintel SONWav™ dynamic tilt antenna and to Neil Baker, Miguel Pineal and Alcatel Lucent for supplying me with the Kensington High Street small cell drive survey data.

My fellow student colleague Richard MacKenzie also deserves thanks for providing me help with the formatting of this thesis.

And finally I would like give special thanks to my wife Kathryn, my children Charlie, Alex, and Thomas, my parents and the rest of my family for their love and support during my studies and dedicate this thesis to them all.

Abstract

The mobile communications market has experienced massive growth over the past 10 years, fuelled by the continuing take up of mobile services in the developing world and the exponential mobile data growth seen in the developed world. Current forecasts predict that today's global mobile data traffic is set to rise by over 1000% by the year 2017 and in order to cope with this demand current 2nd and 3rd generation mobile networks are now evolving toward self-organising 4th generation heterogeneous networks in most markets.

To address these capacity challenges this thesis firstly explores novel means to maximise the capacity of the existing macrocell network, therefore delaying the deployment of small cells and their associated costs. To do this it considers both higher order sectorisation and self-organising dynamic antenna tilt at the macrocell and shows through both detailed simulation and field trials that both techniques provide a reasonable capacity gain and therefore delay the need for the deployment of small cells.

However, given current traffic forecasts, it is accepted that small cells will be required in the future and this thesis also considers the use of Self-Organising Network techniques to ensure that these small cells are located as close as possible to traffic hotspots to maximise their traffic and cost effectiveness. The thesis then goes on to show the effectiveness of low powered small cells to offload traffic from a co-channel macrocell layer and finally proposes a number of Self-Organising Network methods to maximise traffic offload from the macrocell layer onto a deployed small cell layer.

Table of Contents

List of Tables

List of Figures

List of Abbreviations

1G	First Generation
2D	Two Dimensional
2G	Second Generation
3D	Three Dimensional
3G	3rd Generation
3GPP	Third Generation Partnership Project
4G	4th Generation
AoA	Angle of Arrival
A-GPS	Assisted GPS
BSIC	Base Station Identity Code
BTS	Base Transceiver Station
CC	Central Cells
CCCH	Common Control Channel
CCH	Common Channel
CDF	Cumulative Distribution Function
CLA	Clustered Linear Array
CPICH	Common Pilot Indication Channel
dB	Decibel
dBi	Decibels relative to isotropic antenna gain
dBm	Decibels relative to 1mW
DL	Downlink
DSCH	Downlink Shared Channel
eICIC	Enhanced Inter Cell Interference Coordination
Gbps	Gigabits per second
GGSN	Gateway GPRS Support Node
GHz	Gigahertz
GMSC	Gateway Mobile Switching Centre

GPRS	General Packet Radio Service
GPS	Global Positioning System
GSM	Global System for Mobile Communications
HCS	Hierarchical Cell Structure
HLR	Home Location Register
HSDPA	High Speed Downlink Packet Access
HS-DSCH	High Speed Downlink Shared Channel
HSPA	High Speed Packet Access
HSPA+	Evolved HSPA
HSUPA	High Speed Uplink Packet Access
Hz	Hertz
ICIC	Inter Cell Interference Coordination
ID	Identity
IEEE	Institute of Electrical & Electronic Engineers
ISD	Inter-Site Distance
ITU	International Telecommunications Union
kbps	Kilobits per second
KHS	Kensington High Street
km	Kilometre
KPI	Key Performance Indicator
LoS	Line of Sight
LTE	Long Term Evolution
LTE-A	LTE-Advanced
m	Metres
Max. C/I	Maximum C/I
Mbps	Megabits per second
MDT	Minimisation of Drive Test
ME	Mobile Equipment
MHz	Megahertz

MIMO	Multiple Input Multiple Output
MNO	Mobile Network Operator
ms	Millisecond
MSC	Mobile Switching Centre
mW	Milliwatt
NGMN	Next Generation Mobile Networks Alliance
OMS	Operations and Maintenance System
OPEX	Operational Expenditure
OTDA	Observed Time Difference of Arrival
PCI	Physical Cell ID
PDSCH	Physical Downlink Shared Channel
PF	Proportional Fair
PSTN	Public Switched Telephone Network
QAM	Quadrature Amplitude Modulation
QoS	Quality of Service
RAN	Radio Access Network
RF	Radio Frequency
RMS	Root Mean Squared
RNC	Radio Network Controller
RR	Round Robin
RRU	Remote Radio Unit
RSCP	Received Signal Code Power
RSSI	Received Signal Strength Indication
RX	Receiver
s	Second
SC	Scrambling Code
SGSN	Serving GPRS Support Node
SHO	Soft Hand Over
SOM	Self-Organising Maps

SON	Self-Organising Networks
TM7	Transmission Mode 7
TOA	Time of Arrival
TTI	Transmission Time Interval
TX	Transmitter
UARFCN	UTRA Absolute Radio Frequency Channel Number
UE	User Equipment
UMTS	Universal Mobile Telecommunications System
UTRA	Universal Terrestrial Radio Access
VLR	Visitor Location Register
W	Watt
WCDMA	Wideband Code Division Multiple Access
X-Polar	Cross Polar

List of Symbols

β	Antenna horizontal beamwidth
φ	Horizontal bearing from the antenna boresight
φ_{3dB}	Horizontal 3dB beamwidth of the antenna
θ	Vertical bearing from the antenna boresight
θ_{3dB}	Vertical 3dB beamwidth of the antenna
θ_{etilt}	Antenna electrical downtilt
A	Relative antenna gain
A_H	Relative horizontal antenna gain
A_m	Front-to-back antenna attenuation
A_V	Relative vertical antenna gain
$Avr\_Throughput_n$	Average throughput for user n
BW	Bandwidth
BW_{LTE}	LTE system bandwidth
C	Channel capacity
$cell(n).opt\_tilt$	Optimum tilt for cell n
C/I	Carrier to interference ratio
$C/I_{HS\text{-}DSCH}$	C/I of the HS-DSCH
$C/I_{LTE\text{-}PDSCH}$	C/I of the LTE PDSCH
d	Distance
Ec/Io	Energy per chip to the interference spectrum density ratio
I	Interference power
$Inst\_Throughput_n$	Instantaneous throughput for user n
N	Noise power
PF_factor_n	Proportional Fair scheduler fairness factor for user n
PL	Path Loss

$R_{HS\text{-}DSCH}$	Bit rate of the HS-DSCH
RMS_Error	Root Mean Squared Error
$RSCP_{Macro\_Cell}$	RSCP of the best serving macrocell
$RSCP_{Small\_Cell}$	RSCP of the best serving small cell
$RSSI_n$	RSSI for lamppost microcell n
S	Received power
SLA_v	Slide lobe antenna attenuation
tc	Traffic captured
$window\_size$	Sliding window size
x	Horizontal simulation coordinate
y	Vertical simulation coordinate

Chapter 1
Introduction

1.1 Motivation & Objectives

Mobile broadband data traffic is rapidly expanding across the globe as more and more users adopt feature phones, smart phones, connected laptops and tablets [1]. Not only are more users adopting these devices each month, but each month the users that already have adopted these devises consume increasing amounts of data [2].

To cope with this so called "data tsunami" Mobile Network Operators (MNOs) are having to rapidly increase the capacity of their cellular networks through the acquisition of more radio spectrum, through the use of more spectrally efficient radio access technologies such as fourth generation networks based on Long Term Evolution (4G/LTE) radio technology and through the deployment of more, and increasingly smaller, radio cell sites within their networks. However, in order to be cost efficient the MNOs must also maximise their existing assets by increasing the capacity on their legacy second generation/Global System for Mobile Communication (2G/GSM) and third generation/Wideband Code Division Multiple Access (3G/WCDMA) networks, since it will be at least 5 years [3] before the majority of users have a 4G/LTE device and contiguous small cell layers are deployed across the busiest parts of the MNO's networks.

At the legacy macrocell many options exist to increase capacity. These include increasing the number of frequency carriers deployed, increasing the number of sectors and improving the spectral efficiency of the site by moving to a more advanced radio technology such as 3G/High Speed Packet Access (3G/HSPA) or 4G/LTE and/or employing Multiple Input Multiple Output (MIMO) antenna techniques.

Regardless of the steps taken to increase the macrocell layer's capacity, given the traffic forecasts highlighted earlier, it is expected that at some point in the future, in the busiest parts of the network, a network of macrocells will no longer be able to cope with the traffic demand placed upon it and a move to a network of smaller cells will be inevitable. This deployment of a layer of smaller cells under an existing macrocell layer will create a multi-layer network of varying cell sizes often called a Heterogeneous Network or HetNet for short.

Given the number of small cells expected to be deployed [4] and the typical locations at which they are expected to be installed (dense urban areas, retail parks, shopping malls etc.) then small cell Base Transceiver Stations (BTSs) are likely to have a much smaller physical size and therefore lower transmit power than their macrocell equivalent. For this reason the

cell range of the small cell will be much smaller than that of the macrocell and therefore for the small cell to be effective at capturing traffic it will need to be placed precisely at, or very close to, the high traffic locations and have its coverage maximised by the careful adjustment of the small cell and the surrounding macrocell(s) parameters.

Also given the expected increase in the number of cells within the network, the need to dynamically control the interaction between the layers and cells of the HetNet, as well as the constant requirement to reduce Operational Expense (OPEX) of future HetNets, Self-Organising Network (SON) methods are now being proposed to automate the operation and optimisation of HetNets [5].

Taking into account the above challenges, the objectives of the research set out in this thesis were as follows;

1. To explore novel ways to maximise the capacity of the legacy macrocells, through SON where possible, therefore delaying the deployment of small cells and their associated costs.
2. When finally having to deploy small cells, using SON techniques to ensure that these small cells are located as close as possible to traffic hotspots to maximise their traffic and cost effectiveness.
3. Understanding the capabilities of low powered small cells to offload traffic from a co-channel macrocell layer.
4. Maximising the offload onto deployed small cell networks using SON techniques.

1.2 Major Contribution

The work undertaken in this thesis has provided a number of original major contributions and this section gives an outline of these contributions.

The higher order sectorisation work determines for the first time, the optimum horizontal antenna beamwidths for 3, 6, 9, 12 and 15 sectored 3G/WCDMA sites to maximise network capacity whilst respecting a number of network Key Performance Indicators (KPIs). Higher order sectorisation field work also shows for the first time, the gains from wide scale deployment of six-sector 3G/WCDMA sites into a live commercial network, and the potential capabilities of the world's first fifteen-sectored 3G/WCDMA site.

The rapid dynamic antenna downtilt work shows this proposed novel SON method to be effective from both simulation and from field trials of this technique in a live 4G/LTE network.

A number of original small cell placement algorithms based upon the use of geo-located UE measurement reports and RF fingerprinting are also proposed and are shown to be effective at capturing traffic even for highly inaccurate User Equipment (UE) location information.

The actual effectiveness of co-channel, low powered, small cells is proven through both simulation and field results from London's first lamppost mounted 3G/WCDMA small cell network deployment.

Finally a number of original SON algorithms are proposed that maximise the offload from the macrocell layer onto low power, street level small cells.

All simulation results presented in this thesis have been performed using a bespoke MATLAB WCDMA/LTE network simulator developed solely by the author. The Network Simulator has been used to model the proposed capacity enhancement techniques on homogeneous as well as real world Central London network configurations. In addition to the extensive network simulations performed, many of the techniques proposed in this thesis have also been further verified through extensive field trials.

1.3 Structure of Thesis

This section gives an outline of the content of the following chapters of this thesis.

Chapter 2 gives an overview of the mobile broadband industry and the evolution of mobile broadband technologies. It then outlines the network and site capacity upgrade options open to MNOs and finally provides a general literature review of SON.

Chapter 3 proposes a novel rapid dynamic macrocell antenna titling concept that can be used to facilitate a self-organising macrocell network. From simulation and field trials it is shown how this concept can improve the cell capacity and cell edge macrocell performance for both 3G/WCDMA and 4G/LTE network technologies.

Chapter 4 studies the capacity gains of higher order sectorisation on a 3G/WCDMA macrocell network. It presents simulations and field trials undertaken to study the expected capacity gains provided by 6, 9, 12, and 15 sectored sites over the capacity of a standard three sectored 3G/WCDMA macrocell site.

Chapter 5 considers if it is possible to use SON self-planning technique to effectively locate small cells on a limited set of street furniture locations (in this case central London lampposts) using geo-located UE measurement reports of varying location accuracy. Chapter 5 also considers the use of Radio Frequency (RF) information detailed within the UE measurement reports to better determine the traffic hotspots within the network through the use of a proposed RF fingerprinting technique.

Chapter 6 looks at the effectiveness of low power, lamppost mounted, 3G/WCDMA microcells to capture traffic from a co-channel macrocell layer. The chapter details simulations that model the potential offload achieved by the deployment of thirteen low power, 3G/WCDMA microcells on lampposts along Kensington High Street in central London and then compares these simulation results to field measurements taken before and

after the actual deployment of four lamppost mounted 3G/WCDMA microcells along the street.

Chapter 7 proposes a number of SON based methods to maximise traffic offload from surrounding 3G/WCDMA macrocells onto the Kensington High Street lamppost mounted 3G/WCDMA microcells introduced in the previous chapter.

Finally Chapter 8 provides a summary of the work presented in this thesis and highlights the main conclusions of the work. This chapter also outlines some potential areas for further research.

1.4 Publication List

This section lists the publications that were produced during the research work undertaken for this thesis. The list is broken into two sections, the first part of the list contains the publications based on the work described within this thesis. For all of the publications in this part of the list, the author of this thesis has carried out all of the work while the other authors have acted as supervisors for the work or have supplied the raw data on which analysis has been performed.

1. R. M. Joyce, L. Zhang, D. Barker, "HSPA Performance Improvement through Coordinated Dynamic Antenna Tilt & Scheduling", *Proc. IEEE Wireless Communications and Networking Conference*, Shanghai, 2013, pp. 3953 - 3957.
2. R. M. Joyce, L. Zhang, D. Barker, "Coordinated Dynamic Antenna Tilt & Scheduling in a Central London LTE Network", *Proc. European Wireless Conference*, Guildford, 2013.
3. R. M. Joyce, D. Morris, S. Brown, L. Zhang, "Higher Order Horizontal Sectorisation Gains For a Real 3GPP/HSPA+ Network", *Proc. European Wireless Conference*, Guildford, 2013.
4. R. M. Joyce, "Automatic Optimisation of Macro and Micro Cells to Maximise Traffic Offload onto a Central London Small Cell Network", presented at the Small Cell World Summit 2013, London, 2013.
5. R. M. Joyce, L. Zhang, D. Barker, "Coordinated Dynamic Antenna Tilt & Scheduling in a Central London LTE Network", presented at the LTE 2013 World Summit, Amsterdam, 2013.
6. R. M. Joyce, D. Morris, S. Brown, D. Vyas, L. Zhang, "Higher Order Horizontal Sectorisation Gains for 6, 9, 12 and 15 Sectored Cell Sites in a 3GPP/HSPA+ Network", *IEEE Trans. Antennas & Propagation, submitted, under review*.
7. R. M. Joyce, "Small Cells and Heterogeneous Networks", *IEEE spectrum magazine, submitted, under review*.

8. R. M. Joyce, L. Zhang, D. Barker, "Rapid Dynamic Antenna Tilting in 3G/WCDMA and 4G/LTE Networks", *IEEE Trans. Antennas & Propagation, submitted, under review*.
9. R. M. Joyce, L. Zhang, "Locating Small Cells Using Geo-located UE Measurement Reports & RF Fingerprinting", *IEEE International Conference on Communication*, Sydney, 2014 *, submitted, under review.*
10. R. M. Joyce, L. Zhang, "Self Organising Network Techniques to Maximise Traffic Offload onto a 3G/WCDMA Small Cell Network using MDT UE Measurements", *IEEE International Conference on Communication*, Sydney, 2014 *, submitted, under review.*
11. R. M. Joyce, L. Zhang, "The Effectiveness of Low Power Co-channel Lamppost Mounted 3G/WCDMA Microcells", *IEEE Wireless Communications and Networking Conference*, Istanbul, 2014, *submitted, under review.*

The second part of the list shows two further publications that were also produced using the bespoke 3G/WCDMA and 4G/LTE Network Simulator developed by the author to support the research work described within this thesis. However, whilst these publications are related to the work presented here, none of the work produced for these publications is used within this thesis.

12. A.Sholiyi, B. Badic, R.M. Joyce, T. O'Farrell, "A Characterisation of HSDPA Capacity using EXIT Chart Techniques", *Proc. IEEE Third International Conference on Next Generation Mobile Applications, Services and Technologies*, Cardiff, 2009, pp. 204 - 208.
13. B. Badic, Amar H. Kabashi, R.M. Joyce, T. O'Farrell, "A Performance Investigation of Coded MC-CDM with the Chase Detection Algorithm", *Proc. IEEE International Symposium on Personal, Indoor and Mobile Radio Communications*, Tokyo, 2009, pp. 1732-1736.

Chapter 2
The Evolution Towards Self Organising Networks

This chapter provides the relevant background information required for the reader to gain a full appreciation and understanding of the work presented in this thesis.

The first section of this chapter provides an overview of the growing mobile broadband industry and the evolution of mobile broadband technologies in order to cope with increasing voice and data traffic demands placed on today's mobile communications networks. The second section considers the options available to the MNOs to increase the capacity of their mobile networks in order to cope with this ever increasing traffic demand. And finally the third section provides a generalised literature review on SON. Reviews of the earlier work undertaken, if any, for each of the SON concepts explored within this thesis are presented separately in the relevant chapters.

2.1 Mobile Broadband Traffic Growth and the Evolution of Mobile Broadband Technologies

The mobile communications market has experienced enormous growth over the past six years since the introduction in 2007 of the Apple iPhone and other first generation smartphones. During this short period of time cellular mobile communications systems have also made the transition from so called "second and third generation" mobile communication systems to a fourth generation of digital cellular systems, with 4G networks providing even higher capacity and data rates than the previous network generations.

This increase in smartphone functionality and the increase in the data rates offered by 3G and 4G network technologies have changed the way that many people communicate, work, purchase, interact with friends, and in fact have changed the way many people live their lives. Shown in Figure 2.1 taken from reference [1] is the average time a smartphone user spends per day undertaking various activities on their mobile device. In total the survey suggests that each user spends on average over two hours a day using their mobile devices and another survey [6] suggests the average smartphone user looks at their mobile devices over 150 times per day.

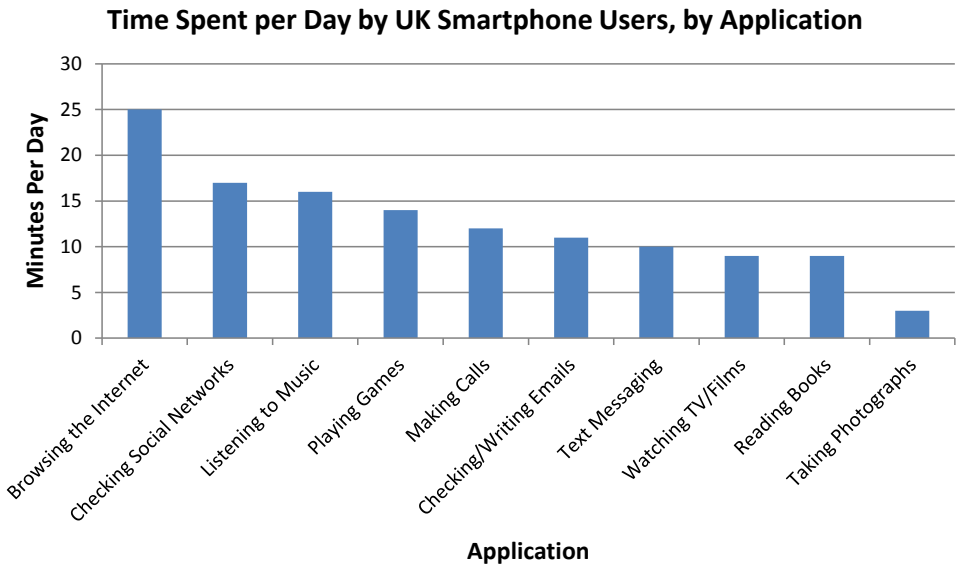

Figure 2.1 Time spent per day by UK smartphone users, by application [1]

Given this dependence on mobile connectivity it is no surprise that the average amount of data consumed by smartphone users has also increased significantly year on year. Shown below in Table 2.1 taken from reference [3] is the average user monthly data consumption seen over the period October 2011 – September 2012, by mobile operating system for users with unlimited data tariff plans. As can be seen from the table for the two major smartphone operating systems (Google's Android and Apple's iOS) these represent annual data growth rates of 66% and 41% respectively.

Table 2.1 Average user data consumption in Mbytes per month usage, by mobile operating system, for users with unlimited data plans, Oct 11 – Sep 12 [3].

Operating System	Oct-11	Nov-11	Dec-11	Jan-12	Feb-12	Mar-12	Apr-12	May-12	Jun-12	Jul-12	Aug-12	Sep-12
Android	968	1036	1002	1036	1132	1068	1305	1303	1365	1469	1498	1610
Proprietary	269	262	258	247	225	220	323	381	642	1184	1220	1300
iOS	782	844	824	838	862	843	979	948	1018	1015	1085	1108
Palm OS	605	651	594	610	703	586	663	805	812	799	771	911
Windows	440	435	347	308	364	388	487	555	694	385	533	481
Linux	90	112	256	264	240	191	301	252	158	148	243	371
Blackberry	184	210	173	173	168	158	182	208	224	257	236	248
Symbian	409	133	143	6	3	0.1	1	1	3	0.4	1	1

In addition to the existing smartphone users' data usage increasing, smartphone penetration rates are still surprisingly low with less than half (48%) of UK mobile phone users owning a smartphone at the time of writing [7]. However, it is also predicted [7] that by 2017, 65% of UK mobile phone users will have a smartphone. This predicted smartphone penetration forecast coupled with the forecast 8-fold increase in data usage per month for smartphone users [3] over the same period (342Mbytes/month to 2.7Gbytes/month per smartphone user), suggests that in just over three years' time, by 2017, the UK mobile networks will carry over 10 times the data volume they carry today. Whilst the UK networks overall may carry 10 times today's data traffic, the data traffic growth will certainly not be uniform across these networks, and in some areas of these networks much greater traffic growth will be seen at specific traffic hotspots. For example shown below in Figure 2.2 is the data traffic density seen on Telefonica UK's central London 3G network in December 2011, clearly showing the non-uniform data traffic distribution seen across today's mobile networks.

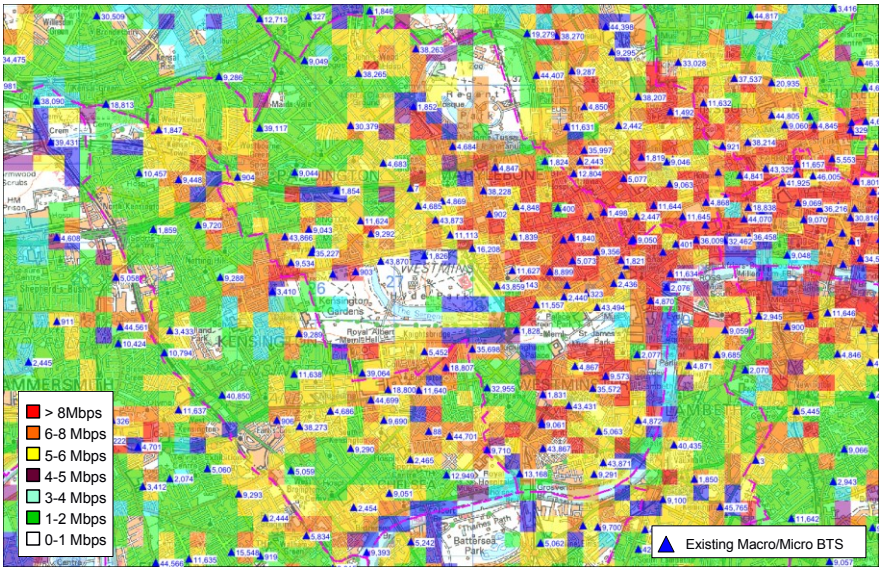

Figure 2.2 Map of Telefonica UK's 3G data traffic density for central London, December 2011.

In order to cope with the ever increasing voice and data volumes seen by mobile networks, the 3rd Generation Partnership Project (3GPP) and other standardisation bodies have constantly been defining new mobile broadband radio standards to increase the capacity and capabilities of mobile networks. Shown in Table 2.2 are the 3GPP releases and the main features included within each of these releases for 3G/WCDMA and 4G/LTE. As can be seen in just 11 years since the introduction of the Release 99 (R99) version of 3G/WCDMA in the year 2000, data rates supported by 3GPP's family of technologies have increased 2600-fold from 384kbps to 1Gbps. Whilst this increase is peak data rates is impressive, this hides the fact that the actual spectral efficiency of the initial releases of 4G/LTE (Figure 2.3)

are not actually that much greater than the later releases of 3G/WCDMA. For example from Figure 2.3 it can be calculated that the spectral efficiency of 3G/HSPA R6 is 0.4bps/Hz whereas the maximum network spectral efficiency for 4G/LTE R8 is only 1.4bps/Hz (only 3.5 times more efficient than 3G/HSPA R6). Given that 4G/LTE is only potentially improving the spectral efficiency of the network by up 3.5 times, yet it is expected, as shown earlier, that data traffic in some areas of the network will increase by 10 times its current levels, then clearly a move to 4G/LTE in existing spectrum bands alone is not enough to cope with the forecasted demand. The following section looks at the other options open to MNOs to increase the capacity of their 3G and 4G mobile networks.

Table 2.2 Main features and the enhancement of throughput from 3GPP releases for 3G/WCDMA and 4G/LTE technologies.

3GPP Release	Year	3G/WCDMA Main Features Delivered	3G/WCDMA Data Rates	
			DL Data Rate	UL Data Rate
99	2000	Initial WCDMA Release	384kbps	384kbps
4	2001	Improvements to R99	384kbps	384kbps
5	2002	HSDPA (DL 16QAM)	14.4Mbps	384kbps
6	2005	HSUPA (UL Existing BPSK)	14.4Mbps	5.76Mbps
7	2007	DL 64QAM, UL 16QAM & MIMO	28.0Mbps	11.5Mbps
8	2008	2 Carrier aggregation	42.2Mbps	11.5Mbps
9	2009	2 Carrier aggregation & MIMO	84.4Mbps	23.0Mbps
10	2011	4 Carrier aggregation & MIMO	168.8Mbps	23.0Mbps

3GPP Release	Year	4G/LTE Main Features Delivered	4G/LTE Data Rates	
			DL Data Rate	UL Data Rate
8	2008	Initial LTE Release	302.0Mbps	75.0Mbps
9	2009	Improvements to R8 LTE & EMBMS	84.4Mbps	23.0Mbps
10	2011	LTE-Advanced, 5 Carrier aggregation	1000.0Mbps	200.0Mbps

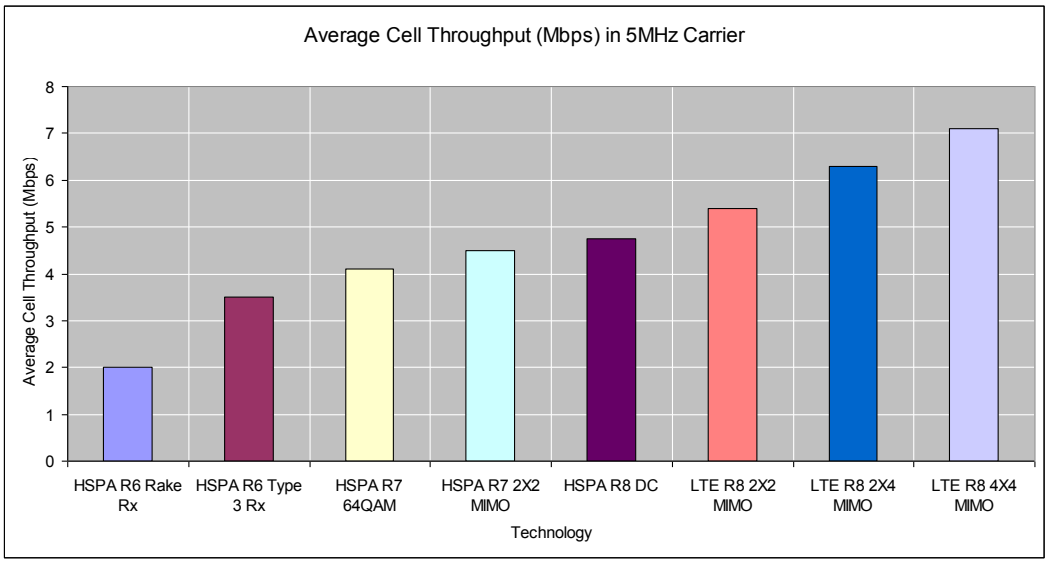

Figure 2.3 Average fully loaded downlink cell throughputs for HSPA, HSPA+ and LTE for a single 5MHz carrier [8].

2.2 Mobile Network Operator Capacity Upgrade Options

Given the forecasted traffic growth on their networks shown earlier, MNOs are now considering a variety of options to increase their network capacities in order to cope with this ever increasing traffic demand. This section highlights the main three options open to the MNOs, namely

- More radio frequency spectrum
- More spectrally efficient network technologies
- More cells & smaller cells

2.2.1 Option 1: More Spectrum

The acquisition of more spectrum by an MNO is a lengthy process and is not always guaranteed to end in success given the typical award processes used by national regulators to allocate new spectrum blocks (spectrum auction, beauty contest etc.). Even if successful in obtaining additional spectrum, the MNO must then decide what technology (2G, 3G or 4G) to deploy in the spectrum, roll out new sites, add new BTS equipment and new antennas to support the new spectrum allocation and also ensure there is a sufficient penetration of mobile devices that support the new allocation/technology. Taking the UK 800MHz digital dividend band as an example, the spectrum was earmarked for future mobile use as early as 2007 by the International Telecommunication Union (ITU) [9]. The UK regulator then issued multiple consultations on the use of this band [10, 11]. The band was finally auctioned in February 2013 [12] and the first launch of a 4G/LTE network in the UK in this band is expected in Q3 2013 [13] some six years after the spectrum was first earmarked for future mobile use.

In addition to the length of time it takes to acquire spectrum, additional spectrum costs money, and as seen from the recent UK 4G spectrum auction [12] and the now infamous UK 3G spectrum auction of 2000 [14], the prices paid for mobile spectrum can run into billions of pounds.

Therefore whilst the acquisition of new spectrum and the deployment of new more advanced spectrally efficient technologies in these new spectrum blocks is an option for MNOs to increase their network capacities, because of the time taken and the significant investment required in both spectrum and network infrastructure, spectrum acquisition is seen as a longer term strategic option rather than an option that can be used to rapidly grow network capacity at key locations within the network.

2.2.2 Option 2: More Spectrally Efficient Network Technologies

As highlighted in Section 2.1, many of the advanced radio technologies and features standardised by 3GPP in the last 10 years have led to improvements in the radio spectral efficiency of the 3G/WCDMA and 4G/LTE air interfaces and deploying these technologies and features at existing sites will clearly help improve network capacity.

However, there are also a number of other promising techniques in addition to deploying the most spectrally efficient radio interface that can also improve the capacity of the MNO's existing macrocell sites and this section considers three such techniques, namely

- Higher Order Antenna Sectorisation
- MIMO antenna techniques
- Rapid Dynamic Antenna Tilting

2.2.2.1 Higher Order Antenna Sectorisation

Higher order horizontal antenna sectorisation has always been seen as a key technique to improve both the coverage and capacity of cellular networks [15, 16]. Today most cellular networks typically employ three sectors per cell site (Figure 2.4) and the reason behind this is due to the fact that three sectors per site works well with the concept that the ideal cellular network is a tessellation of hexagonal cells and because of the limitation of cellular antenna and BTS technology at the time the introduction of 1st generation cellular networks. However, in reality modern cellular networks are not based upon a perfect hexagonal grid of cell sites and nor do the sectors of each cell site perfectly tessellate with one another. Cell sites are typically deployed at high vantage points within the network to provide wide area coverage (e.g. existing TV/radio transmission towers), in areas of high traffic density (e.g. downtown areas/shopping malls) or at locations where the cellular operator may have favourable rental terms with the site provider. Therefore since cellular networks do not follow a perfect hexagonal grid, three sectors per site is really an arbitrary value and higher sector counts are possible and as will be shown in Chapter 4 of this thesis they can yield significant network capacity and coverage benefits.

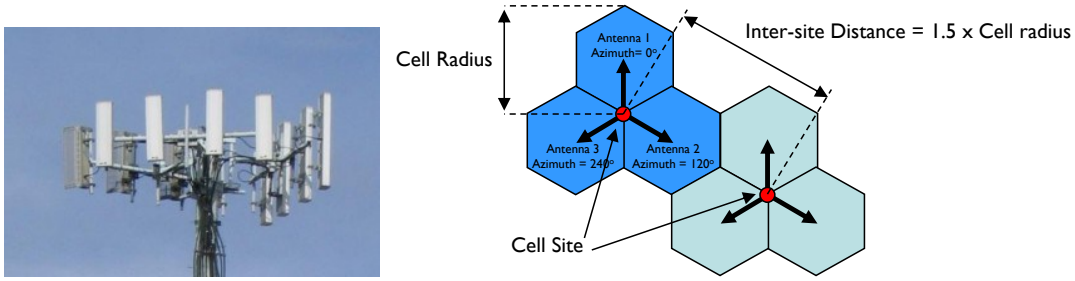

Figure 2.4 Picture of a three sectored site and a diagram showing the theoretical hexagonal tessellation of three sectored sites.

2.2.2.2 MIMO Antenna Techniques

MIMO antenna techniques have been extensively researched over the past 10 years [17] and have been proposed to enhance the performance and capacity of both 3G/WCDMA and 4G/LTE since R7 (3G/WCDMA) and R8 (4G/LTE) of the 3GPP standard. MIMO can be used to support beamforming, spatial multiplexing and both transmit and receive diversity. Whilst 3GPP R8 supports up to 4x4 MIMO for 4G/LTE, higher order modes of MIMO up to 8x8 are proposed for 4G/LTE from 3GPP R10 onwards and it is suggested [18] that 8x8 MIMO may further increase the spectral efficiency of 4G/LTE to over 4.0bps/Hz.

Whilst the capacity gains obtained from MIMO look very attractive, as will be discussed in Chapter 3 MIMO typically require much larger antenna arrays and therefore may not be practical for all existing macrocells or small cells.

2.2.2.3 Rapid Dynamic Antenna Tilting

When optimising a cellular network of any type the MNO will typically optimise the network using a "cluster" based approach [19]. A cluster normally consists of around 10 to 20 cell sites in a particular geographic location (Figure 2.5). During cluster optimisation the MNO deploys drive test teams to drive throughout the clusters and evaluate the network by making a series of voice and data calls using test UEs. In addition to driving the network the operator can also analyse measured statistics from the cell sites such as uplink noise rise and downlink power at each cell to identify any potential problems in addition to those seen from the drive surveys. Based upon these statistics and drive survey results the operator then makes changes to the network in order to optimise and improve the overall performance of the network. These changes may be so called "hard" changes such as antenna tilts (changes to the vertical antenna bearing) and antenna azimuth adjustments (changes to the horizontal antenna bearing) at the cell site or "soft" changes such as parameter changes at the cell site or at other network elements.

Once these changes to the network configuration have been made, further drives are undertaken and the performance of the new drive is assessed against the previous drives and this process is repeated until the cluster meets its performance targets. Once the cluster has met its performance targets and is taken into service, further changes to antenna tilts, antenna azimuths and cell parameters of the cluster are then typically based on the regular and on-going analysis of the network and cell site statistics on a week by week or month by month basis. This normally results in antenna tilt changes being made over the longer term rather than on an hourly or minute or in the extreme millisecond by millisecond basis – the ideal situation given the daily dynamic variation in traffic levels on today's mobile networks.

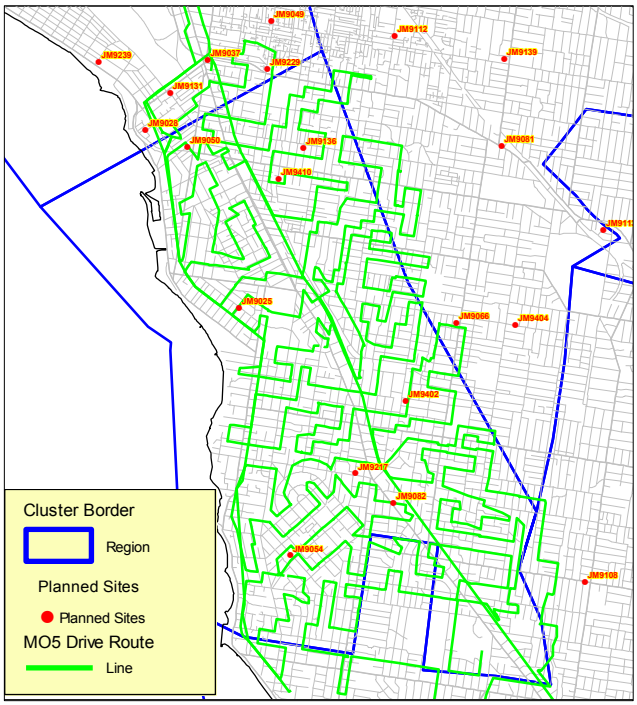

Figure 2.5 A typical cluster of UMTS sites and optimisation drive route.

Instead of this longer term approach, a novel technique proposed in Chapter 3 of this thesis termed Rapid Dynamic Antenna Tilting is a SON antenna tilt technique aligned to the 2ms and 1ms physical layer Transmission Time Intervals (TTIs) of 3G/WCDMA and 4G/LTE, that allows the macrocell sites of these networks to constantly self-optimise their antenna tilts in real time. In Chapter 3 it is shown that this technique when coordinated with the downlink packet scheduler can bring significant capacity gains to sites within already optimised 3G/WCDMA and 4G/LTE networks.

2.2.3 Option 3: More Cells and Smaller Cells

Whilst MNOs will continue to deploy further macrocells where possible, in city centres and high traffic areas, the MNOs are now struggling to find further roof or tower space to increase the macrocell network density and other means must now be found to increase site densities within these areas.

For many years small cells (often termed micro, pico or femtocells depending on their size) have been seen as one of the key techniques in order to improve the capacity of cellular networks [20, 21], however only recently have telecommunication equipment vendors started to produce small, low power BTSs to allow the effective deployments of 2G, 3G and 4G small cell networks. With finite cellular spectrum allocations and LTE and LTE-A spectral efficiencies saturating then small cells (both indoor and outdoor) are the only realistic means to greatly increase an MNO's network capacity in order to cope with the

expected future mobile data demand. Chapters 5, 6 and 7 study the effectiveness of 3G/WCDMA small cells to increase network capacity, by considering the optimum location to place small cells, the actually effectiveness of low power small cells when placed under a co-channel macrocell layer and how to maximise the capacity of small cell networks through SON techniques.

2.3 Literature Review - Self-Organising Networks

From the earlier sections it is clear that the future for MNOs includes networks having sites with more sectors, site supporting 2G, 3G and 4G technologies and networks with multiple layers of macro, micro, pico and femtocells. In order to effectively manage the configuration, optimisation and operation of these future network, MNOs will need to rely on more automated means to perform all of these task. Ultimately this will lead to a fully autonomous self-organising network and this section reviews the history of the SON concept and how SON is being adopted by 3GPP. Reviews of the earlier work undertaken, for each of the concepts explored within this thesis are presented separately at the beginning of the relevant chapters.

2.3.1 A Brief History of Self-Organising Networks

The idea of self-optimising/self-organising Networks has been seen for many years as the "holy grail" for MNOs, enabling them to significantly reduce their OPEX relating to network installation, operation and optimisation. An overview of the estimated benefits of SON on OPEX reduction is given in [22] and suggests that the OPEX improvements in the areas of planning, deployment, operations and optimisation could be in the order of 65% to 80%. Given that [22] also suggests that Network Operations accounts for typically 20% of an operator's OPEX then it can be seen that SON could have a significant impact on the overall OPEX costs for an MNO.

The aim of SON is not only to provide financial benefits to the MNO but to also enhance the Quality of Service (QoS) seen by the users of the network, through higher bit rates, lower latency and improved call performance.

Early papers on SON related mainly to 2G technologies rather than earlier systems due to the lack of digital interfaces between network elements and the lack of significant computer processing capabilities at network nodes. In [23] a method is presented for the dynamic management of GSM neighbour lists using Mobile Equipment (ME) measurement reports as well as neighbour usage statistics. Performance of the proposed scheme is assessed through simulation and the primary gain proposed is not performance but the reduction in manual

planning of the neighbour lists. A secondary gain is the reduction of the length of the GSM neighbour lists and this will have an effect on the handover performance of GSM since the ME will spend less time scanning the neighbours prior to a handover decision being made. It will be shown later that automatic neighbour generation still features heavily in the functional specifications of 4G/LTE SON features.

SON was also proposed for the other major 2G technology deployed globally, IS-95 based Code Division Multiple Access (CDMA). In [24] a method for pilot power optimisation is proposed based on Monte Carlo simulation followed by implementation and measurement in the field. Individual cell pilot powers are adjusted by up to 6dB from their default value in order to maximise the capacity and performance of the network. Again it will be seen that power planning still features heavily in more recent SON proposals.

By the time of 3G network deployments SON proposals became more prevalent, especially relating to 3G/WCDMA, although more generic references also begin to appear during this period. Whilst Raivio *et. al* [25] first propose the use of Self-Organising Maps (SOM) for 3G/WCDMA network optimisation, the reference only states a method of cell classification using SOM. The actual use of SOM for network optimisation is initially presented in [26]. Here a centralised approach to simulate cluster grouping, coverage and capacity enhancement by adjusting the cell's antenna heights, azimuths, tilts and beamwidth is proposed, although in this context relates more to network planning (pre-deployment) than network optimisation (post-deployment and operation).

Real time optimisation is however the aim of the architecture presented in [27]. Here a high level architecture for a fully self-optimising hybrid (cellular & multi-hop) network is presented based on Autonomic Computing, where Autonomic Computing is the term given to placing the intelligence into the nodes of the network. Each node of the network can communicate with other nodes within the network to perform a number of functions introduced in the reference under the umbrella term "Self-Management", these include;

- Self-configuration – In this reference refers to the ability to configure the cell to handle a changing traffic pattern.
- Self-optimization – The re-routing of packet data on route congestion or failure
- Self-healing – Detecting node failures and taking corrective actions to rectify or by-pass these failures
- Self-protecting – In this reference relates more to the protection of relayed links between two mobile parties

It is interesting to note that this terminology is very similar to that now seen within 3GPP relating to SON, although with the meaning of each term here having a slightly different meaning than those currently proposed within 3GPP.

Continuing this theme of real time optimisation references [28, 29] consider more the physical aspects of real time optimisation with both considering the use of near real time antenna tilts or adaptive antennas to maximise cellular coverage and/or capacity to achieve load balancing between cells. Hampel *et al.* [28], presents results from a simplified four cell model that investigated which cell parameters are most effective at balancing the load. The reference concludes that antenna tilting is much more effective than purely pilot power adjustment and this effect is now well known within the industry and exploited in some of the SON algorithms proposed later in this thesis.

Lin *et al.* [29], consider the effect of co-ordinated changes between cells through using what is termed "A Cooperative Negotiation Approach". The method presented uses four element adaptive antennas to contract the coverage of busy cells and expand the coverage of the surrounding cells to offload traffic from the busy cell. A high level protocol is presented for the negotiation between the cells and cells may request "help" only when their load goes above a certain load threshold. Simulations based on hexagonal network geometry are presented using omni-directional adaptive antennas. The results presented suggest that the adaptive antenna approach can avoid network blocking as users migrate to traffic hot spots within the simulation area and the network adapts to maintain a reasonable QoS for each of the users.

Finally prior to the standardisation bodies' involvement in SON, [30, 31] proposed some key, more generic high level concepts on SON relating to 3G and future 4G technologies.

2.3.2 Self-Organising Networks Standardisation

It was not until 2006 that a consolidated push towards a standardised SON approach was put forward by the Next Generation Mobile Networks Alliance (NGMN) in [32]. This document introduced many of the SON concepts now adopted by 3GPP and defined a number of "SON use cases" giving examples of the areas of network operation in which SON could be used to provide cost savings and performance benefits. The functional grouping of the use cases defined by NGMN were as follows;

- Self-Planning
- Self-Configuration
- Self-Optimisation
- Self-Testing & Self-Healing

The Self-Planning category included use cases considering both the location of new sites within the network as well as initial network parameters and site parameters (transmit power, antenna tilt etc.) prior to installation and operation of the new node.

The Self-Configuration category defined use cases relating to the automation of the installation and commissioning of the new network node.

The Self-Optimisation category defined use cases that used SON to automate the on-going optimisation of the network.

And finally in the Self-Testing and Self-Healing category NGMN set out use cases that allow the network to constantly monitor its performance and where necessary make changes to rectify faults detected within the network. In this category NGMN also proposed the automatic collection of drive survey measurements from normal user's UEs - a concept later adopted by 3GPP and renamed Minimisation of Drive Test (MDT) [33, 34]. Many of the SON concepts proposed in this thesis also make use of the MDT concept to identify the location of individual user or to build up coverage and traffic maps on which to make network optimisation decision.

3GPP started to include SON concepts from R8 onwards. In [35] 3GPP defined an overview of the proposed LTE SON architecture and functionality. Three different SON architectures were defined, Centralised SON, Hybrid SON and Distributed SON. For the Centralised SON architecture the SON intelligence is located within the centralised Operations and Maintenance System (OMS). In the Distributed Architecture intelligence is distributed across all network elements. Whilst, in the Hybrid Architecture some of the intelligence is at the OMS and some is situated in the network elements. 3GPP grouped its SON requirements into five categories, namely;

- SON in a Multi-Vendor network
- Self-Establishment of a new eNodeB
- Automatic Neighbour Relation Management
- Self-Optimisation, Self-Healing, Coverage and Capacity Optimisation, and Handover Optimisation
- Continuous Optimisation due to Dynamic Changes in the Network

Further details of the required functions for Self-Establishment/Configuration, Automatic Neighbour Relations and Self Optimisation are given in [36, 37, 38, 39] respectively. Whilst the required high level functional requirements are presented in these documents, no details relating to the actual algorithms are given since it is 3GPP intention that these will be implemented separately by the vendors.

2.4 Chapter Summary

This chapter has shown how the growing demand for mobile data, driven by the increasing use and penetration of smartphones, is forcing MNO to rapidly increase their mobile network capacities through the acquisition of more mobile spectrum, the introduction of more spectrally efficient radio technologies and the deployment of more macrocells and small cells.

All of this leads to a future where the mobile network becomes a heterogeneous network made up of very high capacity macrocells overlaying one or more layers of small cells. In order to cope with the increased complexity of planning, optimising and operating future HetNets, self-organising methods commonly referred to as SON are now being proposed to automate many of the manual activities associated with network operation.

The following chapters explore a number of techniques that address both the macrocell capacity challenge as well as the use of SON for macrocell and HetNet planning and optimisation and show through both simulations and field trials that significant performance benefits can be obtained through the techniques proposed within this thesis.

Chapter 3
Coordinated Dynamic Antenna Tilting & Scheduling in a Macrocellular 3G/WCDMA and 4G/LTE Network

This chapter explores the benefits of coordinated dynamic antenna tilting and scheduling outlined in Section 2.2.2.3 of Chapter 2 as a potential macrocell SON capacity enhancement technique. The chapter begins with an overview of the proposed dynamic antenna titling concept followed by an explanation of the simulation setup used to evaluate the benefits of this novel technique. Simulations undertaken to evaluate the potential benefits of dynamic antenna tilting are presented for ideal hexagonal homogeneous 3G/WCDMA and 4G/LTE networks as well as a real central London 4G/LTE network. Finally, early field trial results using a prototype Quintel dynamic tilt antenna are presented and it is shown that the average user throughput and cell edge throughput gains seen from these field results align very closely to those predicted by the central London simulations.

3.1 Dynamic Antenna Tilting

As was explained in the background chapter MIMO antennas and SON techniques have been the focus of much research in recent years, aimed at improving the spectral efficiency of mobile broadband systems. Traditional SON antenna techniques typically suggest slowly varying electrical tilt changes across multiple cells in order to adapt or optimise to a varying spatial load and distribution of traffic [40, 41, 42]. MIMO techniques on the other hand attempt to optimise spectral efficiency of the individual cell to UE communication links in real time. Traditional SON antenna techniques typically apply tilt to the entire RF channel whereas MIMO maintains a fixed beam or tilt for common/reference channels but exploits spatial multiplexing, diversity and/or beam-forming of the traffic channel(s) [43]. 3GPP R8 and R9 introduce a number of adaptive downlink transmission modes to support a variety of MIMO schemes for both 3G/WCDMA and 4G/LTE.

A popular emerging antenna configuration for 4G/LTE Transmission Mode 7 (TM7) [44], also known as dual-layer beam-forming, is shown in the centre of Figure 3.1 flanked by a traditional cross-polar (X-Polar) antenna on the left and a new type of antenna configuration proposed here on the right. This central antenna configuration is often referred to as a Clustered Linear Array (CLA) with *n* closely spaced X-Polar columns or CLA-*n*X. Typically a 4-port antenna configuration for the base station is proposed (CLA-2X) which would allow for example, two spatial multiplexed layers to be exploited by virtue of two (de-correlated) orthogonal polarisations, or each layer can be steered in azimuthal terms by differential phasing of the signals across each of the pairs of co-polar antenna ports. In such

an antenna configuration, all common channels can be transmitted using one X-Polar array and hence have a fixed azimuth and thus define the cell boundaries, and all traffic channels can be transmitted via adaptive azimuth beam-steering using differential phasing across both arrays. However, because of the need for a side by side antenna array topology, CLA-2X antennas are typically twice the width of a standard X-Polar antenna and can be prohibitively wide (>50cm) at low-band cellular frequencies such as 700-900MHz [45] and are therefore difficult to deploy on macrocell sites because of size, weight, aesthetic and wind loading reasons.

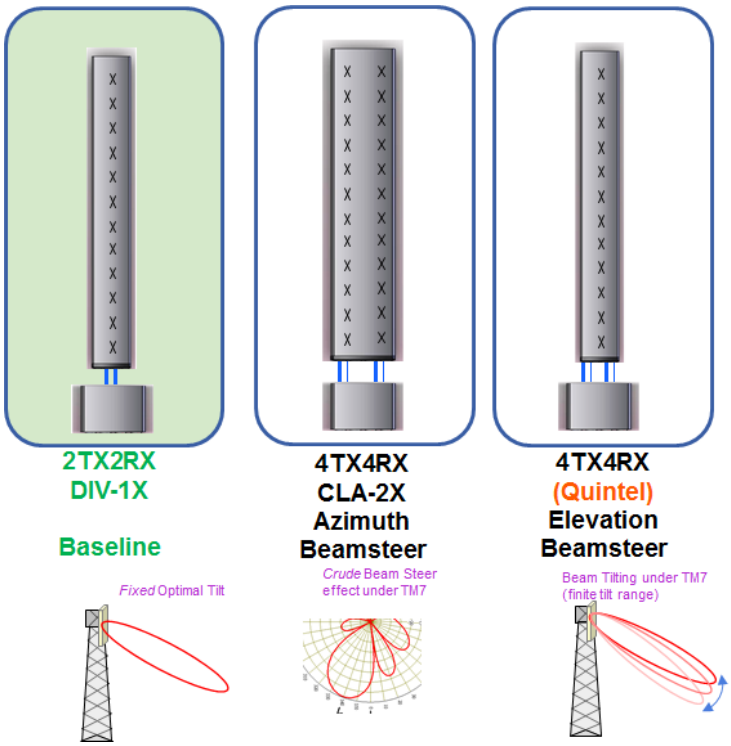

Figure 3.1 Example of cell site cross-polar antenna options and the azimuth and elevation beam-steering possible from each.

Instead an alternative, novel, and completely passive antenna design concept that can also provide 4 ports (i.e. as per the CLA-2X, with 2 pairs of orthogonally polarised ports) but using a single X-Polar antenna column was jointly proposed by the author and Quintel Technologies in 2008 [46]. It is analogous to the CLA-2X arrangement, but instead of beam-forming in azimuth through phase variation across co-polar ports of horizontally separated antenna arrays, the Quintel SONWav four-way Transmit, four-way Receive (4TX4RX) antenna performs beam-forming in the elevation plane. This is perhaps better described as beam-steering or dynamic antenna tilting, with tilts being able to be applied individually to each polarised array (+/-45^{o}) [47].

Using the Quintel SONWav antenna, dynamic tilting can be applied as rapidly as every 1ms TTI and can also be applied independently per code, per frequency and per subcarrier and therefore per individual user. When such dynamic tilting is applied to all channels of the cell it can be viewed as part of a traditional adaptive slow SON implementation, but when applied to traffic channels per TTI it can be viewed as a TM7 dual-layer beam-forming MIMO mode.

Antenna tilts specific to individual users can be calculated through techniques now widely used to geo-locate users in cellular networks such as direction finding on the uplink [48], Assisted Global Positioning System (A-GPS) [49] and Observed Time Difference of Arrival (OTDA) [50] all of which are further discussed in Chapter 5.

The remainder of this chapter considers the system benefits of both the traditional slow SON and MIMO implementations of dynamic antenna tilting using the proposed Quintel SONWav antenna when applied to both 3G/WCDMA and 4G/LTE network technologies.

3.2 Cellular Network Simulator

In order to evaluate dynamic antenna tilting and other advanced cellular network concepts presented in this thesis a bespoke cellular network simulator has been developed solely by the author using the MATLAB technical computing language. The Network Simulator is able to model both ideal hexagonal homogenous as well as heterogeneous network configurations as well as real world network deployments for 3G/WCDMA/HSPA, 4G/LTE and 4G/LTE-Advanced cellular technologies.

This section presents an overview of the version of the Network Simulator used to evaluate dynamic antenna tilting on ideal and real macrocellular network topologies for 3G/HSPA and 4G/LTE. Further enhancements made to the Network Simulator to model other advanced SON concepts studied elsewhere in this thesis are presented in the relevant chapters.

3.2.1 Ideal Homogeneous Network Simulation Setup

In order to create a workbench on which to evaluate combined dynamic tilt and scheduler techniques a macro network simulator was developed initially around a homogeneous hexagonal network geometry (Figure 3.2) based on the network topology described by 3GPP in [51, 52]. Three-sectored sites were assumed for this work, but any number of sectors per site is configurable within the Network Simulator as will be shown in later chapters.

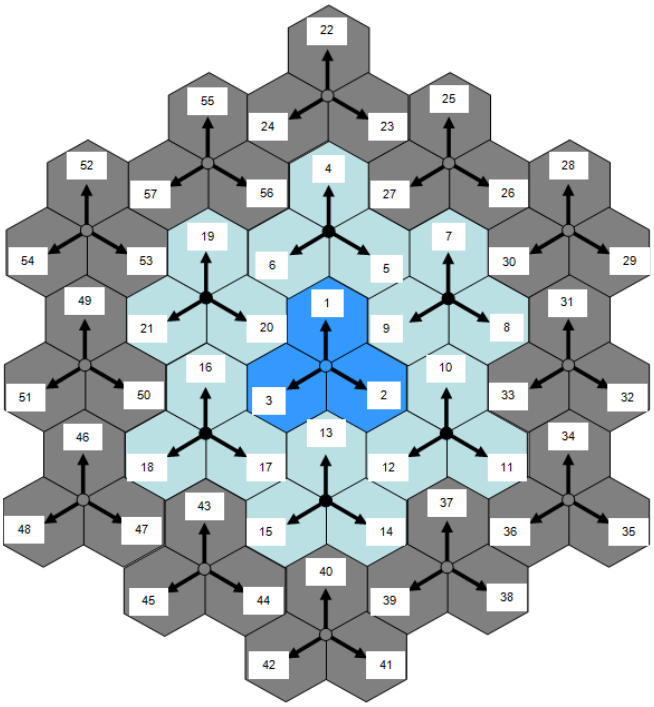

Figure 3.2 Network simulator ideal hexagonal homogeneous network geometry.

The simulated three-tier ideal hexagonal network consisted of 19 sites with 57 cells (3 cells per site). This three-tier approach is typical in cellular network modelling, allowing statistics to be gathered from only the central cells (first tier) or the centre cells plus the second tier of cells to avoid the edge from seen in the third tier of sites. It should be noted however that all cells were active in the simulation and statistics could be gathered from each and every cell in the Network Simulator. The main 3G/HSPA and 4G/LTE ideal network simulation parameters assumed are given below in Table 3.1.

Table 3.1 Ideal HSPA/LTE dynamic antenna tilt network simulation assumptions.

Simulation Assumption	Value
Network sites/sectors per site	19/57 (3 sector per site)
Inter-site Distance	750m
Simulation bin size	10x10m
BTS Height	20m
Sector Azimuths	0^o, 120^o and 240^o
Sector Mechanical Downtilt	0^o - 10^o
Sector Electrical Downtilt	Specified by antenna pattern
Sector Max. TX Power	43dBm
HSPA CPICH Power	33dBm
HSPA Other CCH Power	33dBm
HSPA Downlink Orthogonality	0.6 (Ideal orthogonality = 1)
HSPA HS-DSCH Power	40dBm
LTE Reference Signal Power	15dBm per sub-carrier
LTE DSCH Power	40dBm
LTE Signal RF Bandwidth	20MHz
Operating Frequency	3GPP Band I (2100MHz) [53]
Path Loss Model	COST231 Hata (Dense Urban) [54]
Penetration Loss	20dB
UE Height	1.5m
UE Antenna Gain	0dBi
UE Noise Figure	9dB

3.2.2 Central London Network Simulation Setup

To evaluate rapid dynamic antenna tilt on a realistic network configuration, simulations were also performed using a sample of real site locations from Telefonica UK's central London HSPA+/LTE network. The area of the network that was simulated was a 9km^2 area bounded by the UK Ordnance Survey grid lines E528000, N180000, E531000, N183000 and contained 51 macrocell sites as shown in Figure 3.3. The 51 sites within the central London simulation area vary in height, antenna orientation and tilt, with many sites not following the standard three sector horizontal/azimuthal orientations of 0^o, 120^o and 240^o. Therefore this network provided a much more representative platform on which to evaluate the real benefit of dynamic antenna tilt in addition to the ideal homogeneous networks described in the previous section.

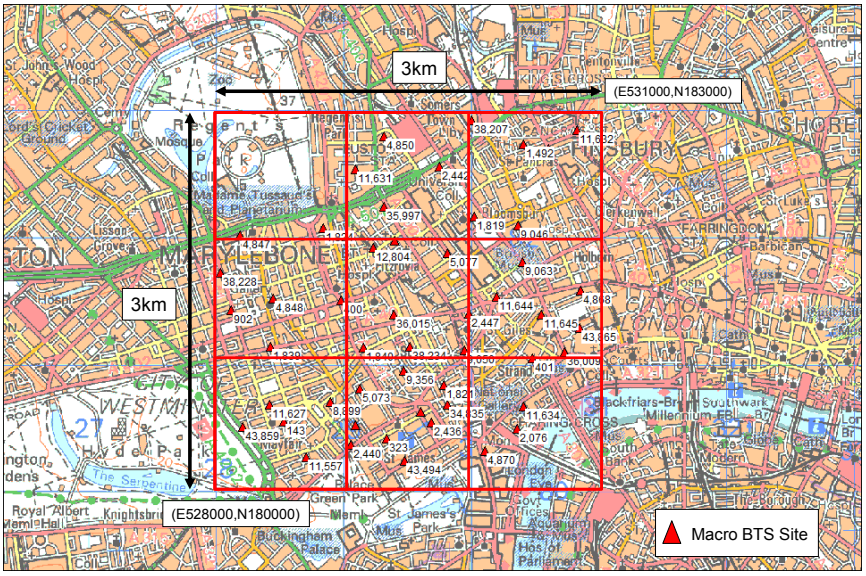

Figure 3.3 Central London macro network simulation area.

The radio propagation path loss model used for the central London simulations was based upon the macrocell model proposed in 3GPP 25.814 [51] and is included in Table 3.2, however rather than use a fixed penetration loss of 20dB as proposed in 3GPP 25.814 a more realistic penetration loss was assumed using land use clutter data made available for central London by Telefonica UK. Cellular traffic was also distributed according to clutter class across the entire simulation area with greater user densities being applied to dense urban and urban areas than for parks and open spaces. Nominal user densities per clutter type are specified in Appendix A - Nominal User Densities per Clutter Category. Examples of the clutter categories and a user distribution of 2000 users based upon this clutter spreading technique are shown in Figure. 3.4.

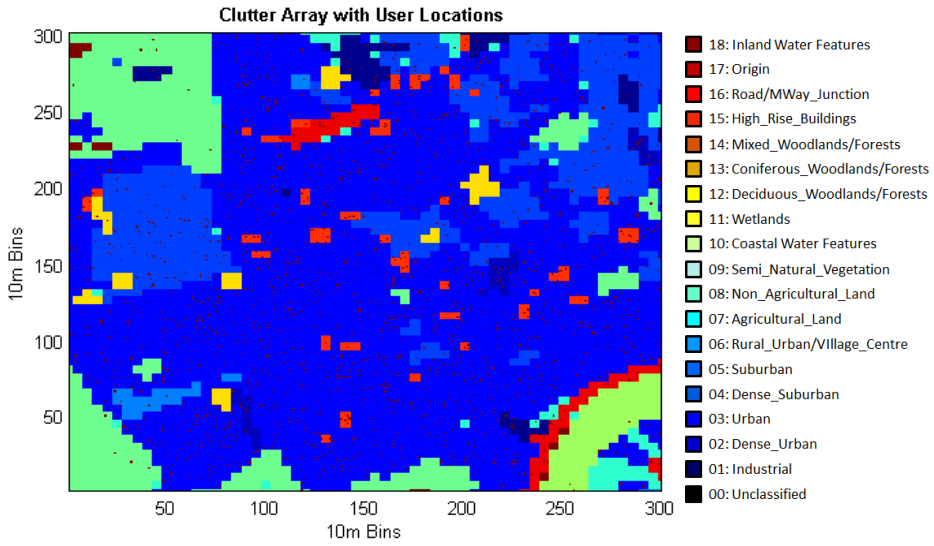

Figure 3.4 Central London clutter and the distribution by clutter class of 2000 users (burgundy pixels).

Whilst all sites/cells were active in the simulations to avoid edge effects statistics were gathered from only the sites and users within the central 2x2km region of the 3x3km simulation area. The main network simulation parameters for the central London 4G/LTE network modelled are given below in Table 3.2. Slow (shadow) fading was also applied to the central London network simulations using a zero mean log-normal variable with a standard deviation of 8dB, on a site by site basis (sectors of the same site had correlated slow fading). An example of the best serving site areas for the central London network following the application of slow fading is shown below in Figure 3.5.

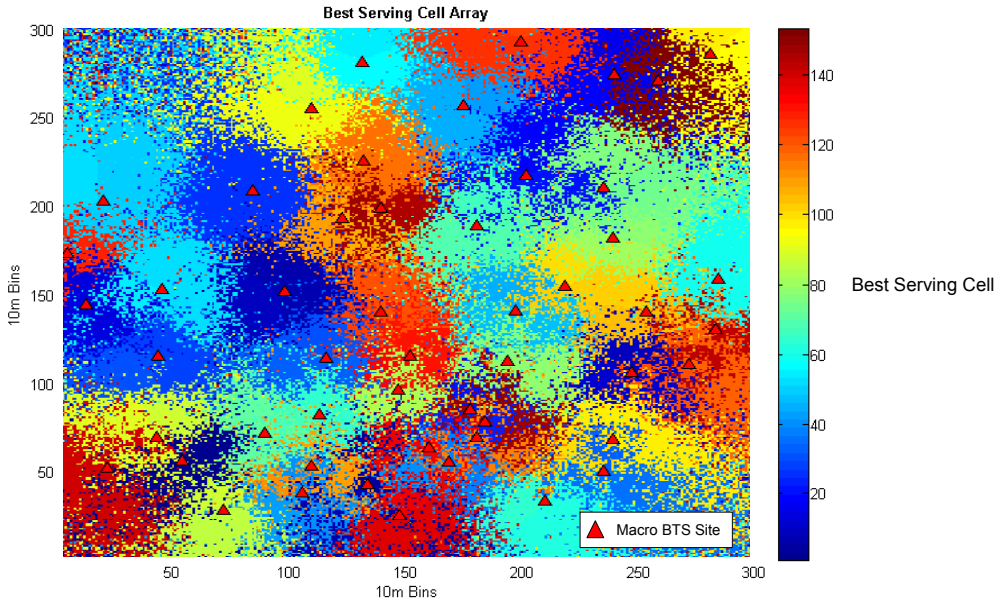

Figure 3.5 Central London best server site areas with shadow fading applied.

Table 3.2 Central London 4G/LTE dynamic tilt network simulation assumptions.

Simulation Assumption	Value
Active users per TTI	2000
Sites/Sectors per Simulation	51/153 (3 Sectors/Site)
Simulation Bin size	10x10m
Cell Site Heights	18 - 52m (Real site heights)
Sector Azimuths	(Real sector azimuths)
Sector Mechanical Downtilt	-5^{o} - $+4^{o}$ (Real sector mechanical tilts)
Sector Horizontal Beamwidth	62^{o}
Sector Electrical Downtilt	0^{o}-10^{o} (Real sector electrical tilts)
Sector Max. TX Power	43dBm
LTE PDSCH Power	40dBm
LTE Signal Bandwidth (BW_{LTE})	20MHz
Operating Frequency	3GPP Band I (2100MHz) [53]
Path Loss Model	PL=128.1 + 37.6$\log_{10}$(d), d in km [51]
Shadow Fading	Sectors of same site correlated, Standard Deviation = 8dB.
Fast Fading	Uncorrelated fast fading per user using ETU3 channel model [55]
UE Height	1.5m
UE Antenna Gain	0dBi
UE Noise Figure	9dB

3.2.3 Antenna Beam Pattern Modelling

The network simulation tool was written to use industry standard PLANET antenna beam patterns [56] and all ideal homogeneous dynamic tilt network simulations were performed using measured Quintel SONWav QA0007 antenna beam patterns - one pattern per electrical antenna tilt applied. The PLANET file format specifies the antenna pattern using two dimensional (2D) horizontal and vertical cross sections of the three dimensional (3D) antenna radiation pattern. Example 2D beam pattern plots for the QA0007 antenna are given below in Figure 3.6. An example of a PLANET antenna pattern file given in Appendix B.

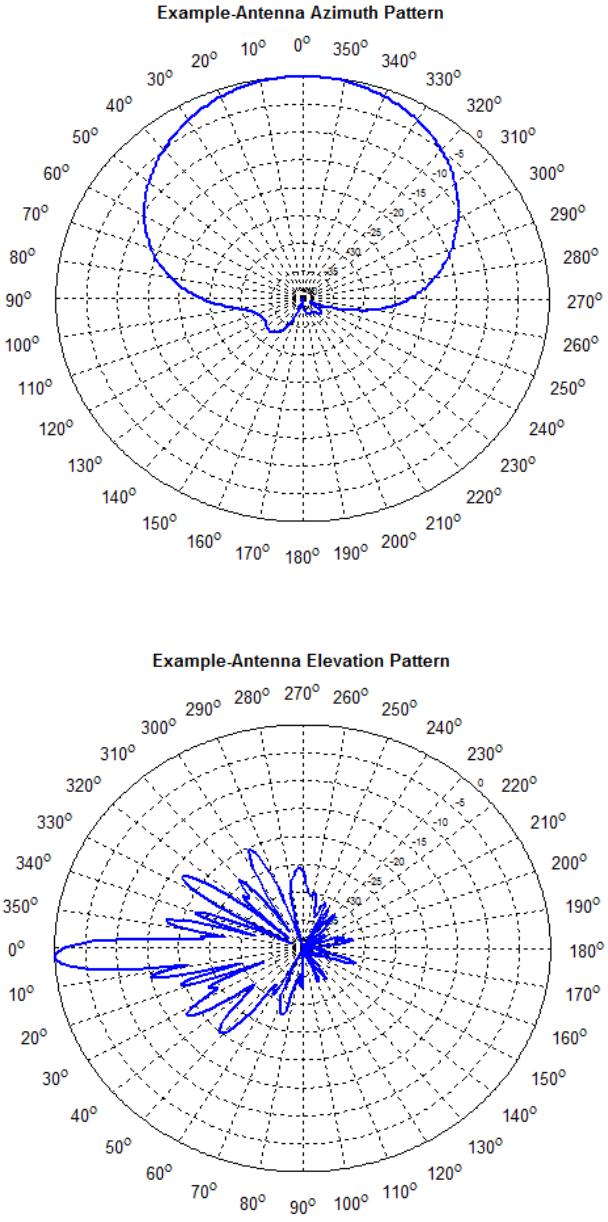

Figure 3.6 QA0007 2D horizontal and vertical antenna radiation patterns for the 2° electrical tilt case showing gain relative to boresight.

All other macrocell antenna patterns used for the remaining research presented in this thesis for both ideal homogeneous and real network simulations were generated using the method proposed by 3GPP in [51]. The 3GPP method uses the following equations to generate the horizontal, $A_H(\varphi)$ and vertical, $A_V(\theta)$ antenna radiation patterns.

$$A_H(\varphi) = -\min\left[12\left(\frac{\varphi}{\varphi_{3dB}}\right)^2, A_m\right] \tag{3.1}$$

$$A_V(\theta) = -\min\left[12\left(\frac{\theta-\theta_{etilt}}{\theta_{3dB}}\right)^2, SLA_v\right] \tag{3.2}$$

where

φ	is the horizontal bearing from the antenna's boresight
φ_{3dB}	is the horizontal 3dB beam width of the antenna
A_m	is the front-to-back attenuation (25dB)
θ	is the vertical bearing from the antenna's boresight
θ_{3dB}	is the vertical 3dB beam width of the antenna
SLA_v	is the side lobe attenuation (20dB)
θ_{etilt}	is the electrical antenna downtilt

As explained earlier the horizontal and vertical antenna patterns generated by the above equations or read from a PLANET antenna file actually represent two perpendicular cross sections of the 3D antenna pattern and therefore to make use of these patterns in a simulation tool or commercial radio planning tool, a 3D antenna pattern must be regenerated from these two perpendicular cross sections. For the purposes of the simulations presented in this thesis the regeneration method also presented in [51] has been assumed, however other techniques are possible such as the method proposed in [57]. The proposed 3GPP method of 3D antenna pattern regeneration is given by the following equation

$$A(\varphi,\theta) = -\min\{-[A_H(\varphi) + A_V(\theta)], A_m\} \tag{3.3}$$

where

$A(\varphi,\theta)$ is the antenna gain at a point with a horizontal bearing from the antenna of φ and a vertical bearing from the antenna of θ.

A_H, A_V and A_m are the horizontal, vertical and front-to-back attenuations previously defined in (3.1) & (3.2).

Two views of the same 3D antenna pattern generated by the 3GPP 25.814 method for the QA0007 beam pattern with a 2^o electrical tilt applied are given below in Figure 3.7.

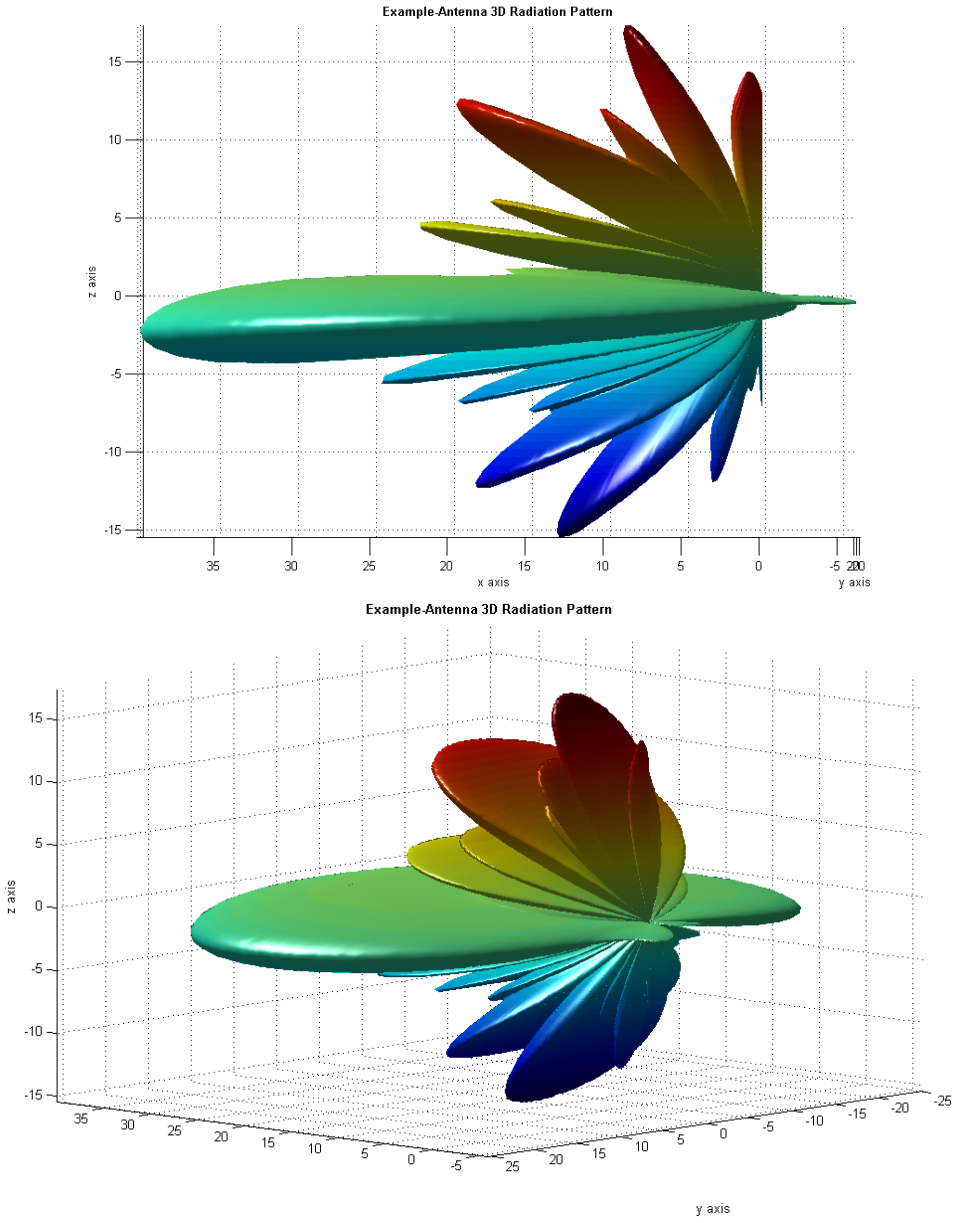

Figure 3.7 Example of a generated QA0007 3D antenna radiation pattern.

3.2.4 Downlink Shared Channel Throughput Modelling

According to Shannon [58] channel capacity C in bps is given by

$$C = BW \log_2\left(1 + \frac{S}{N}\right) \tag{3.4}$$

where

BW	is the bandwidth available in Hz
S	is the received signal power in Watts
N	is the noise power in Watts

Simulation studies by Nokia [59] suggest that the performance of 3G/HSDPA using 15 channelisation codes in the downlink is within 2dB of the Shannon limit, the shortfall is claimed to be mainly due to decoder limitations and receiver estimation inaccuracies. Ericsson also propose a similar relationship between 3G/HSPDA downlink throughput and Shannon's Equation (3.4) and propose an equation in [60] which quantifies the relationship between the High Speed Downlink Shared Channel (HS-DSCH) bit rate, $R_{HS\text{-}DSCH}$ and the HS-DSCH signal to noise ratio, $C/I_{HS\text{-}DSCH}$ as

$$R_{HS-DSCH}[Mbps] = BW_{WCDMA} \cdot \begin{cases} 0, & C/I_{HS-DSCH} < 10^{-1.4} \\ \log_2\left(1 + \dfrac{C/I_{HS-DSCH}}{2}\right), & C/I_{HS-DSCH} \geq 10^{-1.4} \end{cases} \tag{3.5}$$

where BW_{WCDMA} is the WCDMA transmission bandwidth. Given LTE's more spectrally efficient air interface the relationship between the LTE Physical Downlink Shared Channel (LTE-PDSCH) bit rate $R_{LTE\text{-}DSCH}$ and the LTE PDSCH's C/I has been assumed as

$$R_{LTE-PDSCH}\ [Mbps] = BW_{LTE} \cdot \begin{cases} 0, & C/I_{LTE-PDSCH} < 10^{-1.4} \\ \log_2\left(1 + \dfrac{C/I_{LTE-PDSCH}}{1.5}\right), & C/I_{LTE-PDSCH} \geq 10^{-1.4} \end{cases} \tag{3.6}$$

where BW_{LTE} is the LTE transmission bandwidth. Typical 3G/HSDPA category 10 UEs and 4G/LTE category 3 UEs were assumed in all simulations resulting in a theoretical maximum HS-DSCH and LTE-PDSCH throughputs of 14.4Mbps and 100Mbps respectively. Applying this maximum bit rate capping to equations (3.5) and (3.6) results in the 3G/HSPA and 4G/LTE throughput performance curves shown in Figure 3.8 and these performance curves have been used for all the simulations performed throughout this thesis.

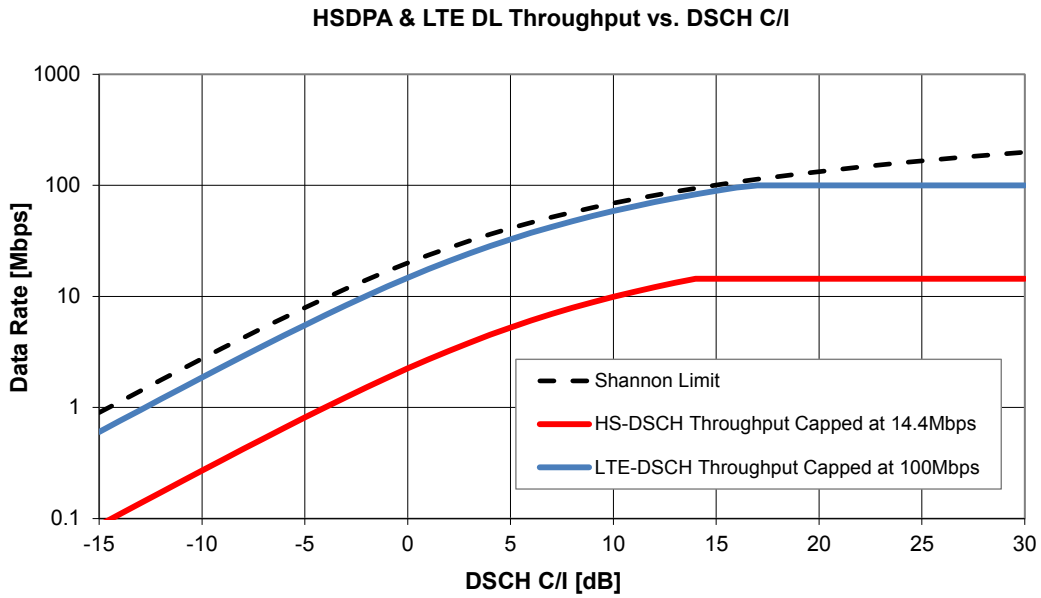

Figure 3.8 HS-DSCH & LTE-DSCH performance vs. DSCH C/I

3.2.5 Monte Carlo Simulation Approach for the Ideal Hexagonal Homogeneous Network Simulations

The Network Simulator used a Monte Carlo simulation approach to evaluate the benefits of dynamic antenna tilting for both the ideal homogeneous and real network simulations. The Monte Carlo simulation for the ideal homogeneous 3G/HSPA network simulations can be summarised by the following steps;

1. Randomly distribute users – single/multiple users per cell (see following sections).
2. Calculate coverage arrays and gather cell and user statistics.
3. Make network changes (antenna tilts eqn. (3.7), & scheduler decisions).
4. Calculate new coverage arrays and gather new cell and user statistics and compare to original statistics and record results.
5. Repeat steps 1-4 to allow the results to converge.

3.2.6 Monte Carlo Simulation Approach for 4G/LTE Central London Network Simulations

The Monte Carlo simulations performed for the central London 4G/LTE network can be summarised by the following steps;

1. Calculate the 4G/LTE network coverage arrays.
2. Randomly distribute users based on clutter data – multiple users per cell (2,000 users across whole simulation area in this case).

3. Cell specific schedulers individually make decision on which users to schedule in the next scheduler period based on specified scheduler type (Round Robin, Proportional Fair, Maximum C/I – see later Section 3.3.2).
4. Calculate cell and user statistics using the fixed antenna tilts of the original central London sites.
5. Antennas then tilted directly towards scheduled users for each cell as per eqn. (3.7).
6. Calculate new coverage/interference arrays and gather new cell and user statistics and compare to original fixed antenna tilt results calculated in step 4 and record results.
7. Repeat steps 3-6 for a predefined time period (10,000 scheduler periods in this case).
8. Repeat steps 1-7 to allow results to converge.

3.3 Simulation Results

Dynamic antenna tilt network simulations were performed for the ideal homogeneous network for both 3G/HSPA and 4G/LTE technologies and for the central London network for 4G/LTE only.

3.3.1 Ideal Homogeneous 3G/HSPA Results

3.3.1.1 Multiple Active Users per Cell

In order to test the dynamic antenna tilt technique as a traditional slow SON implementation, multiple users were initially distributed across the whole simulation area and the network was allowed to optimise its tilts on a cell by cell basis as required to provide the best service the multiple users within each cell. The initial tilt algorithm assumed simply attempted to point the antenna's main vertical beam at the location of the users within the cell. If there was a single user in the cell then the antenna would be downtilted to point directly at the user. If there was more than one user in the cell, then the antenna would be downtilted to point at the user furthest from the cell site in order to provide a level of fairness to the cell edge users. The algorithm for calculating cell *n*'s optimum tilt *cell(n).opt_tilt* is given below as

$$cell(n).opt\_tilt=min(max(round(min(user(1).tilt, user(2).tilt \ldots. user(u).tilt)),2),7) \quad (3.7)$$

where

u	is the user index
$user(u).tilt$	is the downtilt towards user u.

The restriction of the antenna tilt between 2^o and 7^o was because the Quintel QA0007 prototype antenna was physically limited to integer tilts within the range $2\text{-}7^o$. Effectively the tilt algorithm (3.7) attempts to maximise the cell's antenna tilt and was therefore given the name *Max_Tilt*. Only cells containing users were tilted, otherwise cells with no users active had their tilts left unchanged. Maximising the downtilt towards each active user of the cell provides the following benefits;

- Maximises the user's wanted signal in this case Received Signal Code Power (RSCP) and the received HS-DSCH power.
- Minimises downlink interference to the surrounding cells.
- Reduces the uplink path loss which in turn reduces uplink interference to serving and surrounding cells and increases UE battery life.
- Improves the cell edge performance.

Snapshots of one iteration of a Monte Carlo run using the *Max_Tilt* algorithm is shown below in Figure 3.9, with the initial best server plot on the left and the optimised best server plot on the right following changes to the cells' downtilts. The different best serving cells are shown as different colours and the active user locations are shown in the figure as yellow pixels. The effect of optimising the tilts towards the users can be seen by the slight changes in the shape of the best server areas of some of the cells in the right hand figure.

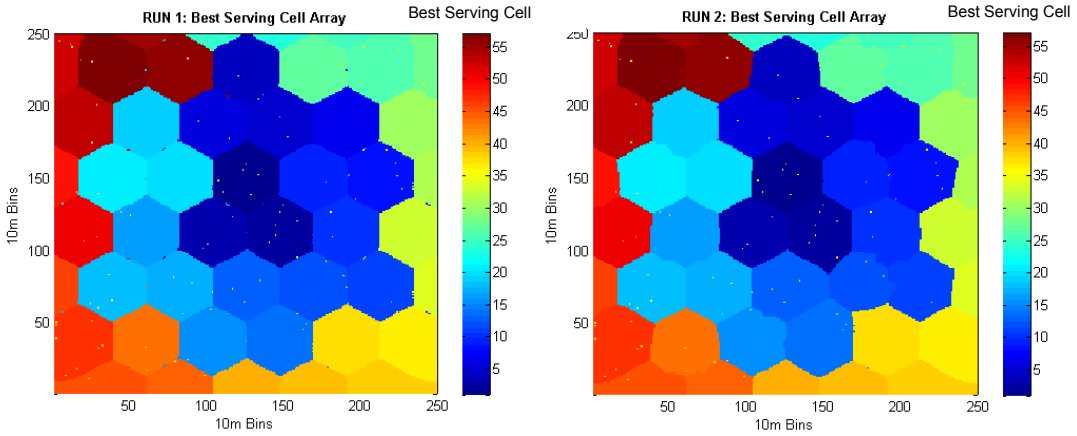

Figure 3.9 100 users distributed randomly across the simulation area, users shown as yellow dots on top of best server plots. Left – original, right – optimised tilts using the *Max_Tilt* algorithm.

The results of the simulation run for the multiple user case are given in Table 3.3 showing a gain of 19.87% (2.71Mbps to 3.25Mbps) in the average HSDPA throughput per user over the fixed tilt case. While this initial run appears to provide promising results, the problem with the traditional slow SON approach presented here was that the antenna tilts were affecting all channels of the site (common, dedicated and shared). Therefore implementing such an approach in practice whilst maximising active users' downlink throughput could also led to reduced Common CHannel (CCH) coverage and outage for non-active users. This limitation is addressed by applying rapid antenna tilting to only the traffic channels as explained in the following sections.

Table 3.3 Results for 100 users randomly distributed across the entire simulation area.

Run	1
No. Users	100
User Distribution	Random
Initial Tilt (Degs.)	2
Original Av. HS-DSCH TP. (Mbps)	2.71
Tilt Algorithm	Max_Tilt
Monte Carlo Snap Shots	1000
Avr. RSCP Gain (dB)	1.33
Avr. Ec/Io Gain (dB)	0.36
Avr. HS-DSCH C/I Gain (dB)	0.98
Avr. HS-DSCH TP Gain (Mbps)	0.54
Avr. HS-DSCH TP Gain (%)	19.87%

3.3.1.2 Single Instantaneous Scheduled User per Cell

Although the multiple users per cell case results were promising, a more realistic HSPA scenario is now consider. Typically vendor scheduling limitations result in only 1-3 active HSPA users per cell in each scheduling period/TTI. If 5 codes are allocated for the HS-DSCH and there is no code multiplexing then there will be zero or one active HSPA user per cell in each scheduling period. Even if 10 or 15 codes are allocated to the HS-DSCH, vendors may still choose to schedule a single user per TTI to reduce scheduler complexity, BTS processor load, common channel load and intra-cell interference on the downlink.

Therefore based on the assumption of a single active user per cell per TTI the Network Simulator was further enhanced to allow the random distribution of one active user per cell across the entire simulation area (equating to 100% HSDPA utilisation per cell – data to send in each scheduling period – sometimes termed full buffer in 3GPP simulations). Further Monte Carlo simulations runs were then performed using the *Max_Tilt* algorithm for this single user per cell per TTI case and the results are given in Table 3.4.

Table 3.4 Dynamic antenna tilt results for a single active user per cell. Initial antenna tilts = 2^o & 5^o.

Run	2	3
No. Users	1 user per cell	1 user per cell
User Distribution	Random Across Cell	Random Across Cell
Initial Tilt (Degs.)	2	5
Original Av. HS-DSCH TP. (Mbps)	2.72	3.93
Tilt Algorithm	Max_Tilt	Max_Tilt
Monte Carlo Snap Shots	5000	5000
Avr. RSCP Gain (dB)	3.01	0.80
Avr. Ec/Io Gain (dB)	0.67	0.17
Avr. HS-DSCH C/I Gain (dB)	1.92	0.40
Avr. HS-DSCH TP Gain (Mbps)	1.10	0.20
Avr. HS-DSCH TP Gain (%)	40.54%	5.02%

Again on first appearance the results for the single active user per cell case appear very encouraging with a 3dB reduction in path loss (3dB increase in RSCP) and a 40.54% increase in average HS-DSCH throughput. However upon further investigation it became clear that the main reason for the large gains was due to the fact that the initial antenna electrical downtilt of 2^o was far from ideal. The tilt to the cell edge at 500m (Inter Site Distance (ISD) = 750m) with a BTS height of 20m is around 2.3^o and therefore with a 2^o tilt the main beam hits the ground beyond the cell edge and causes unnecessary interference to the surrounding cells. Therefore a further simulation exercise was undertaken to ascertain the most optimal fixed tilts based on RSCP and Ec/Io metrics and this resulted in a best all round fixed tilt of 5^o. Also shown in Table 3.4 are the results for the case when the initial tilt was optimal at 5^o and clearly it can be seen that a much lower gain of 5.02% in average user throughput was obtained for this optimised initial tilt. Whilst this result suggested that the worst case throughput/capacity gain achieved by dynamic tilt and the *Max_Tilt* algorithm was around 5% for a perfectly optimised network, typical sector throughput/capacity gains using the tilt per single users per TTI method in a deployed network are expected to be between the 5-40% range assuming that in practice perfect tilt will not be applied to each and every sector of the network for each and every users.

Another way to visualise the performance improvement provided by the dynamic antenna tilt concept is to plot throughput before and after tilting for each user versus the distance between the user and the cell site across multiple simulation runs. Gathering data from across just the main horizontal beam (+/-30^o either side of the antenna's horizontal boresight) of the antenna results in the graphs presented in Figures 3.10 & 3.11.

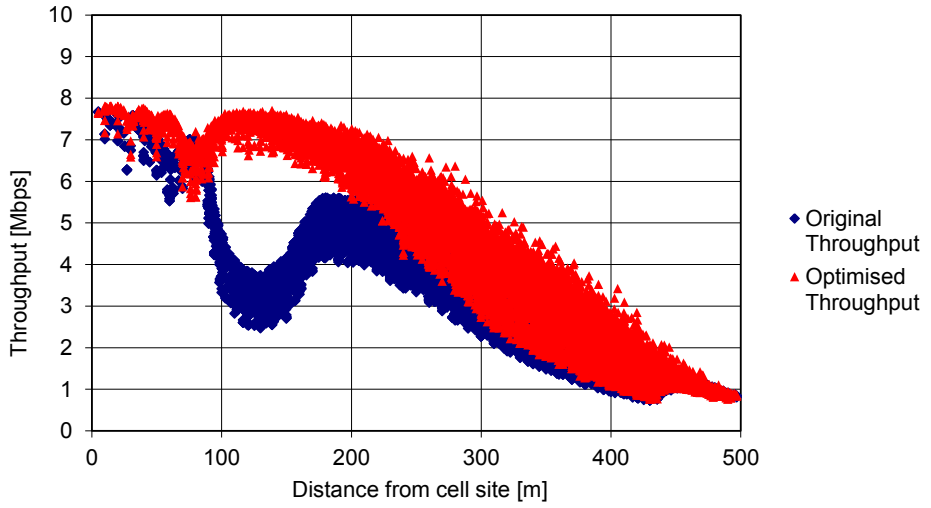

Figure 3.10 User throughput vs. distance plot. Initial antenna electrical tilt = 2°.

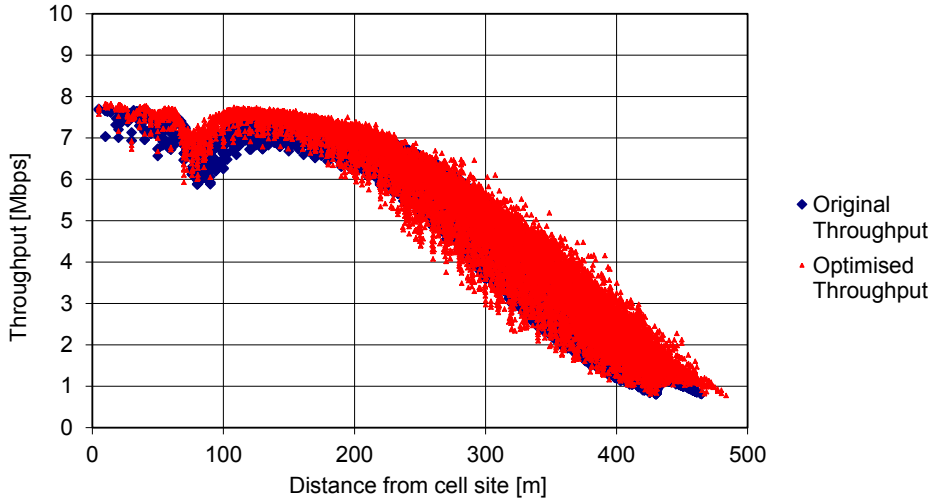

Figure 3.11 User throughput vs. distance plot. Initial antenna electrical tilt = 5°.

3.3.1.3 Fixed Common Channel Tilts & Dynamic HS-DSCH Tilts

Up until now all previous 3G/HSPA simulations presented have assumed the dynamic antenna tilt is applied to all of the cell's physical channels. However as explained earlier using the Quintel SONWav antenna it is also possible to separately tilt the dedicated and common/reference channels from the same BTS realising a MIMO beam-forming implementation on the dedicated and/or shared channels. For example a fixed tilt could be applied to the common and R99 channels on one antenna polarisation (+45°) and a dynamic tilt could be applied to the HS-DSCH on a second antenna polarisation (-45°) (Figure 3.12). This would be the preferred approach with a 3G/WCDMA system in order to maintain a consistent cell footprint/reference for common channels for cell selection and mobility/handover purposes.

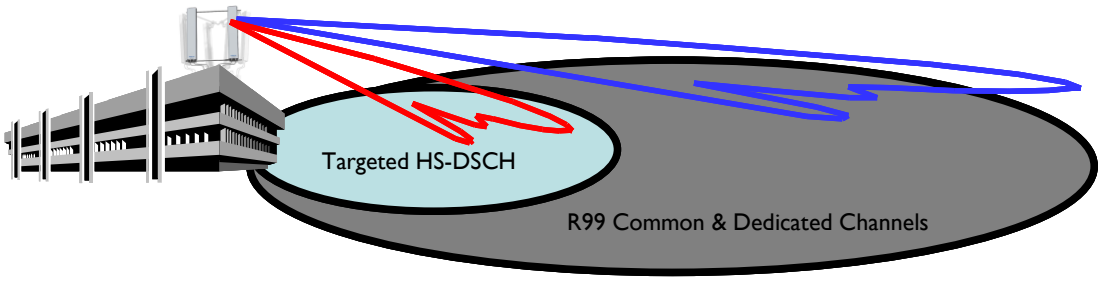

Figure 3.12 Separate tilting of 3G/WCDMA R99 and HS-DSCH channels.

Further enhancements were made to the simulator to model the ability to separately tilt the R99 common and dedicated channels from the HS-DSCH. The modified simulator was then used to perform further Monte Carlo simulation runs to quantify the user performance improvement across the cell with this more practical technique. Shown in Figure 3.13 is a throughput versus distance plot showing the performance of the separate HS-DSCH tilt approach over the original optimal 5° fixed tilt performance. From the figure it can be clearly seen that a much greater throughput is possible closer to the cell as the HS-DSCH can be tilted independently from the CCH/R99 channels hence maximising the HS-DSCH wanted signal, HS-DSCH C/I, and throughput. Also there is still a significant improvement in cell edge throughput compared to the fixed tilt because of the reduction in interference from the surrounding cells.

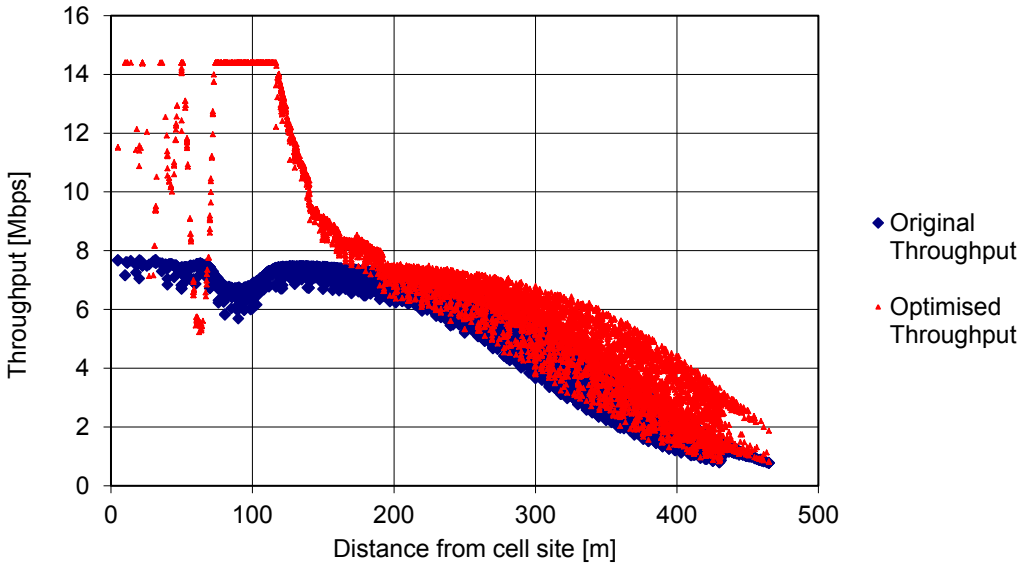

Figure 3.13 Throughput vs. distance plots for fixed tilt case and for case with dynamic tilts applied only to HS-DSCH. Initial mechanical/electrical tilt = 3/2°.

Based upon these modifications simulation runs were performed to assess the overall performance improvement of the separate HS-DSCH tilt approach for various initial antenna tilts. The results are shown in Table 3.5 and show a significant cell throughput gain of 89.28% in the case of an un-optimised network (initial electrical tilt = 2^o) but still a modest gain of 22.94% for the case of an optimised network (combined initial mechanical/electrical downtilt = 5^o). As expected in both cases the RSCP remains unchanged since the tilt applied to the common channels remains fixed in all cases.

The results suggest that significant performance gains are possible by applying a dynamic tilt to just the HS-DSCH even for the optimised network case.

Table 3.5 HS-DSCH dynamic tilting results for single active users per cell. Initial antenna mechanical/electrical tilts = $0/2^o$, $0/5^o$,$0/7^o$ and $3/2^o$. *Max_Tilt* tilt algorithm

Run	32	33	34	35
No. Users	1 user per cell	1 user per cell	1 user per cell	1 user per cell
User Distribution	Random	Random	Random	Random
Initial Tilt (Degs.)	0M+2E	0M+5E	0M+7E	3M+2E
Original Av. HS-DSCH TP. (Mbps)	2.71	3.93	4.44	3.94
Tilt Algorithm	Max_Tilt	Max_Tilt	Max_Tilt	Max_Tilt
Monte Carlo Snap Shots	500	500	500	500
Avr. RSCP Gain (dB)	0.00	0.00	0.00	0.00
Avr. Ec/Io Gain (dB)	-1.93	-0.52	-2.39	-0.70
Avr. HS-DSCH C/I Gain (dB)	3.49	0.57	0.42	1.25
Avr. HS-DSCH TP Gain (Mbps)	2.42	0.37	0.21	0.90
Avr. HS-DSCH TP Gain (%)	89.28%	9.49%	4.82%	22.94%

Two modified tilt algorithms were also considered, both based on the *Max_Tilt* algorithm. The first named *Round_Up* simply took the value calculated by the *Max_Tilt* algorithm and rounded up to the next integer tilt rather than rounding to the nearest integer tilt as in the case of the *Max_Tilt* algorithm (it should be noted that typically only integer tilts are implemented in electrically tiltable antennas). The second modified algorithm named *Round+1* took the value calculated by the *Max_Tilt* algorithm and increase this by 1^o, effectively further over tilting the antenna towards the user(s) than the *Round_Up* algorithm.

The idea here was that since the vertical beam pattern of the antenna rolls off slowly across the vertical plane close to the antenna's main boresight beam, but more rapidly at higher tilt angles (see Figure 3.6) then these two algorithms would lead to very little reduction in the wanted signal at the user's location but would give a greater reduction to the inter-cell interference generated by the cell towards the surrounding cells. The results using the modified tilt algorithms are shown below in Tables 3.6 and 3.7. As can be seen over tilting the antennas gives a marginal improvement with the *Round+1* algorithm giving the better results overall.

Table 3.6 HS-DSCH dynamic tilting results for single active users per cell. Initial antenna mechanical/electrical tilts = 0/2°, 0/5°,0/7° and 3/2°. *Round_Up* tilt algorithm.

Run	36	37	38	39
No. Users	1 user per cell	1 user per cell	1 user per cell	1 user per cell
User Distribution	Random	Random	Random	Random
Initial Tilt (Degs.)	0M+2E	0M+5E	0M+7E	3M+2E
Original Av. HS-DSCH TP. (Mbps)	2.71	3.93	4.44	3.94
Tilt Algorithm	Round Up	Round Up	Round Up	Round Up
Monte Carlo Snap Shots	500	500	500	500
Avr. RSCP Gain (dB)	0.00	0.00	0.00	0.00
Avr. Ec/Io Gain (dB)	-1.86	-0.50	-2.32	-0.66
Avr. HS-DSCH C/I Gain (dB)	3.57	0.72	0.64	1.29
Avr. HS-DSCH TP Gain (Mbps)	2.44	0.46	0.36	0.92
Avr. HS-DSCH TP Gain (%)	90.13%	11.71%	8.05%	23.28%

Table 3.7 HS-DSCH dynamic tilting results for single active users per cell. Initial antenna mechanical/electrical tilts = 0/2°, 0/5°,0/7° and 3/2°. *Round+1* tilt algorithm.

Run	40	41	42	43
No. Users	1 user per cell	1 user per cell	1 user per cell	1 user per cell
User Distribution	Random	Random	Random	Random
Initial Tilt (Degs.)	0M+2E	0M+5E	0M+7E	3M+2E
Original Av. HS-DSCH TP. (Mbps)	2.71	3.94	4.46	3.94
Tilt Algorithm	Round+1	Round+1	Round+1	Round+1
Monte Carlo Snap Shots	500	500	500	500
Avr. RSCP Gain (dB)	0.00	0.00	0.00	0.00
Avr. Ec/Io Gain (dB)	-1.77	-0.33	-2.13	-0.64
Avr. HS-DSCH C/I Gain (dB)	3.64	0.75	0.73	1.34
Avr. HS-DSCH TP Gain (Mbps)	2.47	0.46	0.42	0.93
Avr. HS-DSCH TP Gain (%)	91.39%	11.80%	9.44%	23.59%

3.3.2 Ideal Homogeneous 4G/LTE Network Simulations

The work detailed in the previous section of this chapter has focussed on the overall effect of dynamic antenna tilting on the performance of a 3G/HSPA network by mainly considering user location relative to the cell site and what gains could be achieved by tilting the antenna towards the users and potentially away from other surrounding cells thereby minimising inter-cell interference. The gains were calculated using a Monte Carlo simulation approach with the simulator calculating its results over many user distributions across the cells of the simulation area.

Whilst the approach provided a good approximation of the overall gains of dynamic tilt in an HSPA/LTE network, the approach did not fully model realistic scheduling behaviour seen in most mobile broadband systems when the UE is undergoing multipath fading [61]

(sometimes referred to elsewhere as fast fading or Rayleigh fading). Therefore to more accurately model the benefits of dynamic antenna tilt on a 4G/LTE network the Network Simulator was further enhanced to model multipath fading per user and to incorporate the dynamic tilting of the antenna with more realistic scheduling procedures of a 4G/LTE network.

The main purpose of the scheduler in both 3G/HSPA and 4G/LTE is to efficiently share the cell's uplink/downlink resources amongst the active users of the cell and where possible exploit the time varying channel conditions seen by each user. To do this effectively requires some measure of the channel quality such that users are scheduled when they have favourable channel conditions and such approaches are referred to as channel-dependent scheduling. The three generic schedulers commonly referred to in the literature are Round Robin, Maximum C/I and Proportional/Fair and the Network Simulator was updated to include the ability to model all three generic schedulers. Only the Maximum C/I and Proportional/Fair can be classed as channel-dependent schedulers since they both base their decisions on the instantaneous channel quality.

3.3.2.1 Round Robin Scheduler Implementation

The Round Robin (RR) scheduler is the simplest of the generic scheduling algorithms considered. The RR scheduler allows users to take it in turns to use the shared resources and does not take into account the instantaneous channel conditions when scheduling the users. In order to model the performance of the RR and other schedulers in the network simulation a multipath fading channel model based on the Enhanced Typical Urban 3km/h (ETU3) channel model [55] was added to the Network Simulator to model independent multipath fading per user. Any number of active users per cell can be modelled by the Network Simulator and shown in Figure 3.14 is an example of independent multipath fading for two users within the same cell for a 4G/LTE network simulation run.

Shown in Figure 3.15 is an example of the RR scheduler employed in the Network Simulator in the case of a 4G/LTE cell with two active users. As can be seen the instantaneous channel conditions are not taken into account and the users are scheduled sequentially every scheduling period (one LTE sub frame = 1ms). The benefits of the RR scheduler are its simplicity and that all users within the cell will be granted some resource. The disadvantage of the RR scheduler is that it does not maximise the throughput per user or per cell since the instantaneous channel condition are not exploited by the scheduler.

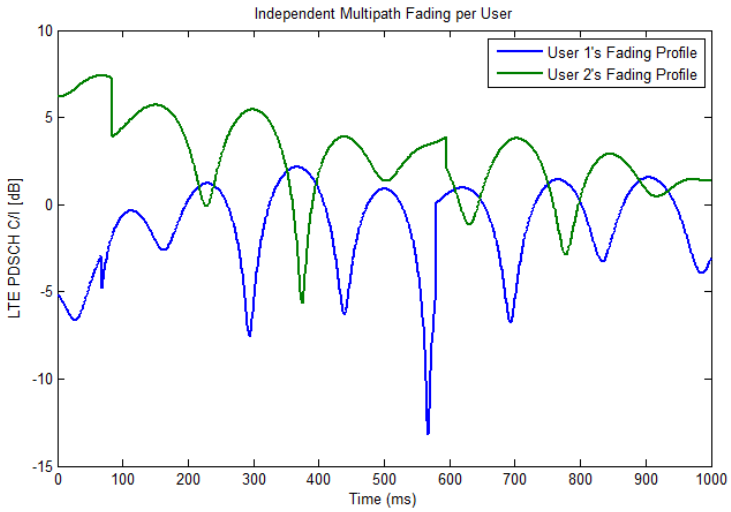

Figure 3.14 Example of independent multipath fading per user for a 4G/LTE network simulation run.

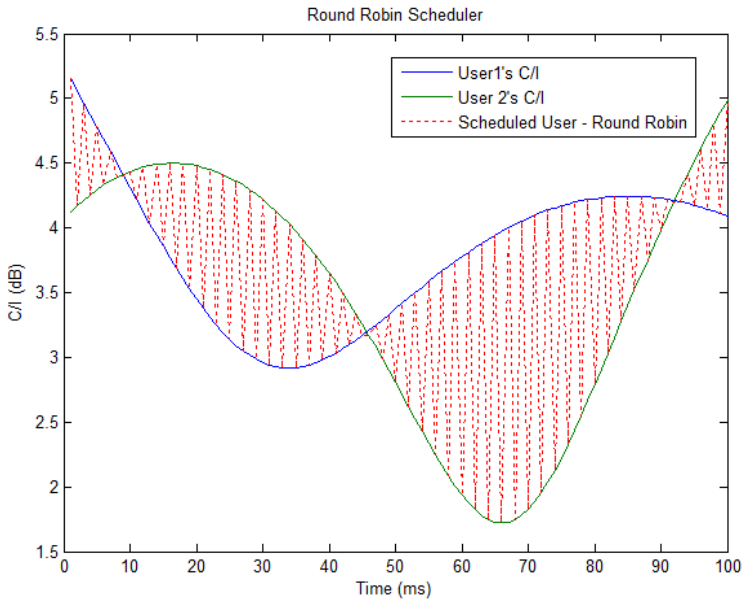

Figure 3.15 Example of Round Robin scheduling with independent multipath fading per user for a 4G/LTE network simulation run.

3.3.2.2 Maximum C/I Scheduler Implementation

The Maximum C/I (Max. C/I) scheduler implemented in the Network Simulator always scheduled the user with the best instantaneous channel conditions. Whilst this approach maximised cell throughput and peak user data rates the drawback was that users with poor channel conditions (e.g. cell edge users) could be starved of resource. Shown in Figure 3.16 is an example of the Max. C/I scheduler employed in the Network Simulator in the case of a 4G/LTE cell with two active users.

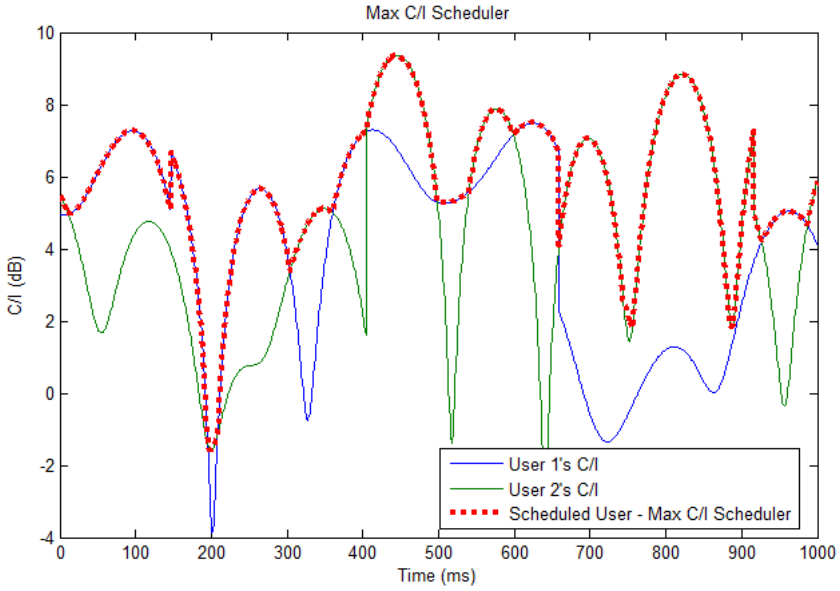

Figure 3.16 Example of Max. C/I scheduling with independent multipath fading per user for a 4G/LTE network simulation run.

3.3.2.3 Proportional/Fair Scheduler Implementation

The third and final generic scheduler incorporated into the Network Simulator was the Proportional Fair (PF) scheduler. The PF scheduler implemented was based on the PF scheduler outlined in [62] and aimed to exploit the instantaneous channel conditions to maximise radio resource utilisation but at the same time keeping a check on all users' underlying average throughputs so that no user was starved of resource if their channel conditions remained poor for a long period of time. To do this the implemented PF scheduler scheduled the user having the highest *PF_factor*, where the *PF_factor* was calculated for each user as

$$PF\_factor_n = \frac{Inst\_Throughput_n}{Avr\_Throughput_n} \tag{3.8}$$

where

$Inst\_Throughput_n$ is the instantaneous throughput that is possible given the current instantaneous channel conditions for user n.

$Avr\_Throughput_n$ is the average throughput experienced by the user n over a pre-defined user throughput averaging period (in this implementation a 1s averaging period was assumed).

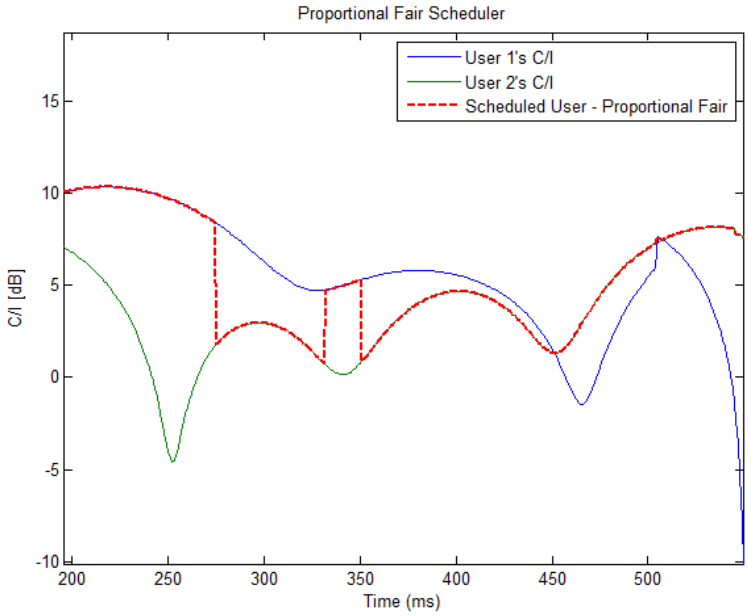

Figure 3.17 Example of Proportional Fair scheduling with independent multipath fading per user for a 4G/LTE network simulation run.

Shown in Figure 3.17 is an example of the PF scheduler employed in the Network Simulator for the case of a 4G/LTE cell with two active users. Perfect channel quality estimation has been assumed for all simulations. As can be seen the PF scheduler will grant resources to the user with the lower C/I when required to maintain that user's average throughput.

3.3.2.4 Ideal Homogeneous 4G/LTE Network Simulation Results

4G/LTE downlink simulations were performed assuming five active users per cell. All active users were constantly consuming data (full buffer implementation) and the *Max_Tilt* algorithm was applied to tilt the LTE PDSCH. A CDF plot of the three schedulers' performance with and without dynamic antenna tilt is shown in Figure 3.18 for the un-optimised network case where the initial mechanical/electrical tilt was 0/2^{o} and shown in Figure 3.19 for the optimised network case where the initial mechanical/electrical tilt was 3/2^{o}. Also shown below in Tables 3.8 and 3.9 are the average user and cell throughputs seen for the three different schedulers combined with dynamic antenna tilt for the two initial mechanical tilts considered. As can be seen from both the graphs and the tables, capacity gains were achieved for all three schedulers considered for both the optimised and un-optimised networks.

The highest user throughput gains were seen for the un-optimised network with gains ranging from 27.1% for the PF scheduler to 36.5% for the RR scheduler. From the CDF curves for the un-optimised network it can be seen that a significant cell edge gain was achieved for the RR (32%) and PF (31%) schedulers but not for the Max C/I. scheduler. The

reason for this is that the Max C/I will always avoid serving cell edge users since they will generally have poor C/I and therefore these users will not see any benefit from the dynamic tilt being applied. Whereas the RR and PF schedulers will always serve cell edge users and therefore these users will experience a dynamic tilt gain.

For the optimised network case much smaller user throughput gains ranging from 4.6% for the RR scheduler to 8.1% for the Max C/I. scheduler were seen since the network tilts are optimised and the interference into the surrounding cells is already greatly reduced. Whilst further tilts maximise the wanted signal they do not reduce the interference as much as was the case for the un-optimised network. This effect is similar to that seen in the 3G/HSPA results presented earlier.

Comparing the results to those presented for the ideal 3G/HSPA network, a much reduced dynamic tilt gain for both the optimised and un-optimised network case is seen due to the inclusion of fast fading and a realistic scheduler in the simulations. However as previously mentioned since a deployed real world network can never be fully optimised for all user distributions, the gains from dynamic antenna tilting for a real network are expected to be closer to the un-optimised rather than the optimised network case presented here and in the following sections this is shown to be the case in reality.

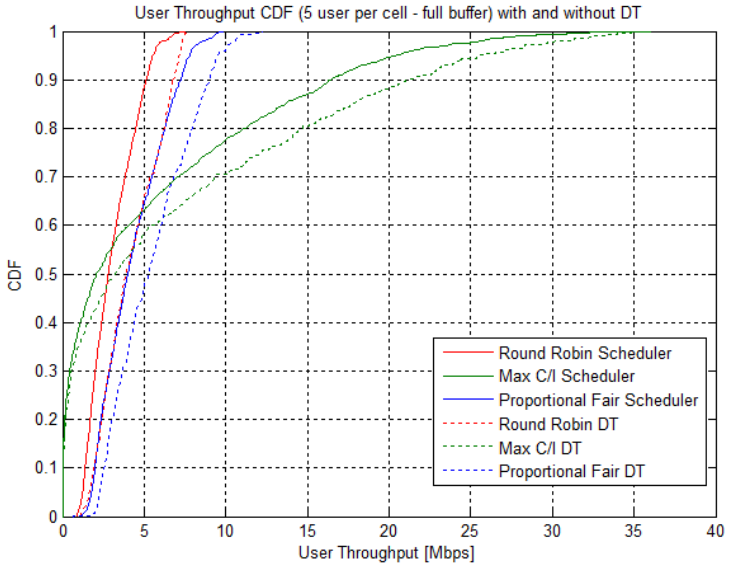

Figure 3.18 CDF of Combined tilt/scheduler LTE user throughput distribution for the three generic schedulers combined with dynamic tilt. Initial mechanical/electrical tilt = 0/2°.

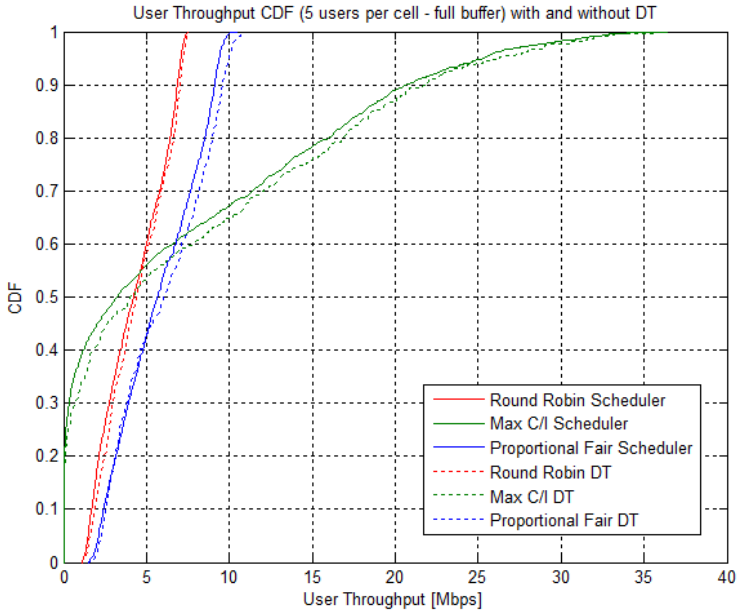

Figure 3.19 CDF of Combined tilt/scheduler LTE user throughput distribution for the three generic schedulers combined with dynamic tilt. Initial mechanical/electrical tilt = 3/2°.

Table 3.8 Combined tilt/scheduler 4G/LTE throughput improvements. Initial mechanical/electrical tilt = 0/2°.

Scheduler	Measure	Throughput [Mbps] no dynamic tilt	Throughput [Mbps] with dynamic tilt	% Gain
Round Robin	Average User Throughput	3.07	4.19	36.5%
	Average Cell Throughput	15.33	20.94	36.5%
Max C/I	Average User Throughput	5.56	7.25	30.3%
	Average Cell Throughput	27.82	36.25	30.3%
Proportional Fair	Average User Throughput	4.33	5.51	27.1%
	Average Cell Throughput	21.67	27.53	27.1%

Table 3.9 Combined tilt/scheduler 4G/LTE throughput improvements. Initial mechanical/electrical tilt = 3/2°.

Scheduler	Measure	Throughput [Mbps] no dynamic tilt	Throughput [Mbps] with dynamic tilt	% Gain
Round Robin	Average User Throughput	4.26	4.46	4.6%
	Average Cell Throughput	21.32	22.29	4.6%
Max C/I	Average User Throughput	7.43	8.03	8.1%
	Average Cell Throughput	37.15	40.14	8.1%
Proportional Fair	Average User Throughput	5.77	6.04	4.7%
	Average Cell Throughput	28.85	30.20	4.7%

3.3.3 Central London 4G/LTE Simulations

In order to assess the gains achieved through dynamic antenna tilting on a realistic network, simulations were performed for the portion of Telefonica UK's central London LTE network described in Section 3.2.2. All sites were simulated with an antenna having 62^{o} horizontal and 7^{o} vertical beamwidth generated using the 3GPP method presented earlier in Section 3.2.3. The fixed antenna tilts were the fixed mechanical and electrical tilts actually applied to the real central London sites. The electrical tilt range was this time allowed to be varied by the antenna tilt optimisation algorithm from 0-10^{o} since Quintel's commercial SONWav antenna will have this larger tilt range. In order to provide the dynamic tilt antenna maximum freedom to optimise the network (uptilt as well as downtilt from the current fixed tilt setting) the initial electrical tilt of the dynamic tilt antenna was set to 5^{o} and the mechanical tilt was set such that the combined mechanical and initial electrical tilt of 5^{o} was equal to the combined mechanical and electrical tilts currently applied to the central London sites.

3.3.3.1 Central London 4G/LTE Dynamic Tilt Simulation Results

Shown in Figure 3.20 are the 4G/LTE downlink PDSCH C/I distributions for the three generic schedulers with and without dynamic antenna tilting applied. As expected tilting the antenna towards the scheduled users in each cell provides a C/I gain, and again the overall gains achieved are dependent on the scheduler type. As expected the Max. C/I scheduler provides the highest C/I for the scheduled users and a median dynamic tilt PDSCH C/I gain of 2.4dB. Since by its nature the Max. C/I scheduler will concentrate on serving close in users with the highest C/I values a much bigger C/I gain for this scheduler is expected since by directing the tilt towards the close-in users not only will this maximise the users' wanted signals it will also minimise the interference into the surrounding cells when compared to the RR and PF schedulers.

The RR scheduler on the other hand does not consider the users' instantaneous C/I in its scheduling decision and independently schedules users in each cell in a sequential fashion. Therefore it will typically allocate resources equally to close-in and far-out users across the cells of the network. Whilst the dynamic tilt PDSCH C/I gain in this case (median gain = 2.0dB) will be due to mainly to the combined scheduler/tilt algorithm maximising the users' wanted signals, because each cell will randomly serve both close-in and cell edge users then some interference reduction to the surrounding cells will also occur contributing to the C/I gain.

The PF scheduler is almost a hybrid between the Max. C/I and RR schedulers in that whilst it tries to make use of the favourable instantaneous channel conditions of each user, it also strives to provide all users with some level of service, even those with unfavourable channel

conditions, many of whom are likely to be towards the cell edge. Therefore whilst a dynamic tilt PDSCH C/I gain for the PF scheduler (median gain = 1.3dB) is seen, it is not as large as that seen for the other two schedulers. This is due to the scheduler spending much of its time trying to deliver service to cell edge users and therefore whilst maximising the wanted signals to these users it does not provide the same amount of interference reduction seen by either the RR and Max. C/I schedulers.

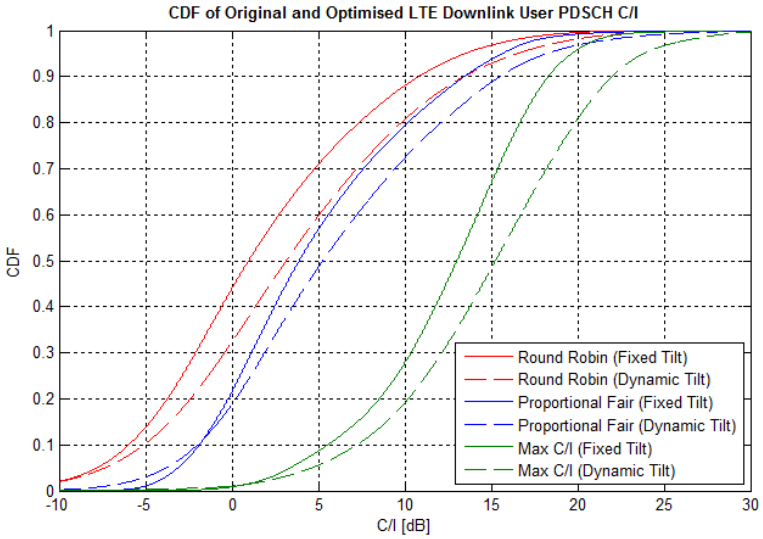

Figure 3.20 Central London user downlink LTE PDSCH C/I distribution for the three generic schedulers with and without dynamic antenna tilt.

The downlink user throughput distributions for the three generic schedulers with and without dynamic tilt are shown in Figure 3.21. Here it is seen that as expected the Max. C/I scheduler only delivers service to those users with a very high C/I and for the central London network starves the majority of users (63%) of downlink resource. That said the dynamic tilt technique still provides some capacity gain when combined with the Max. C/I scheduler, but not as much throughput gain as is seen with the RR or PF schedulers. The reason that the gains in C/I achieved by the Max. C/I scheduler and dynamic tilt do not result in significant throughput gains is because the users served by the Max C/I scheduler already have a very high C/I and an increase in C/I of say 2dB beyond this does not result in as large a relative throughput gain when compared to what a C/I increase of 2dB would provide a user with a very low C/I as per the situation for the RR and PF schedulers' users. In fact in some cases the increase in C/I for the Max C/I scheduler's user is redundant since the UE may already be at or close to its 100Mbps throughput limit (Figure 3.8).

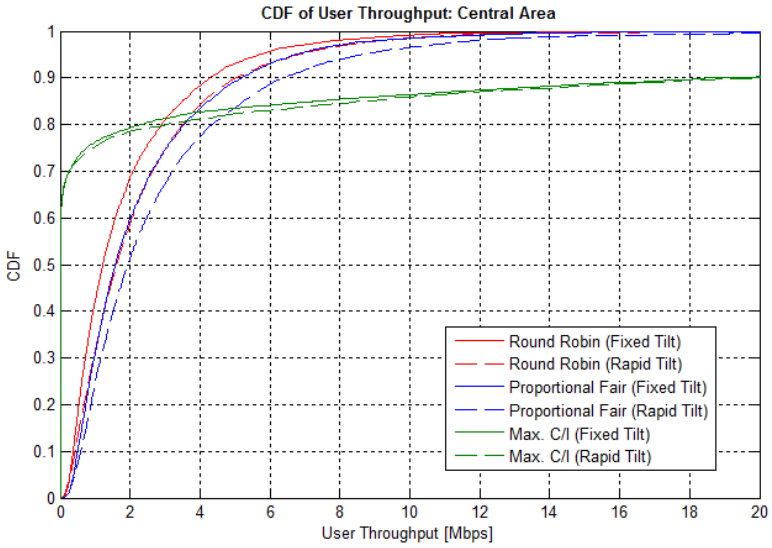

Figure 3.21 Central London downlink user throughput distribution for the three generic schedulers with and without dynamic antenna tilt.

A summary of the capacity gains per user, per cell and across all cells of the central 2x2km area of the network is shown in Table 3.10. As can be seen for the RR and PF schedulers, dynamic tilt provides a user/network capacity gain of around 25% and ties in well with the ideal homogeneous results presented in the previous section for the un-optimised homogeneous network. For the Max. C/I scheduler, a user throughput gain of 8% and a cell/network capacity gain of 11% was observed. This is much lower than was found for the ideal homogeneous network case and is due the greater traffic load per cell (on average 13 users per cell for the central London network compared to the 5 users per cell used for the ideal network case) and the more realistic radio channel environment used in the central London simulations. This resulted in a much lower percentage of users obtaining downlink resource (37%) and also led to the throughput saturation situation for the served users mentioned previously. The reasons for the slight difference in the percentage gains between the mean user and central network throughputs was because the mean users throughput was calculated across the throughput of all users within the central 2x2km area, whereas the central network throughput was calculated across the cells within the 2x2km whose coverage may or may not extend outside the central 2x2km area.

Table 3.10 Central London 4G/LTE simulation results summary table.

Scheduler Type	Measure	Fixed Tilt	Dynamic Tilt	% Gain
Round Robin	Mean User Throughput [Mbps]	1.9	2.3	23%
	Mean Cell Throughput [Mbps]	24.9	31.2	25%
	Central Network Throughput [Gbps]	2.0	2.5	25%
Maximum C/I	Mean User Throughput [Mbps]	5.8	6.3	8%
	Mean Cell Throughput [Mbps]	68.5	76.0	11%
	Central Network Throughput [Gbps]	5.55	6.16	11%
Proportional Fair	Mean User Throughput [Mbps]	2.4	2.9	25%
	Mean Cell Throughput [Mbps]	31.0	39.1	26%
	Central Network Throughput [Gbps]	2.51	3.17	26%

Finally Figure 3.22 shows the average site throughput for the PF scheduler with and without dynamic antenna tilt for all 27 sites of the central 2x2km area. Clearly not all cells benefit equally from the dynamic tilt technique and this is dependent on the suitability of each original cell's fixed antenna tilt to provide service across all of the service area of the cell. However Figure 3.22 does show that even for what is classed as an optimised central London 4G/LTE network, dynamic tilt provides significant cell capacity gains for the majority of sites for a commonly deployed scheduler such as the PF scheduler assumed in this example.

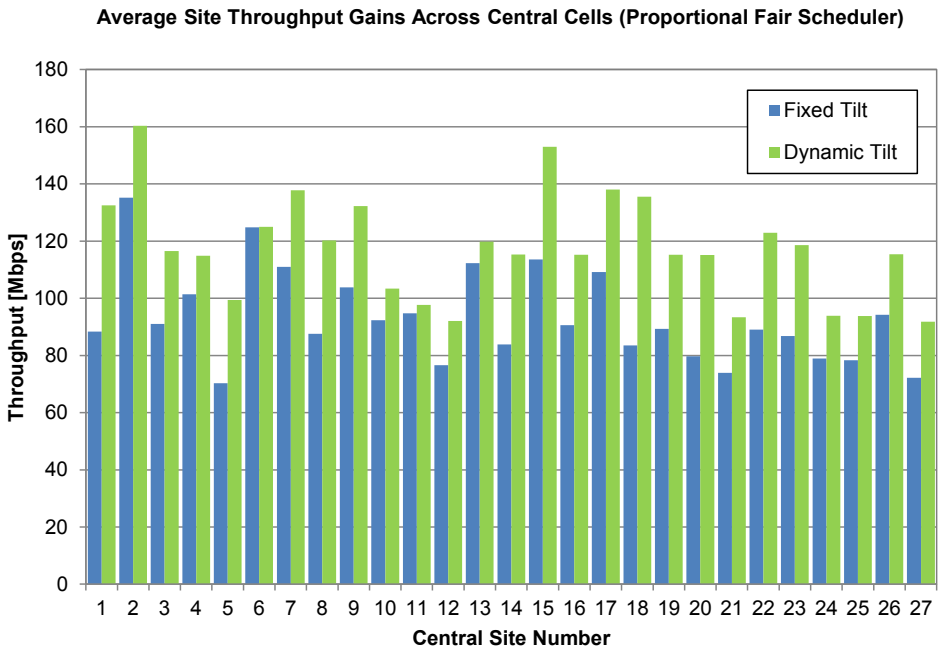

Figure 3.22 Central London individual site throughput gains from dynamic antenna tilt for the 27 sites within the central 2x2km region of the simulation area.

3.4 Dynamic Tilt Initial Field Trial Results

A recent field trial of Quintel's SONWav antennas was completed in February 2013 by a North American mobile operator [63]. Unfortunately the name of the operator cannot be disclosed at this stage for commercial reasons. The trial considered the use of the SONWav antenna for uplink rather than downlink performance improvements since only 4-branch uplink diversity rather than 4-branch downlink diversity radio equipment was available from the RAN vendor chosen for the trial.

Figure 3.23 below illustrates how the SONWav antenna operates in the uplink mode. The figure shows an uplink signal from a UE arriving at the SONWav antenna. The uplink signal can be considered as a plane wave in a macrocell radio channel, which would have a relatively small angular multi-path dispersion in the elevation plane, and as such can be considered as having an approximately linear phase front arriving at the antenna's array of elements with a particular Angle of Arrival (AoA). Considering only one of the two orthogonal slant polarizations of the antenna (+45° or -45° polarization), the uplink signal is collected by each of the individual antenna elements for the slant considered and these are then converted by the antenna distribution network (which in this case can be considered as a vector processing or combining network) into a single pair of signals which have equal amplitude but have a differential phased between them, where the phase difference is a function of the AoA of the UE's signal.

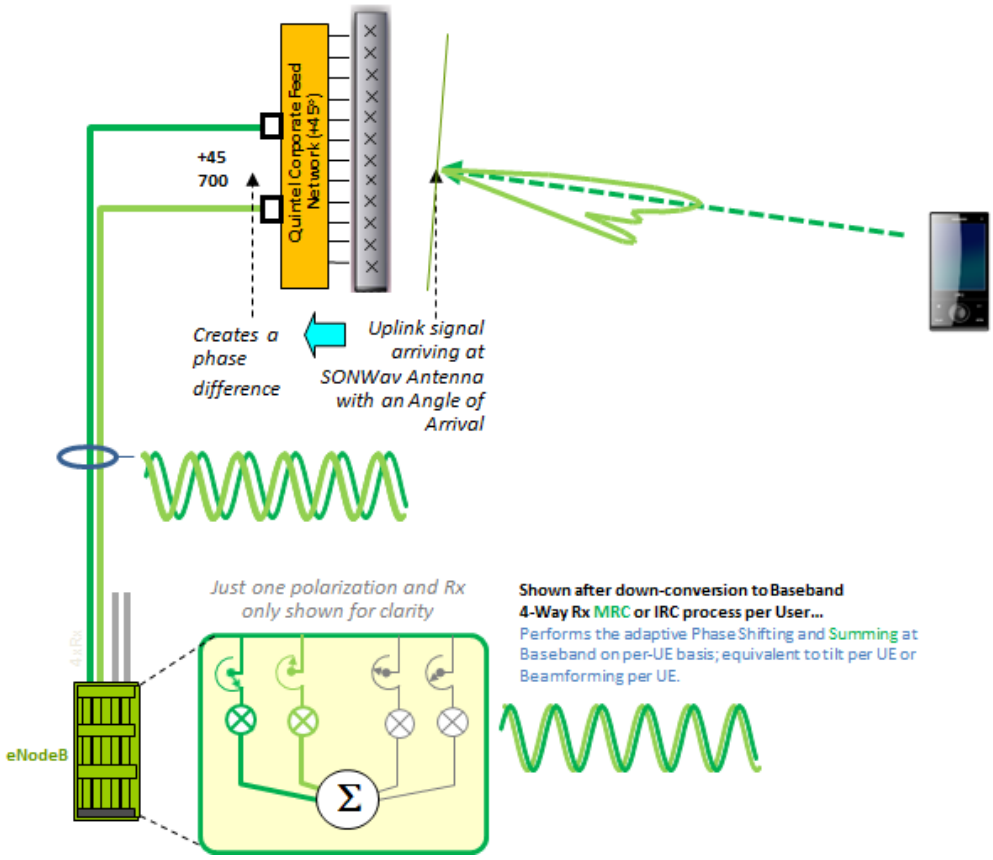

Figure 3.23 eNodeB MRC combining when connected to Quintel SONWav antenna.

This pair of differentially phased signals together with the associated signals from the orthogonal polarization of the antenna are down-converted from RF to baseband. The four baseband signals are then vectorally summed in a 4-branch combining process at baseband within the eNodeB. Known reference signals are periodically transmitted by the UE which allow the eNodeB to measure the phase differences (and any amplitude differences) between all four signals and apply an appropriate baseband phase shifts and weights on each of the branches of the receiver such that coherent signal addition maximises the wanted information signal. In a noise limited radio channel, Maximal Ratio Combining (MRC) would be an optimal combining process. As the UE moves around the cell the AoA may change resulting in a change in the phase difference in each of the pairs of signals, but the receiver combining process will always combine coherently. This is in fact equivalent to having the main beam of the antenna array directed toward and tracking the UE. Furthermore, because multiple UEs are being served simultaneously in the cell then there are several independent receiver combining processes running at baseband, hence this is also equivalent to having directed a beam toward each active uplink user.

Whilst downlink adaptive tilting was not able to be trialled due to 4TX4RX base station solutions not being available at the time of the trial, it might be reasonable to assume that the downlink tilt angle to serve a particular UE would be approximately the same as the uplink AoA for that UE since the scattering geometry and angular dispersion characteristics for uplink and downlink in a macrocell radio channel might be very similar, and of course would be almost identical for a TDD based system. Therefore the uplink AoA could be derived from the uplink channel estimation process, which could then be used for downlink beam steering or adaptive tilting and scheduling.

The North American trial undertaken involved the deployment of two SONWav antennas on adjacent sites in a suburban area of a 10MHz bandwidth LTE network operating in the AWS band (3GPP Band IV [53]). The sector configuration of both sites, prior to, and after deployment of the SONWav antenna is shown below in Figure 3.24. The scheduler deployed on the network was a proprietary vendor PF based scheduler.

The trial sites (sites A and B) were spaced 1.1km apart and had tower heights of 28m and 30m respectively. The area of the network between two sectors of the two adjacent sites was driven by a vehicle containing a test UE running an FTP data session before and after the deployment of the two SONWav antennas and the uplink throughput performance seen by the test mobile was recorded. Adjacent cell uplink interference was generated by six UEs in the adjacent cell north of the two sites, with each UE constantly uploading high definition video content, and thus presenting a modest uplink interference load into the cells of the trial region. Traces of the test UE's instantaneous uplink bit rate before and after the deployment of the SONWav antennas are shown in Figures 3.25 and 3.26.

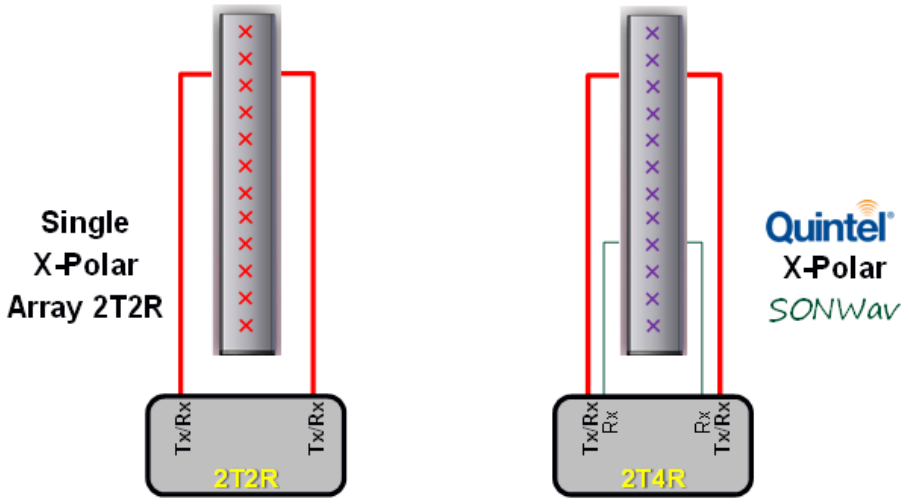

Figure 3.24 Site configuration before (left) and after (right) the deployment of the Quintel SONWav antenna.

Analysis of the measured data revealed that on average the test UE's mean and cell edge throughputs had increased by 29.4% and 78.2% respectively and this gain aligns extremely well to the overall PF scheduler results for the central London simulations presented in the previous section. The reason for the much greater cell edge gain is most likely due to the modest rather than full interference uplink load experienced by this trial network.

Further trials are planned with other operators including trials for the downlink once 4-branch TX/RX radio units become available.

Figure 3.25 Test UE's throughput trace for site configuration with standard X-polar antenna.

Figure 3.26 Test UE's throughput trace for site configuration with SONWav antenna.

3.5 Chapter Summary

This chapter has introduced the concept of rapid dynamic antenna tilting made possible by Quintel's SONWav antenna technology. Initial simulation based upon a homogeneous 3G/HSPA network showed that theoretical single user per cell gains for this ideal network range between 22% and 89%. Further simulations were also performed to evaluate the potential benefit of a modified tilt algorithm that "over-tilts" the antenna towards the users and it was shown that this resulted in some further, yet modest gains in user and cell average throughput.

Ideal homogeneous simulations were then performed with a more realistic 4G/LTE network simulator that included the implementation of fast fading and generic downlink packet schedulers and these results indicated a more realistic downlink capacity gain of between 4% and 36% depending on the scheduler type and level of optimisation already applied to the network.

Further simulations applying rapid dynamic antenna tilt to a real central London 4G/LTE network employing three generic schedulers on top of a fast and slow fading radio channel also resulted in user and cell throughput gains of between 8% and 26% depending on the scheduler type. These results tie in well with previous homogeneous network simulations and suggest a significant user throughput/cell capacity gain can be achieved through the technique even when applied to an already optimised network. The technique is also applicable to both MIMO and non-MIMO capable UEs and can therefore provide a capacity gain for both legacy 3G networks as well as MIMO capable 4G networks. Since in reality most network operators deploy RR or PF schedulers in their network, it was concluded from the simulation work that gains of 25% can be expected in most cases.

Finally some high level results from the first field trial of Quintel's SONWav antenna were presented for the uplink case which show that uplink capacity gains of 30% and cell edge improvements of up to 80% are being seen in the field using dynamic antenna tilt technique. These results align well with the central London simulation results presented earlier in this chapter and the results confirm that rapid dynamic antenna tilt does provide a reasonable macrocell capacity gain.

Chapter 4
Higher Order Horizontal Sectorisation

As was mentioned in Section 2.2 of Chapter 2, in addition to dynamic vertical antenna tilting, higher order horizontal antenna sectorisation has always been seen as a key technique to improve both the coverage and capacity of cellular networks. This chapter begins by reviewing earlier work on higher order horizontal antenna sectorisation and the capacity gains predicted by these earlier references. The chapter then presents the findings of simulation of sectorisation beyond three sectors per site, undertaken on an ideal hexagonal network model proposed by 3GPP in [51, 52] as well as on Telefonica UK's central London 3G/WCDMA network grid. The chapter considers not only the predicted capacity gains but for the first time the ideal horizontal antenna beamwidth required to maximize the downlink capacity for 3, 6, 9, 12, and 15 sector sites whilst maintaining coverage and other typical network operator Key Performance Indicators (KPIs) applicable to a 3G/WCDMA network.

The chapter then presents field trial results from live 3G/WCDMA cell sites within Telefonica UK's network upgraded from three to six sectors as well as results from the deployment of the what is believed to be the Industry's first fifteen sector 3G/WCDMA site and compares these measured results to those found from the simulations. Finally the chapter summarizes the most practical antenna beamwidths that should be deployed for 3, 6, 9, 12 and 15 sectored cell sites.

4.1 Review of Previous Work on Higher Order Horizontal Sectorisation

There have been a number of key papers considering higher order horizontal sectorisation mainly for 3G/WCDMA cellular networks based upon earlier versions of the 3GPP standard prior to the introduction of HSPA in 3GPP R6.

In [64] the authors mainly consider the effect of three fixed antenna beamwidths of 90^{o}, 65^{o} and 33^{o} on the capacity and coverage for three, four and six sector 3G/WCDMA sites. As with all previous papers found on the subject no reason is given why these particular beamwidths should be the ones used for the different sector counts. A homogenous network simulator is used with even traffic spreading to generate the results and it is proposed that six sectors, with each sector utilizing a 33^{o} horizontal antenna beamwidth gives the best coverage and capacity for the network configurations studied. The paper also presents a theoretical uplink calculation for the sectorisation gain for a sector count greater than six but

only for the three fixed antenna beamwidths considered. The paper concludes that the gains determined from the simulations suggest a six sector gain of 1.72 for a 6x33^{o} site configuration over a standard 3x65^{o} configuration.

Reference [65] considers the performance of three, six, nine and twelve sector sites for an IS-95 based 2G/CDMA network. Here real sector coverage measurements are taken from a smart antenna on the roof of a building located in typical European city (city name not given). These measurements are then imported into a network simulator consisting of a network of only seven sites (a test site and a single tier of sites generating the surrounding interference). Simulation results presented suggest a six sector gain of 1.52, a nine sector gain of 2.59 and a twelve sector gain of 2.67 over the capacity of a standard three sector site. These gains assume the non-ideal overlap seen from the field measurements on which the simulations were based.

In [66] again the antenna beamwidth is considered as an important factor in the capacity of three and six sector 3G/WCDMA sites, however once again only fixed beamwidths of 33^{o}, 65^{o} and 90^{o} are considered. Simulations are performed on a homogenous network configuration of ten sites with a non-uniform traffic distribution. Simulation results suggest a six sector gain of 1.8 for the 6x33^{o} site configuration over a standard 3x65^{o} site configuration.

References [67] and [68] consider the impact of angular spread on the capacity gains of three, six and twelve sector sites and use a homogeneous 19 site network simulation setup very similar to that proposed by 3GPP in [51] but with a 3km inter-site distance. Traffic is spread uniformly across the simulation area and capacity gains over a three site configuration (3x63^{o}) of 1.8 and 3.0 are reported for the 6x35^{o} and 12x20^{o} configurations respectively.

Reference [69] considers higher order sectorisation gains in both homogenous and real network deployments. The simulation results from a homogenous network with a uniform traffic distribution suggest a six sector gain of 1.86 and a twelve sector gain of 3.24 over three sectors. Again fixed antenna beamwidths of 65^{o}, 33^{o} and 16^{o} were assumed for the three, six and twelve sector site configurations respectively. Real network simulations (undertaken for a central Stuttgart network) were performed with just a central set of five out of 134 sites being upgraded from three to six sectors and therefore the paper considers six sectors more as a single site hotspot solution rather than a network wide capacity upgrade. Only three and six sector configurations were considered, with the six sector sites providing on average a capacity gain of 1.8 over the previous three sector configuration. The results also suggest that the soft hand over (SHO) overhead remains very similar for both three and six sector deployments since the roll off of the gain of the narrower beam antenna deployed for the six sector configuration is sharper and therefore whilst there are more cell

boundaries between adjacent sectors for the six sector sites, the area of equal Common Pilot Indication Channel (CPICH) powers between sectors is also reduced.

Finally reference [70] is the only reference found to date that considers the potential gains of higher order sectorisation for 4G/LTE. The simulations performed are based upon the 19 site 3GPP homogenous network model defined in [52] using ideal antenna patterns also specified in [52]. A fixed antenna beamwidth of 70^o was assumed for the three sector site configuration and beamwidths of 35^o, 40^o, and 45^o were assumed for the six sector site configurations with the 40^o, and 45^o beamwidths being used to model the effect of angular spreading on a 35^o beamwidth antenna. The simulation results suggest a six sector network capacity gain of 1.88 (6x35^o) over a network deployed using three sector sites (3x70^o) and an standalone site six sector gain of up to 2.1 for individual hotspot sites upgrade from three to six sectors.

In summary previous work indicates a capacity gain can be obtained from higher order sectorisation with predicted capacity gains in the range of 1.5 – 2.1 when moving from three to six sector configuration. Only some of the papers look beyond six sectors to higher order configurations such as nine and twelve sectors. None of the papers consider the optimum beamwidth for the different sector configurations and none support their findings with real network field trials of higher order sectorisation.

4.2 Network Simulations Undertaken to Model the Capacity Benefits of Higher Order Horizontal Sectorisation

In order to evaluate the capacity benefits of higher order antenna sectorisation the Network Simulator introduced in the previous chapter was modified to allow the simulation of both real and ideal hexagonal homogeneous networks of sites with greater than three sectors per site.

4.2.1 Ideal Hexagonal Homogeneous Network Simulations Performed

The network model used to evaluate the benefits seen for higher order sectorisation on an ideal hexagonal homogenous network was again based on the model described in [51, 52] and consisted of a central site encircled by two tiers of surrounding sites giving a total of 19 sites within the simulation area. The ISDs considered here were those presented in [52] as Case 1 (ISD = 500m) and Case 3 (ISD = 1732m). These distances are typical of ISDs found in real urban and suburban mobile network deployments although much smaller ISDs (~250m) are possible for networks deployed in dense urban areas as will be seen for the central London case. Further homogenous network simulation parameters assumed are presented in Table 4.1.

Static Monte Carlo network simulations were performed for the homogeneous network (Cases 1 & 3) for networks of sites having 3, 6, 9, 12, and 15 sectors per site, for varying horizontal beamwidths per sector. Since higher order sectorisation may not necessarily be deployed uniformly across the network, the homogeneous network was also used to evaluate the capacity benefits of a single higher order site being placed at the centre of the network surrounded by a network of three and six sector sites.

Table 4.1 Ideal Hexagonal HSPA+ network simulation assumptions.

Simulation Assumption	Value
Network sites/sectors per site	19/57 (3 sect.) – 19/285 (15 sect.)
Simulation bin size	10x10m ($100m^2$)
BTS Height	32m
Sector Mechanical Downtilt	Case 1: 10^o, Case 3: 5^o
Sector Electrical Downtilt	0^o - specified by antenna pattern
Sector Max. TX Power	43dBm
HSPA CPICH Power	33dBm
HSPA Other CCCH Power	33dBm
HSPA Downlink Orthogonality	0.5 (Ideal orthogonality = 1)
HSPA HS-DSCH Power	40dBm
Operating Frequency	3GPP Band I (2100MHz)
Path Loss Model	PL = 128.1 + $37.6\log_{10}(R)$, R in km [52]
Penetration Loss	20dB
UE Height	1.5m
UE Antenna Gain	0dBi
UE Noise Figure	9dB

4.2.2 Central London Network Simulations Performed

In order to evaluate higher order horizontal sectorisation on a more realistic network configuration, simulations were also performed using the sample of actual site locations (51 sites) from Telefonica UK's central London 3G/WCDMA network shown previously in Figure 3.3. The sites within the central London simulation vary in height and antenna orientation and therefore provide a much more representative network on which to evaluate the benefit of higher order sectorisation than the uniform homogeneous networks assumed in previous studies.

The radio propagation path loss model used for the central London simulations was based upon the macrocell model proposed in [52] but again as previously described in section 3.2.2 the penetration loss was derived from central London land use clutter data made available by Telefonica UK. Cellular traffic was again also distributed according to clutter class across the entire simulation area with greater user densities being applied to the dense urban and urban areas than for parks and open spaces.

Central London simulations were performed for all 51 sites of the network having three, six, nine, twelve and fifteen sectors using the optimal beamwidths determined during the homogeneous network simulations for Case 1, since the Case 1 ISD was more representative of the ISDs of the central London network (central London ISD for the portion of the network considered varied between 100 and 700m). Again in order to evaluate the potential capacity benefits of higher order sectorisation on individual sites further runs were also performed to evaluate the gains a higher sector count had when deployed on just five out of the 51 network sites, with all the remaining sites having three and then six sectors per site. For these simulations, where only five sites were upgraded to have a higher sector count the site gains calculated for these sites had also to take into account the loss of traffic from the surrounding sites. This was not the case for the contiguous higher order simulations where statistics were gathered across all sites and therefore all traffic gains/losses were accounted for.

4.2.3 Antenna and 3G/HSPA Throughput Modelling

In order to determine the ideal horizontal antenna beamwidth for 3, 6, 9, 12, and 15 sector sites a large number of antenna patterns with varying horizontal beamwidths were required. Since it could not be guaranteed that real antennas and their associated patterns actually existed for each and every beamwidth considered then all antenna patterns used during this study for both the homogeneous and central London simulations were generated using the method proposed by 3GPP in [52] presented previously in Section 3.2.3 of Chapter 3.

All beam patterns generated for this study had a fixed electrical tilt of 0^o, a fixed vertical beamwidth of 7^o and only the horizontal beamwidth β was varied from 14^o to 90^o in steps of

2^o in order to generate some 39 different antenna beam patterns. The boresight gain *G(β)* of each antenna was set relative to the 17dBi gain of the 70^o horizontal beamwidth antenna *G(70)* using the following simple relationship

$$G(\beta) = G(70) \times 10\log_{10}\left(\frac{\beta}{70}\right) \tag{4.1}$$

HSPA downlink throughput was again calculated using the equation proposed by Ericsson [60] and presented in Section 3.2.4 of Chapter 3.

4.3 Network Quality Key Performance Indicators Used to Assess the Performance of the Different Horizontal Antenna Beamwidths Considered

In order to assess other effects the introduction of higher order horizontal sectorisation may have on network quality such as increased areas of soft/softer handover, loss of coverage and increased areas of outage due to pilot pollution, a set of typical cellular network performance KPIs were utilized to assess both homogeneous and central London simulation results. The KPIs chosen to be used for the evaluation of simulation results are outlined in the following subsections.

4.3.1 KPI 1: Ec/Io Outage Area

The Energy per chip to Interference Ratio (Ec/Io) is a measure of the serving cells' received signal quality. It is used by the mobile to periodically select the best cell and when all 3G/WCDMA cells are below a certain Ec/Io threshold then it is used to trigger the mobile to reselect to another access technology, for example reselection to an underlying 2G radio access technology such as GSM. The trigger level at which a 3G/WCDMA mobile reselects to GSM is an operator specific parameter but for the purposes of this study a cautious GSM reselection Ec/Io trigger level of -14dB has been assumed. In areas where the best serving cell's Ec/Io is less than or equal to -14dB it has been assumed that all mobiles in this area will re-select to GSM and will therefore not be able to access the enhanced services offered by 3G/WCDMA. Minimising these so called "3G outage areas", caused by too many serving cells and the lack of dominance by a single cell (often referred to as "pilot pollution") is one of the key optimisation tasks in any CDMA or OFDMA single frequency based cellular network.

4.3.2 KPI 2: Ec/Io Mean

As mentioned previously Ec/Io is a measure of the quality of the signal of the serving cell(s). In order to maintain reliable communications the value of Ec/Io must be kept well above the reselection threshold, and therefore mean Ec/Io was used as a further network KPI to assess the performance of horizontal sectorisation.

4.3.3 KPI 3: RSCP Mean

The RSCP is defined as the received signal level of a serving or nearby neighbour cell. It provides a measure of the strength of the serving cells in the area and is used by the network planning/optimisation Engineer to determine the level of coverage provided by the network. Clearly any attempt to increase capacity through higher order sectorisation should not severely compromise coverage and therefore the mean RSCP was chosen as a further evaluation KPI.

4.3.4 KPI 4: Cell Edge RSCP (5^{th} Percentile RSCP)

Whilst mean RSCP is a measure of coverage across the entire cell, it is the cell edge users who will be most affected by loss of coverage. For this reason a second RSCP based KPI was defined based upon the 5^{th} percentile RSCP.

4.3.5 KPI 5: Mean Downlink Cell Throughput

Mean HSPA downlink cell throughput measured in Mbps was used to measure any capacity increased caused by higher order sectorisation.

4.3.6 KPI 6: Downlink User Cell Edge Throughput

In order to measure the downlink throughput at cell edge a second throughput KPI was defined as the 5^{th} percentile of the user's downlink throughput.

4.3.7 KPI 7: Percentage of Users in Soft Handover (SHO)

This KPI measured the total percentage of users that would be in soft (inter-cell handover) or softer (intra-cell) handover or a combination of the two (soft/softer). Whilst handover is required within a 3G/WCDMA network for mobility purposes, since soft/softer handover typically requires resources from two or more cells then generally it is best to keep the number of users in SHO as small as possible whilst still maintaining reliable mobility within the 3G/WCDMA network.

4.3.8 KPI 8: Mean Downlink Cell Site Throughput

This KPI provides a measure of the total downlink throughput across the entire cell site and is the summation of the mean downlink throughput across all cells and sectors of the site.

4.4 Homogeneous Network Simulation Results

The most optimal beamwidths to maximise the site capacity whilst maintaining network quality for the different sector counts considered were determined by evaluating the homogeneous simulation results against the KPIs presented in the previous section. Whilst assessing the results it was seen that the choice of the optimal beamwidth for each configuration considered (3, 6, 9 12, and 15 sectors) is really a compromise between conflicting KPIs. For example shown in Figures 4.1 and 4.2 is the effect that the horizontal antenna beamwidth has on KPIs 2:*Mean Ec/Io*, 3:*Mean RSCP* and 7:*Percentage of users in SHO*, for the three sector, Case 1, network. As expected, from Figure 4.1 it is seen that that better coverage is achieved with a wider antenna beamwidth, but at the cost of signal to noise ratio (*Ec/Io*). In Figure 4.2 again as expected a wider beamwidth antenna leads to greater sector overlap and much greater percentage of users in SHO.

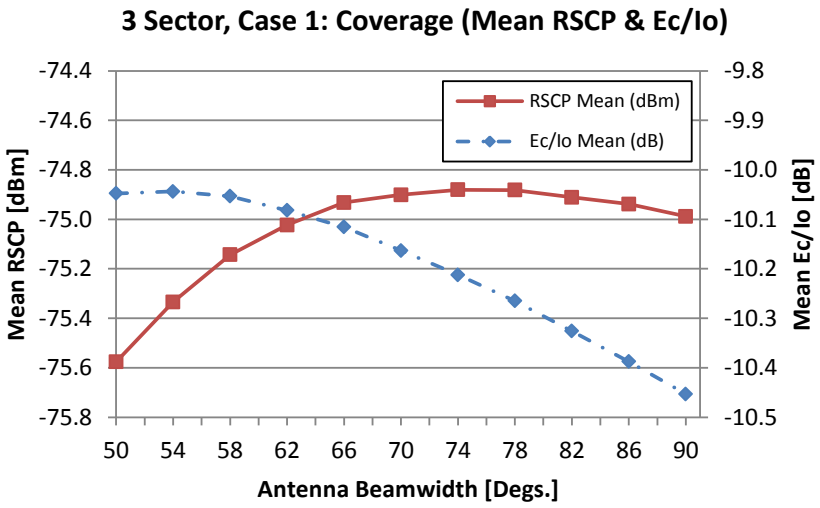

Figure 4.1 Mean RSCP and Ec/Io for the horizontal antenna beamwidths considered for the three sectored Case 1 homogeneous network.

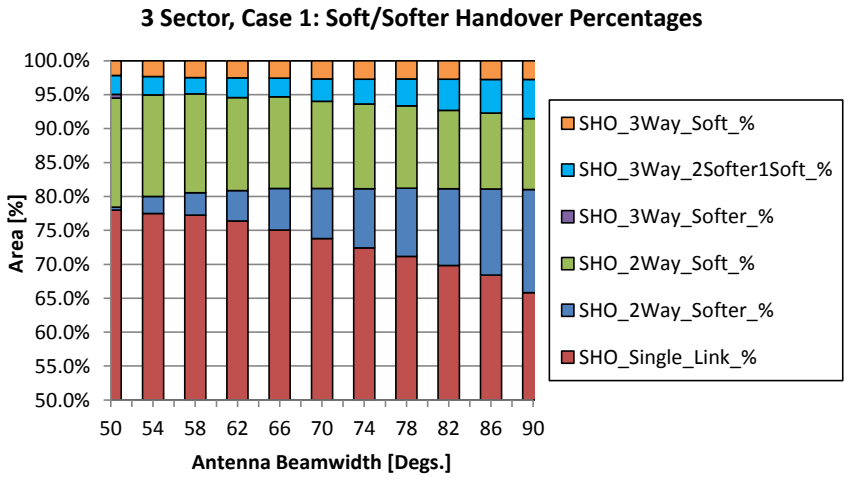

Figure 4.2 Soft/Softer handover percentages for the horizontal antenna beamwidths considered for the three sectored Case 1 homogeneous network

In order to find the horizontal beamwidth that provided the best compromise across all KPIs, targets were set against each of the KPIs as either an absolute threshold for example Ec/Io outage <= 5% or as a relative threshold across the results for the different antenna horizontal beamwidths considered. Each configuration then was assessed against these KPI targets. Configurations that did not meet one or more of the KPI targets were discounted and the most optimal beamwidth was determined as the configuration that maximise the remaining KPIs. Tables 4.2-4.11 present a full summary of the results for all sector counts considered for the ideal homogeneous Case 1 & Case 3 networks against the aforementioned KPIs and their associated targets. In the tables the green cells indicate where the KPI targets have been met and in each case the antenna beamwidth considered to be optimal is indicated by a yellow shaded value.

For example considering the results in Table 4.3 for the six sector Case 1 network configuration, here it can be seen that of the beamwidths considered, 34^{o}, 38^{o} and 42^{o} were the most optimal beamwidths providing the best compromise across all the KPIs. In this case it was concluded that 34^{o} was the optimum beamwidth since it provided the highest cell site capacity out of the three beamwidth meeting all KPI targets.

It was also found from the results that sector tessellation plays an important part in determining the effectiveness of higher order sectorisation for the ideal homogeneous network. Site configurations with an odd numbers of sectors were seen to provide better inter-site sector tessellation (Figure 4.3) than those with an even number of sectors. Site configurations with an even number of sectors tended to have inter-site sectors pointing directly at one another leading to areas where there was no dominance and high pilot pollution as can be seen in the Case 3 KPI summaries of the six and twelve sector configurations (Tables 4.8 and 4.10).

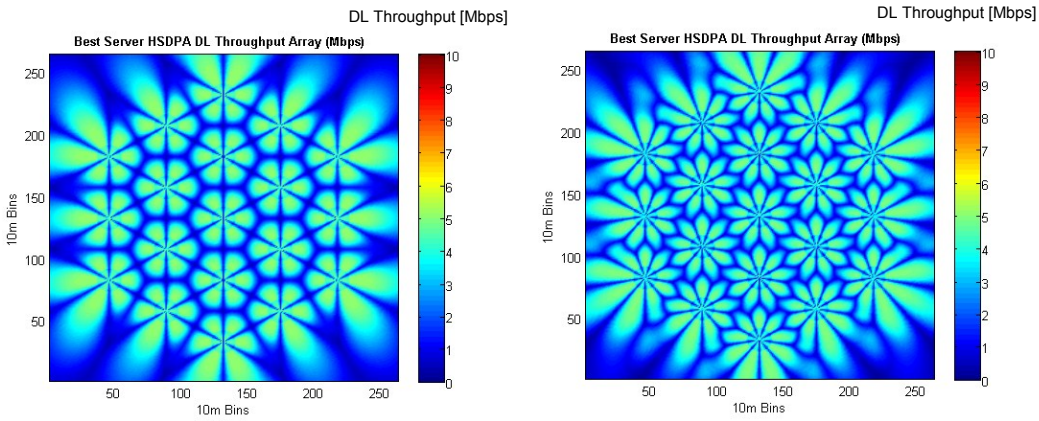

Figure 4.3 Best server HS-DSCH throughput arrays for 6 and 9 sectors per site, showing better inter-sector tessellation for 9 sector configuration.

Table 4.12 presents an overall summary of the optimum horizontal beamwidths determined by the homogenous network simulations and the capacity gains obtained over a baseline three sector configuration of 3x62°. The Case 1 gains of 1.8, 2.7 and 3.2 for the six, nine and twelve sector configurations tie in well with some of the earlier work referenced and it is interesting to see that the homogeneous simulation results also suggest yet further gains (>4) are possible by using fifteen sectors – assuming a practical 14° horizontal beamwidth antenna could be produced and deployed.

Table 4.2 Ideal Hexagonal Network, Case 1, Three Sector Results

		Antenna Horizontal Beamwidth [Degrees]										
Key Performance Indicator	Target/ Peak	50	54	58	62	66	70	74	78	82	86	90
Ec/Io Outage Area <= 5%	5.0%	0.2%	0.2%	0.1%	0.0%	0.0%	0.0%	0.0%	0.0%	0.0%	0.0%	0.0%
Ec/Io Mean >= 11dB	-11.0	-10.0	-10.0	-10.1	-10.1	-10.1	-10.2	-10.2	-10.3	-10.3	-10.4	-10.5
RSCP Mean <= 1dB from Peak	-74.9	-75.6	-75.3	-75.1	-75.0	-74.9	-74.9	-74.9	-74.9	-74.9	-74.9	-75.0
Cell Edge RSCP <= 2dB from Peak	-81.2	-82.9	-82.3	-81.9	-81.6	-81.3	-81.3	-81.2	-81.2	-81.2	-81.2	-81.2
Throughput Mean <= 10% from Peak	3.51	3.51	3.50	3.48	3.44	3.39	3.32	3.25	3.17	3.08	2.99	2.89
Cell Edge Throughput <= 10% from Peak	1.16	1.15	1.16	1.16	1.15	1.15	1.13	1.11	1.10	1.08	1.06	1.03
Total SHO	40.0%	22.0%	22.5%	22.8%	23.6%	25.0%	26.2%	27.6%	28.8%	30.2%	31.6%	34.2%
Site Throughput	N/A	10.52	10.51	10.45	10.32	10.17	9.96	9.74	9.50	9.23	8.96	8.67

Table 4.3 Ideal Hexagonal Network, Case 1, Six Sector Results

		Antenna Horizontal Beamwidth [Degrees]										
Key Performance Indicator	Target/ Peak	22	26	30	34	38	42	46	50	54	58	62
Ec/Io Outage Area <= 5%	5.0%	11.2%	3.4%	1.3%	0.9%	0.8%	0.7%	0.7%	0.8%	0.9%	1.1%	1.4%
Ec/Io Mean >= 11dB	-11.0	-10.9	-10.5	-10.3	-10.3	-10.4	-10.5	-10.6	-10.7	-10.8	-11.0	-11.1
RSCP Mean <= 1dB from Peak	-71.9	-74.3	-73.0	-72.3	-72.0	-71.9	-71.9	-72.0	-72.1	-72.3	-72.4	-72.6
Cell Edge RSCP <= 2dB from Peak	-78.2	-87.4	-83.3	-80.9	-79.5	-78.6	-78.3	-78.2	-78.3	-78.4	-78.5	-78.6
Throughput Mean <= 10% from Peak	3.18	2.8	3.1	3.2	3.1	3.0	2.9	2.7	2.6	2.4	2.2	2.0
Cell Edge Throughput <= 10% from Peak	1.03	0.5	0.8	1.0	1.0	1.0	1.0	1.0	1.0	0.9	0.9	0.9
Total SHO	40.0%	25.9%	22.5%	25.9%	28.6%	31.4%	34.3%	37.0%	39.7%	44.9%	47.6%	52.9%
Site Throughput	N/A	16.93	18.61	19.05	18.81	18.20	17.38	16.42	15.37	14.29	13.22	12.23
Capacity Gain Over 3 Sector	N/A	1.64	1.80	1.85	1.82	1.76	1.68	1.59	1.49	1.38	1.28	1.18

Table 4.4 Ideal Hexagonal Network, Case 1, Nine Sector Results

		Antenna Horizontal Beamwidth [Degrees]									
Key Performance Indicator	Target/ Peak	12	14	16	18	20	22	24	26	28	30
Ec/Io Outage Area <= 5%	5.0%	14.5%	8.5%	3.9%	1.7%	0.6%	0.2%	0.1%	0.1%	0.1%	0.2%
Ec/Io Mean >= 11dB	-11.0	-11.3	-10.8	-10.5	-10.3	-10.3	-10.3	-10.4	-10.4	-10.5	-10.6
RSCP Mean <= 1dB from Peak	-70.1	-72.5	-71.7	-71.1	-70.6	-70.3	-70.2	-70.1	-70.1	-70.2	-70.2
Cell Edge RSCP <= 2dB from Peak	-76.8	-84.7	-82.4	-79.7	-78.0	-77.2	-76.9	-76.9	-76.8	-76.8	-76.8
Throughput Mean <= 10% from Peak	3.07	2.72	2.88	2.99	3.06	3.07	3.05	2.98	2.90	2.80	2.68
Cell Edge Throughput <= 10% from Peak	1.05	0.21	0.47	0.79	1.00	1.05	1.05	1.04	1.03	1.01	0.99
Total SHO	40.0%	23.1%	20.7%	20.9%	21.2%	24.7%	25.2%	27.6%	29.8%	33.4%	33.8%
Site Throughput	N/A	24.45	25.89	26.93	27.53	27.65	27.42	26.84	26.10	25.17	24.16
Capacity Gain Over 3 Sector	N/A	2.37	2.51	2.61	2.67	2.68	2.66	2.60	2.53	2.44	2.34

Table 4.5 Ideal Hexagonal Network, Case 1, Twelve Sector Results

		Antenna Horizontal Beamwidth [Degrees]								
Key Performance Indicator	Target/ Peak	8	10	12	14	16	18	20	22	24
Ec/Io Outage Area <= 5%	5.0%	33.0%	22.3%	10.4%	6.1%	4.4%	3.1%	2.9%	2.8%	2.9%
Ec/Io Mean >= 11dB	-11.0	-13.4	-12.2	-11.2	-10.8	-10.7	-10.7	-10.7	-10.8	-10.9
RSCP Mean <= 1dB from Peak	-69.1	-73.9	-72.2	-70.8	-69.9	-69.5	-69.2	-69.1	-69.1	-69.2
Cell Edge RSCP <= 2dB from Peak	-76.4	-90.1	-87.1	-82.6	-80.0	-79.0	-77.8	-77.0	-76.5	-76.4
Throughput Mean <= 10% from Peak	2.73	1.85	2.16	2.45	2.65	2.73	2.73	2.67	2.57	2.44
Cell Edge Throughput <= 10% from Peak	0.86	0.12	0.15	0.43	0.67	0.72	0.80	0.84	0.86	0.84
Total SHO	40.0%	45.2%	39.6%	33.5%	33.3%	32.1%	35.4%	34.7%	40.1%	42.4%
Site Throughput	N/A	22.16	25.93	29.37	31.78	32.76	32.75	32.04	30.82	29.27
Capacity Gain Over 3 Sector	N/A	2.15	2.51	2.84	3.08	3.17	3.17	3.10	2.99	2.84

Table 4.6 Ideal Hexagonal Network, Case 1, Fifteen Sector Results

		Antenna Horizontal Beamwidth [Degrees]						
Key Performance Indicator	Target/Peak	8	10	12	14	16	18	20
Ec/Io Outage Area <= 5%	5.0%	16.5%	5.7%	1.7%	0.6%	0.3%	0.4%	0.7%
Ec/Io Mean >= 11dB	-11.0	-11.7	-10.8	-10.6	-10.5	-10.6	-10.7	-10.9
RSCP Mean <= 1dB from Peak	-67.9	-70.0	-68.7	-68.2	-68.0	-67.9	-68.0	-68.2
Cell Edge RSCP <= 2dB from Peak	-74.6	-82.4	-77.4	-75.4	-74.8	-74.6	-74.6	-74.6
Throughput Mean <= 10% from Peak	2.78	2.42	2.67	2.78	2.77	2.67	2.52	2.34
Cell Edge Throughput <= 10% from Peak	0.97	0.18	0.65	0.86	0.97	0.97	0.95	0.91
Total SHO	40.0%	22.8%	18.0%	24.4%	25.7%	31.9%	32.8%	39.9%
Site Throughput	N/A	36.25	40.11	41.71	41.50	40.07	37.85	35.15
Capacity Gain Over 3 Sector	N/A	3.51	3.89	4.04	4.02	3.88	3.67	3.41

Table 4.7 Ideal Hexagonal Network, Case 3, Three Sector Results

		Antenna Horizontal Beamwidth [Degrees]										
Key Performance Indicator	Target/ Peak	50	54	58	62	66	70	74	78	82	86	90
Ec/Io Outage Area <= 5%	5.0%	0.6%	0.5%	0.5%	0.6%	0.7%	0.7%	0.8%	0.9%	1.1%	1.3%	1.5%
Ec/Io Mean >= 11dB	-11.0	-10.4	-10.5	-10.5	-10.5	-10.6	-10.6	-10.7	-10.8	-10.8	-10.9	-11.0
RSCP Mean <= 1dB from Peak	-92.9	-93.4	-93.2	-93.1	-93.0	-92.9	-92.9	-92.9	-92.9	-92.9	-93.0	-93.0
Cell Edge RSCP <= 2dB from Peak	-101.0	-101.6	-101.3	-101.2	-101.1	-101.0	-101.0	-101.0	-101.0	-101.1	-101.1	-101.2
Throughput Mean <= 10% from Peak	3.02	3.02	3.01	2.98	2.94	2.89	2.83	2.76	2.69	2.62	2.54	2.46
Cell Edge Throughput <= 10% from Peak	0.94	0.94	0.93	0.92	0.91	0.89	0.87	0.86	0.84	0.83	0.81	0.79
Total SHO	40.0%	24.7%	26.1%	27.0%	28.2%	29.4%	30.7%	32.0%	33.4%	34.6%	36.0%	38.4%
Site Throughput	N/A	9.07	9.03	8.94	8.81	8.66	8.49	8.29	8.08	7.86	7.63	7.39

Table 4.8 Ideal Hexagonal Network, Case 3, Six Sector Results

		Antenna Horizontal Beamwidth [Degrees]										
Key Performance Indicator	Target/ Peak	22	26	30	34	38	42	46	50	54	58	62
Ec/Io Outage Area <= 5%	5.0%	15.9%	10.9%	6.0%	3.9%	3.2%	3.0%	3.1%	3.4%	3.8%	4.6%	5.7%
Ec/Io Mean >= 11dB	-11.0	-11.5	-11.1	-10.9	-10.8	-10.9	-10.9	-11.0	-11.1	-11.3	-11.4	-11.6
RSCP Mean <= 1dB from Peak	-90.0	-92.4	-91.2	-90.4	-90.1	-90.0	-90.0	-90.1	-90.2	-90.3	-90.5	-90.6
Cell Edge RSCP <= 2dB from Peak	-98.3	-104.3	-103.6	-101.3	-99.7	-98.8	-98.4	-98.3	-98.3	-98.5	-98.6	-98.8
Throughput Mean <= 10% from Peak	2.73	2.43	2.64	2.73	2.72	2.64	2.53	2.39	2.24	2.09	1.94	1.80
Cell Edge Throughput <= 10% from Peak	0.78	0.49	0.50	0.64	0.75	0.78	0.78	0.77	0.76	0.74	0.71	0.68
Total SHO	40.0%	34.7%	31.9%	30.7%	32.8%	35.9%	38.7%	41.3%	43.9%	48.9%	51.4%	56.5%
Site Throughput	N/A	14.57	15.83	16.39	16.31	15.84	15.16	14.35	13.46	12.53	11.63	10.78
Capacity Gain Over 3 Sector	N/A	1.65	1.80	1.86	1.85	1.80	1.72	1.63	1.53	1.42	1.32	1.22

Table 4.9 Ideal Hexagonal Network, Case 3, Nine Sector Results

		Antenna Horizontal Beamwidth [Degrees]									
Key Performance Indicator	Target/ Peak	12	14	16	18	20	22	24	26	28	30
Ec/Io Outage Area <= 5%	5.0%	15.0%	8.1%	3.0%	1.3%	0.9%	0.7%	0.7%	0.8%	1.2%	1.5%
Ec/Io Mean >= 11dB	-11.0	-11.5	-11.0	-10.7	-10.6	-10.6	-10.6	-10.7	-10.8	-10.9	-11.0
RSCP Mean <= 1dB from Peak	-88.1	-90.5	-89.5	-88.8	-88.5	-88.3	-88.2	-88.1	-88.1	-88.2	-88.3
Cell Edge RSCP <= 2dB from Peak	-96.5	-102.7	-99.5	-97.7	-97.0	-96.6	-96.5	-96.5	-96.5	-96.6	-96.6
Throughput Mean <= 10% from Peak	2.78	2.45	2.61	2.73	2.78	2.78	2.74	2.68	2.59	2.50	2.40
Cell Edge Throughput <= 10% from Peak	0.94	0.21	0.51	0.82	0.91	0.94	0.93	0.90	0.87	0.84	0.81
Total SHO	40.0%	24.9%	21.8%	23.1%	24.8%	28.4%	29.7%	32.0%	34.2%	37.9%	38.5%
Site Throughput	N/A	22.09	23.53	24.54	24.99	24.98	24.65	24.09	23.35	22.50	21.58
Capacity Gain Over 3 Sector	N/A	2.51	2.67	2.78	2.84	2.83	2.80	2.73	2.65	2.55	2.45

Table 4.10 Ideal Hexagonal Network, Case 3, Twelve Sector Results

		Antenna Horizontal Beamwidth [Degrees]								
Key Performance Indicator	Target/ Peak	8	10	12	14	16	18	20	22	24
Ec/Io Outage Area <= 5%	5.0%	35.6%	23.3%	12.9%	8.8%	7.8%	7.2%	6.5%	6.2%	6.5%
Ec/Io Mean >= 11dB	-11.0	-13.6	-12.5	-11.6	-11.2	-11.1	-11.1	-11.1	-11.1	-11.2
RSCP Mean <= 1dB from Peak	-87.2	-91.9	-90.2	-88.6	-87.8	-87.4	-87.2	-87.2	-87.2	-87.3
Cell Edge RSCP <= 2dB from Peak	-96.5	-109.2	-106.8	-101.7	-99.3	-98.2	-97.8	-97.1	-96.7	-96.5
Throughput Mean <= 10% from Peak	2.47	1.71	1.99	2.25	2.41	2.47	2.46	2.40	2.31	2.19
Cell Edge Throughput <= 10% from Peak	0.65	0.13	0.16	0.40	0.58	0.61	0.62	0.63	0.65	0.65
Total SHO	40.0%	51.2%	45.4%	39.5%	38.8%	38.4%	41.2%	40.7%	45.0%	47.0%
Site Throughput	N/A	20.57	23.87	26.99	28.86	29.63	29.47	28.76	27.69	26.29
Capacity Gain Over 3 Sector	N/A	2.33	2.71	3.06	3.27	3.36	3.34	3.26	3.14	2.98

Table 4.11 Ideal Hexagonal Network, Case 3 Fifteen Sector Results

		Antenna Horizontal Beamwidth [Degrees]						
Key Performance Indicator	Target/Peak	8	10	12	14	16	18	20
Ec/Io Outage Area <= 5%	5.0%	17.4%	7.2%	2.5%	1.2%	1.3%	2.1%	3.0%
Ec/Io Mean >= 11dB	-11.0	-11.8	-11.0	-10.8	-10.8	-10.9	-11.1	-11.2
RSCP Mean <= 1dB from Peak	-86.0	-87.9	-86.7	-86.1	-86.0	-86.0	-86.1	-86.2
Cell Edge RSCP <= 2dB from Peak	-94.3	-100.1	-96.4	-94.8	-94.4	-94.3	-94.4	-94.5
Throughput Mean <= 10% from Peak	2.56	2.24	2.47	2.56	2.53	2.43	2.29	2.12
Cell Edge Throughput <= 10% from Peak	0.86	0.23	0.57	0.82	0.86	0.84	0.80	0.76
Total SHO	40.0%	26.8%	22.9%	27.9%	30.7%	36.4%	37.9%	44.7%
Site Throughput	N/A	33.65	37.04	38.39	37.88	36.42	34.30	31.85
Capacity Gain Over 3 Sector	N/A	3.82	4.20	4.36	4.30	4.13	3.89	3.61

Table 4.12 Overall Homogeneous Network Results Summary & Optimum Horizontal Beamwidths for 3, 6, 9, 12, & 15 Sector Sites

No. Sectors	Homogeneous Network Case	Optimum Antenna Horizontal Beamwidth [Degs.]	Capacity Gain Over 3 Sector Config.
3	1	62	N/A
	3	62	N/A
6	1	34	1.82
	3	34	1.85
9	1	20	2.67
	3	18	2.84
12	1	18	3.17
	3	16	3.36
15	1	14	4.02
	3	12	4.36

The results of the standalone higher order sectorisation simulations using the optimal antenna beamwidths determined from the Case 1 network simulations are presented in Tables 4.13 and 4.14. Here it is seen that the higher order standalone configurations provide a slightly greater gain than they provide as a contiguous network of sites all having the same sector count. This is due to the fact that in these cases the central site has a higher antenna gain than the surrounding sites and is therefore able to provide greater coverage dominance than the surrounding sites with a lower sector count and therefore captures more traffic.

Table 4.13 Case 1 Standalone Results, 3 Sector Network

Central Site Sector Count	6	9	12	15
Central Site Beam Width [Degs.]	34	20	18	14
Central Site Coverage Area Increase [%]	14%	22%	26%	31%
Central Site Mean RSCP Improvement [dB]	2.1	3.1	4.2	4.9
Central Site Mean Ec/Io Improvement[dB]	-0.1	-0.2	-0.3	-0.3
Central Site Throughput Gain Over 3 Sectors	1.89	2.75	3.49	4.30

Table 4.14 Case 1 Standalone Results, 6 Sector Network

Central Site Sector Count	9	12	15
Central Site Beam Width [Degs.]	20	18	14
Central Site Coverage Area Increase [%]	6%	11%	15%
Central Site Mean RSCP Improvement [dB]	1.2	2.3	3.0
Central Site Mean Ec/Io Improvement[dB]	0.0	-0.1	-0.1
Central Site Throughput Gain Over 6 Sectors	1.48	1.88	2.31

4.5 Central London Network Simulation Results

An example downlink RSCP coverage prediction from the central London network simulations is shown in Figure 4.4 for the case of six sectors per sites. Here it is seen that the non-uniform site placement and varying antenna heights leads to much more site/sector overlap than was present in the homogeneous simulations. This in turn leads to the situation that not all sites benefit equally from higher order sectorisation and some may actually lose traffic through higher order sectorisation for example site 323 in Figure 4.5. However on average higher order sectorisation does improve the throughput per site and the results from the simulations of the central London network are given in Table 4.15.

From the results it is clear that the amount of traffic (Table 4.15) and how this traffic is spread (Figure 4.5) effects the gains seen, with the lowest gains being seen for the lowest amount of traffic (500 active users per scheduling period). For the 2,000 user case the gains seen are very similar to those presented for the ideal hexagonal network, suggesting that the gain from higher order sectorisation can be achieved even for a network with non-ideal site placement such the central London network.

The average capacity gains seen from the results of the simulation of the five standalone sites deployed into a London network of three and six sectors are shown in Tables 4.16 and 4.17 for the different sector configurations deployed. Again as with the previous all-site network simulation results a greater gain is typically achieved for a higher traffic load and even though the traffic stolen from the surrounding sites has been taken into account in the gain calculations, as with the homogeneous runs the standalone higher order sectorisation sites take more traffic individually than when deployed contiguously across the network.

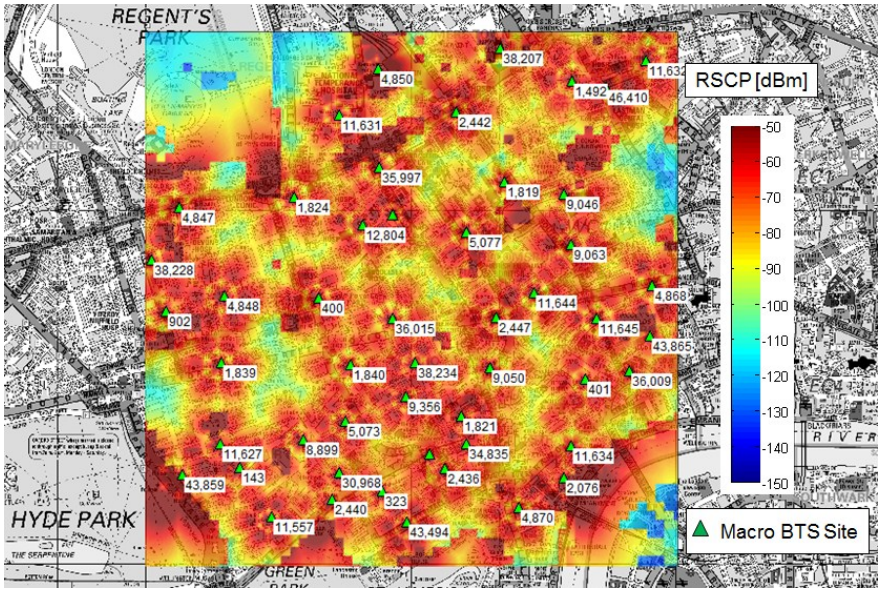

Figure 4.4 Six sector RSCP coverage plot for central London simulation area.

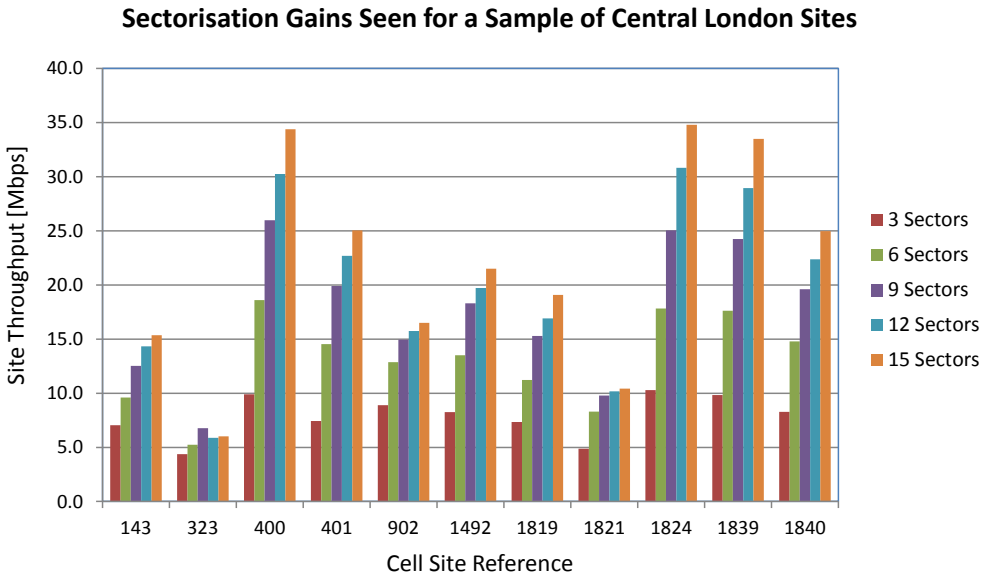

Figure 4.5 Higher order sectorisation gains across a sample of the central London sites.

Table 4.15 Central London Simulation Capacity Gains

	Sectors per site			
Traffic	6	9	12	15
500 users	1.41	1.73	1.82	1.92
1000 users	1.71	2.28	2.54	2.80
2000 users	1.85	2.64	3.08	3.56
Uniform Traffic	1.87	2.74	3.42	4.13

Table 4.16 Central London Standalone Gains – Surrounding Network Consisting of Three Sectored Sites

Average standalone gain over three sector site capacity				
Traffic	Sectors per site			
	6	9	12	15
500 users	1.55	2.05	2.30	2.61
1000 users	1.73	2.49	2.91	3.47
2000 users	1.78	2.66	3.21	3.96

Table 4.17 Central London Standalone Gains – Surrounding Network Consisting of Six Sectored Sites

Average standalone gain over six sector site capacity			
Traffic	Sectors per site		
	9	12	15
500 users	1.18	1.27	1.39
1000 users	1.30	1.50	1.72
2000 users	1.37	1.63	1.97

4.6 Field Verification of Higher Order Sectorisation

4.6.1 Six Sector Field Results

Telefonica UK has deployed six sector 3G/WCDMA sites across most of its high traffic areas including much of central London and statistics from some of these sites have been analysed before and after their upgrade to six sectors in order to assess the capacity benefit seen from the upgrade. Shown in Figures 4.6 and 4.7 is the daily HSDPA traffic seen on two of Telefonica UK's central London 3G/WCDMA sites before and after their upgrades from three to six sectors. In the case of Site A, it can be seen that the average weekday HSDPA traffic volume increases from approximately 20,000 Mbytes/day prior to the upgrade to just over 30,000 Mbytes/day after the upgrade, representing a site capacity gain of around 1.5. In the case of Site B, a similar jump in weekday HSDPA traffic volume is seen this time from around 17,000 Mbytes/day prior to the upgrade to around 27,000 Mbytes/day after the upgrade, representing a site capacity gain of around 1.6. Interestingly this site was included in the central London simulations which predicted a capacity gain of 1.7. Whilst the gains seen for these two sites seem lower than the average predicted by the London simulations, it must be remembered that the actual traffic gains seen are due to the increase in offered traffic to the site and therefore do not necessarily represent the actual maximum gain possible from the upgrade which will only be see when the site is fully loaded.

Statistics are also shown for a larger sample of sites across the whole of Telefonica's UK network (Figure 4.8) considering the average weekday HSDPA data volume on each of these sites two weeks before and two weeks after the site's six sector upgrade. This sample of sites is much more representative of how six sector sites are being used by Telefonica UK as a general 3G/WCDMA network capacity upgrade mechanism since it includes city centre sites as well as standalone six sector sites in smaller towns and suburban areas. From Figure 4.8 it can be seen that not all six sector upgrades have resulted in the site taking more traffic in the period considered - although some carry more than double their previous amount of traffic. Traffic reduction on some sites may be due to season variations in the traffic for that site, or because of the lack of offered traffic following the upgrade. However the majority of sites have benefited from the upgrade with an average capacity gain of 1.5 seen across all 34 sites considered.

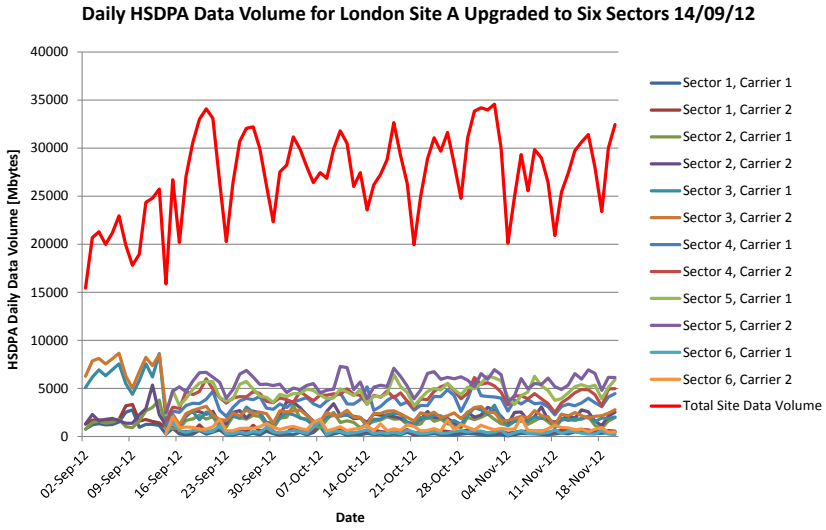

Figure 4.6 Central London Site A traffic increase after upgrade from 3 to 6 sectors.

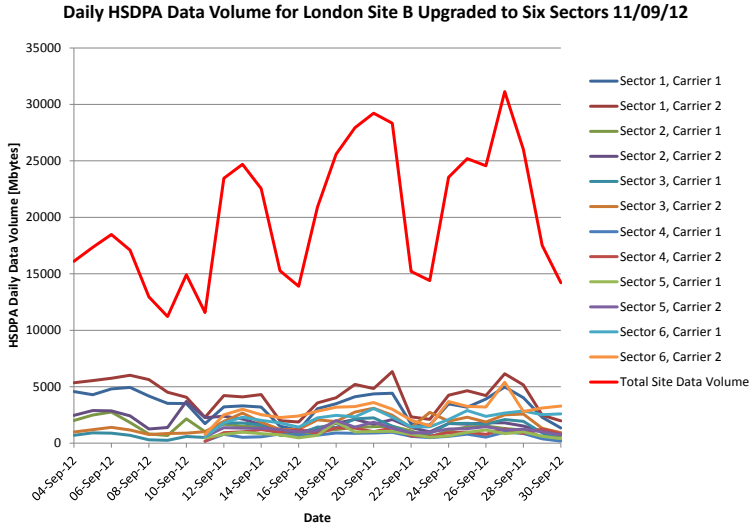

Figure 4.7 Central London Site B traffic increase after upgrade from 3 to 6 sectors.

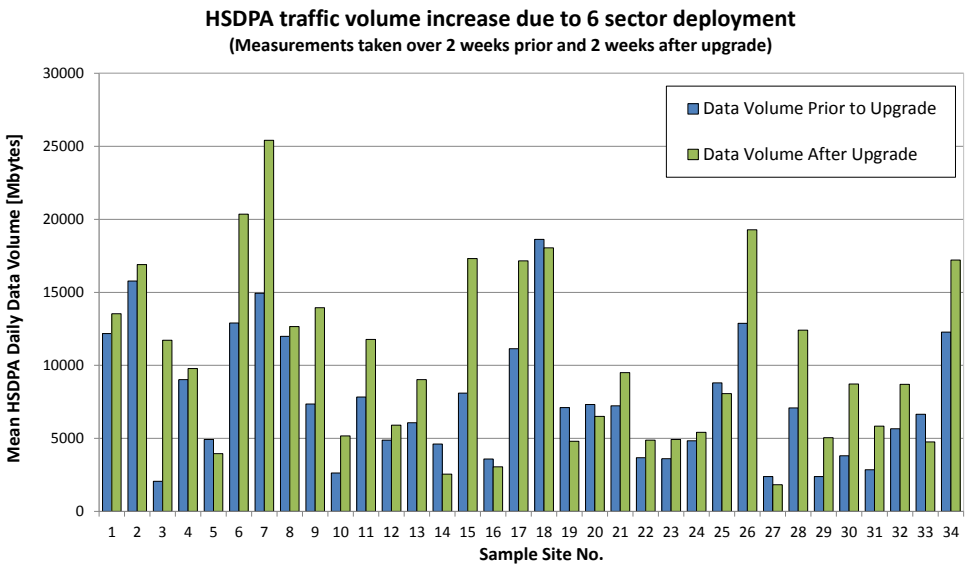

Figure 4.8 Higher order sectorisation gains observed over a sample of Telefonica UK's sites upgraded from three to six sectors.

4.6.2 Fifteen Sector Field Results

Shown in Figure 4.9 is a fifteen sector special event site deployed by Telefonica UK for a concert held in London's Hyde Park on the eve of the London 2012 Olympics, 26th July 2012. The site is believed to be the first of its kind to be deployed into a live 3G/WCDMA network and consisted of three Nokia/Siemens Networks Flexi^{TM} BTSs. Each BTS supported five sectors of the site, with two carriers per sector (10 cells per BTS). The antennas used to create the fifteen sectors were three Argus 5NPX1006F antennas. Each antenna produced five beams, with each beam having a horizontal beamwidth of 12^{o}, a vertical beamwidth of 11^{o}, a mechanical downtilt of 0^{o} and a fixed electrical downtilt of 6^{o}. The specification for this antenna is given in Appendix C.

Downlink data throughput statistics from the site during the event are shown in Figure 4.10. As can be seen from the statistics not all fifteen sectors were equally loaded but the peak traffic occurred in the hour between 5pm and 6pm when the site carried some 5.44Gbytes of data per hour, equivalent to 12.1Mbps on average over the hour. Not quite the 41Mbps or the 35Mbps predicted by the homogeneous and central London simulations for a fifteen sectored site, but for a site to average 12Mbps over an hour means it was very likely there will have been periods during this hour when this site carried far more than 12Mbps.

If the busiest sector that carried 1.2Gbytes of data in the busy hour is considered, then had this been the case on all sectors then the site would have carried 18Gbytes of data in the busy hour, equivalent to 40Mbps on average over the hour – very similar to the simulation results presented earlier. Further work is planned to evaluate the performance of the site at a finer time resolution than that used during this first deployment.

Figure 4.9 Photograph of the fifteen sector cell site deployed at a special event in London's Hyde Park 26th July 2012.

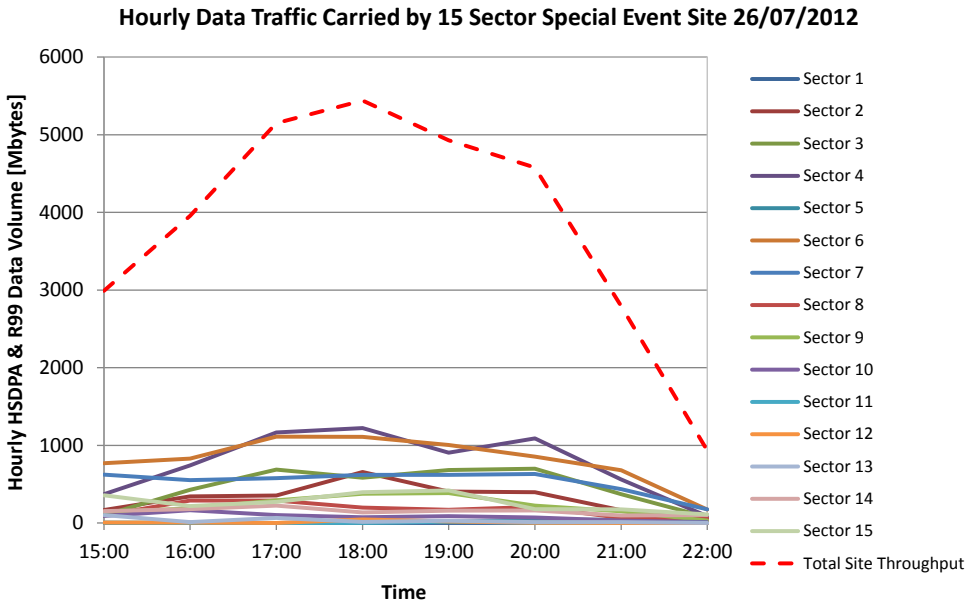

Figure 4.10 Traffic volume carried by a 3G fifteen sector site during Olympic 2012 concert in London's Hyde Park, 26th July 2012.

4.7 Chapter Summary

This chapter has evaluated the gains from higher order horizontal sectorisation for a 3G/HSPA network using both simulations and field trials. Simulations upon an ideal hexagonal network have not only been used to evaluate the potential capacity gains achievable through this technique but by evaluating the results using typical cellular operator network performance KPIs they have also been used to determine the most optimum antenna horizontal beamwidths for 3G/WCDMA cell sites employing horizontal sectorisation.

- Three sector site - optimum horizontal beamwidth = 62^{o}
- Six sector site - optimum horizontal beamwidth = 34^{o}
- Nine sector site - optimum horizontal beamwidth = 20^{o}
- Twelve sector site - optimum horizontal beamwidth = 18^{o}
- Fifteen sector site - optimum horizontal beamwidth = 14^{o}

Central London simulation results have shown that for the optimum beamwidths determined from the ideal hexagonal simulations, significant capacity gains also appear achievable in real deployment scenarios with non-ideal site placement. The analysis of live network statistics from numerous six sector 3G/WCDMA cell sites deployed into Telefonica UK's network in both central London and across the UK have verified an average downlink capacity gain of at least 1.5 from six sector deployment is typical and aligns well with the unloaded central London simulations.

Finally results from the deployment of a 15 sector special event site for the London 2012 Olympic Games have been presented. Whilst the results from this particular 15 sector trial are by no means conclusive, the trial has shown it is possible to deploy and operate a 15 sectored 3G/WCDMA site, the site took a considerable amount of data traffic and further trials are planned in the future to better understand the potential of 15 sector sites.

Chapter 5
Small Cell SON: Determination of Optimum Small Cell Locations Using Geo-located UE Measurement Reports

As explained in Chapter 2, the three available techniques to increase the capacity of a cellular network are to add spectrum, to increase spectral efficiency and finally to add more cells. As MNOs struggle to find more macrocell sites within city centres more are now turning to the deployment of small cells in order to increase the cell count and network capacity.

Where to deploy these small cells is a key question facing the MNOs and this chapter considers the issue of small cell placement in order to maximise the capture of traffic onto the small cell or microcell layer from the macrocell layer given a limited small cell coverage footprint and a limited set of potential small cell locations. During a recent small cell deployment in central London the total cost of deploying a lamppost based 3G/WCDMA small cell was found to be between £10,000 and £15,000 per lamppost [71]. Therefore it is essential given these high costs that placement methods are developed that ensure that each small cell is deployed at a location where it will capture a significant amount of traffic.

The work detailed in this chapter considers if it is possible to effectively locate small cells on a limited set of street furniture locations (in this case central London lampposts) using geo-located UE measurement reports of varying location accuracy. The chapter also considers the use the RF information contained within these measurement reports to estimate the potential size of the small cell when deployed on a shared carrier frequency with the macrocell layer and then uses this cell size estimation to choose the most effective locations for small cell deployment.

5.1 Review of Previous Small Cell Placement Work

There have been many studies into methods of finding the optimal location for both macrocells and microcells in cellular networks, however many references reviewed assume that a cell site can be placed anywhere and do not approach the problem with a limited set of potential small cell locations as was considered in this chapter. Nor do any of the references found use a geo-located UE measurement based approach to create a traffic distribution on which to base the small cell placement decisions or to better estimate the effectiveness of small cells placed under a co-channel macrocell layer.

In terms of macrocell placement there is a wealth of references on this matter, with all references of note approaching the placement problem by considering there is already a

perfect pre-defined (albeit granular in some cases) traffic distribution map on which to base the placement decision, few if any specify how such a map could be generated. For example, in both [72, 73] a divide and conquer approach is proposed which calculates optimum macro site placement across the whole network, but with no reference to available infrastructure or indeed existing cell sites. In [74] the existing cell sites are taken into consideration, however the placement of additional cells into the network is to improve coverage rather than improve capacity and the granularity of the traffic map is only suitable for macrocell placement. Finally [75] presents an example of a paper considering heuristic techniques (in this case simulated annealing) to select the optimum set of existing 2G/GSM cell sites on which to co-located 3G/WCDMA cells but only considers macrocellular placement.

For the microcell case, there appears very few references relating to optimal placement especially placement on street furniture, although some considering the placement of WLAN access points [76] also suggest their applicability for the placement of cellular small cells. In [77] heuristic techniques are this time proposed for the placement of small cells under a macrocell layer and their effectiveness is modelled on a real deployment in a large European city but once again the technique is used to find only ideal locations rather than choose existing available locations. Finally reference [78] looks at the macro-micro co-channel interference problem for 3G/WCDMA showing that the location of the co-channel microcell with respect to the macrocell is key to the effectiveness of the microcell to offload traffic from the macrocell layer. The reference also considers in depth the optimum CPICH setting on the microcells in order to strike a balance between coverage and capacity on the microcell layer.

In summary, to date there seems to have been very little work undertaken considering small cell traffic geo-location using geo-located UE measurement based techniques to place small cells. Whilst some reference have addressed optimal small cell placement, none have considered the problem of small cell placement on a set of fixed street furniture locations. And whilst [78] acknowledged that the placement of a 3G/WCDMA small cell with respect to the macrocell is critical to the effectiveness of the microcell, it did not go on to provide small cell size estimations for the different macrocell RSCP levels considered in the paper.

Therefore it is concluded that the combination of traffic distribution generation through geo-located UE measurements, the selection of existing street furniture based upon this distribution, the estimation of small cell size using geo-located UE measurement of the macrocell and the use of RF fingerprinting to correct any location errors within the UE measurements appear to be areas where there has been little if any significant work performed to date.

5.2 Geo-location of UE Measurement Reports & Minimisation of Drive Test

The UE in a 2G, 3G or 4G cellular network regularly sends measurement reports relating to, for example, the signal strength or quality of the serving and neighbour cells back to the network in order that the network can instruct the UE to reselect to a nearby cell with better coverage, an alternative carrier frequency, or a different radio access technology [79]. Up until and including 3GPP R9, these UE measurement reports did not contain any information regarding the exact location of the UE.

Given that all UEs within the network at some point are sending measurement reports back to the network, the opportunity to use these measurements to build up an exact picture of the actual coverage and performance of the network in real time is very appealing to network operators. Therefore a number of techniques have been proposed to augment the received UE measurements with geo-location data in order to build up a picture or what is termed here an Xmap (a map of processed geo-located measurements) in order to allow network operators to visualise the coverage and performance of their networks.

The most widely used techniques for geo-location of measurements for 3G/UMTS prior to the introduction of the MDT feature [34] introduced in 3GPP R10 were proprietary techniques proposed by a number of vendors [80, 81] which used network probes deployed typically on the Iub, Iur, Iu-cs and Iu-ps interfaces of the 3G network (Figure 5.1) to collect network data. Data collected by these probes was then triangulated using proprietary methods typically based on Time of Arrival (TOA) techniques [82] to produce geo-locations for the measurements collected. These proprietary solutions then use the geo-located data to perform network analysis and recommend network changes in order to improve network quality.

In 3GPP R10 however a feature known as Minimisation of Drive Test (MDT) was introduced for both 3G/UMTS and 4G/LTE in order to standardise the geo-location of UE measurement reports and is a mandatory feature in the UE from 3GPP R10 onwards. The main aims of MDT were to add the ability of the UE to include geo-location data in its measurement reports and to allow the UE to record radio measurements when in an idle state - for subsequent transmission back to the network. MDT primarily uses the Global Positioning System (GPS) to geo-locate the UE but will fall back to other geo-location techniques such as OTDA and Cell Identity (Cell-ID) described later in this chapter, if GPS is not available. A new network entity known as the MDT Server is also introduced in 3GPP R10 and this removes the need for network probes to be placed within the network. As with all 3GPP network entities the MDT Server is specified with open interfaces so that 3rd party products may be used to analyse the data collected through MDT.

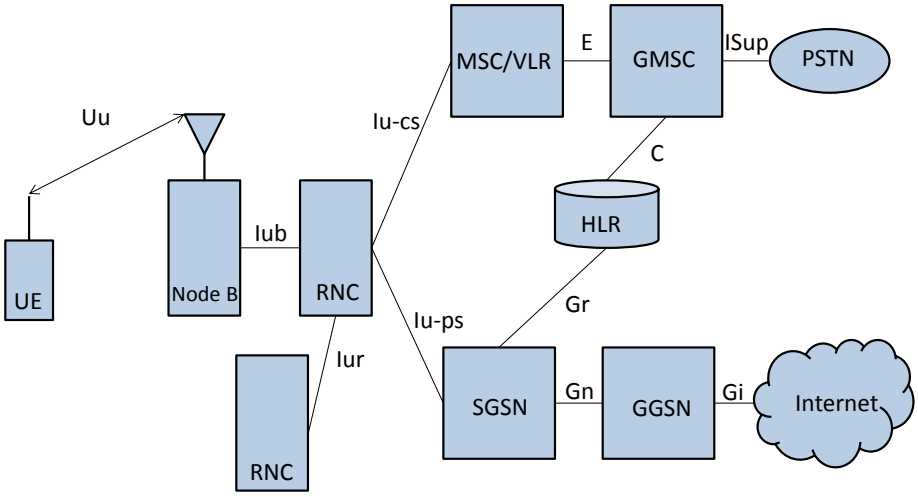

Figure 5.1 3G/WCDMA Network Architecture.

Another interesting approach to the automatic collection of geo-located UE measurements is that based upon using smart phone applications to collect measurements from the UE and then send these back over the cellular network and internet to a remote server (not necessarily hosted by the network operator) for further analysis [83]. The benefits of this approach are that potentially a far greater range of measurements are available using a UE based application such as general user application behaviour and data transfer rate as well as the RF related measurements. Also since all data is delivered to a 3rd party server there is greater flexibility in the analysis of the data than the MDT Server based approach. The application based approach also primarily uses GPS to geo-locate the UE but again can fall back to OTDA and Cell-ID technique if GPS is not available.

The disadvantages of the application based approach is that it requires the installation and operation (although such an application can be programmed to run in the background) of the geo-location/measurement application on many users' smartphones to be able to collect enough measurements to be effective. Also the sending of the measured data back to the remote server will consume some of the user's data allowance. And finally the continued operation of an application that may require the operation of the GPS within the smartphone and the transmission of data back to the server is likely to have an impact on battery life.

Regardless of the techniques used to collect the geo-located data one thing is certain, depending on the geo-location technique used, there will always be some form of uncertainty relating to the accuracy of the geo-location measurement and therefore being able to understand the impact this uncertainty has on for example the accurate placing of a 50m radius small cell on a traffic hotspot is key to being able to exploit techniques such as MDT to their fullest potential. The following section provides an overview of the potential accuracy of the geo-location methods introduced so far.

5.3 Review of the Accuracy of Geo-location Methods

Given below is a list of the most prevalent techniques currently used to geo-locate measurement reports. Note that the cell placement and SON techniques presented in this and subsequent chapters assume a method of geo-location but are not dependent on a particular technique being used. The work here is more concerned coping with the inaccuracy of the location information rather than the method used to provide the geo-location information.

5.3.1 Standalone UE Measurement Reports

UE measurement reports already provide a fairly crude estimation of the location of the UE since the network knows the location of serving cell site as it is included in the UE measurement report. The accuracy of the location estimation based on this method is therefore dependent on the size of the serving cell which in metropolitan areas can be as small as 50m but in rural area can be as large as 200km. However, even in city centres this method of geo-location still has its problems since not all UEs will be in a 50m radius microcell and surrounding overshooting cells can lead to some UEs still being a number of kilometres from their serving cells. Earlier work [84] suggests geo-location through the use of the knowledge of the serving cell alone provides a location accuracy of between 500m and 800m. Therefore this technique alone is not suitable for creating detailed coverage/traffic distributions on which to locate/optimise 100 - 200m radius small cells.

5.3.2 Time of Arrival and Observed Time Difference of Arrival

TOA and OTDA use triangulation of either the uplink (computation performed in the network) or the downlink (computation performed in the UE) signals to estimate the UE's location. Various related techniques exist for 2G/GSM [85, 86], 3G/WCDMA [50] and 4G/LTE [87], with median location accuracies for 3G/WCDMA and 4G/LTE being reported to be 75m [88] and 20m [89] respectively.

5.3.3 GPS Based Geo-location Techniques

With most 3G and 4G smartphones now being shipped with an internal GPS receiver, very accurate location estimation (median location error < 5m) is now available directly at the UE when the UE has good visibility of three or more GPS satellites [90]. However with over 80% of mobile data traffic estimated to be generated/consumed indoors [91] then the availability of an accurate GPS fix for MDT or similar will not always be possible and therefore some reliance on earlier methods will also be required.

5.3.4 RF Fingerprinting Techniques

In addition to the three techniques mentioned above a novel technique now being proposed in the literature based primarily upon the analysis of RF measurement from the UE is RF fingerprinting [92, 93]. Here a database of expected serving and neighbour cells and their expected signal levels is constructed - ideally for all possible locations within network though dedicated measurement surveys or by the processing of geo-located UE measurement reports. This database can then be used to "look-up" UE locations based purely on the RF fingerprint reported by the UE.

RF fingerprinting alone has been estimated to provide an accuracy of between 20-50% of the serving cell size [94] and therefore for a central London macrocellular network with a typical cell radius of 250m, this equates to a location accuracy of around 50m to 125m.

It is therefore clear from the review of the different UE geo-location methods that no single geo-location method is available or accurate in all locations. For the majority of indoor users a reliable GPS fix will not be available and therefore other less accurate methods are expected to be utilised for geo-location in these area. Assuming that fall back to OTDA is possible for a 3G UE in such circumstances then in most cases 3G users without GPS will have a median location error of 75m [88] equating to a typical Root Mean Square (RMS) location error of between 90 - 100m [95].

5.4 Small Cell Location Simulation Assumptions

Up until now the Network Simulator had been used to model only macro cellular networks and therefore changes were required in order to adapt the model to simulate the small cell networks studied in this and subsequent chapters.

5.4.1 Small Cell Location Simulation Area

All small cell modelling detailed in this and subsequent chapters was performed upon the Kensington and Chelsea area of central London. The reason for the choice of this location was because both macro cellular and lamppost location and configuration data had been made available for this area to the University of Leeds by Telefonica UK. The detailed small cell simulation area was a 3x3km area bounded by the UK Ordnance Survey grid lines E524000, N178000, E527000, N181000 containing 31 macrocell sites and 5832 lamppost (potential small cell locations). The location of the 31 macrocell sites is shown in Figure 5.2, whilst those of the 5832 lampposts within the simulation area are shown in Figure 5.3.

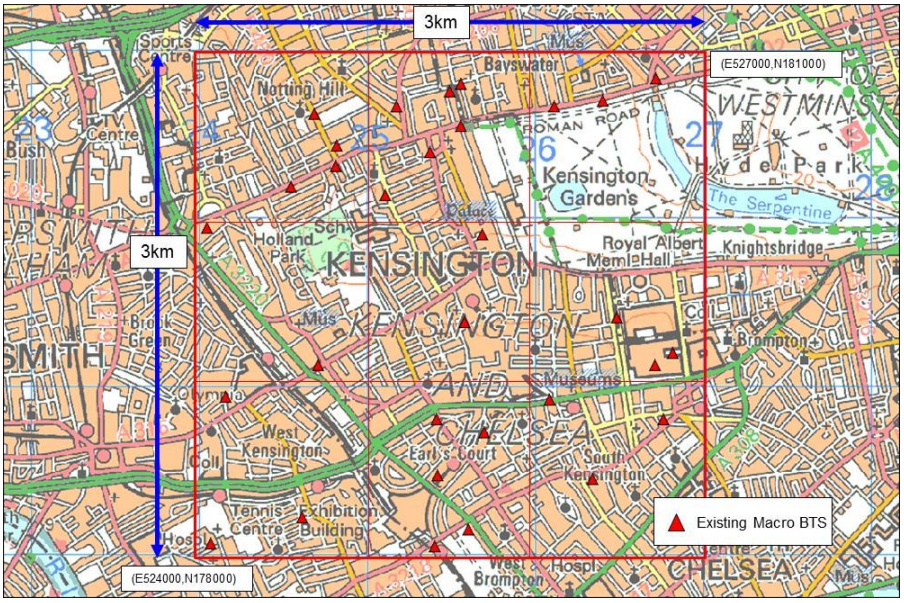

Figure 5.2 Kensington 3x3km Small cell simulation area — showing the location of the existing Telefonica UK macrocells within the simulation area.

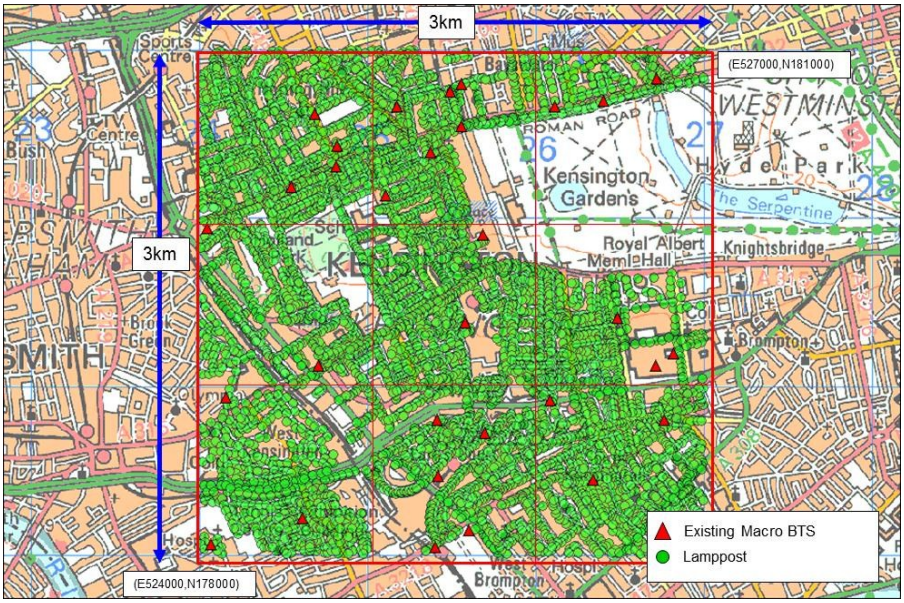

Figure 5.3 Kensington 3x3km small cell simulation area — showing the location of the 5832 lampposts within the simulation area.

Again as with the macrocell simulation area the 31 macrocell sites within the small cell simulation area also vary in height, antenna orientation and tilt with many not following the standard three/six sector horizontal/azimuthal orientations and therefore provided a much more representative platform on which to evaluate the real benefit of small cell SON than the ideal hexagonal homogeneous networks such as those previously proposed [51]. The 5832 lamppost within the simulation area varied in height between 8 and 10m. Lampposts less than 8m in height were not included in the simulations since these lampposts were considered too low for small cell deployment.

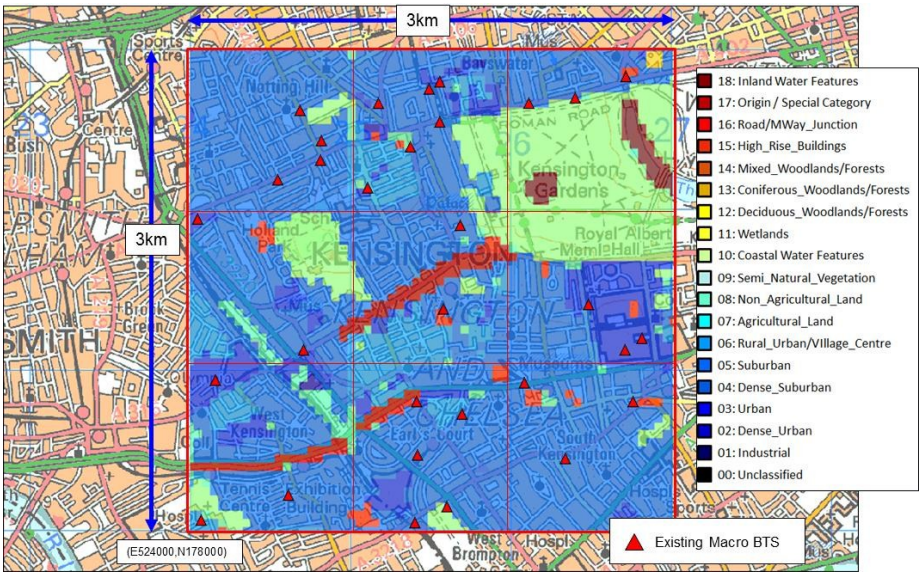

Figure 5.4 Clutter data and classification for Kensington small cell simulation area.

5.4.2 Simulation Area Clutter Data

A portion of the 50m resolution London clutter data made available by Telefonica UK was also used for the small cell simulations (Figure 5.4). The clutter data was used to place data traffic hotspots in realistic locations (avoiding parks and lakes for example) and was also used to apply building penetration losses during the macro and microcell coverage calculations. The building penetration losses assumed for the small cell simulations are shown below in Table 5.1 and are typical of those assumed by MNOs. The origin/special category and additional clutter categories were also used in some simulations to separately identify key area of interest such as Kensington High Street as shown in this example (clutter category = 17) or traffic hotspots. By identifying key areas separately using different clutter categories allowed different user densities to be applied to these areas and also allowed traffic and coverage statistics to be collected specifically for just these key areas.

5.4.3 Macro and Microcell Propagation Models

The macrocell radio propagation path loss model used for the small cell location simulations was again based upon the heterogeneous macrocell model proposed in 3GPP Specification 36.814 [52], as described in Chapter 3 for the macrocell simulations, with the penetration loss again being derived from land use clutter data available for central London (Table 5.1).

The microcell propagation model used for the small cell location simulations was based upon the "Urban Micro Outdoor to Indoor" propagation model proposed in [51] and modelled the combined path loss and building penetration loss (20dB) as a single Path Loss (PL) in dB as

$$PL = 7 + 56\log_{10}(d) \tag{5.1}$$

where

d is the distance in metres between the transmitter and the receiver.

In addition to the propagation and penetration losses antenna gains of 2dBi and 0dBi were assumed for the small cell and UE's antennas respectively.

5.4.4 Summary of Small Cell Simulation Assumptions

Table 5.2 summarises the main small cell simulation assumptions.

Table 5.1 Assumed Building Penetration Losses for each Clutter Category.

Clutter Category	Description	Assumed Building Penetration Loss [dB]
0	Unclassified	0
1	Industrial	14
2	Dense Urban	24
3	Urban	20
4	Dense Suburban	16
5	Suburban	14
6	Rural Urban/Village Centre	8
7	Agricultural Land	0
8	Non Agricultural Land	0
9	Semi Natural Vegetation	2
10	Coastal Water Features	0
11	Wetlands	0
12	Deciduous Woodlands/Forests	4
13	Coniferous Woodlands/Forests	4
14	Mixed Woodlands/Forests	4
15	High Rise Buildings	16
16	Road/Motorway Junction	6
17	Origin/Special Category	0/16
18	Inland Water Features	0

Table 5.2 Small Cell Placement Network Simulation Assumptions.

Simulation Assumption	Value
No. Surrounding Macro Sites	31 sites, 71 sectors
No. KHS Lampposts	5832
Simulation bin size	5m
Macro Sector Max. TX Power	37-43dBm (SON Adjustable)
Macro CPICH Power	10% Macro TX Power
Macro Other CCCH Power	10% Macro TX Power
Macro HSPA HS-DSCH Power	50% Macro TX Power
Macro Antenna Mechanical Tilt	As per Telefonica network setting
Macro Antenna Electrical Tilt	0-10^{o} (SON Adjustable)
Micro Max. TX Power	10dBm
Micro CPICH Power	10% Micro TX Power
Micro Other CCCH Power	10% Micro TX Power
Micro HSPA HS-DSCH Power	50% Micro TX Power
Downlink Orthogonality	0.5 (Perfect orthogonality = 1)
Operating Frequency	3GPP Band I (2100MHz)
Macro Path Loss Model	3GPP 36.814 [52]
Macro Penetration Loss	Clutter based loss
Micro Path Loss Model	3GPP 25.814 [51]

5.4.5 Distribution of Traffic Hotspots within Small Cell Simulation Area

In order to model how small cells could cope with the offloading of traffic from the macrocell network for the case of localised traffic hotspots within the network, a method of hotspot distribution within the simulation area was required.

Although the Network Simulator was enhanced such that random hotspot sizes were possible, in order to simplify the analysis a fixed hotspot size of 100x100m typical of those seen in central London was assumed during the small cell placement work. The Network Simulator was then modified such that the 100x100m traffic hotspots could then be randomly distributed across the simulation area an example of which is shown in Figure 5.5.

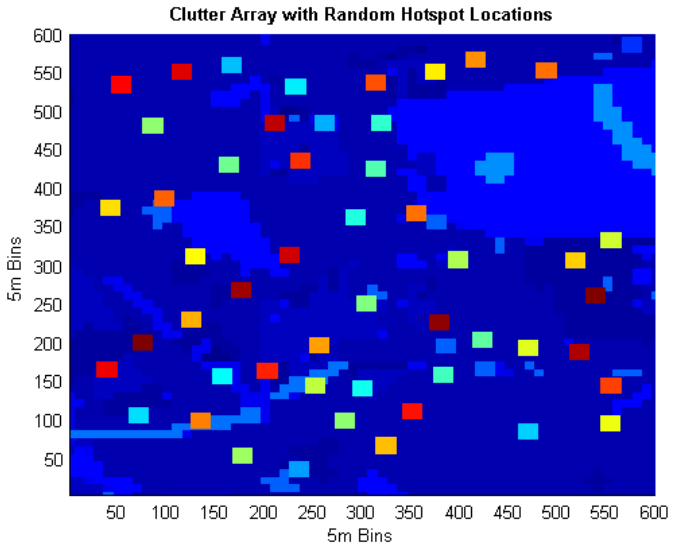

Figure 5.5 Example of random placement of fifty 100x100m hotspots across simulation area. (Clutter data shown in background).

5.4.6 Distribution of Users within Traffic Hotspots and Modelling of User Location Inaccuracies

Since the aim of the work detailed in this chapter was to consider how to effectively detect and place small cells on or close to traffic hotspots using geo-located UE measurement reports, a method of modelling the inaccuracies of the locations reported by the UEs regardless of the geo-location method used was required. Reference [90] for example considers in detail the reasons for errors in GPS location and the classification of these errors, but perhaps the most useful reference found presenting a method of modelling the inaccuracies of GPS was [95]. This reference shows that if the Root-Mean-Squared error (*RMS_Error*) in GPS geo-location accuracy is given by

$$RMS\_Error = \sqrt{\frac{\sum_{i=1}^{N} Error_i^2}{N}} \tag{5.2}$$

where

N is the number of location samples

Error is the location error

Then the linear distance between the reported location and the actual location can be modelled by a Weibull distribution with a shape factor = 2, where the probability of the location error being less than a given distance *d* is given by

$$\text{Probability}(Error \le d) = 1 - e^{-\left(\frac{d}{RMS\_Error}\right)^2} \tag{5.3}$$

This method was used by the Network Simulator to generate a "reported" user location as opposed to the "actual" user location – the actual user location being the original location generated within a traffic hotspot. Show below in Figures 5.6 and 5.7 are examples of an "actual" *user distribution matrix* (Figure 5.6 show the real location of the users within the various traffic hotspots) and a "reported" *user distribution matrix* (Figure 5.7 shows the reported location of the user with the geo-location inaccuracies generated using the Weibull distribution approach described above).

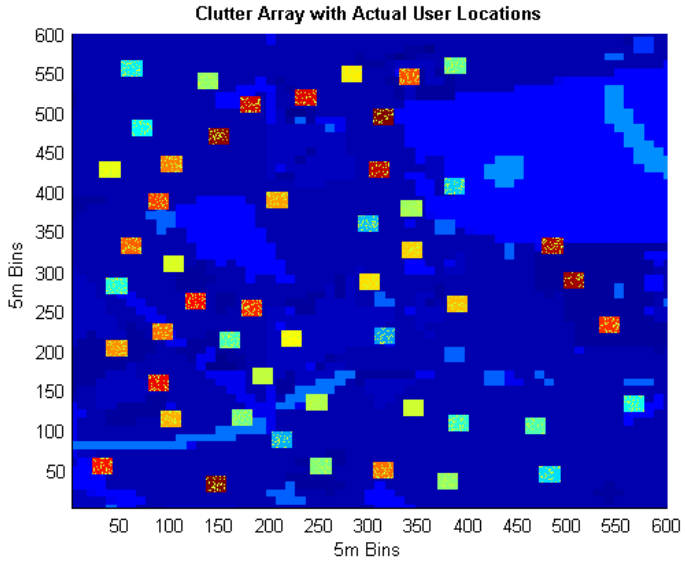

Figure 5.6 Example of random user placement within hotspot areas – actual user location shown as yellow pixels within hotspot areas. (Clutter data shown in background).

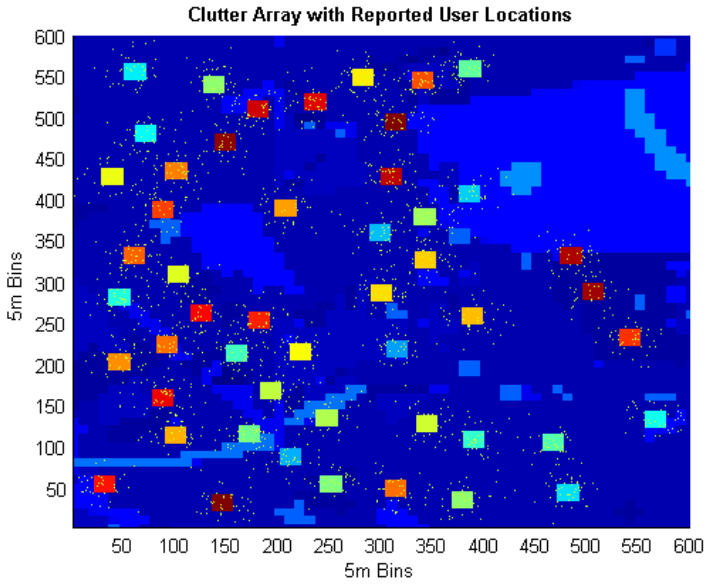

Figure 5.7 Example of random user placement within/around hotspot areas. Reported user location derived from actual user locations (Weibull location error function applied RMS_Error = 100m) shown as yellow pixels. (Clutter data shown in background).

5.5 Optimum Lamppost/Small Cell Location Methods

As explained in the introduction to this chapter, the placement of a small cell on or close to a traffic hotspot is key to the effectiveness of the small cell in capturing traffic and offloading the macrocell layer. For this reason there is a clear need to accurately identify the precise location of the traffic hotspots and choose the closest available location to the hotspot to place the small cell.

This section considers the performance of the two methods developed during this work that estimate the hotspot locations through the use of geo-located UE measurement reports and then locate small cells on nearby lampposts to best capture traffic from the detected hotspots. The section also considers the effect that the UE measurement report location accuracy has on such methods. As will be shown in this and subsequent sections of this chapter the key consideration when using geo-located UE measurement report is the overall wide area availability and the location accuracy of the measurement reports.

5.5.1 Distribution of Users for Optimum Lamppost/Small Cell Location Identification Methods

The Network Simulator was used to model the distribution of 50 traffic hotspots with 500 users per hotspot (a total of 25,000 users) using the methods described earlier, with the geo-location RMS error being varied from 0m to 200m in steps of 25m.

5.5.2 Small Cell Location Method 1: Lamppost by Lamppost Evaluation Method

The first method developed (Method 1) used to locate lamppost mounted small cells close to detected traffic hotspots using geo-located UE measurement reports was a method that simply evaluated the potential traffic captured by each of the 5832 lamppost in a post by post fashion using a fixed small cell radius around each post. One could imagine that when evaluating the placement of small cells on a dedicated carrier frequency, the assumption of a fixed cell radius per small cell would be valid given the lack of dominant interference from the macrocell layer. The overall method, written in pseudo code is given in Figure 5.8, with the Method 1 parameters being given in Table 5.3. The method should be viewed as a benchmark that other enhanced methods of small cell location will be compared against.

A snapshot of the simulator placing 50 small cells with a fixed cell radius of 50m on a reported traffic distribution with an RMS location error of 50m using Method 1 is shown below in Figure 5.9. As can be seen in this case, not all hotspots are addressed by the placement algorithm and this can be for one of two reasons. Firstly there is not a nearby lamppost that can capture any traffic from the hotspot and secondly some hotspots can be

addressed by two lampposts because of the spread of the reported UE locations around the lamppost. This then leads to hotspots not being addressed because of the 50 small cell limit imposed in this particular case.

```
initialise simulation area.
load lamppost locations.
for 1 to number of Monte Carlo runs
        distribute hotspots
        distribute users randomly within each hotspot
        apply user location errors and generate reported UE geo-locations
        for each potential lamppost
            evaluate potential users captured based on reported UE geo-locations for a
            fixed cell radius
        end for
        for 1 to number of small cells to place
            choose and record lamppost capturing the most users
            remove users captured by chosen lamppost from surrounding lampposts
        end for
end for
```

Figure 5.8 Pseudo code for small cell location Method 1.

Table 5.3 Small Cell Placement: Method 1 Parameters

Parameter	Value
Name	Method 1: Lamppost by lamppost evaluation
Monte Carlo runs per parameter set	100
Hotspots per run	50
Users per hotspot	500
Fixed cell sizes evaluated	50, 100, 200m
UE location RMS errors evaluated	0, 25, 50, 75, 100, 125, 150, 175, 200m

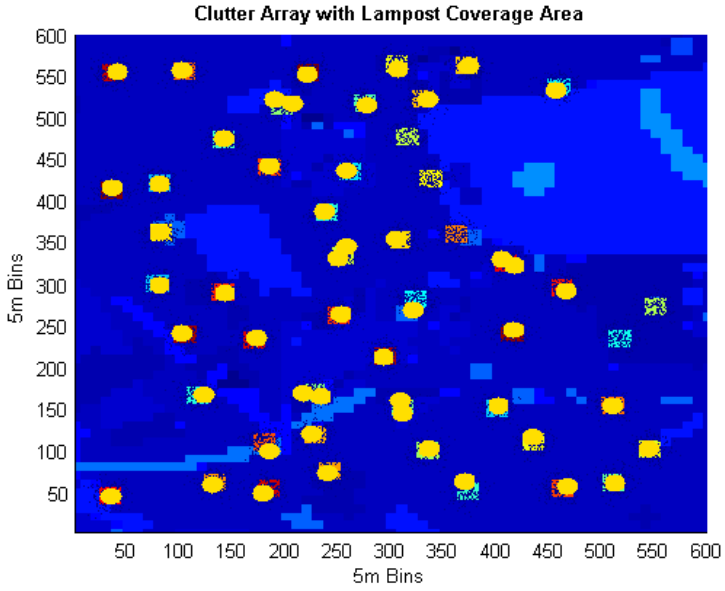

Figure 5.9 Example of small cell placement (yellow circles) using Method 1. (Small cell radius = 50m, RMS location error = 50m).

5.5.3 Small Cell Location Method 2: Hotspot Location Through 2D Circular Filtering

The second small cell placement method developed (Method 2) was a method that used 2D sliding window filtering of the reported *user distribution matrix* (Figure 5.7) to try to identify the traffic hot spot locations. The potential traffic capture value *tc* for each bin *(x,y)* within the simulation area was calculated as

$$tc(x,y) = \sum_{i=x-window\_size/2}^{x+window\_size/2} \sum_{j=y-window\_size/2}^{y+window\_size/2} user\_distribution\_matrix(i,j) \qquad (5.4)$$

where

window_size was the size of the sliding window applied to the *user distribution matrix*.

Since the above calculation applies a square sliding window to the traffic and actually the theoretical small cell coverage footprint is circular, the sliding window method was further enhanced to apply a circular rather than a square sliding window by only considering values from the *user distribution matrix* within the square sliding window where

$$(i-x)^2 + (j-y)^2 - \left(\frac{window\_size}{2}\right)^2 \le 0 \qquad (5.5)$$

In order to optimise the window size a number of runs were performed for the case of user distributions with an RMS location error = 100m. The results of these runs are shown in Figure 5.10. Here it is seen that runs performed with a window size of 30 bins (150m) captured the most users and this was the window size chosen and applied for Method 2. This window size is large enough to gather together uses of a single hotspot, but not too large to start capturing users from nearby hotspots.

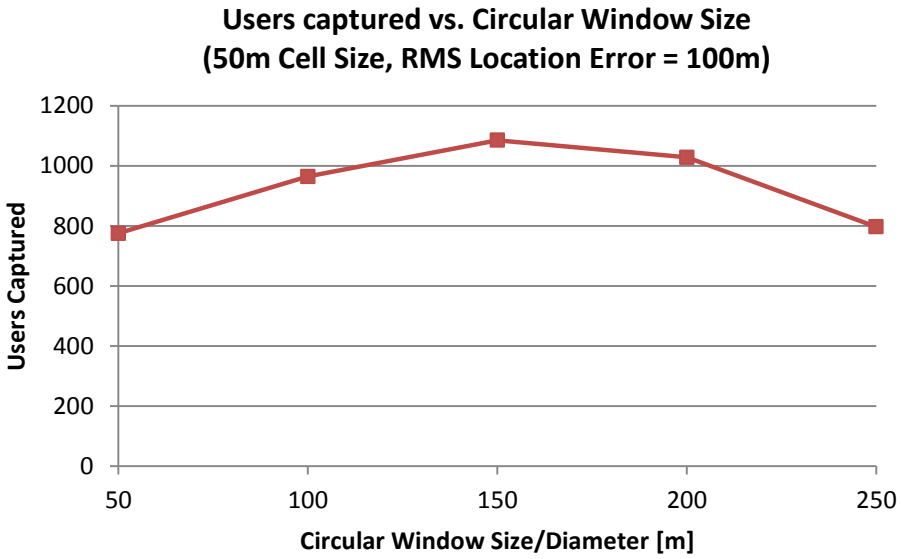

Figure 5.10 Results of initial circular window tuning runs suggesting a circular window with a diameter of 150m was most effective at locating 100x100m hotspot centres from erroneous geo-location data with an RMS location error of 100m.

The outline of the filter based Method 2, written in pseudo code is given below in Figure 5.11, with the associated parameters being given in Table 5.4.

```
initialise simulation area.
load lamppost locations.
for 1 to number of Monte Carlo runs
        distribute hotspots
        distribute users randomly within each hotspot
        apply user location errors and generate reported UE geo-locations
        apply 2D circular sliding window filter to reported user distribution
        for each potential lamppost
            evaluate potential users captured based on filtered user distribution
        end for
        for 1 to number of small cells to place
            choose and record lamppost capturing the most users
            remove users captured by chosen lamppost from surrounding lampposts
        end for
end for
```

Figure 5.11 Pseudo code for small cell location Method 2.

Table 5.4 Small Cell Placement: Method 2 Parameters

Parameter	Value
Name	Method 2: 2D circular filter approach
Monte Carlo runs per parameter set	100
Hotspots per run	50
Users per hotspot	500
Fixed cell sizes evaluated	50, 100, 200m
UE location RMS errors evaluated	0, 25, 50, 75, 100, 125, 150, 175, 200m

Examples of the output of Method 2's sliding 2D circular window filter for user location distributions with RMS location errors of 50, 100 and 200m are shown below in Figures 5.12 to 5.14. Clearly it can be seen that as the RMS location error increases so does the accuracy at which Method 2 is able to locate the centre of the traffic hotspot.

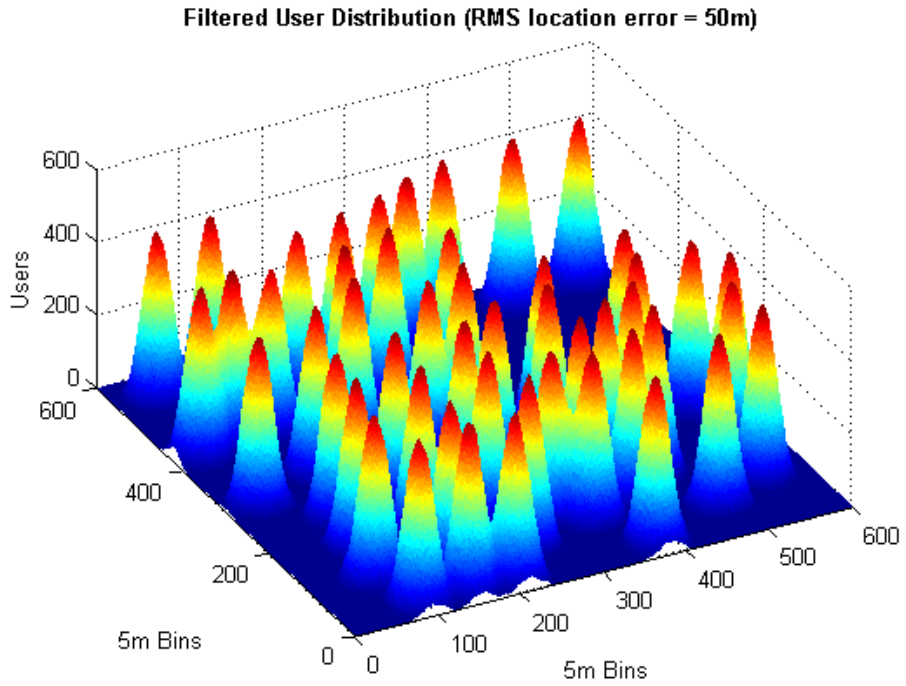

Figure 5.12 Method 2's circular sliding filter results (RMS location error = 50m).

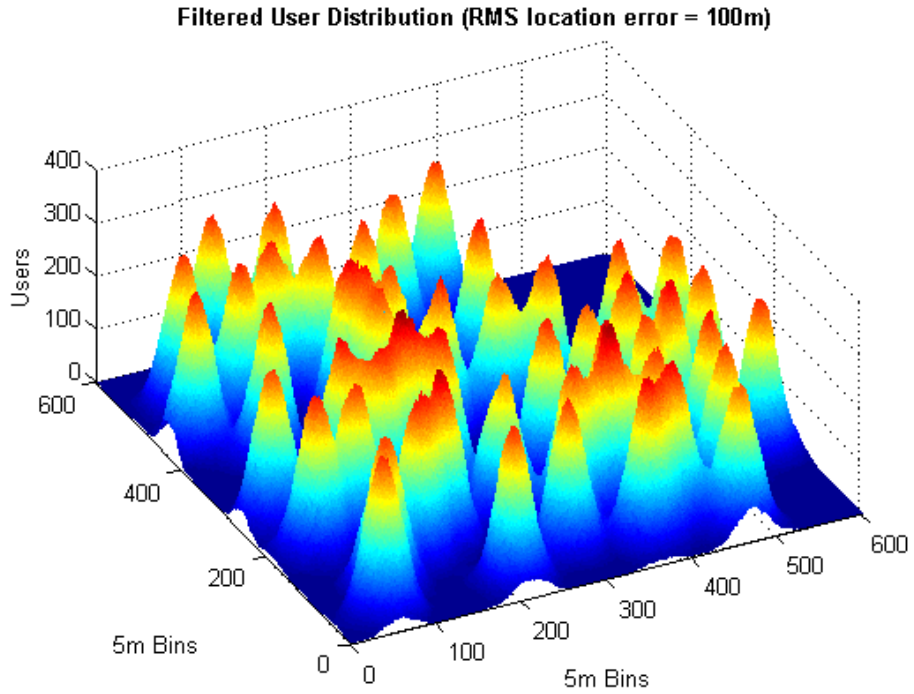

Figure 5.13 Method 2's circular sliding filter results (RMS location error = 100m).

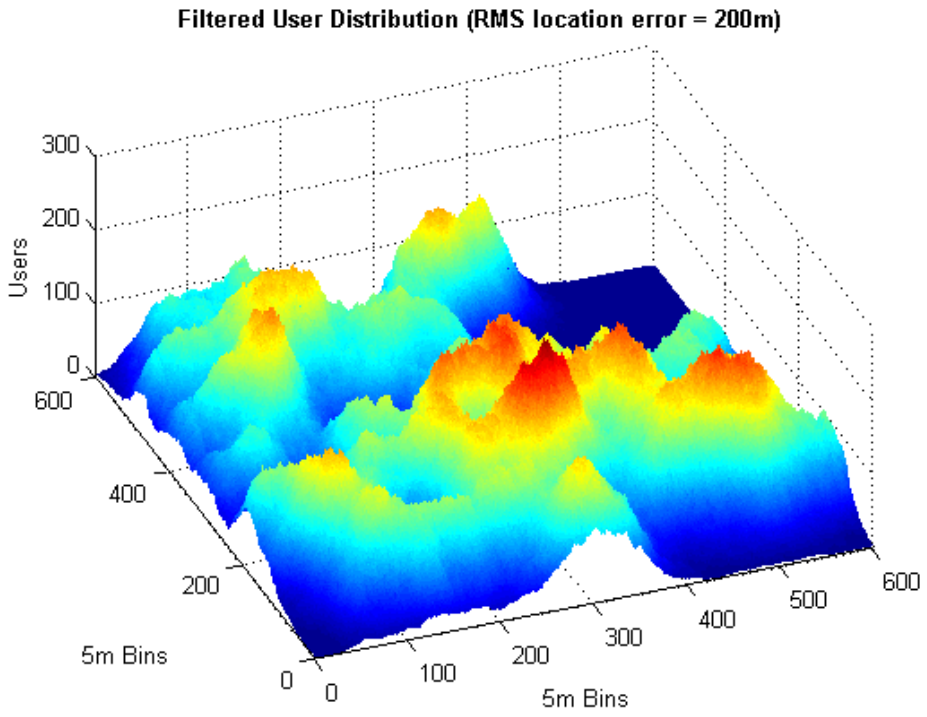

Figure 5.14 Method 2's circular sliding filter results (RMS location error = 200m).

5.5.4 Initial Small Cell Placement Method Results

Tables 5.5 and 5.6 show the total users captured across the whole simulation area for the two placement methods (Methods 1 & 2) considered, with varying fixed cell sizes and varying user RMS location errors applied. These results are also shown graphically in Figure 5.15.

Table 5.5 Total Users Captured by Placement Method 1.

	RMS Location Error								
Microcell Radius	0m	25m	50m	75m	100m	125m	150m	175m	200m
50m	15067	14610	13600	11610	9010	7114	5220	4138	3030
100m	23952	23913	23870	23760	22510	19456	17180	15067	12970
200m	24782	24702	24651	24662	24618	24124	23573	22459	21655

Table 5.6 Total Users Captured by Placement Method 2.

	RMS Location Error								
Microcell Radius	0m	25m	50m	75m	100m	125m	150m	175m	200m
50m	15302	14373	13940	12901	10916	7945	5843	4659	3897
100m	24463	24377	24311	24211	23481	20728	18284	16103	14208
200m	24911	24897	24841	24788	24740	24673	24550	24172	23840

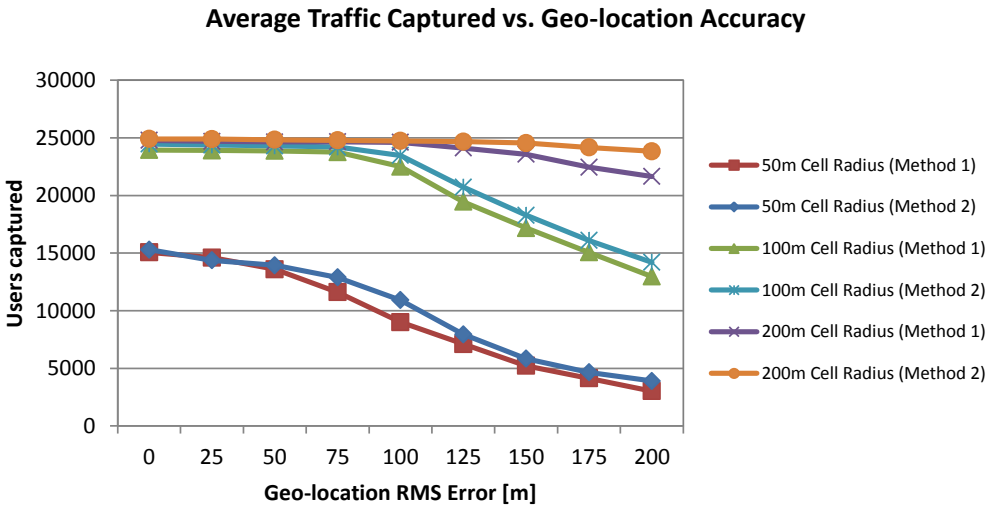

Figure 5.15 Average traffic captured by methods 1&2 for varying cell radii and RMS location errors.

What is clear from the initial placement results is that there is little difference between the post by post approach of Method 1 and the 2D circular filter based approach of Method 2, although Method 2 does slightly outperformed Method 1 in all cases. This is not surprising since both methods are in effect working to the same principle of evaluating the reported UEs within a particular radius around each post, Method 1 doing this explicitly and Method 2 doing this using a filter and then post selection method.

What is perhaps more interesting to consider from these initial results is the relationship between users captured, cell size and RMS location error. The first thing to note here is that for the simulation area under study an assumed 50m cell radius is not capable of capturing all the available users and this should not be too much of a surprise given the hotspot areas are 100mx100m (10,000m^2) and the 50m radius small cell area is 7,854m^2. Therefore even perfect placement at the centre of every hotspot was possible, a 50m radius small cell would only be capable of capturing approximately 19,500 users out of a potential 25,000 users assuming uniform user distribution across each hotspot. However both methods were

limited by the lamppost that they can chose to address the hotspots, then this lack of being able to place a small cell at the centre of each hotspot further reduces the total number of users captured by the fifty 50m radius small cells for both methods to at best around 15,000 users.

Therefore for the smallest cell radius of 50m considered, even with perfect user location knowledge (RMS location error = 0m), both placement methods are only able to capture around 15,000 users. As the RMS location error increases the users captured decreases and at an RMS location error of 200m, Methods 1 and 2 are only able to capture around 3,000 and 3,900 users respectively equating to just 12% and 16% of the users available within the hotspot areas. Clearly at this low yield small cell deployment would not be cost effective given the typical cost of a lamppost mounted small cell deployment highlighted in the introduction to this chapter.

For the larger cell radius of 100m, for small RMS location errors (0-75m), 50 cells are able to capture almost 100% of the available users. Again a small reduction is seen because of inability to place small cells precisely at the hotspot centre because of the limited locations of the available lampposts. For higher RMS locations errors beyond 75m, the total uses captured by the small cells then decreases with increasing location error until at an RMS location error of 200m Methods 1 and 2 capture 12,970 (52%) and 14,208 (57%) of users respectively.

For the largest cell radius considered (200m), both methods capture over 98% of the potential hotspot users for RMS location errors from 0 to 125m, showing that the inaccuracy of the hotspot location method is compensated by the larger cell size and that even with an RMS location error of 200m, both methods capture over 85% of the hotspot users.

Studying the results as a whole what does become clear is that the effectiveness of small cells to capture traffic is greatly dependent on the accuracy of the user location information, however this can also be offset to some degree by increasing the size of the small cell. For the simulation setup considered there appears to be a direct correlation between the size of the cell, and the RMS location error at which the traffic captured by the two placement methods considered begins to decrease, i.e. for a 50m cell radius, beyond an RMS location error of 50m and for a 100m cell radius, beyond an RMS location error of 100m – and this also appears true for the 200m case.

5.5.5 Initial Small Cell Placement Method Summary

In summary, for the simulation assumptions presented, the initial results suggest that there is very little performance difference between Methods 1 and 2. However, for a typical UE RMS location error of between 75-125m, a cell size at least twice the radius of the hotspot radius is required to ensure sufficient capture of hotspot users.

5.6 Increasing the Accuracy of Small Cell Placement Using a Simple RF Fingerprinting Method

As shown in the previous section, there appeared to be little difference between the results of the small cell placement Methods 1 & 2. Therefore further enhancements were explored to increase the accuracy of Method 2 to detect and locate the centre of a traffic hotspot even when doing so using very inaccurate (>150m RMS location error) reported UE locations.

As mentioned earlier one promising technique now being proposed within the literature to geo-locate users is RF fingerprinting and this section presents the findings of the work undertaken to enhance the filter based approach of Method 2 with simple RF fingerprinting.

The problem that was being experience by the original Method 2 for high RMS location errors (>100m) was that the output of the 2D circular filtering did not have clearly defined peaks unlike the more favourable case for the lower RMS values (Figures 5.12 and 5.13), and therefore the estimation of the centres of the traffic hotspots was much more difficult. This obviously was due to the spreading of the reported UE locations away from each hotspot with increasing RMS location error. Therefore in order to have better defined peaks in the output of the 2D circular filter so that Method 2 could better estimate the centre of the hotspot, a reduction, or correction, of this UE location spreading was required.

Since the majority of 2G/GSM, 3G/WCDMA and 4G/LTE UE measurement reports also contain data such as Cell ID., Frequency, Base Station Identity Code (BSCI) for 2G/GSM, Scrambling Code (SC) information for 3G/WCDMA, Physical Cell ID (PCI) for LTE as well as signal level measurements of the best serving and the neighbouring cells seen by the UE, then further information other than the reported location is available on which to base a better estimate of the UEs location than the reported geo-location alone. This extra information can be used to discard UE location reports that clearly suggest the UE is somewhere it cannot be given the reported RF measurements, or it can be used to correct or provide a better estimate of the likely position of a UE whose reported location does not match its associated RF measurements.

5.6.1 Method 2+RF: Combining 2D Circular Filtering with RF Fingerprinting

An enhanced method (Method 2+RF) was therefore developed based upon a method of discarding UE location reports where the reported location did not match with the associated RF measurements. An RF fingerprint table was constructed for each location within the simulation area using coverage plots produced by the Network Simulator. It was assumed that the construction of such a table would be possible in a reality using a predicted multi-cell 3D RSCP fingerprint matrix generated from a commercial RF planning tool combined

over time with UE measurement reports known to have very accurate location information to correct any discrepancies between the planned and actual coverage arrays, similar to that proposed in [94]. The 3D RSCP fingerprint matrix generated by the Network Simulator contained an RF fingerprint for each 5x5m bin, an example of such a fingerprint generated by the simulation tool is given below in Table 5.7.

Table 5.7 Example RF Fingerprint Entry in the 3D RSCP Fingerprint Matrix.

Serving Cell	Cell Scrambling Code	Cell RSCP [dBm]
1st	49	-85.52
2nd	47	-94.51
3rd	33	-95.80
4th	34	-95.97
5th	58	-98.65

In order to discard erroneous user locations from the *user distribution matrix* used as input into the 2D circular filter process, each UE measurement report was given a *location reliability rank* based upon the comparison of its reported location and best serving cells against the 3D RSCP fingerprint matrix as follows:

> If the UE measurement report's best serving cell matched the best serving cell stored in the 3D RSCP fingerprint matrix for the location reported in the UE measurement report then the UE measurement was given a *location reliability rank* of 1.
>
> If the UE measurement report's 1st and 2nd best cells matched the 1st and 2nd best cells stored in the 3D RSCP fingerprint matrix for the location reported in the UE measurement report then the UE measurement was given a *location reliability rank* of 2.
>
> If the UE measurement report's 1st, 2nd and 3rd best cells matched the 1st, 2nd and 3rd best cells stored in the 3D RSCP fingerprint matrix for the location reported in the UE measurement report then the UE measurement was given a *location reliability rank* of 3.
>
> If the UE measurement report's 1st, 2nd, 3rd and 4th best cells matched the 1st, 2nd, 3rd and 4th best cells stored in the 3D RSCP fingerprint matrix for the location reported in the UE measurement report then the UE measurement was given a *location reliability rank* of 4.

If the UE measurement report's 1st, 2nd, 3rd, 4th and 5th best cells matched the 1st, 2nd, 3rd, 4th and 5th best cells stored in the 3D RSCP fingerprint matrix for the location reported in the UE measurement report then the UE measurement was given a *location reliability rank* of 5.

It should be noted that only the order of the cells and not the actual RSCP levels were used in this case to perform the fingerprint look up and location report ranking. The reason for this was that it was felt that because of shadow fading and inaccuracies of the RSCP values actually reported by the UE (3GPP TS 25.133 [96] specifies a +/- 11dB absolute accuracy requirement and a +/- 3dB relative requirement) then the RF fingerprinting method proposed here was more likely to be a practical reality if it only considered the relate rankings rather than absolute RSCP levels. That is not to say that methods based on both cell ranking and absolute or relative RSCP levels are not possible and this is definitely an area worthy of further investigation.

Having given each UE location report a *location reliability rank*, it was then possible to build up user distribution Xmaps using only measurement reports with particular location reliability rankings. For example shown in Figures 5.16 to 5.19 are examples of user distributions Xmaps constructed from the same reported UE locations but with different location reliability rankings used to filter the users used to create the users distribution Xmap. As can be seen clearly from these examples the higher the location reliability ranking threshold applied to the reports the much greater the location accuracy becomes of the retained samples.

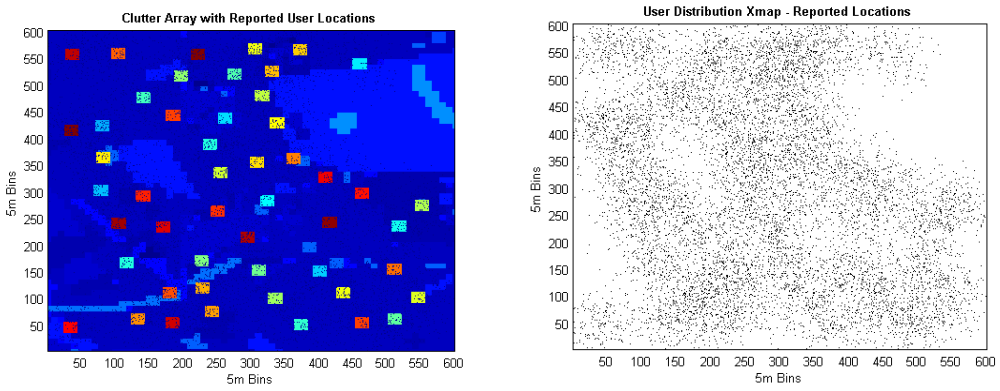

Figure 5.16 Left-hand side: Original Hotspot location with reported UE locations. Right-hand side: All reported UE locations. (RMS location error = 200m).

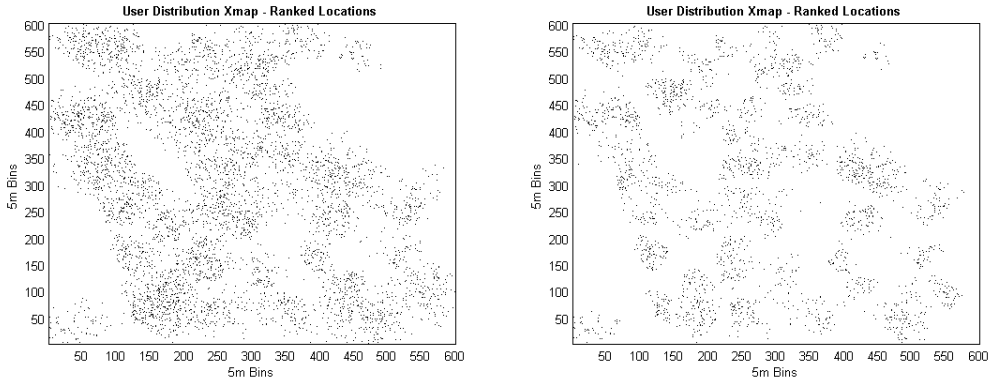

Figure 5.17 Left-hand side: Only UE reports with RF fingerprint reliability rank ≥ 1 retained. Right-hand side: Only UE reports with RF fingerprint reliability rank ≥ 2 retained. (RMS location error = 200m).

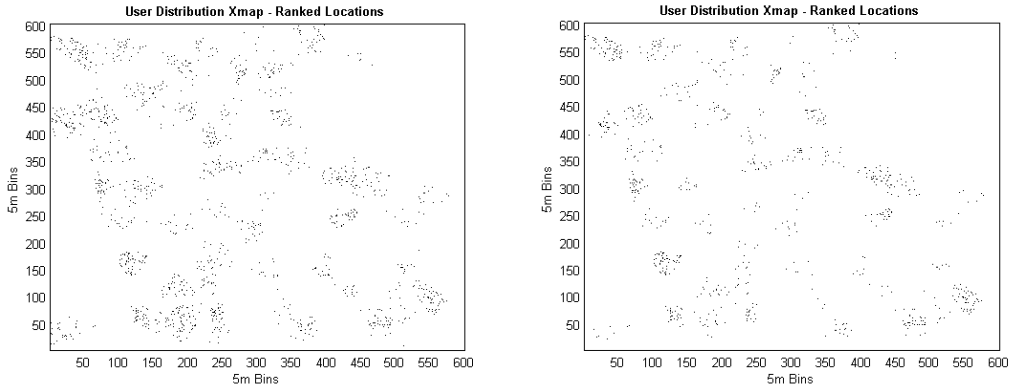

Figure 5.18 Left-hand side: Only UE reports with RF fingerprint reliability rank ≥ 3 retained. Right-hand side: Only UE reports with RF fingerprint reliability rank ≥ 4 retained. (RMS location error = 200m).

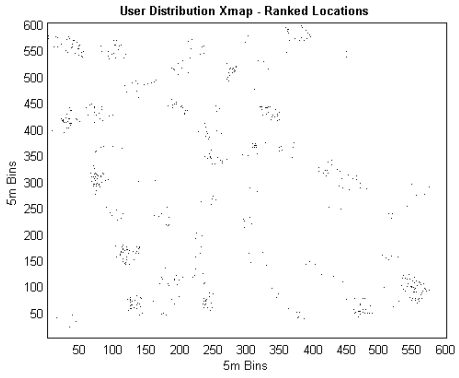

Figure 5.19 Reported UE locations (RMS location error = 200m), only UE reports with RF fingerprint reliability rank = 5 retained.

5.6.2 Placement Results using Method 2+RF: Combining 2D Circular Filtering with RF Fingerprinting

As stated previously the aim of applying the RF fingerprinting technique to the user locations was to provide the 2D circular filter with much more reliable UE locations in order for it to better estimate the location of the traffic hotspots. Shown in Figures 5.20 and 5.21 are the output from the 2D circular filter process before and after applying the RF fingerprint location reliability ranking prior to application of the filter. As can be see applying the user location reliability ranking prior to the 2D circular filtering process certainly produces better defined peaks in the output of the filtering process and as will be shown allows the lamppost placement algorithm to place lampposts much closer to the traffic hotspots than was the case without RF fingerprinting being applied.

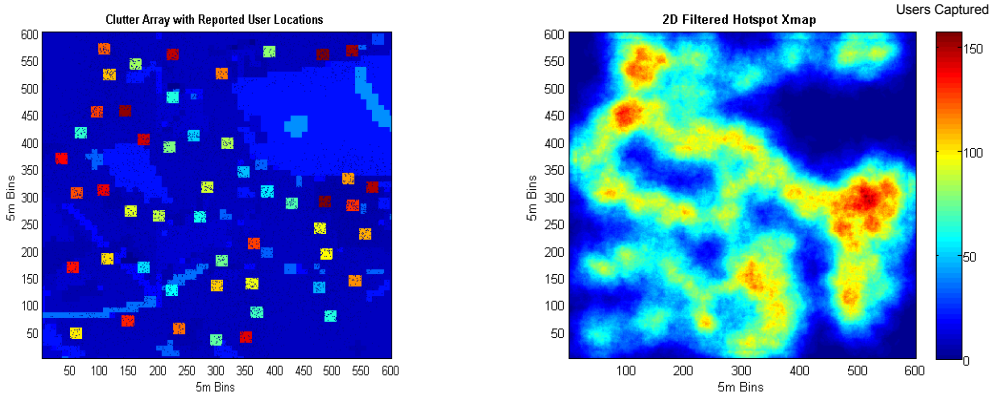

Figure 5.20 Original hotspot locations and circular sliding filter results without RF fingerprinting applied (RMS location error = 200m).

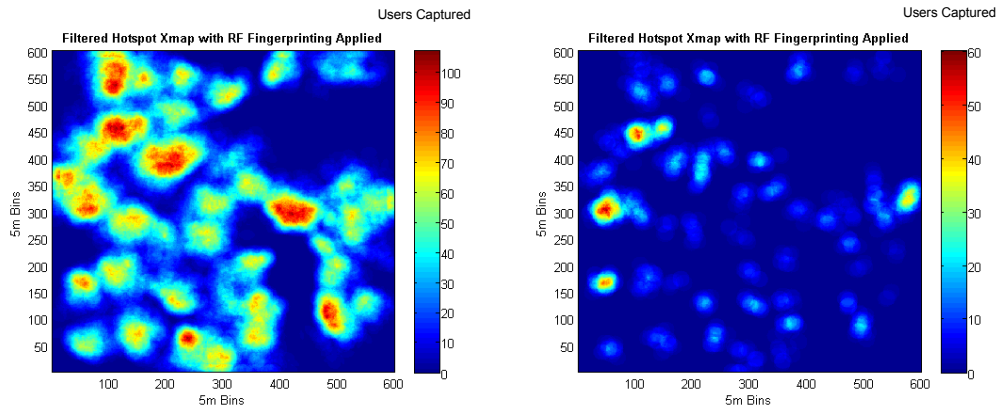

Figure 5.21 Circular sliding filter results after RF fingerprinting applied (RMS location error = 200m). Reliability rank ≥ 1 applied (left-hand figure) and reliability rank = 5 applied (right-hand figure).

Further Monte Carlo simulation runs were performed with placement Method 2+RF in order to evaluate whether the RF fingerprinting provided significant gains over the previous Methods 1 & 2. Shown in Figures 5.22 and 5.23 are the detailed results for the 100m cell radius case for RMS location errors of 150m and 200m . As can be seen from the figures the RF fingerprinting technique definitely improves the ability of the placement algorithm to estimate the location of the hotspots especially for an RMS location error of 200m. Also it can be seen that only considering the UE reports with a reliability rank = 5 provides the greatest gains in terms of the users captured per post by the placement algorithm.

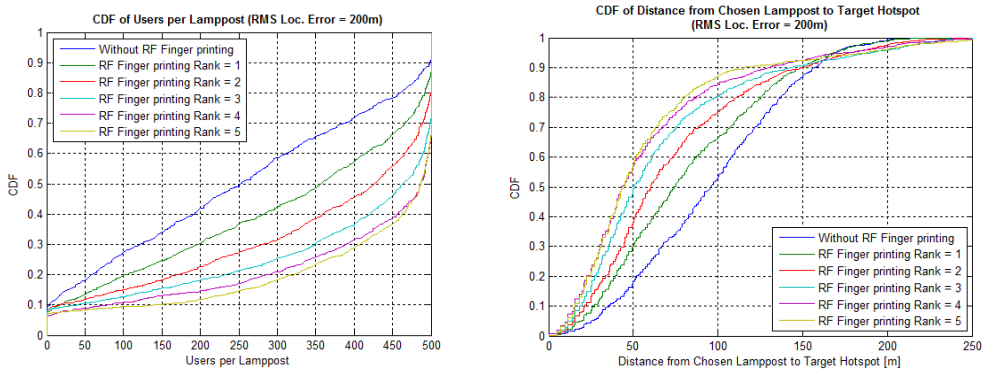

Figure 5.22 Method 2+RF results. Left-hand figure: CDF of users per Lamppost. Right-hand figure: CDF of distance from lamppost to target hotspot. (Cell radius = 100m, RMS location error = 200m).

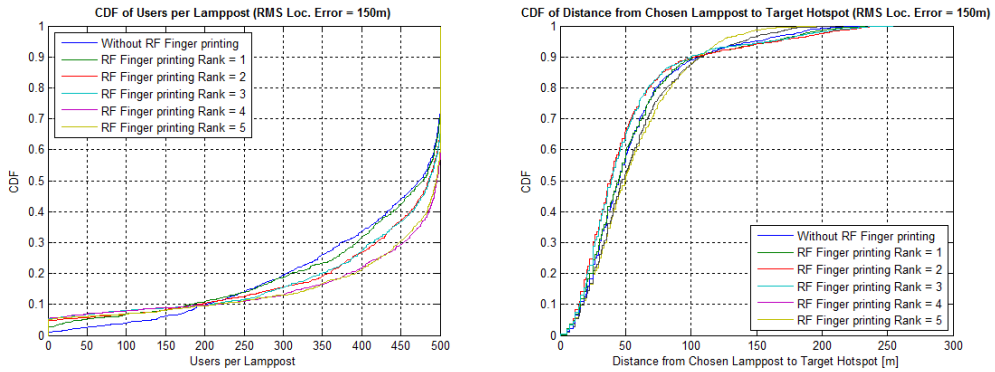

Figure 5.23 Method 2+RF results. Left-hand figure: CDF of users per lamppost. Right-hand figure: CDF of distance from lamppost to target hotspot. (Cell radius = 100m, RMS location error = 150m).

The overall results for Method 2+RF applied to all three small cell radii considered are given below in Table 5.8 and represented graphically in Figure 5.24. Starting with the 200m cell radius case, as seen for both Methods 1, 2 and 2+RF cells of this size tend to capture the majority of traffic because of their size compared to the inaccuracy of the hotspot location estimation. Although Method 2+RF does provide a gain over Method 1 at the largest RMS

location error of 200m, it does not provide any gain over Method 2, and therefore it is concluded that no further gains are seen when applying RF fingerprinting compared to Method 2 in the case of the placement of 200m radius small cells.

However for the cases of 50 and 100m radii small cell placement, whilst it is seen that for low RMS location error values Method 2+RF provides little benefit over that of Method 1 for larger RMS location errors of 100m or greater significant captured traffic gains as high as 139% are possible especially for the largest RMS location error of 200m.

Table 5.8 Method 2+RF (Reliability Rank=5) overall results showing traffic gains over Method 1.

	RMS Location Error									
	0m		50m		100m		150m		200m	
Microcell Radius [m]	Users Served	% Gain over Meth. 1	Users Served	% Gain over Meth. 1	Users Served	% Gain over Meth. 1	Users Served	% Gain over Meth. 1	Users Served	% Gain over Meth. 1
50	15295	2%	13941	3%	10916	21%	8187	57%	7237	139%
100	24457	2%	23937	0%	22852	2%	21288	24%	20209	56%
200	24951	1%	24797	1%	24716	0%	24533	4%	23826	10%

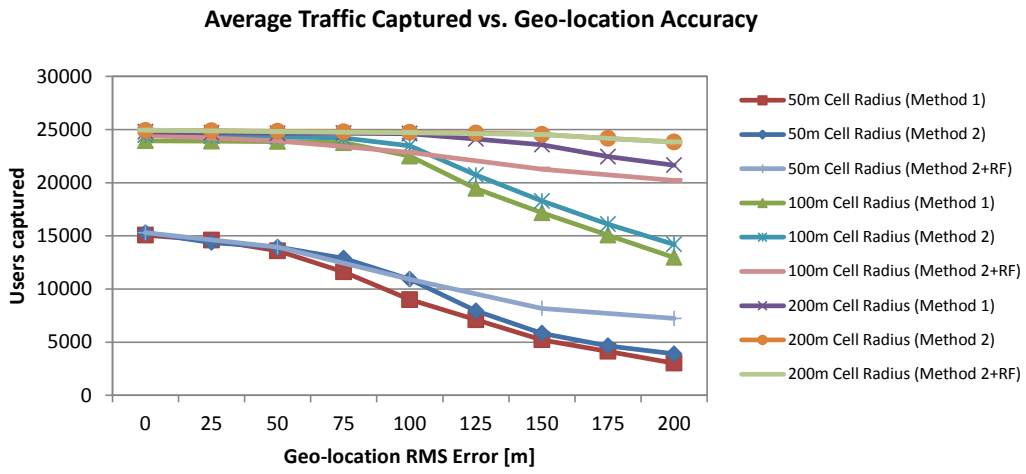

Figure 5.24 Method 2+RF (Reliability Rank=5) overall results compared against those of placement Methods 1 & 2.

5.6.3 Small Cell Placement Enhancement Through RF Fingerprinting Summary

This section has investigated whether RF fingerprinting can be used to increase the accuracy of small cell placement based upon unreliable UE geo-location information in a realistic central London small cell network. A very simple RF fingerprinting technique has been proposed to determine the reliability of each UE location report and give each of them a reliability ranking depending on a match between the reported best servers and a reference list of best servers stored in an pre-defined RF fingerprint matrix.

It has been shown that when addressing 100x100m traffic hotspots using small cells with radii of 50 and 100m, the additional gains provided by the simple RF fingerprinting technique are significant for UE reports with large RMS locations errors and that in these cases traffic gains of up to 56% (100m small cell radius) and 139% (50m small cell radius) are possible through the more accurate estimation of the traffic hotspot location using this technique.

In terms of further work, it should be noted that so far only RF fingerprinting techniques based on the order of the best servers reported by the UE were considered, and it is possible that further gains are possible by also considering the absolute or relative strengths/quality of the best servers' signal levels. Also the RF fingerprinting was used to merely exclude UE location reports deemed to be too inaccurate to be used in the hotspot estimation calculation, but there may also be gains to be had by attempting to correct inaccurate UE location reports and adding these corrected reports to the reliable UE location reports prior to the hotspot estimation 2D circular filter algorithm.

5.7 Small Cell Size Determination from Geo-Located UE Measurement Reports

Up until now this chapter has assumed fixed small cell radii of 50, 100 and 200m and as mentioned earlier such an approach may be valid if the small cell is being deployed on a dedicated carrier frequency and the small cell's range is noise limited rather than interference limited. However in the case where the small cell layer must share a carrier frequency with the macrocell layer then the potential cell size of the small cell will be very much dependent on the amount of interference received from the macrocell layer at the small cell's proposed location.

This section proposes a method to estimate the potential cell size of a small cell when deployed on a shared carrier frequency with the macrocell layer through the spatial processing of geo-located UE measurement reports. The section considers how the accuracy of the UE location reports may affect the accuracy of the cell size estimation of the small

cell and to do this it proposes a method to estimate the macrocell's coverage across areas for which there are no UE measurement reports available. Finally the section considers the gains possible by having an approximate estimation of the cell size when attempting to place small cells at traffic hotspots in a central London network.

5.7.1 Macrocell Coverage Estimation & RSCP Sample Interpolation Methods

In order to calculate the potential cell size of a small cell deployed on a shared carrier frequency a good estimation of the interference generated by the existing macrocells and small cells at and around the proposed small cell's location is required.

As the small cells could be placed anywhere, a cell size estimation maybe required in an area where only a few measurement reports from the macrocell are available. Therefore a method is required to interpolate between macro UE measurement reports to ensure that a macrocell RSCP value is available at all locations to enable a small cell size estimation at these locations.

Since many 2D interpolation methods already exist and are easily implemented in a MATLAB or similar, a number of these existing methods [97] were studied to see which provided the best RSCP estimation across all locations within the Network Simulator without UE measurement reports. To do this the Network Simulator was used to simulate the collection of 1,000, 5,000 and 25,000 geo-located UE measurement reports across the Kensington simulation area (bin size = 5x5m) for the macrocell layer with the UE location reports having RMS location errors of 0, 50, 100, 150 and 200m. These reports were then used to create an partial RSCP Xmap and then the standard 2D grid interpolation methods available in MATLAB were applied to the partial Xmaps to determine which method of interpolation provided the best RSCP estimation for the locations without measurement reports. This was performed by comparing the interpolated Xmaps produced against the original RSCP raster predicted by the Network Simulator for the different RMS location errors considered. Shown below in Figures 5.25 to 5.27 are graphs showing the RMS error of the RSCP estimation for the four 2D interpolation methods and UE RMS location errors considered for the 1,000, 5,000 and 25,000 user cases. Here it can be seen that the "Natural Neighbour" method of 2D interpolation provided the most accurate RSCP estimation across all RMS location error values and all user cases and therefore was method of 2D interpolation chosen as the interpolation method to be used in the small cell size estimation method described in the next sections.

Shown in Figures 5.28 to 5.30 are examples of interpolated RSCP Xmaps using the chosen Natural Neighbour method of 2D interpolation between UE measurement reports.

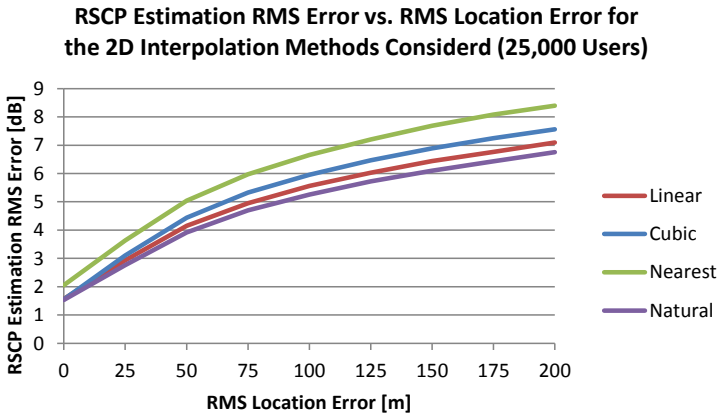

Figure 5.25 RSCP estimation RMS error for the four MATLAB 2D interpolation methods considered (25,000 users).

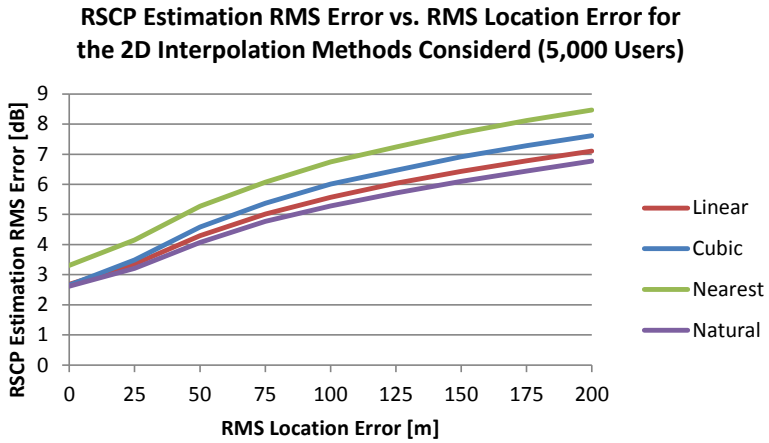

Figure 5.26 RSCP estimation RMS error for the four MATLAB 2D interpolation methods considered (5,000 users).

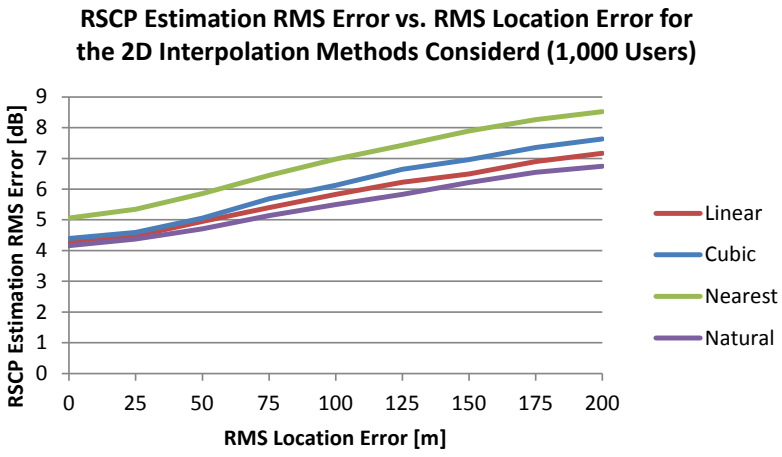

Figure 5.27 RSCP estimation RMS error for the four MATLAB 2D interpolation methods considered (1,000 users).

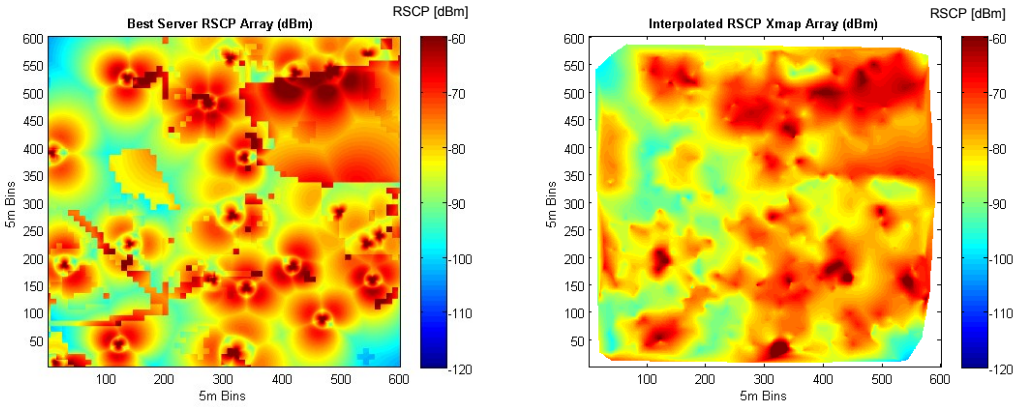

Figure 5.28 Original Best Server RSCP array generated by simulator and interpolated RSCP Xmap (RMS location error = 50m, 1,000 users).

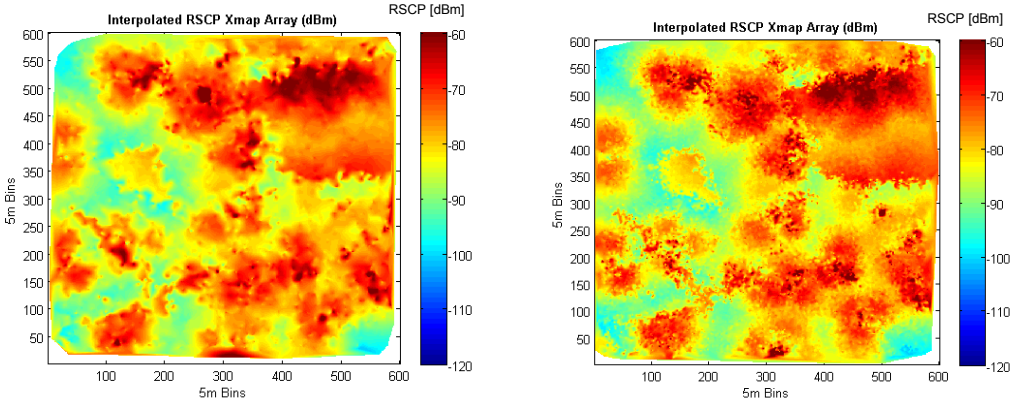

Figure 5.29 Interpolated RSCP Xmaps. Left-hand figure (RMS location error = 50m, 5,000 users). Right-hand figure (RMS location error = 50m, 25,000 users).

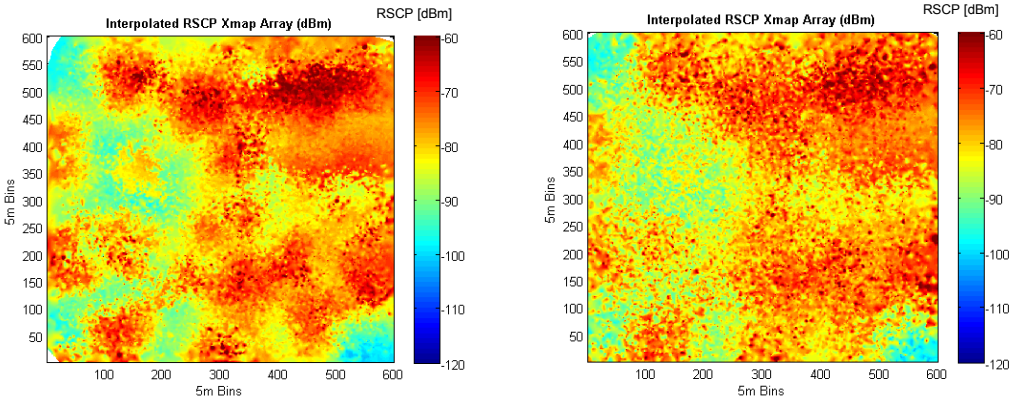

Figure 5.30 Interpolated RSCP Xmaps. Left-hand figure (RMS location error = 100m, 25,000 users). Right-hand figure (RMS location error = 200m, 25,000 users).

5.7.2 Simple Small Cell Size Estimation Method

Given the estimation of the macrocell coverage across the simulation area the next stage was to find a method of estimating the small cell's size at any given point within the simulation area. To do this the two assumptions were made, the first was that handover between the macrocell and the small cell would occur at a location where

$$RSCP_{Small\_Cell} = RSCP_{Macro\_Cell} \tag{5.6}$$

where

$RSCP_{Small\_Cell}$ is the RSCP of the small cell.

$RSCP_{Macro\_Cell}$ is the RSCP of the best serving macrocell.

And the second assumption was that the small cell size would be based upon the average macro RSCP level across an area within a 50m radius from the potential small cell location rather than using a single point value at the proposed small cell's location.

The microcell propagation model given in equation (5.1) was then used to generate a lookup table (Table 5.9) of small cell sizes for the different average macrocell RSCP interference levels and small cell output powers considered. The small cell radii estimates in this table are also shown graphically in Figure 5.31.

A snap shot of the Network Simulator employing the simple small cell size estimation method for the case of small cells with output power = +30dBm is shown in Figure 5.32. The orange areas are the small cells' coverage area estimates using knowledge of the macrocell RSCP and the yellow areas indicate a fixed cell radius estimate of 50m. Here it can be clearly seen that the Network Simulator is estimating different cell sizes for the different locations chosen by the placement algorithm depending on the macrocell interference received at that particular location. In some cases the estimated cell sizes are much greater than 50m, whilst in others they are significantly smaller than 50m.

This example highlights the need for some method of small cell size estimation, whether it be a simple method such as the one presented here, or a much more complex pixel by pixel evaluation method to accurately predict the small cell's best server area – another possible area for future research.

Table 5.9 Small cell radius estimation lookup table given average macrocell RSCP level using 3GPP 25.814 microcell propagation model.

Small Cell Radius Estimation Given Average Macrocell RSCP Levels [m]						
Average Macrocell RSCP Level [dBm]	Microcell TX Power [dBm]					
	10	15	20	24	30	37
-100	50	60	75	90	115	155
-95	40	50	60	70	95	122.5
-90	32.5	40	50	60	75	100
-85	27.5	32.5	40	47.5	60	82.5
-80	22.5	27.5	32.5	40	50	67.5
-75	17.5	22.5	27.5	32.5	40	55
-70	15	17.5	22.5	25	32.5	45
-65	12.5	15	17.5	22.5	27.5	35
-60	10	12.5	15	17.5	22.5	30
-55	7.5	10	12.5	15	17.5	25
-50	5	5	10	12.5	15	20
> -50	0	0	0	0	0	0

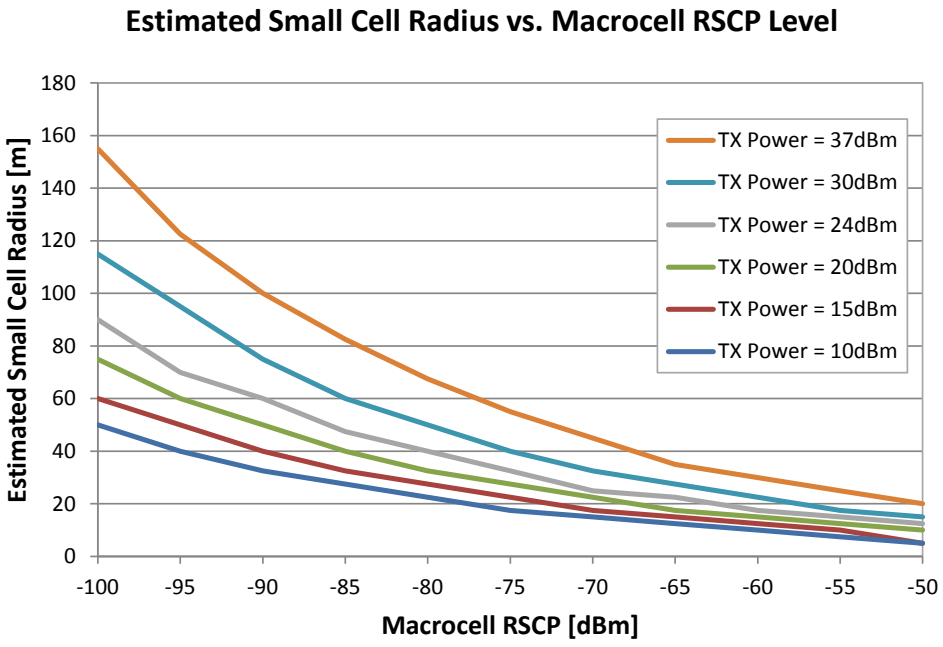

Figure 5.31 Estimated small cell size given macrocell RSCP level using the 3GPP 25.814 microcell propagation model for different small cell transmitter powers.

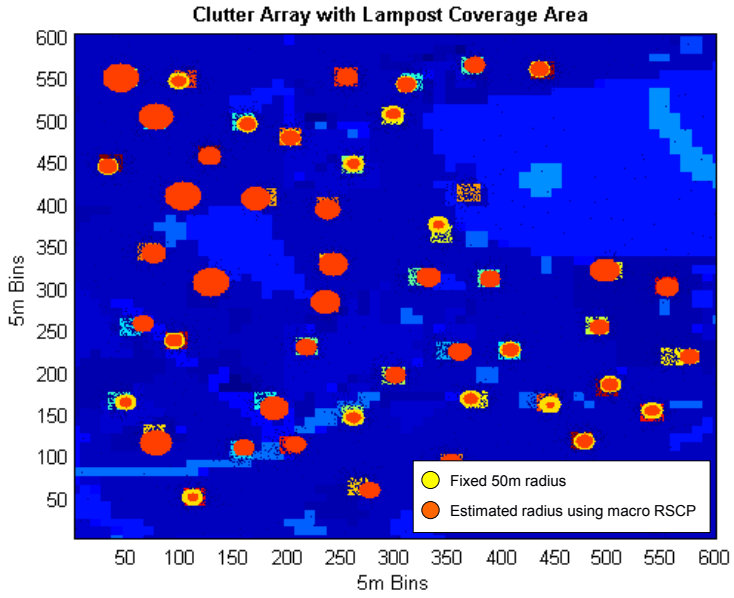

Figure 5.32 Example of estimated small cell sizes using macrocell RSCP level for lamppost mounted small cells with a transmitter power of 30dBm.

5.7.3 Accuracy of Simple Small Cell Size Estimation Method for Increasing UE RMS Location Errors

Using this simple look up method of small cell size estimation a number of runs were performed to study the accuracy of the simple cell size estimation method as the reported UE measurement RMS location error was increased. This was done by comparing the cell size estimated using the interpolated RSCP Xmap method to a cell size estimate using the actual original RSCP coverage array generated by the Network Simulator.

Shown below in Figure 5.33 are the results from the cell size accuracy simulation runs. The CDF curves show the absolute cell size estimation errors for the different UE RMS location errors and UE counts considered. The steps in the curves are due to the discrete cell size estimates used in the cell size look up table (Table 5.9). Whilst this could have been avoided by deriving a cell size lookup function, rather than using a discrete valued lookup table, the ultimate aim of the cell size estimation work was to estimate whether a lamppost deployment was viable, i.e. the chosen lamppost provided worthwhile (>50m radius) coverage rather than whether its radius was precisely 64m or 65m.

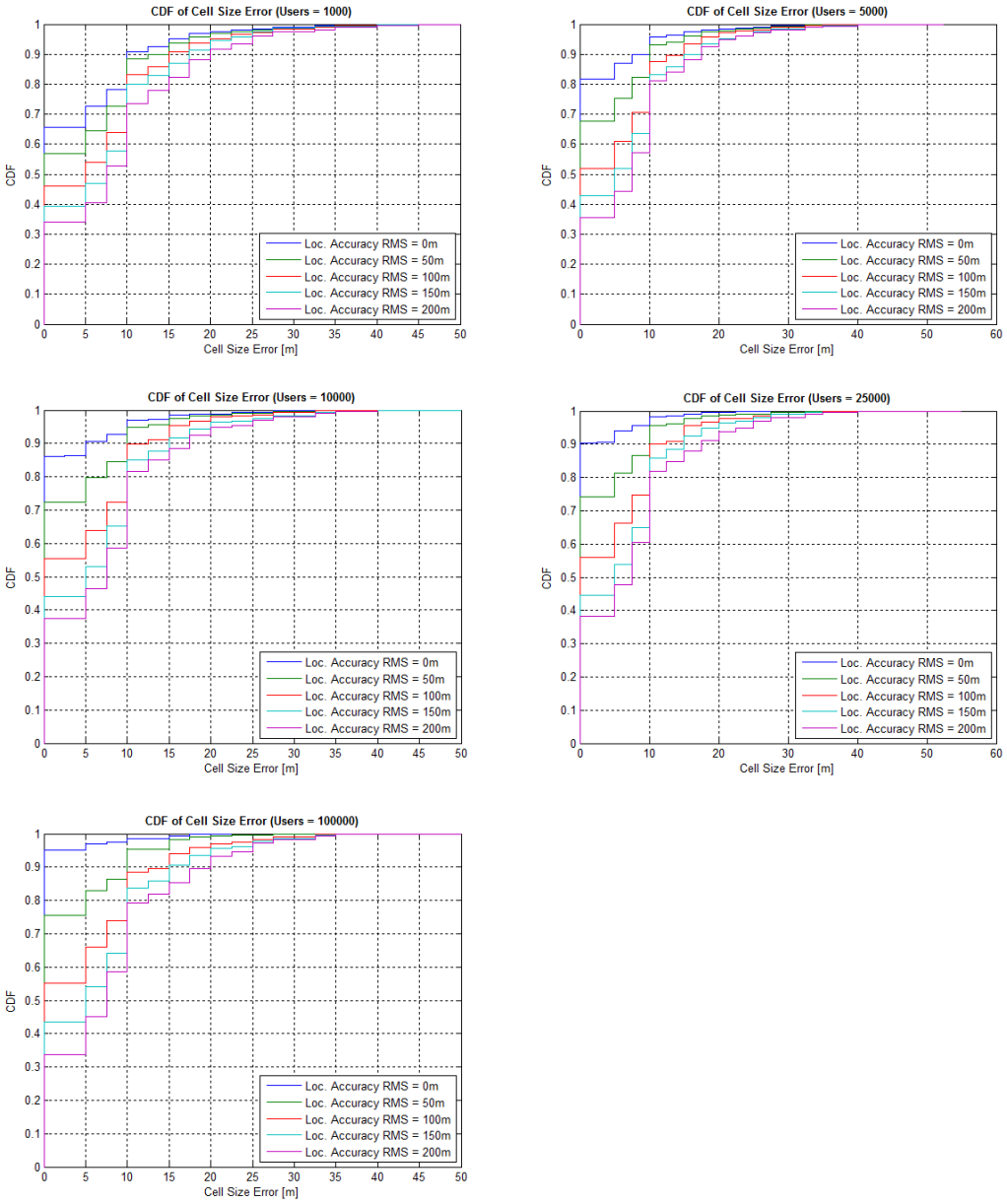

Figure 5.33 CDF curves of absolute cell size estimation errors for the different UE RMS location errors and UE counts considered.

As expected the results show that as the RMS location error increases the reliability of the cell size estimates decreases and also that the greater the number of measurement reports available across the macrocell coverage area, the more reliable the cell size estimates are. Even so, for a moderate number of UE measurement reports, 10,000 for example and typical RMS location error of 100m, over 90% of cell size estimates using the interpolated RSCP Xmap are within 10m of the cell size estimate performed with perfect knowledge of the macrocell's RSCP and over 95% of cell size estimates using the interpolated RSCP Xmap are within 15m of the cell size estimate performed with perfect knowledge of the macrocell's RSCP.

It was therefore concluded that the proposed small cell size estimation method works well with unreliable UE location information. The method appears to provide a sensible first approximation of small cell size and with typical UE RMS location errors achieves a cell size estimation accuracy of +/- 15m, 95% of the time.

Whilst more complex methods of evaluating the RSCP delta between the macrocell and the small cell layers on a pixel (bin) by pixel basis are possible and would lead to non-circular small cell coverage areas, for this approach to be effective it would also require an equally reliable small cell tuned propagation model or ray tracing techniques to be employed to accurately predict the coverage of the proposed small cell.

Given that the aim here was merely to give a red/green/amber indication of whether a small cell was viable at a particular location given real UE measurement reports for the macrocell within the vicinity of the proposed small cell location, it is concluded that the proposed method achieves this goal.

5.7.4 Benefits of Estimating Small Cell Size When Choosing Small Cell Locations

This section builds on much of the previous work within this chapter to show by example the benefits of being able to accurately estimate the location of the traffic hotspots, chose the closest lamppost to this hotspot on which to deploy a small cell as well as being able to estimate the size of the small cell radius when the cell is deployed on the same carrier frequency as the macrocell.

For this example it has been assumed that a MNO wishes to address hotspots located in the Kensington area by deploying just 20 small cells on the lampposts that will provide the biggest offload from the macrocell layer onto the microcell layer.

Using the Method 2 placement algorithm combined with the small cell size estimation method described earlier a number of simulation runs were undertaken to show the effectiveness of being able to estimate the cell size and use this to effectively choose which lampposts would be most cost effective. Shown in Figures 5.34 to 5.36 are the CDFs for the number of users captured for the case where the fixed estimated cell radius was 50m and the RMS location error was 50, 100 and 200m. The blue curve in each graph shows the number of users the Method 2 algorithm estimates it is capturing by choosing what it thinks are the best 20 lampposts to serve the hotspots given a fixed estimated cell radius of 50m. The green curves shows the number of actual users Method 2 has captured when the small cell radii of Method 2's chosen lampposts are adjusted to take into account the co-channel interference from the macrocell layer. And finally the red curves shows the users captured by an algorithm named Method 3 which uses Method 2's placement algorithms but on top

of this takes into account the macrocell interference power to estimate the small cell's size in order to choose the most effective lampposts to maximise the users captured.

Method 2's inability to estimate the small cell size means that it blindly chooses lampposts based upon its fixed 50m cell radius assumption and in some cases this means the lampposts chosen carry very little traffic (40% of chosen lampposts carry no users for the case where the RMS location error = 200m). Whereas for the case of Method 3, since it has visibility of potential small cell size, all lampposts chosen carry some traffic and in the case where the RSM location error = 100m all chosen locations carry greater than 220 users per post and 50% of them carry greater than 400 users per post.

On average Method 3's lamppost small cells carry 420, 400 and 162 users compared to the 317, 298, and 73 users carried by Method 2's lampposts for the three RMS location error values of 50, 100 and 200m considered. This represents an increase in the effectiveness of Method 3 lampposts of 32%, 34% and 121% over Method 2 and clearly shows the need for an estimate, even an approximate one, of the small cell radius when determining the optimum location for small cells on a shared carrier frequency with the macrocell layer.

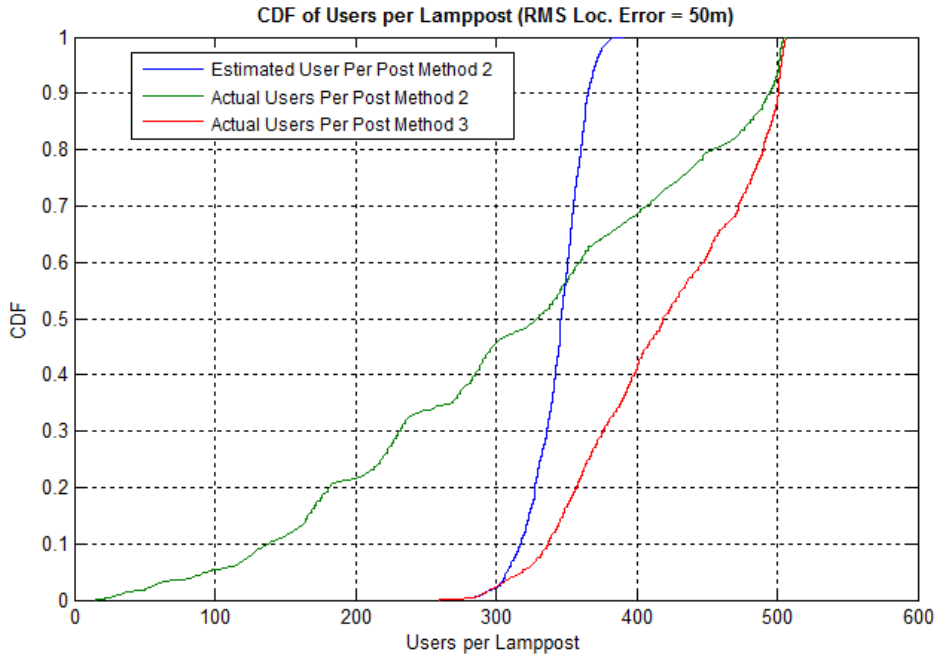

Figure 5.34 CDF curves of users captured per lamppost small cell for Method 2 and Method 3 placement algorithms. Estimated cell size = 50m, RMS location error = 50m.

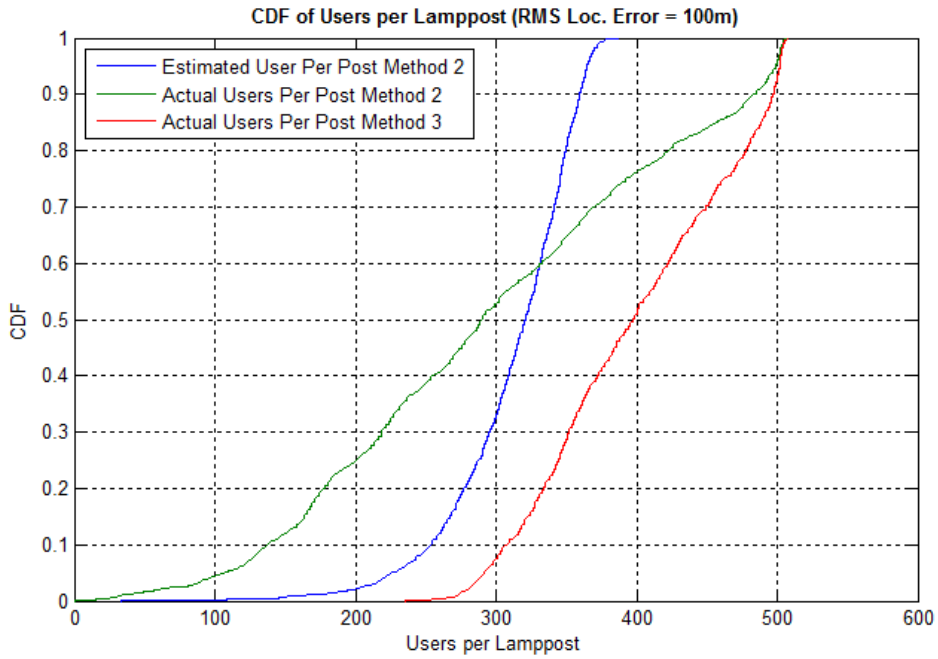

Figure 5.35 CDF curves of users captured per lamppost small cell for Method 2 and Method 3 placement algorithms. Estimated cell size = 50m, RMS location error = 100m.

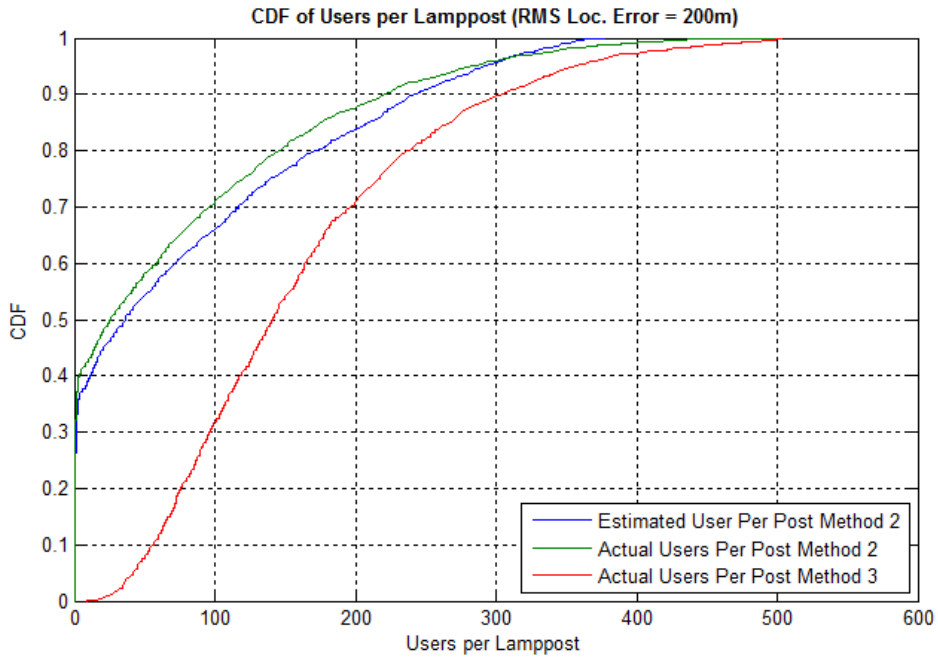

Figure 5.36 CDF curves of users captured per lamppost small cell for Method 2 and Method 3 placement algorithms. Estimated cell size = 50m, RMS location error = 200m.

5.8 Chapter Summary

This chapter has considered small cell placement and cell size estimation using geo-located UE measurement reports. A number of methods for the placement of small cells in order to maximise traffic offload from the macrocell layer have been presented and have been evaluated using enhancements made to the Network Simulator in order to model heterogeneous network deployments.

The results suggest that the effectiveness of the SON placement methods proposed are very much dependent on the accuracy of the location information contained within the UE measurement report and that if cell placement decisions are to be effective based upon UE measurement reports with very inaccurate location information, either an increased cell size or some form of location report cleansing is required. In this case the cleansing has been achieved through a proposed simple RF fingerprinting technique which has been shown to be very effective at locating hotspot locations even at very large RMS location errors of 150m or greater.

Finally the chapter proposed a small cell size estimation method based upon interpolation of geo-located UE measurement reports for the macrocell layer and how this method could be used to greatly increase the effectiveness of the lampposts chosen for small cell deployment when sharing a carrier frequency with the macrocell layer.

Chapter 6
The Effectiveness of Low Power Lamppost Mounted 3G/WCDMA Microcells to Offload Traffic from a Co-Channel Macrocell Layer

Whilst the previous chapter considered SON self-planning methods to determine where to place small lamppost mounted 3G/WCDMA microcells in order to capture the most traffic from the macrocell layer, this chapter looks at the actual effectiveness of low power lamppost mounted 3G/WCDMA microcells to capture this traffic when deployed on a common carrier frequency with the 3G/WCDMA macrocell layer.

The chapter begins by reviewing earlier work on macrocell offloading using outdoor microcells and the challenges identified within these references. The chapter then models the potential offload achieved by the deployment of thirteen low power (+24dBm maximum output power) lamppost mounted 3G/WCDMA microcells along a busy street in central London through simulation using a modified version of the Network Simulator described earlier. The simulation results are then compared to field measurements taken before and after the deployment of four lamppost mounted Alcatel Lucent 3G/WCDMA microcells along Kensington High Street and finally conclusions are drawn as to the effectiveness of low power lamppost microcells at capturing traffic from a co-channel macrocell layer.

6.1 Review of Previous Low Power Co-Channel 3G/WCDMA Microcell Offload Studies & Field Trials

There appears to be very little earlier work considering macrocell offload using lamppost mounted low power 3G/WCDMA cells. Some reference regarding offload to higher power street level microcells or indoor femtocells were found and are worthy of consideration since they also address macrocell offloading onto a shared carrier small cell network.

Jami & Tao [78] study co-channel microcell offload in a R99 3G/WCDMA network, using high power microcells with an output power of 10W (+40dBm). The paper considers the issues of rapid re-selection between the co-channel macro and microcell layers of the network and suggest fast moving mobiles should be kept on a separate carrier to the microcell layer through the Hierarchical Cell Structure (HCS) feature of 3G/WCDMA [98]. A modified Walfisch-Ikegami model [54] is proposed based on field measurements made around a single microcell and it is proposed that given these findings a separate model per microcell would be required for accurate microcell coverage prediction. The paper then considers analytically the radius and capacity of a single microcell located at varying distances from a nearby single co-channel macrocell using a Hata based channel model for

the macrocell path loss prediction [54]. The paper concludes that for a microcell output power of 10W, the cell radius of the co-channel microcell will be 100m, 150m and 200m at distances of 1km, 1.5km and 2km from the macrocell respectively. Whilst the approach appears sound, there is no mention of the effect of shadowing or penetration loss on the macrocell signal's path loss and therefore it is expected that the cell radii presented will be somewhat smaller than those actually seen from a deployed 10W co-channel microcell.

In a later reference Chang-Young [99] also considers the effect of microcell powers of 1W, 5W, 10W, 15W and 20W on Rel-5 3G/WCDMA HSPA microcell radii when the microcell is deployed on a shared carrier with the macrocell layer. Unfortunately it appears that the paper does not model the HSDPA downlink SINR correctly since values as high as 70dB are presented and as shown in the description of the Network Simulator in Chapter 3, because 3G/WCDMA uses co-channel common channels, then even with good orthogonality between the 3G/WCDMA cell's downlink channels an HSDPA SINR much above 25dB is unlikely to be seen in a deployed network. Even so the paper does show that the further from the co-channel macrocell the microcell is placed the better the throughput of the microcell, with 3G/HSPA microcells at 900m from the macrocell achieving approximately twice (2.1 Mbps) the capacity of microcells located at 300m from the macrocell (1.0Mbps).

Erceg & Whitehead [100] determined estimates, purely from field measurements of the cell size that can be achieved from lamppost mounted small cells operating in the 900MHz, 2GHz and 6GHz frequency bands for US 1G Advanced Mobile Phone Service [101], 2G/IS-54 [102] and 2G/IS-95[16] cellular systems. The reference also considered capacity limited ranges for a given user distribution and suggests that powers as low as +5dBm power may be suitable for street level coverage at 2GHz for an interference limited microcell only network. With a transmit power of +10dBm the paper suggest an IS-95 microcell could provide a coverage area of $1km^2$, corresponding to a microcell radius of 560m. Unfortunately the paper does not address the interaction between co-channel macro and microcell layers.

Since it proved difficult to find references relating directly to microcell offload from the macrocell layer using a shared carrier frequency a number of papers that considered offloading onto co-channel femtocells were also studied.

References [103, 104] look at the offloading of the macrocell network through indoor femtocell rather outdoor microcell deployment using a simulation approach with a Shannon based throughput C/I mapping very similar to that used in the simulations presented in this thesis. It is shown that femtocells can operate on a shared carrier with very little uplink interference into the macrocell network. The work concludes that offloading a single deep indoor user from the macrocell provides up to 2.5 times its capacity for outdoor users and that for the scenarios studied the co-channel deployment of femtocells not only offloaded

the macros but also provided what was termed in the paper an “offloading capacity gain” on the macrocells of between 30-100%.

Finally reference [105] evaluates through field measurement the effectiveness of low power (+13dBm) co-channel indoor 3G/WCDMA femtocells to provide coverage to a dense urban environment. Simultaneous field measurements of both 3G/WCDMA (2100MHz) and IEEE 802.11 Wi-Fi (2.4GHz) are taken throughout central Vienna and the signal levels seen at 540 distinct locations throughout the city are analysed. It is shown that given the proliferation of Wi-Fi access points, for central Vienna at around 55% of sample location the Wi-Fi signal is stronger than the 3G/WCDMA signal. At these locations it is therefore proposed that the deployment of a femtocell alongside the associated Wi-Fi access point would provide better coverage for the 3G/WCDMA users than that currently provided by the macrocell layer. The methods presented in this paper provide both a method for placement of indoor small cells and also suggests that low power +13dBm outdoor small cells may also be effective in offloading traffic from the macrocell layer.

In summary many papers were found regarding offload from the 3G/WCDMA macrocell layer to co-channel indoor femtocells, a number of papers were found that considered the cell size of outdoor lamppost mounted microcells but did not consider explicitly offload onto these microcells. Finally a novel technique using combined Wi-Fi measurements to both place and predict the coverage of low power 3G/WCDMA small cells was found that suggests low power outdoor small cells with powers as low as +13dBm may be viable for co-channel 3G/WCDMA offload in a large European city.

6.2 Output Power Considerations for Lamppost Mounted Small Cell Deployments

There are a number of key technical considerations to be addressed when deploying any small cell network, these include;

- The maximum size and weight of the cell site equipment allowed to be installed at the proposed small cell location.
- The availability of power at the proposed small cell location.
- The availability of backhaul connectivity (fixed or wireless) at the proposed small cell location.
- The distance between each small cell location.
- The required output power of the small cell to ensure the cell’s dominance in the area surrounding the small cell – and this will be different for dedicated and shared carrier deployments.

Whilst the physical size and weight of the unit and the availability of power and backhaul connectivity are key to the deployment aspects of small cells this section concentrates on the

effect the output power has on the dominance of the small cell in a shared carrier scenario and whether low power small cells with an output power of +30dBm (1W) or less can effectively capture traffic from the macrocell layer. As was shown in Chapter 5 using the macro and microcell propagation models proposed in [51,52] results in the following cell sizes for microcells with output powers ranging from +10 (10mW) to +37dBm (5W) for the co-channel deployment case.

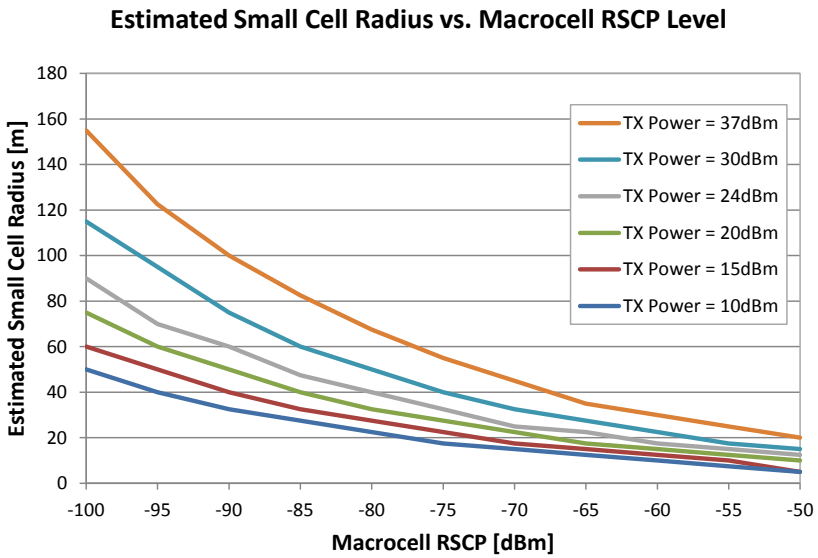

Figure 6.1 Estimated co-channel small cell size given macrocell RSCP level using the 3GPP 25.814 microcell propagation model for different small cell transmitter powers.

Here in Figure 6.1 it is seen that the small cell's size is not only a function of output power of the small cell but also the level of interference seen from the surrounding co-channel macrocell layer. From the graph it is seen see that for a +24dBm output power small cell its effective cell size (with indoor penetration loss - since this was included in the 3GPP 25.814 Urban Micro Outdoor to Indoor model used) will range from 20m to 60m when deployed in an environment with a macrocell RSCP power range of -60dBm to -90dBm.

Whilst these sizes initially appear very limited it should also be remembered that the spacing between lampposts can be as low as 10m in an urban environment and outdoor coverage ranges will be significantly larger than the indoor ranges given above. Therefore it would appear from the above graph that co-channel small cell dominance should be possible using +24dBm output power small cells providing that the lamppost spacing chosen between these small cells is adequate for the level of macrocell interference experienced in the area of small cell deployment.

6.3 Telefonica UK Kensington High Street Microcell Network

Telefonica UK deployed over 100 outdoor 3G/Wi-Fi small cell access points into central London throughout 2012 [71] in readiness for the anticipated mobile data traffic increase during the London 2012 Olympics games. Deployment was focused on areas with high 3G/WCDMA traffic levels as reported from 3G macrocell network statistics. A traffic density raster created from the analysis of Telefonica's 3G/WCDMA traffic in central London in late 2011, shown previously in Chapter 2 and shown again for ease of reference in Figure 6.2, clearly shows the non-uniform nature of the data traffic distribution across Telefonica's central London 3G/WCDMA network.

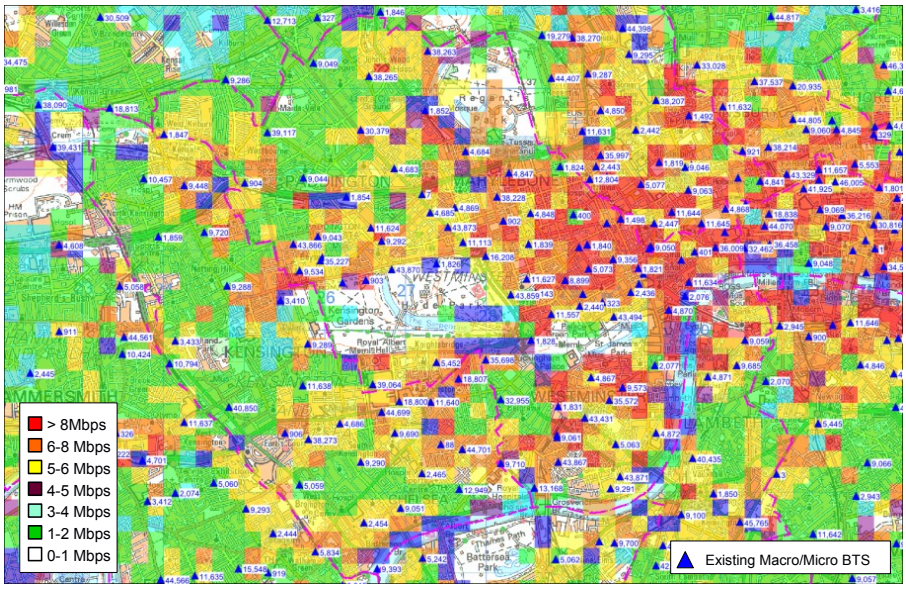

Figure 6.2 Map of Telefonica's 3G data traffic - Central London, December 2011.

Based upon this traffic raster and a requirement by Westminster and Kensington councils for Telefonica UK to deliver free public Wi-Fi to key areas of central London during the London 2012 Olympic games, the following nine areas were chosen for the initial Phase 1 deployment of Telefonica UK's central London small cell network. A map of the Phase 1 deployment areas is shown in Figure 6.3.

- Exhibition Road
- Kensington High Street
- Oxford Street
- Regent Street
- Piccadilly Circus
- Leicester Square
- Trafalgar Square
- Parliament Square
- Covent Garden

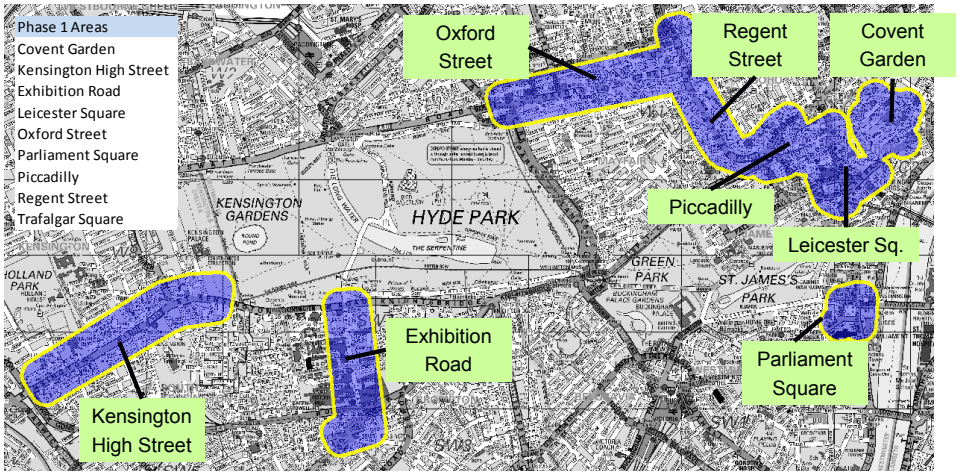

Figure 6.3 Telefonica UK London small cell phase 1 deployment areas.

This chapter focuses on just the Kensington High Street (KHS) small cell network since this has been used by Telefonica UK as its small cell testbed and far more measurements and observations have been made of this area than any of the other small cell deployment areas.

The KHS small cell network consists of thirteen 3G/Wi-Fi microcells deployed upon existing lampposts along a 1.4km stretch of KHS. The layout of the KHS microcell network is shown in Figure 6.4 which also shows the position of the surrounding macrocell sites in relation to the KHS small cell network.

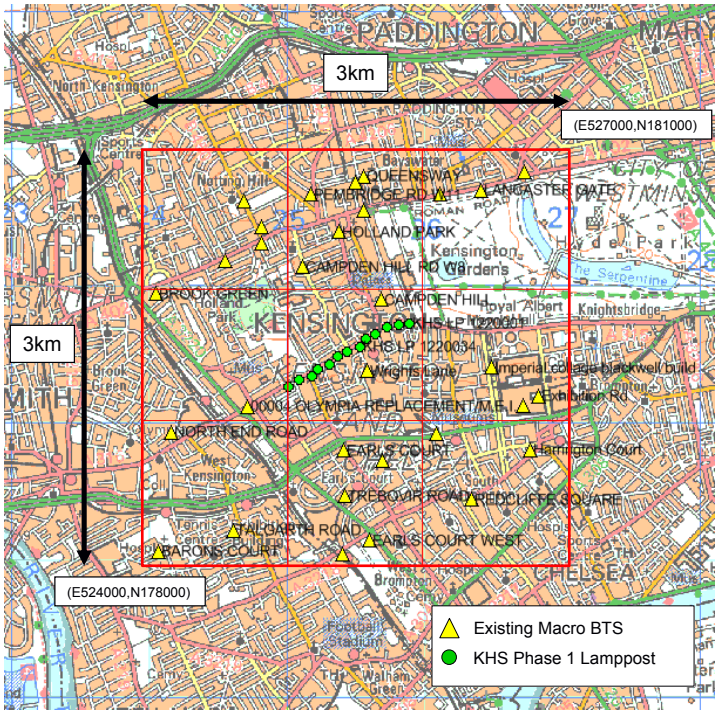

Figure 6.4 Map showing KHS microcell network in relation to existing macrocells and the 3x3km simulation area used during the work detailed within this chapter.

Each KHS small cell consists of a hybrid 3G/Wi-Fi microcell located at a height of 8m on an existing KHS lamppost. The Wi-Fi Access Point (AP) was a Ruckus Wireless 8800 AP and the 3G microcell unit was an Alcatel Lucent Metro V2 outdoor microcell. Datasheets for both products are given in Appendices D & E. Based on a design proposed by the author both units were mounted back to back using a special mounting bracket developed by Ruckus Wireless (Figure 6.5) and when mounted together appear as an integral single unit (Figure 6.6).

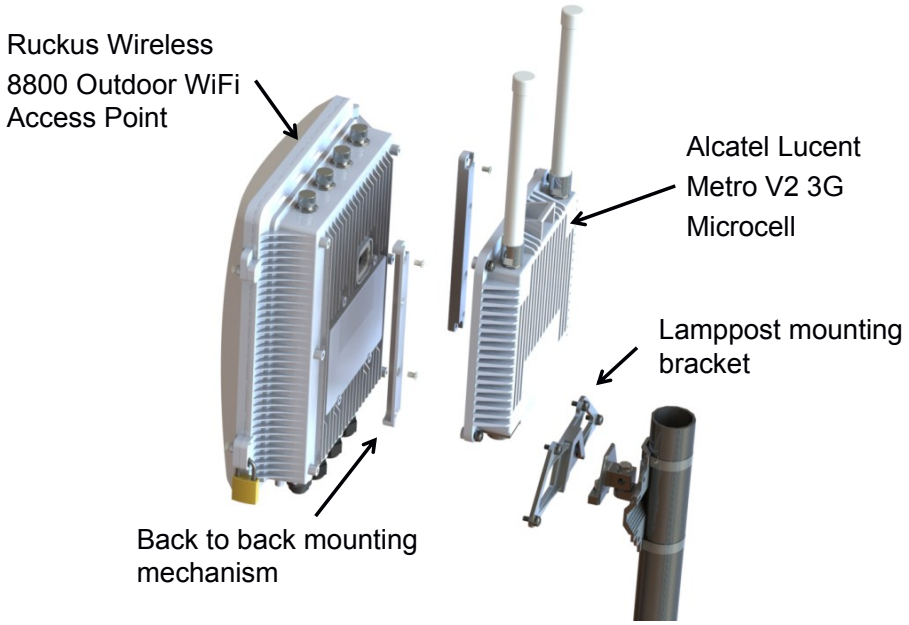

Figure 6.5 Exploded schematic of the Telefonica 3G/Wi-Fi microcell.

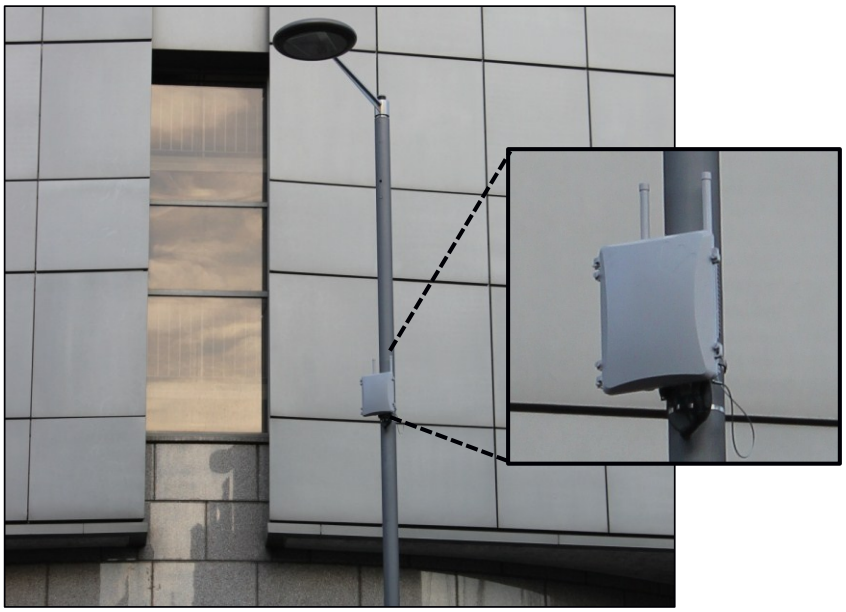

Figure 6.6 Deployment example of a Telefonica 3G/Wi-Fi microcell on Kensington High Street lamppost LP1220001.

Shown in Figure 6.7 is the detailed street design for the KHS microcell network. It shows the lampposts chosen for 3G/Wi-Fi microcell deployment and the inter-site distances between each lamppost. The inter-site distances were chosen based upon a recommendation from Ruckus due to the limited range (100m) of their proprietary 5GHz point to multipoint meshing technology used to provide backhaul transmission between the microcells. Backhaul connectivity to Telefonica's core network was provided to the network at four "Root" AP locations, shown as green nodes in Figure 6.7. Three 100Mbps fibre Ethernet circuits were deployed to the lampposts LP1220060, LP1220034 and LP1220014 and one 50Mbps point to point link was deployed to LP1110012 from the nearby macrocell site 40850 (the location of this cell site is also shown in Figure 6.8). The remaining nine lamppost microcells without direct transmission to the core network connected to the lampposts that had core connectivity using a dynamic 5GHz mesh network established between all of the Ruckus 8800 units. Early integration tests proved that this meshing coupled with the number of lampposts deployed provided on average 25Mbps of available transmission per lamppost.

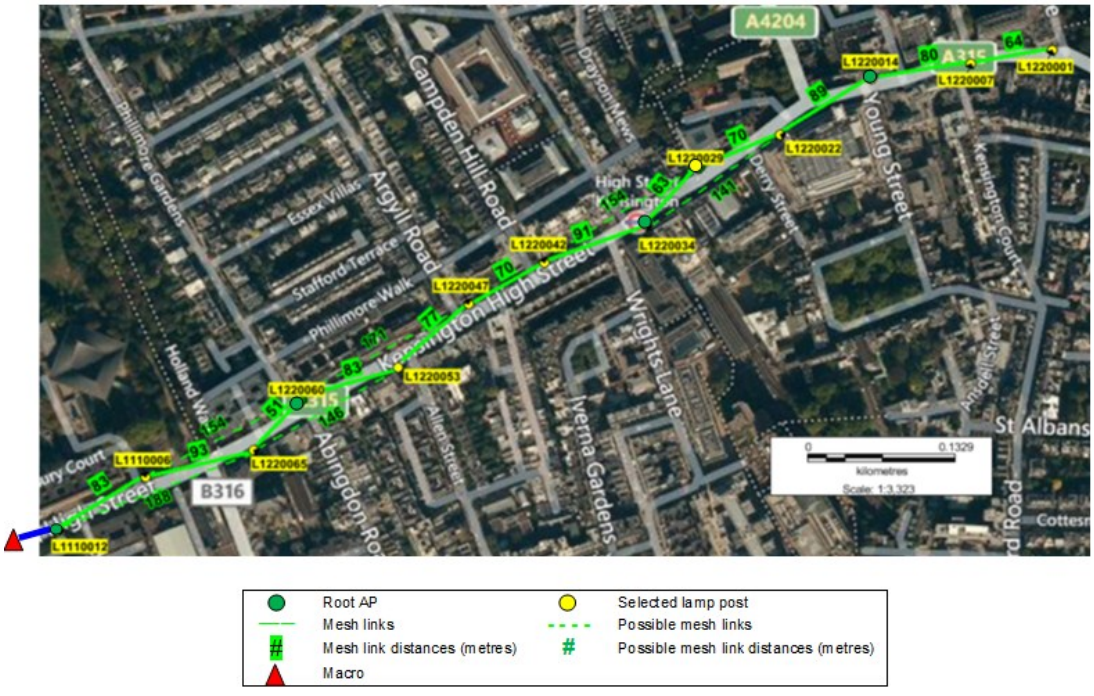

Figure 6.7 Detailed design of KHS microcell network showing the selected lamppost. Reference numbers shown in yellow text, inter-site distances shown as green text and root APs/transmission hubs show as green nodes.

6.4 Kensington High Street Microcell Network Modelling & Predicted Traffic Offload

This section considers through simulation the expected coverage and traffic offload that the KHS microcells will provide. In order to study specifically the effect this would have on users located on KHS, again as shown in Section 5.4.2 of the previous chapter a special clutter category (category 17) was used to define the KHS high traffic area (area = 0.1225km^2). The users/km^2 applied for each clutter category, normalised to match the total number of users distributed for the simulations, is given in Appendix A. The clutter loss for the KHS clutter category was set to 16dB, the same as the Dense Suburban clutter category surrounding the KHS area (the penetration losses for the other clutter categories were shown in Table 5.1 of the previous chapter).

6.4.1 KHS Macro and Microcell Coverage Predictions

The Network Simulator was used to predict the coverage of both the 3G/WCDMA macrocells and the lamppost microcells along and around KHS for the co-channel case. The propagation model used for the macrocells was the 3GPP 25.814 "Macrocell distance-dependent path loss model" given in [51] but with a clutter based penetration loss applied as explained previously in Section 3.2.2 of Chapter 3. Shown below in Figures 6.8 and 6.9 are the best server RSCP coverage plots for the case with and without the KHS microcells deployed. In Figure 6.8 the cell identities, sector numbers and the scrambling codes for the nearby surrounding sectors area also given.

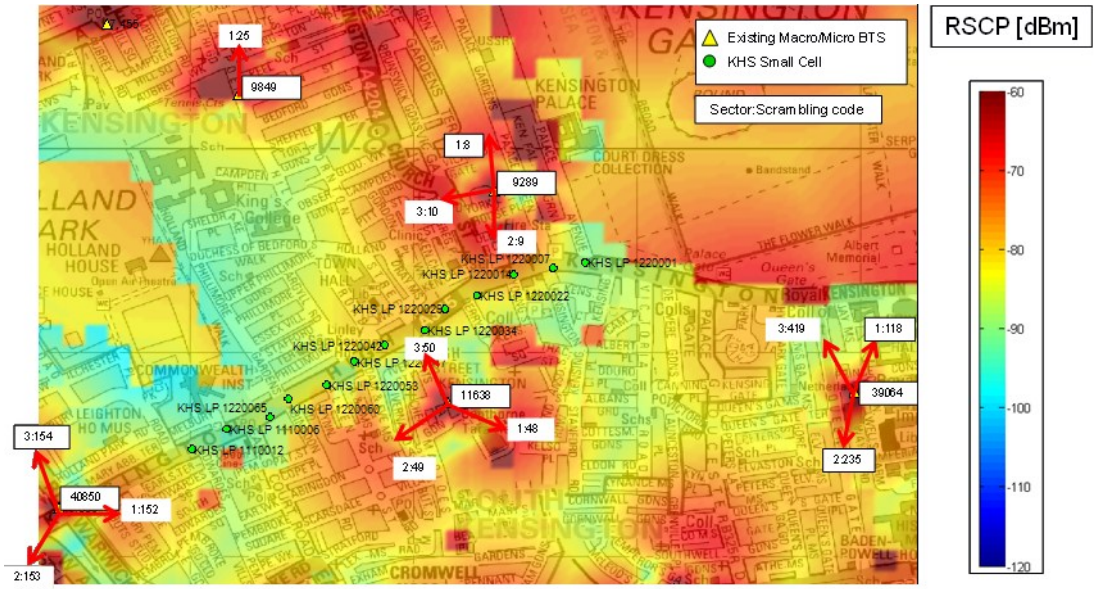

Figure 6.8 Simulated macrocell best server RSCP coverage along KHS prior to activation of KHS microcells. Also shown are the cell identities, sector identities and scrambling codes for the macrocell sectors closest to KHS.

Figure 6.9 Simulated macrocell & microcell best server RSCP coverage along KHS following activation of the thirteen +24dBm KHS microcells.

As can be seen from the KHS coverage predictions it appears that for the 3GPP models chosen, the +24dBm lamppost mounted microcells provide clear dominance along KHS and this is better shown in the best server area coverage plot for the microcells shown below in Figure 6.10.

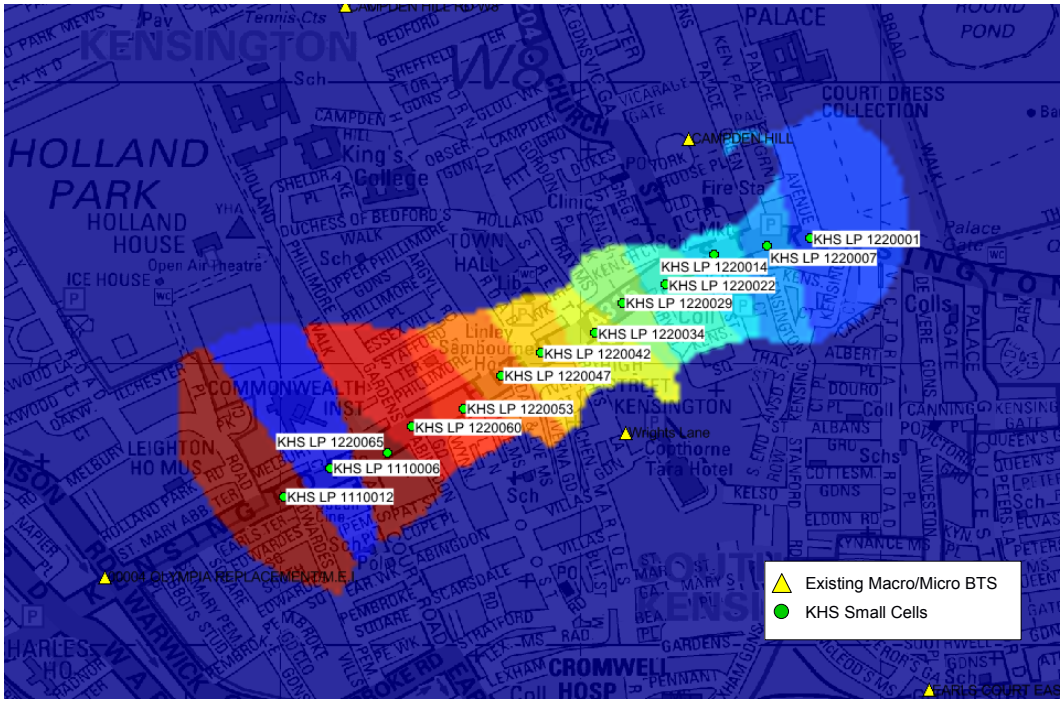

Figure 6.10 Simulated microcell best server coverage areas along KHS.

6.4.2 KHS Microcell Offload Predictions

The results of the above coverage predictions were then used to perform simulations to estimate the amount of traffic offloaded from the surrounding macrocells onto the KHS microcells. Monte Carlo simulation runs were performed with and without the KHS microcells active for 1,000 Monte Carlo snap shots each with an arbitrary 500 users distributed according to clutter category across the entire 3x3km simulation area. Of the 500 users, normalised clutter spreading led to 92 users being distributed within the 0.1225km^2 KHS high traffic area leading to an average user distribution of 751 users/km^2 within the KHS high traffic area and 105 users/km^2 on average in the surrounding macrocell served area. Cell and user statistics were gathered from the simulations for both the central 2x2km area and the KHS high traffic area.

Shown below in Figure 6.11 is the percentage of the KHS high traffic area served by each of the dominant nearby macrocell sectors (see Figure 6.8 for sector locations with respect to KHS) prior to the introduction of the KHS microcells. Here it can be seen that coverage along KHS is predicted to be provided by just five macrocell sectors prior to the deployment of the KHS microcells, and therefore it can be assumed that any traffic offloaded from the macrocell layer will be captured by studying the effect the microcells have on the traffic carried by just these five dominant sectors.

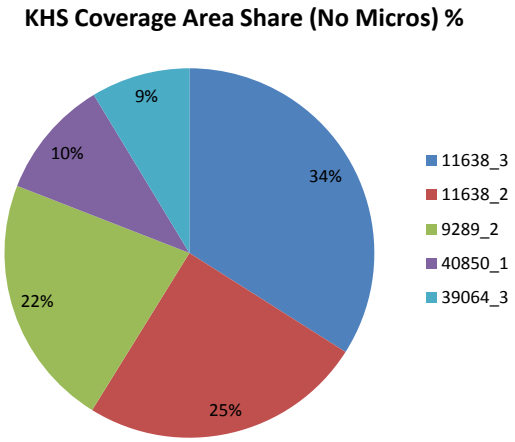

Figure 6.11 Percentage of the 0.1225km^2 KHS high traffic area served by each of the nearby dominant macrocell sectors prior to the KHS microcell deployment.

Shown in Figure 6.12 is a graph showing the predicted change in the coverage areas of the five dominant macrocell sectors within the central 2x2km area, before and after the deployment of the thirteen KHS microcells. Also shown in the graph is the total combined coverage area of all the microcells when deployed. It can be seen from the graph that as shown previously in Figure 6.10 the combined coverage footprint of the microcells (0.3768 km^2) is significantly bigger than KHS high traffic area (0.1225km^2).

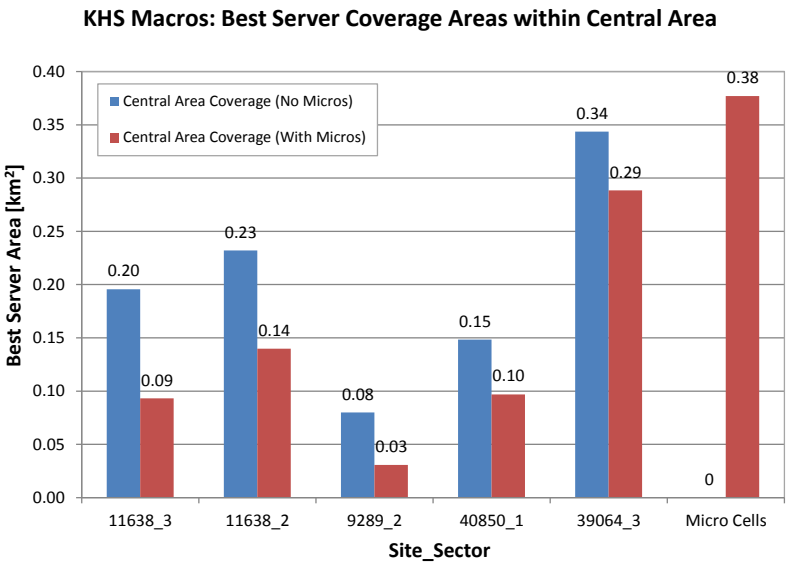

Figure 6.12 Predicted best server areas of the five dominant macrocells before and after the deployment of the thirteen KHS microcells. Also shown is the predicted combined coverage area of the KHS microcells.

Whilst the reduction in the best server area for most of the KHS serving macrocell sectors is around 50%, since the users within the simulation are not evenly distributed but skewed towards the KHS high traffic area, a more dramatic effect is seen the effect the introduction of the microcells has on the number of users served by each of the five dominant macrocell sectors is considered (Figure 6.13). Here it can be seen that all of the dominant five serving macrocell sectors experience a significant reduction in the number of served users with the introduction of the KHS microcells.

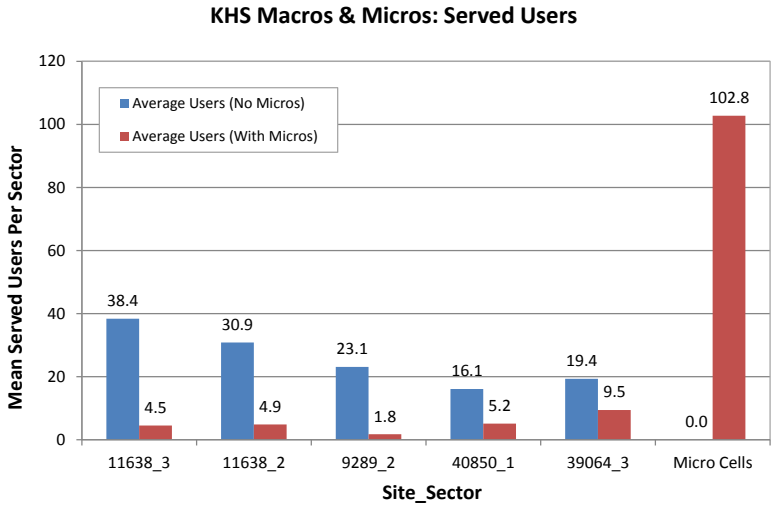

Figure 6.13 Predicted users served for the five dominant macrocell sectors before and after the deployment of the thirteen KHS microcells. Also shown is the predicted users served across all of the KHS microcells following their deployment.

The reduction in served users per macrocell sector for the five dominant KHS macrocell sectors in turn leads to a better user experience for the users remaining on the macrocell sectors and this is shown in Figure 6.14 and this offloading gain is similar to the effects also observed by Claussen *et. al.* in [103].

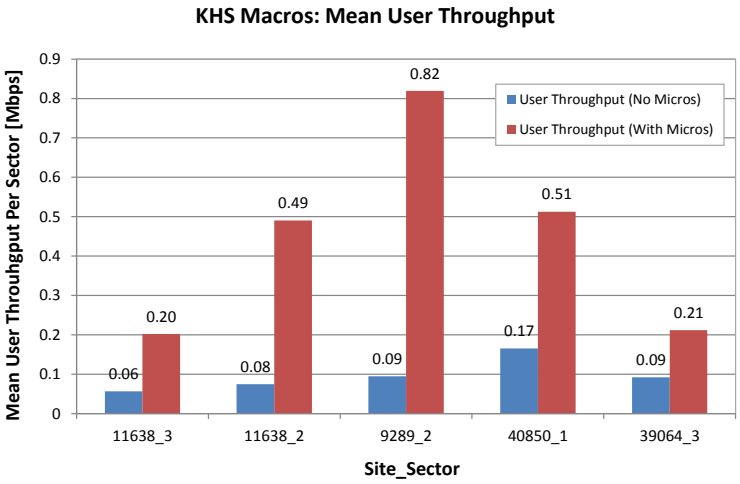

Figure 6.14 Predicted mean user throughput for the users of the five dominant macrocell sectors before and after the deployment of the thirteen KHS microcells.

Regarding the users offloaded onto the KHS microcells, shown in Figure 6.15 and 6.16 are the average number of users served by each of the KHS microcells and the percentage of the KHS high traffic area covered by each microcell. Here it can be seen that the microcells at lampposts LP1110012 and LP1220001 that have coverage footprints that reach well beyond the KHS high traffic area (Figure 6.10) as expected capture the most users.

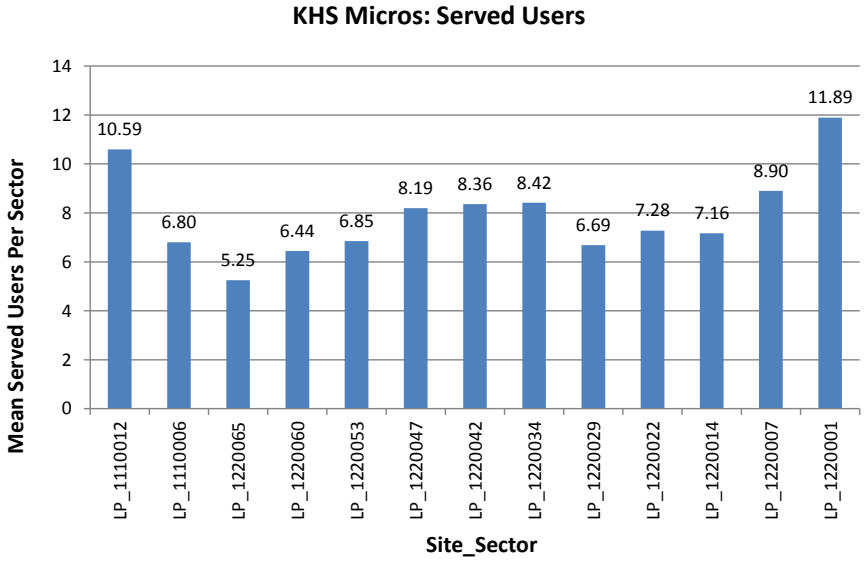

Figure 6.15 Predicted users served by each of the thirteen KHS microcells.

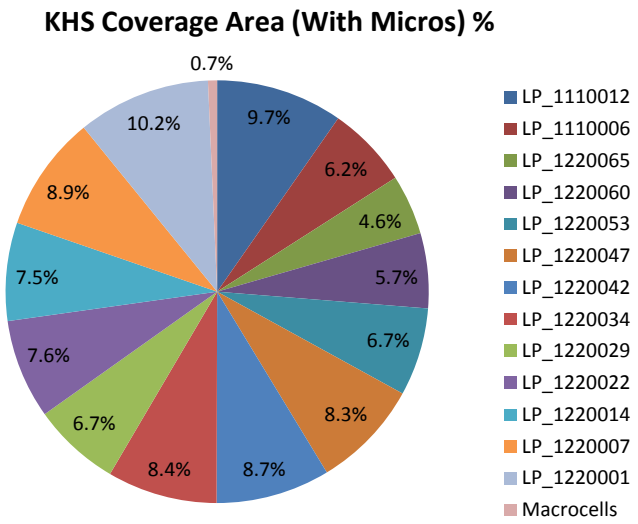

Figure 6.16 Predicted percentage of KHS high traffic area covered by each microcell.

Whilst from the above results it appears that the Monte Carlo simulations predict that the +24dBm microcells will have dominant coverage on KHS and that they will also capture a significant number of users from the macrocell layer, the key question still to be answered is how will the microcell deployment enhance the user experience in KHS and across the wider network? Shown in Figures 6.17 is a CDF distribution of the user throughput seen in just the KHS high traffic area and Figure 6.18 shows the CDF distribution of the user throughput across the whole central 2x2km area of the simulation area before and after the deployment of the KHS microcells. From Figure 6.17, a marked improvement in the user experience for the users located within the KHS high traffic area can be seen, with the median throughput per user increasing some 214% from 0.07Mbps to 0.22Mbps. For the wider area surrounding KHS, the offloading of users to the microcell layer also is seen to have a significant impact on the user experience with median user throughput rates increasing by 100% from 0.12Mbps to 0.24Mbps.

An overall summary of the gains and losses predicted by the simulation of the KHS microcell deployment is given in Table 6.1. From an RF perspective the microcells have little change on the average RSCP and Ec/Io across the central 2x2km area of the simulation area. The reduction in Ec/Io is due to the increased number of pilots seen around KHS, and whilst this does have a slight negative effect on the average throughput per sector of the surrounding macrocells, because there are now fewer users on these surrounding macrocells, the average user throughput seen on these surrounding macrocells actually increases from 0.27Mbps to 0.36Mbps following microcell deployment.

Overall the KHS microcells offload on average 102.8 users from the macrocell layer and this leads to a 22.49Mbps increase in total network throughput, representing a 22% increase

in the capacity of the network. The most significant impact of the microcells however is the effect they have on the user experience for the users located in the KHS high traffic area. Prior to the deployment of the microcells, these users experienced an average throughput of just 0.08Mbps, whereas after deployment their average throughput of 0.26Mbps is more in line with the average throughput seen by the surrounding macrocell users.

The simulation result therefore suggest that +24dBm microcells will provide contiguous coverage dominance along KHS and if there is significant traffic within this area they will also, as shown in the simulation example here, provide significant traffic offload from the surrounding macrocell sectors.

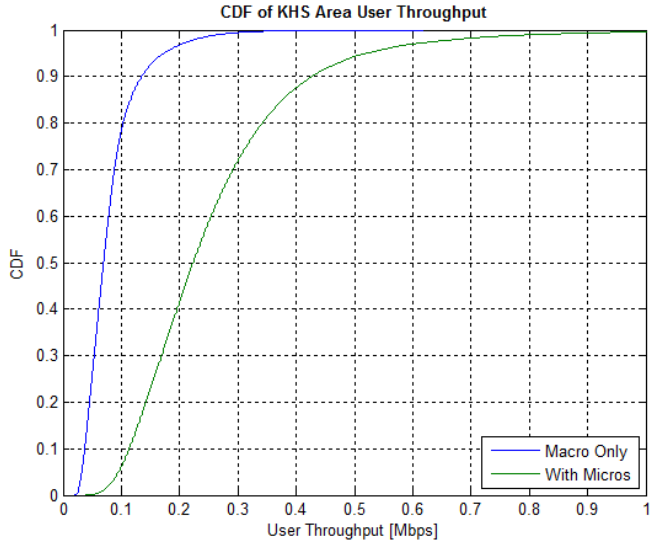

Figure 6.17 CDF of user downlink throughput experienced in KHS high traffic area before and after KHS microcell deployment.

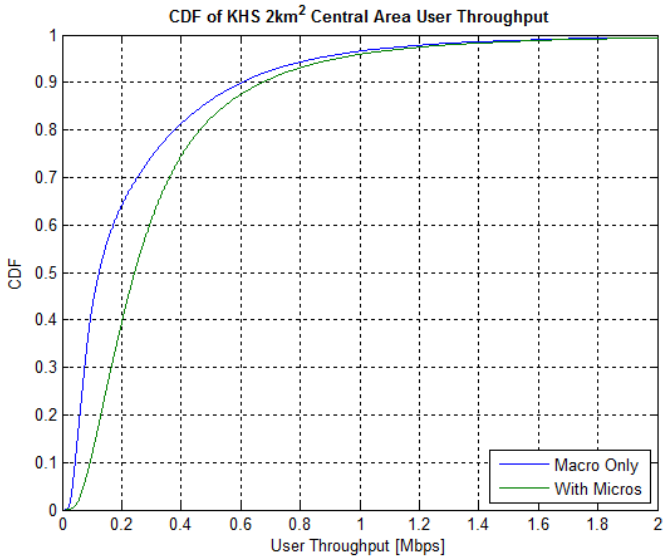

Figure 6.18 CDF of user downlink throughput experienced in central 2x2km area before and after KHS microcell deployment.

Table 6.1 Summary of KHS microcell simulation results.

Central 2x2km Area			
Key Performance Indicator	Macros Only	Macros & Micros	Gain/Loss
Mean RSCP [dBm]	-78.90	-78.06	0.85
Mean Ec/Io [dB]	-11.21	-11.49	-0.28
Macro Network Throughput [Mbps]	101.99	99.30	-2.69
Network Throughput (Macro & Micro) [Mbps]	101.99	124.48	22.49
Mean Macro Sector Throughput [Mbps]	2.32	2.26	-0.06
Mean Macro Users Per Sector [Users]	8.63	6.30	-2.33
Mean Macro User Throughput [Mbps]	0.27	0.36	0.09
Mean Users In Central Area on Macros [Users]	379.84	277.10	-102.74
Mean Macro & Micro User Throughput [Mbps]	0.27	0.34	27%

KHS High Traffic Area			
Key Performance Indicator	Macros Only	Macros & Micros	Gain/Loss
Micro Network Throughput [Mbps]	-	25.18	25.18
Mean Micro Sector Throughput [Mbps]	-	1.87	1.87
Mean Micro Users Per Sector [Users]	-	7.68	7.68
Mean Users Microcell Layer [Users]	-	102.80	102.80
KHS Area Mean User Throughput [Mbps]	0.08	0.26	218%

6.5 Kensington High Street Macrocell Coverage Measurements

In order to validate the actually effectiveness of the KHS microcells a number of field measurements were performed by Telefonica UK before and after the activation of the 3G/WCDMA KHS microcells. This section analyses the results of the first of these field measurement campaigns which measured the signal strength of the surrounding macrocells received along KHS in order to better understand the existing macrocell interference at and around the chosen microcell locations and whether as predicted in the previous sections, the microcells would have dominance along KHS itself.

6.5.1 KHS Macro Coverage Measurements

Coverage measurements of the surrounding 3G/WCDMA macrocell sectors incident on KHS were made by Telefonica UK's Radio Engineering team using a PCTEL Seagull EX scanner on 4th December 2012. Measurements were made for all three 3G/WCDMA carrier frequencies currently deployed by Telefonica in central London (Table 6.2). The translation between the UMTS Terrestrial Radio Access (UTRA) Absolute Radio Frequency Channel Number (UARFCN) and the carrier centre frequency is given in [106]. Since it was Telefonica's intention to operate the KHS microcells on its second UMTS2100 carrier (F2), the rest of this section concentrates its analysis on just the F2 macrocell coverage measurements.

Table 6.2 Telefonica UK 3G/WCDMA carriers deployed in central London.

Carrier	UARFCN	Downlink Carrier Centre Frequency
F1 (UMTS2100)	10637	2126.2 MHz
F2 (UMTS2100)	10661	2132.2 MHz
F3 (UMTS900)	2963	932.6 MHz

Shown in Figure 6.19 is a plot of the measurement route taken and the best serving macrocell scrambling codes detected on carrier F2. The detected scrambling codes and serving sectors in the figure are shown with common colours to aid in the identification of the best serving macrocell sectors along KHS.

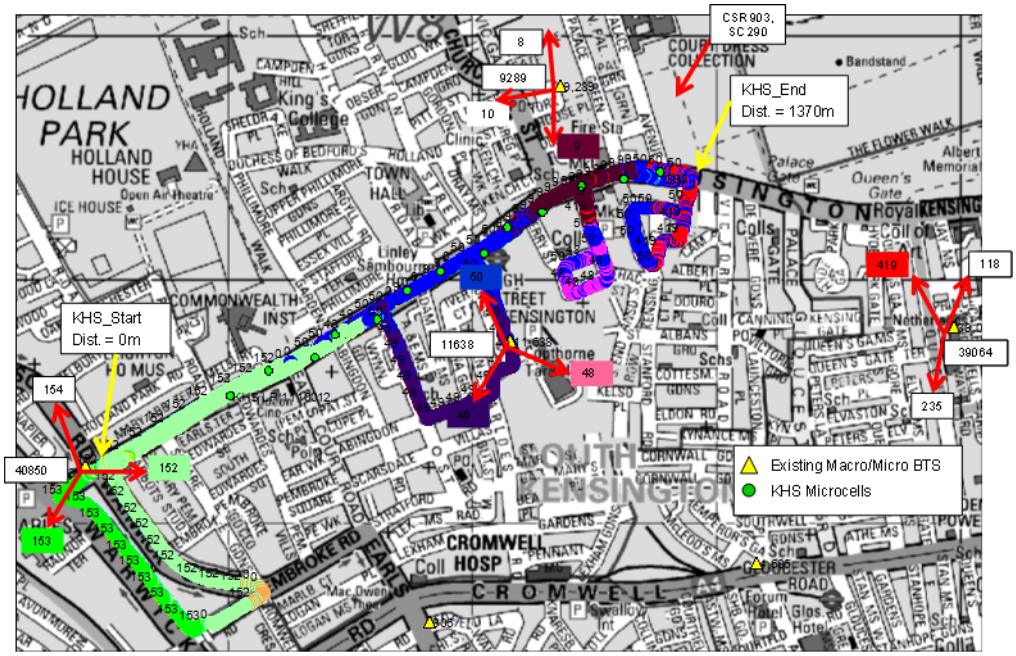

Figure 6.19 Plot showing best serving scrambling codes detected from macrocell carrier F2 (2132.2MHz) during drive surveys along KHS.

Analysis of the scrambling codes detected purely along KHS itself and not the surrounding side streets was performed and resulted in the pie chart presented in Figure 6.20. This figure shows the dominant macrocell sectors detected during the drive survey along KHS. Comparing this chart to that generated from the simulation coverage predictions (Figure 6.11) it is seen that the coverage predictions match well with the measured data. As predicted sector 3 of site 11638 provides the greatest coverage on KHS with cells 40850_1 and 9289_2 covering most of the remainder of KHS. The main difference between the coverage predictions and the measurement results was that the predictions suggested that

sector 2 of site 11638 would also cover a significant portion of the KHS area. However as seen from the drive survey measurements (Figure 6.19) in reality this is not the case and cell 40850_1 covers the areas of KHS that 11638_2 was predicted to cover. The most likely reason for this is because of cell 40850_1's direct line of sight to most of the western end of KHS, something not modelled by the propagation models used within the simulations.

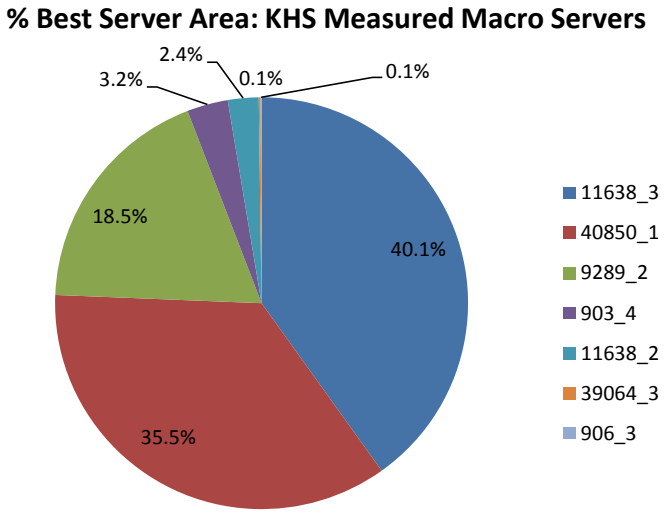

Figure 6.20 Pie chart of measured best serving macrocell coverage along KHS.

6.5.2 KHS Microcell Coverage Area Predictions Using Macrocell Measurements

As shown in Section 6.4.1, the original co-channel microcells' coverage areas were predicted by comparing through simulation, the macrocell and microcell signal levels predicted using the appropriate 3GPP propagation models. This section describes how this process was repeated but using the actual macrocell signal level measured during the drive surveys.

The microcell RSCP signal levels were once again predicted using the 3GPP 36.814 Urban Micro LoS propagation model [52] for the thirteen KHS microcells. The coverage prediction (Received Signal Strength Indication (RSSI) and RSCP)) of these microcells was then superimposed upon the F2 macrocell coverage measurements for length of KHS over which the microcells would be deployed. The result of this process is shown in Figure 6.21. It should be noted that the distances given along the x-axis in this and the subsequent figures are relative to an abstract datum defined to be at the junction of Warwick Gardens and KHS shown as "KHS_Start" in Figure 6.19. From the figure it is clear that the co-channel microcells were still predicted to have dominant coverage along KHS even when compared to the actual measured co-channel macrocell coverage.

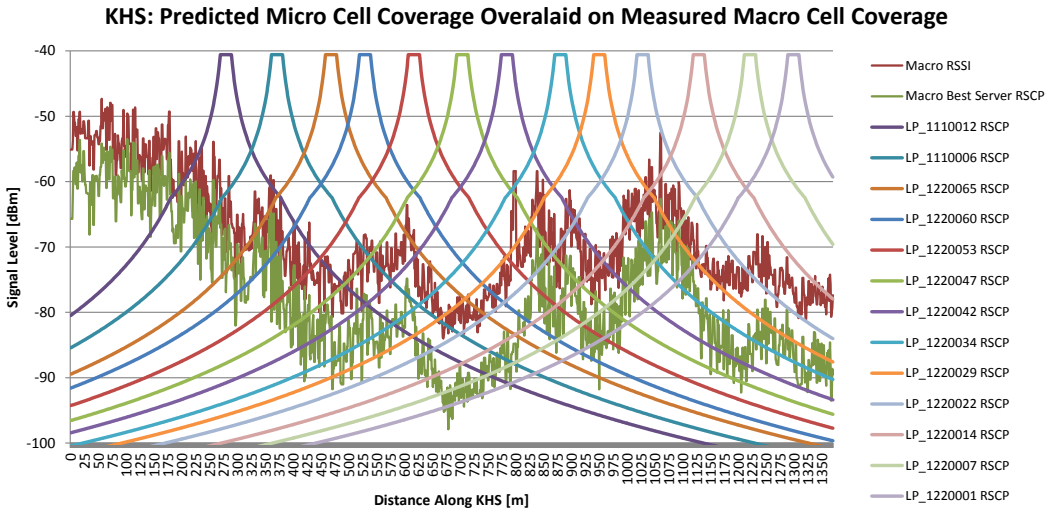

Figure 6.21 Predicted coverage of KHS microcells overlaid upon measured F2 RSSI and RSCP along 1.37km length of KHS.

6.6 Kensington High Street Microcell Coverage Measurements

At the time of writing (August 2013) whilst all thirteen KHS microcells have been enabled for Wi-Fi service, only four have been enabled for 3G/WCDMA service due to transmission issues. However, RF measurements have still been performed on the initial four 3G/WCDMA microcells deployed and this section outlines the measurements performed and analysis undertaken on these measurements.

The four lamppost initially enabled for 3G/WCDMA service were lampposts LP1220001, LP1220007, LP1220022 and LP1220029 (Figure 6.22).

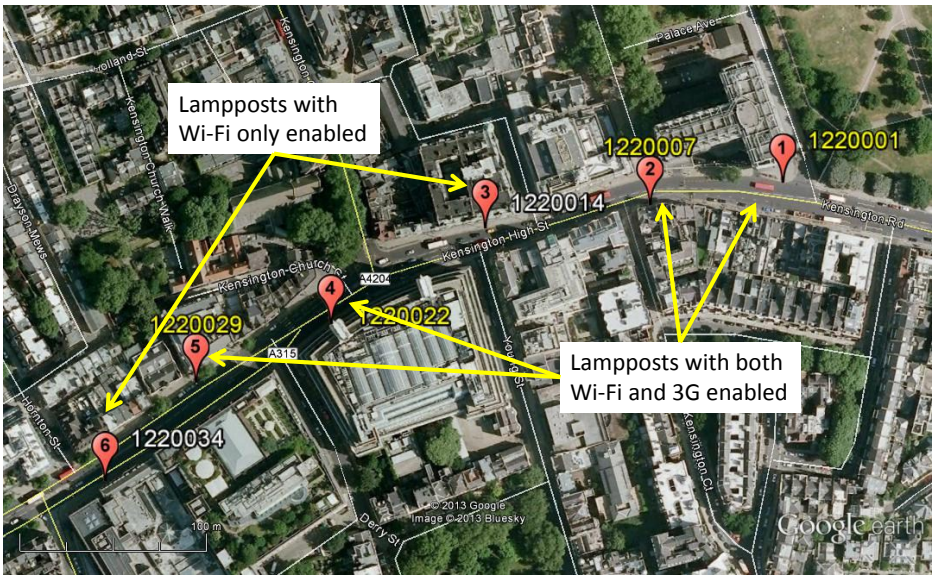

Figure 6.22 The four KHS lamppost microcells initially enabled for 3G/WCDMA service.

6.6.1 KHS Microcell Best Server Area Measurements

Further drive surveys were performed using a PCTEL Seagull EX radio scanner following the activation of the initial four 3G/WCDMA microcells. A plot of the best server scrambling codes detected from the drive surveys of KHS following the activation of the initial four 3G/WCDMA microcells is shown in Figure 6.23. Here it can be seen that clear dominance is achieved by the four microcells along the eastern end of KHS, even with lampposts LP1220014 and LP1220034 not enabled for 3G/WCDMA service. The plot also shows the serving macrocell sectors that cover the remainder of KHS and the surrounding side streets and these macrocell coverage areas align well with those predicted by the earlier simulations.

Shown in Figure 6.24 is a plot showing the best server areas for the section of KHS over which active 3G microcells were dominant together with the length of KHS over which each of the microcell was the dominant server. The maximum length of KHS over which a microcell was dominant was 250m (L1220001) and the minimum length was 115m (L1220022). From the figure it can also be seen that continuous dominance along KHS is not actually fully achieved by the four microcells deployed, with sector 9289_2 achieving dominance for a short distance (25m) between lampposts LP1220014 and LP1220022. This was due to the lack of coverage from missing microcell on lamppost LP1220014 and as was shown earlier in the macrocell coverage plots (Figure 6.8) and macrocell drive surveys (Figure 6.19), it is this precise area the most interference from the macrocell network to occur and in particularly interference from sector 9289_2 was expected.

However, it is also worth mentioning that given significant traffic may be offloaded from the macrocell layer, then in some cases for example in the case of sector 9289_2, where significant traffic is expected to be offloaded from this sector, yet the sector still causes unwanted interference, it may be possible to alleviate this interference by reducing the power or changing the antenna tilt or both for the F2 carrier of sector 9289_2. This idea is further explored in the following chapter.

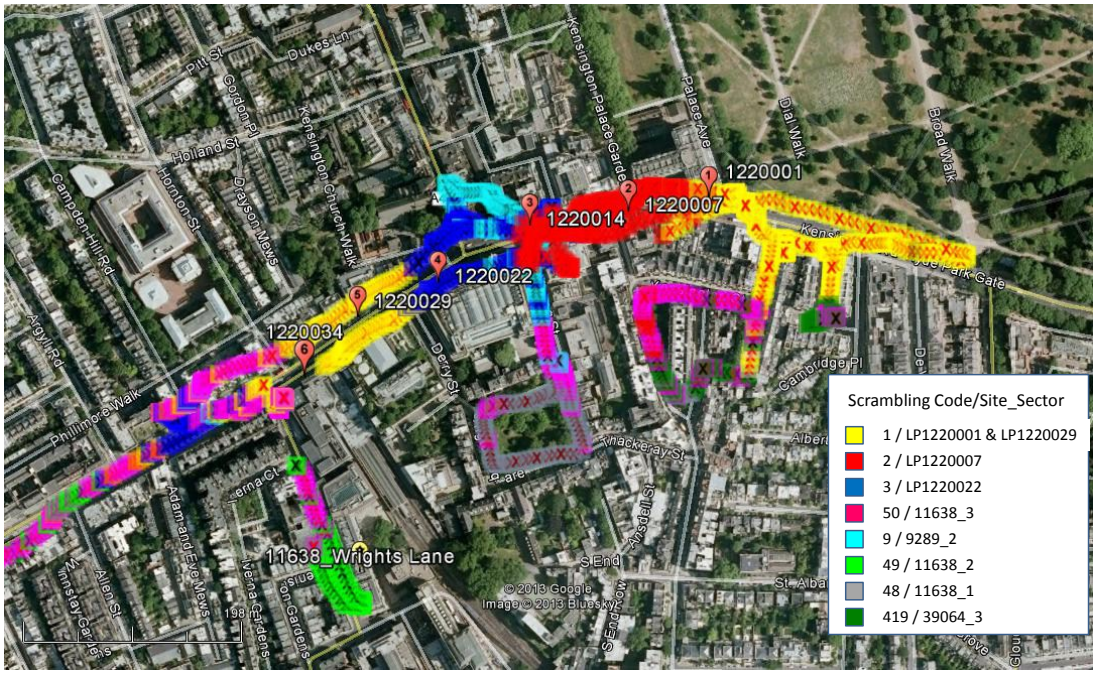

Figure 6.23 Best server scrambling code plot for the F2 carrier following activation of 3G/WCDMA microcells at lampposts LP1220001 (SC=1), LP1220007 (SC=2), LP1220022 (SC=3) and LP1220029 (SC=1).

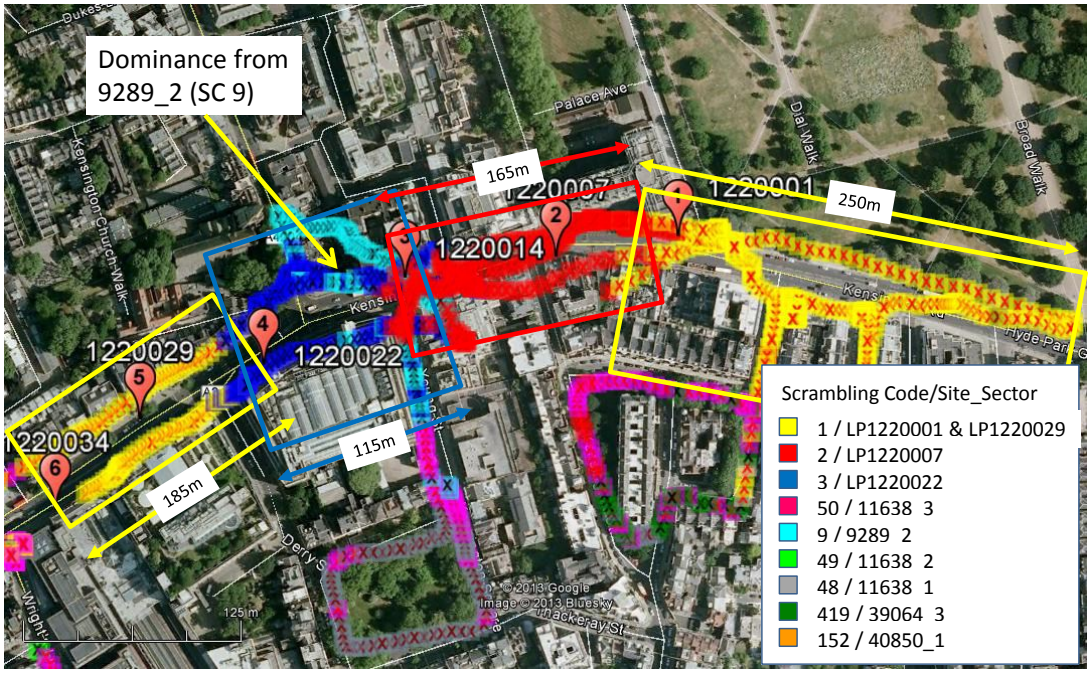

Figure 6.24 Best server scrambling code plot for the F2 carrier for the section of KHS over which 3G/WCDMA microcells were the dominant servers.

6.6.2 KHS Microcell RSCP Measurements

The graph presented in Figure 6.25 shows the best server RSCP before and after the activation of the initial four microcells and the predicted coverage from the five lampposts microcells LP1220001, LP1220007, LP1220014, LP1220022 and LP1220029. Here it can be seen the four microcells provide significant dominance over the macrocell coverage as predicted by the earlier simulations. The predicted coverage from the microcell LP1220014, also shows that complete coverage dominance is expected to be achieved between microcells LP1220007 and LP1220022 once LP1220014 is activated for 3G/WCDMA service.

Although predicted signal levels of -40dBm were not measured from the microcells during the surveys, this was not a surprise since the 3GPP model did not take into account any shadowing or reduction in the antenna gain of the microcell seen when directly underneath the microcell. Further out the line of sight microcell measurements appear to match well with the 3GPP microcell LoS model and this is further shown by the individual RSCP vs. distance scatter plots for microcells LP1220007 and LP1220022 shown in Figures 6.26 and 6.27.

From these results it is seen that the 3GPP LoS microcell model does indeed provide a good model for outdoor microcell coverage and as predicted by this model and now measured in the field, +24dBm low power lamppost mounted microcells can provide dominance when deployed on a shared carrier with the macrocell layer.

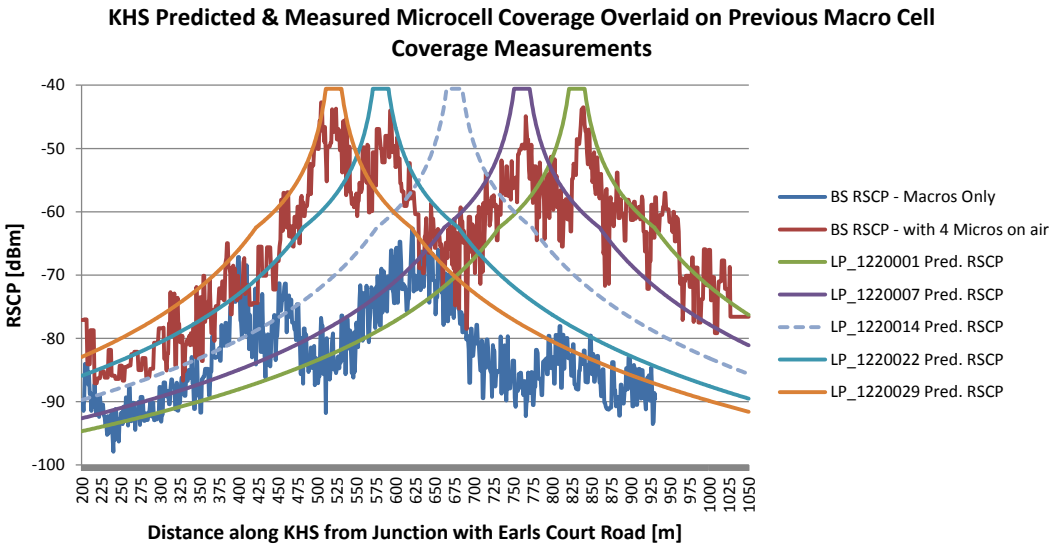

Figure 6.25 Measured best server RSCP coverage before and after the activation of the initial four KHS microcells, together with the predicted coverage from the these four microcells and the inactive microcell at lamppost LP1220014.

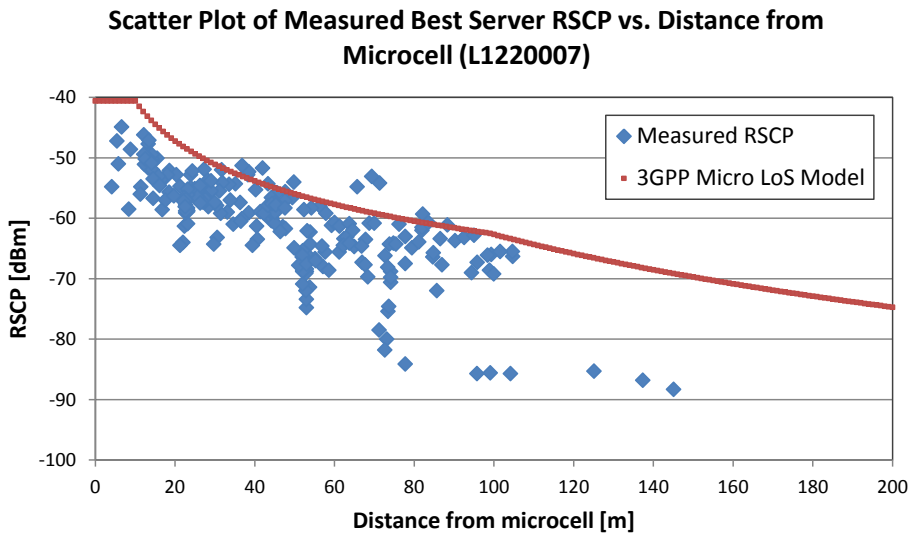

Figure 6.26 Measured RSCP vs. distance from serving microcell (L1220007).

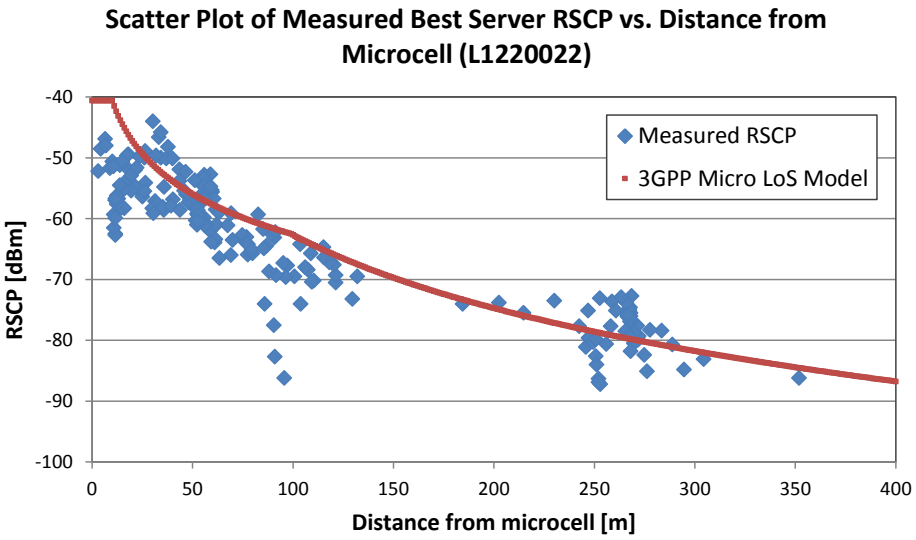

Figure 6.27 Measured RSCP vs. distance from serving microcell (L1220022).

6.6.3 KHS Microcell Ec/Io Measurements

Finally shown in Figure 6.28 is the effect the activation of the first four microcells had on the Ec/Io seen along KHS. As expected the microcells provide a much higher Ec/Io in the areas where they have dominance, however a slightly worse Ec/Io is seen in the overlapping dominance areas between the microcells and the macrocells. As mentioned in Section 6.4.1, the simulations did suggest that this would occur because of the increase in the pilot pollution caused by the increased number of pilots incident in these areas. However, as also expected the area pilot pollution is very limited because of the rapid reduction of the microcells signals especially for the non-LoS case.

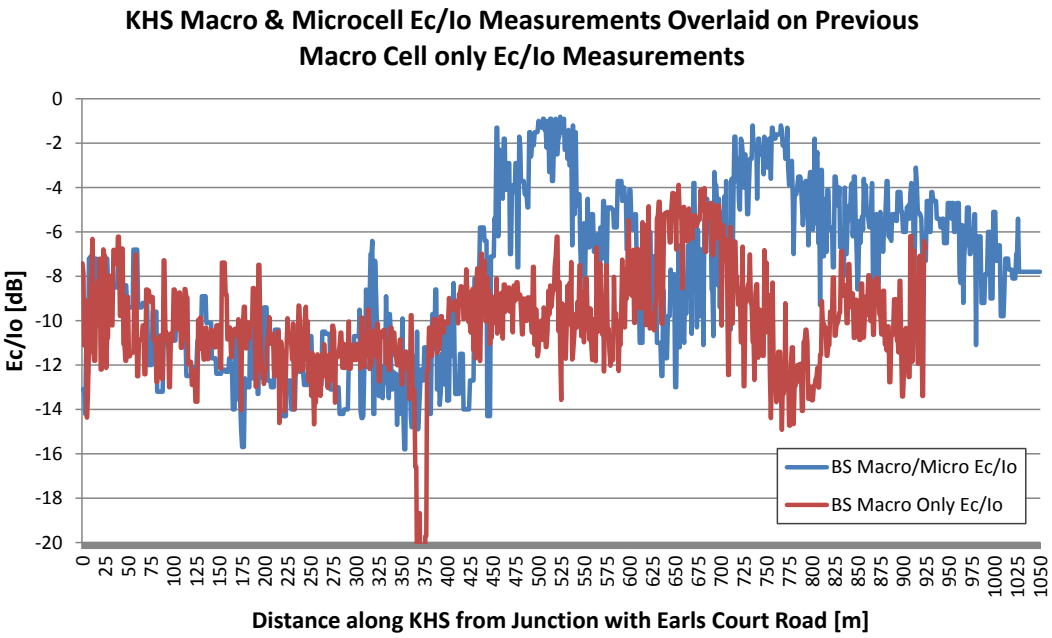

Figure 6.28 Measured Ec/Io along KHS before and after the activation of the initial four KHS microcells.

6.7 Chapter Summary

This chapter has studied the effectiveness of low power lamppost mounted 3G/WCDMA microcells to capture traffic from a co-channel macrocell layer. Simulations and measurements were undertaken for a 3G/Wi-Fi small cell network deployment on thirteen lampposts along Kensington High Street, London.

Both modelling and simulations suggested that dominance could be achieve by +24dBm 3G/WCDMA microcells when deployed under a co-channel macrocell layer and it was shown that the microcell range achieved depended primarily on the level of interference from the macrocell layer. Typical microcell radii predicted from modelling and simulation assuming a 20dB building penetration loss ranged from 30 – 90m (Figure 6.1), and it was also expected that the outdoor microcell range would be much greater than this.

Simulations were also performed to study the potential of the 3G/WCDMA microcells to offload traffic from the macrocell sectors surrounding the area of KHS. These simulations suggested that the proposed network of thirteen low power 3G/WCDMA microcells would indeed capture significant traffic from the surroundings macrocells providing that traffic was located on or close to KHS.

A series of RF measurement drive surveys were also conducted before and after the activation of the initial four 3G/WCDMA microcells in order to validate the macro and microcell coverage simulations and to measure the effective dominance area of the

microcells once they had been activated. Analysis of the drive survey measurements showed that the active 3G microcells clearly provided dominance along KHS and that when all thirteen microcells are enabled for 3G service then contiguous 3G microcell dominance along KHS is expected.

It is concluded that from modelling, simulation and measurements that low power +24dBm 3G/WCDMA microcells do have the potential to significantly offload a co-channel macrocell layer, provided that the microcells are placed in areas of high traffic and are spaced close enough together (<100m) to provide contiguous microcell dominance.

Chapter 7
Small Cell SON: Maximising Small Cell Traffic Capture Through SON Techniques

As was shown in the previous chapter in order to maximise the benefit of microcells located at non-ideal locations within the network, a great deal of network optimisation will be required by the network radio engineering team. This includes neighbour list optimisation, antenna tilt optimisation, careful cell power planning and parameter tuning on both the macro and micro cell layers. However this manual method of optimisation, often involving drive testing the area before and after any microcells have been installed, as was the case in the KHS example, is very labour intensive and cannot always deliver optimal results. Therefore ideally an automated SON method that avoids the need to drive an area to optimise the street level microcell's performance, as well as one that approaches the "optimum" solution (note there will be many optimum solutions depending on whether, coverage, capacity or quality of service are the key performance targets) is required.

This chapter proposes a number of SON based methods that attempt to maximise the microcell network's performance. The first two methods proposed use only microcell based measurements on which to make macrocell network optimisation decisions. The third proposed method is based upon automatic collection of UE measurements using a 3GPP Minimisation of Drive Test (MDT) [34] approach or similar and the analysis of these geo-located UE measurements using three-dimensional Xmaps, an extension to the work undertaken in the Seventh Framework Socrates Project [107], itself based upon an earlier reference [108]. Finally a fourth method based upon a hybrid of the first three methods is proposed and is shown to be the most effective method maximising traffic offload onto the microcell layer.

This chapter begins by reviewing earlier work on SON for microcell offload using MDT and the approaches used in these earlier references. The chapter then describes the four SON methods developed during this study. Simulations are presented which model the four SON methods when applied to the KHS lamppost microcell network. The results of the simulations are then presented and finally conclusions are drawn.

7.1 Review of Previous Small Cell SON Optimisation Techniques

There have been many papers regarding SON for macrocell networks and many papers for applying SON to small cell (micro/pico/femto) networks but very few on using SON together with MDT to maximise the offload from the macrocell layer onto the small cell layer.

SON for macrocell networks has been the topic of many research papers and indeed entire European research projects [107]. References [28, 109, 110] for example present three typical approaches to SON when applied to antenna tilt in macrocellular networks, namely brute force, simulated annealing and methods based on network KPI feedback. Whilst all macrocell methods presented in the literature generally result in an improved network performance, none specifically address the problem of offload to a lower microcellular layer by applying SON techniques to the tilt and power settings of the macrocell layer as is done here in this chapter.

SON for small cell networks (micro, pico and femto) has also received a great deal of focus over recent years, especially given that according to the Small Cell Forum as of November 2012 there were more small cells deployed than macrocells [4]. Many papers, for example [111, 112, 113] consider changes at the small cell only and not the macrocell in order to maximise the coverage and capacity offload provided by standalone small cells. And whilst some papers clearly state the benefit of macrocell to small cell offload for both the macro and small cell users [103, 114], none can be found that propose a joint macro/microcell approach to maximise this offload nor can any references be found on MDT based methods for optimising clusters/linear deployments of 3G/WCDMA outdoor lamppost mounted microcells.

Perhaps one of the reasons that very little focus has been given particularly to SON for outdoor 3G/WCDMA microcells, is that many in the industry believe that 3G/WCDMA traffic growth will flatten over the coming years as more mobile broadband traffic migrates to 4G/LTE networks and therefore mobile operators will deploy outdoor 4G/LTE microcells rather than outdoor 3G/WCDMA microcells in the medium term. In addition 4G technologies such as 4G/LTE allow the implementation of Inter-Cell Interference Coordination (ICIC) schemes that exploit the time/frequency orthogonal properties of OFDMA in order to maximise offload to the 4G/LTE microcell, and lend themselves more to heterogeneous network deployments. The ICIC and enhanced ICIC (eICIC) approach to macro/micro offload has received a great deal of attention and good examples of this can be found in [115, 116].

However, one only has to look at the widely referenced “Cisco Global Mobile Data Traffic Forecast Update, 2012–2017” [3] or the similar GSMA Mobile Economy 2013 forecast [1] to see that whilst the current and forecasted 3G/WCDMA to 4G/LTE device migration rate is faster than it was for case of 2G/GSM to 3G/WCDMA, it will still be many years before 3G/WCDMA traffic is expected to stop increasing and Cisco [3] believes this will be well beyond the year 2017.

Therefore another school of thought is that significant numbers of 3G/WCDMA microcells will be required in some markets and by some operators, prior to the need for the wide scale deployment of 4G/LTE small cells especially for operators who fail to acquire significant

new 4G/LTE spectrum bands and are forced to re-farm existing spectrum holdings for 4G/LTE. Since 3G/WCDMA does not have the time/frequency grid of 4G/LTE to allow ICIC techniques to help solve the underlay/overlay problem, other more traditional approaches for increasing the effectiveness of 3G microcells will therefore be required such as the methods proposed in this chapter.

7.2 Maximising Traffic Offload onto the Kensington High Street Small Cells

As explained in the previous chapter the KHS microcell network is surrounded by many existing Telefonica UK macrocells as shown in Figure 6.4 of the previous chapter.

Since these macrocells are located within central London most are high capacity three carrier 3G/WCDMA macrocells, typically having two carriers at 2100MHz and a third carrier at 900MHz (re-farmed from Telefonica UK's 2G/GSM spectrum allocation). Some of these surrounding sites have also been upgraded from three to six sector configuration in order to increase their capacities. Therefore, as seen from the drive surveys presented in the previous chapter, KHS is already well served by the surrounding macrocells and in order to optimise the coverage and offload capability of the deployed KHS microcell network, antenna and parameter adjustments will be required to a number of the surrounding macrocells.

The problem identified by the Network Engineers during the network optimisation performed to maximise the coverage of the KHS microcells was which surrounding macrocells should be targeted, and what parameters would be most effective in increasing the coverage footprint of the microcells? Whilst on this occasion drive surveys were available which were used to identify the most dominant macrocells (Section 6.5.1), it was clear that the manual optimisation process was non-optimal, i.e. it was very difficult for the Network Engineers to have a full understanding of how the changes they were making to the macrocell network would improve the coverage of KHS microcell and what performance effects these changes would have on the macrocell network and whether their final solution was the most optimum solution in terms of traffic offload, coverage or overall network performance.

It therefore became clear that what was actually required by the Engineers was a method to automatically adjust the parameters (predominantly antenna tilts and CPICH powers) of the surrounding macrocells in order to maximise the chosen target KPI(s) be they microcell coverage or traffic offload for example, whilst still maintaining the overall performance on the surrounding macrocells.

Whilst on this occasion the Engineers had detailed RF drive surveys of the entire deployment area, it was also apparent that in future as the volumes of small cells deployed

increases, the ability to survey before and after deployment will not always be possible because of access or OPEX issues or both. Therefore there was also identified a second requirement of being able to estimate the actual macrocellular coverage by means other than dedicated drive surveys and as shown in Chapter 5, MDT or similar geo-location techniques are now being proposed to achieve this understanding of actual macrocell coverage across all areas of the network without the need for dedicated detailed drive or walk surveys.

Based upon the above two requirements it became apparent that an automated network optimisation method to maximise traffic offload onto small cells might be possible based upon the use of geo-located UE measurement reports. Therefore it was decided that simulations would be performed to further model the KHS network in an attempt to derive an automated means to optimise both macro and micro coverage in order to maximise the capacity offload from the macrocells onto the KHS microcell layer – without compromising the network quality on the macrocell layer.

One other factor that also had to be borne in mind when investigating possible SON technique based upon analysis of collected measurements was the period over which measurements must be taken in order to have a representative view of the network. Generally, Network Engineers analyse and compare daily weekday statistics in order to observe trends within the network following a network change, since analysing statistics collected across a whole day captures the entire traffic patterns seen by the cell. Therefore if SON algorithms are expected base their decisions by analysing the entire traffic patterns then it is also likely that they are programmed to consider daily statistics on which to base their decisions. This means that a SON algorithm that analyses daily statistics may only make one network change per day and then will wait until the next day to review this change and then make another change and so on. SON algorithms that take many steps to reach an optimised solution based on daily statistics are therefore unlikely to keep up with the pace of change of the network as new cells are added and removed and other urgent manual changes are made to the network. Therefore in order to be effective, SON algorithms based on the analysis of daily statistics requiring the least number of changes to arrive at an optimised solution are likely to be the most effective when deployed in a live, ever changing, cellular network.

7.3 Small Cell SON Simulation Assumptions

In order to evaluate SON methods for small cell offload using MDT or similar on a realistic and known heterogeneous network configuration, further changes were made to the Network Simulator to model more precisely the interaction of the coverage between the KHS lamppost microcells and the surrounding Kensington macrocell sites.

The simulation area used was the same 3x3km simulation area as was used for the earlier small cell placement and microcell coverage analysis work of the previous chapters. Again in this case as with the coverage analysis work the simulation area contained 31 surrounding macrocell sites as well as the thirteen KHS lamppost mounted microcells as shown previously in Figure 6.4.

The macrocell radio propagation path loss model used for the small cell SON offload simulations was again based upon the heterogeneous macrocell model proposed in [51]. Building penetration loss was once again derived from the London land use clutter data made available by Telefonica UK. The microcell propagation model chosen for the small cell SON offload simulations was the "Urban Micro Line of Sight" model proposed in [52]. A Line of Sight (LoS) based model was chosen since the target traffic for the KHS lamppost microcells will typically have visibility of the lampposts (outdoor users or users in shops/restaurants along Kensington High Street). Again the same clutter based penetration loss was applied for this microcell propagation model as for the macrocell model.

Cellular traffic was distributed according to clutter class across the entire simulation area with greater user densities being applied to dense urban and urban areas than for parks and open spaces. A special hotspot class of clutter was also defined for the KHS area, and the traffic density for this area was set at five times the traffic density applied to the dense urban clutter area (Figure 7.1).

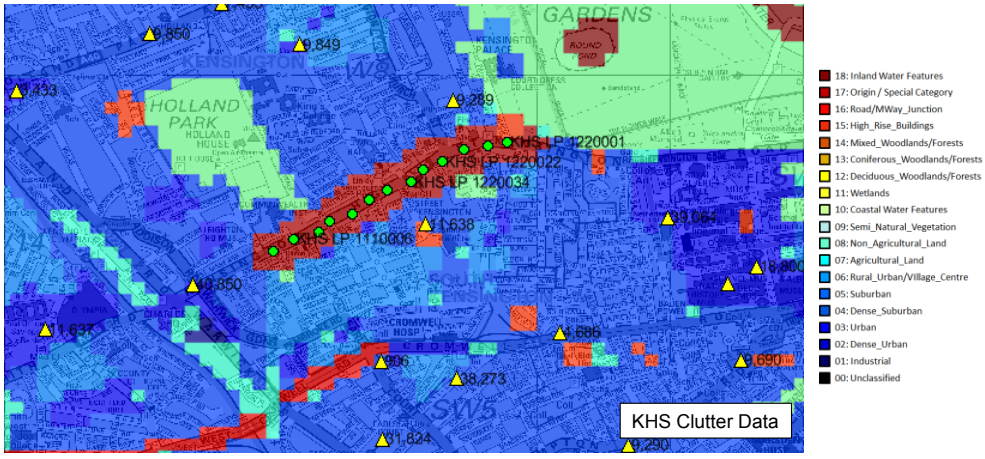

Figure 7.1 Clutter Categories for Kensington Small Cell Simulation Area — showing the use of clutter category 17 to define the KHS high traffic area surrounding the thirteen lamppost microcells.

Whilst all sites and cells were active in the simulations to avoid edge effects macrocell statistics were gathered from only the sites and users within the central 2x2km region of the simulation area. This area obviously included all street level microcells as well as the key sites surrounding KHS. The main network simulation parameters for the KHS network are given below in Table 7.1.

Table 7.1 Small Cell SON Network Simulation Assumptions.

Simulation Assumption	Value
No. Surrounding Macro Sites	31 sites, 71 sectors
No. KHS Lampposts	13
Macro Sector Max. TX Power	37-43dBm (SON adjustable)
Macro CPICH Power	10% Macro TX. power
Macro Other CCCH Power	10% Macro TX. power
Macro HSPA HS-DSCH Power	50% Macro TX. power
Macro Antenna Mechanical Tilt	As per Telefonica network setting
Macro Antenna Electrical Tilt	0-10^{o} (SON adjustable)
Micro Max. TX Power	10dBm
Micro CPICH Power	10% Micro TX. power
Micro Other CCCH Power	10% Micro TX. power
Micro HSPA HS-DSCH Power	50% Micro TX. power
Micro Antenna Gain	2dBi
Downlink Orthogonality	0.5 (Perfect orthogonality = 1)
Operating Frequency	3GPP Band I (2100MHz)
Macro Path Loss Model	3GPP 25.814 [51]
Macro Penetration Loss	Clutter based loss
Micro Path Loss Model	3GPP 36.814 [52]
Micro Penetration Loss	Clutter based penetration loss
UE Height	1.5m
UE Antenna Gain	0dBi
UE Noise Figure	9dB
Accuracy of geo-location (RMS)	25m
Users Distributed	500 per snap shot, of which 136 were within the KHS high traffic area

7.4 Macro to Microcell Offload SON Methods Evaluated

As was shown in the previous chapter, simulations and measurements of the KHS microcell network had shown that 3G/WCDMA microcells deployed with a maximum transmit power of +24dBm on the thirteen lampposts of KHS provided dominant outdoor coverage along KHS. Therefore in order to provide a challenge for any SON algorithms being developed as part of this work, the simulated KHS microcells had their maximum transmit power reduced to just +10dBm, leading to a much reduced and therefore more challenging microcell coverage footprint from which to begin network optimisation. The best server areas of only the +10dBm microcells prior to SON optimisation is shown in Figure 7.2. This limited microcell coverage area provided just 0.08km^2 of coverage, covered just 34% of the KHS high traffic area and served on average only 47 out of the potential 136 users distributed in the KHS high traffic area.

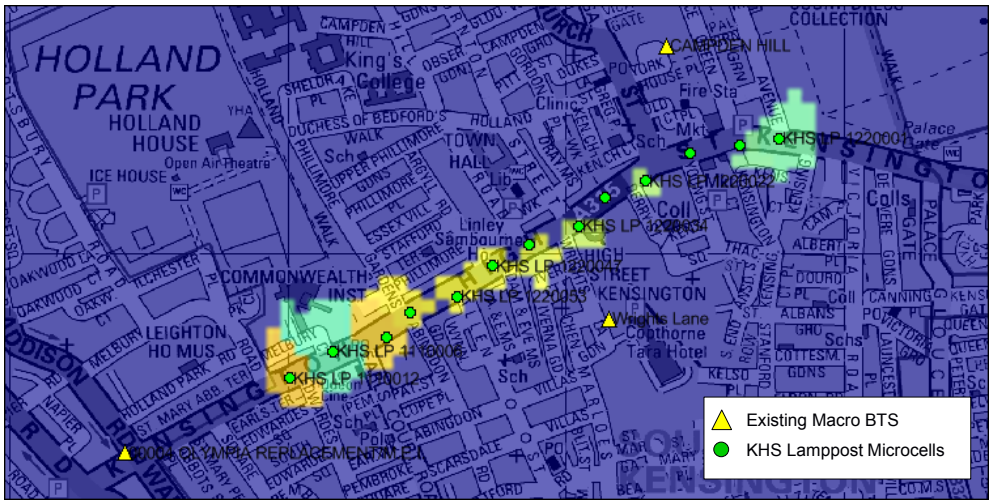

Figure 7.2 KHS Lamppost microcell best server areas prior to network optimisation. Microcell BTS maximum output power = +10dBm.

7.4.1 SON Offload Method 1 – Post Based Measurement Method

The first SON method evaluated was a method that attempted to maximise the microcells coverage footprint by making adjustments to the surrounding macrocells' antenna tilts and transmitter powers based upon measurements taken only at the lamppost microcells themselves. This of course would mean that the microcell would also need some additional hardware in order to be able to measure the co-channel downlink signals from the macrocells and of course to be effective the downlink transmission of the microcell making the measurement would have to cease whilst such measurements were being made. In fact to ensure as many macrocells were detected as possible, all lamppost microcells would need to

halt downlink transmissions during a short period whilst the measurements were being taken to avoid saturation of their receivers from nearby microcells.

Method 1's microcell measurement based SON algorithm operated as follows:

1. *Each lamppost microcell reported the strongest measured macrocell to the SON algorithm.*
2. *The SON algorithm then generated a* ***Target Macrocell List*** *ranked by the number of reports from the microcells for each unique best serving macrocell detected.*
3. *The SON algorithm then worked through the cells of the ranked* ***Target Macrocell List*** *considering the following conditions until a candidate macrocell to change (tilt or power) was found*

   if *the current candidate macrocell's downtilt could be increased (i.e. the antenna electrical tilt was not at the maximum downtilt angle of 10°)*
   then *the macrocell's antenna was downtilted by a further tilt step size (in this case 1°).*
   else if *the current candidate macrocell's transmit power could be reduced (i.e. the cell's transmit power was not at the minimum value of +37dBm)*
   then *the macrocell's transmit power was reduced by the power step size (in this case 0.5dB)*

4. *Steps 1-3 were repeated until no further changes could be made to the macrocells of the current* ***Target Macrocell List****.*

This basic post-based measurement algorithm made no attempt to avoid tilting macrocells further towards the KHS microcell network, nor did it take into account the effect it was having on the macrocell coverage since its only source of information was the measurements received by the lamppost microcells.

In order to overcome some of the obvious shortfalls of Method 1 a refined post-based measurement algorithm (Method 1+) was also developed to avoid macrocell tilts that increased rather than reduced the macrocell's signal level received at the KHS lamppost microcells.

This was done by calculating the linear average of the RSSI reported by each KHS lamppost microcell ($RSSI_{KHS}$) as

$$RSSI_{KHS} = 10\log_{10}\left[\frac{1}{n}\left(\sum_{i=1}^{n} 10^{\frac{RSSI_i - 30}{10}}\right)\right] \quad \text{[dBm]} \qquad (7.1)$$

where

n	was the number of lamppost microcells over which the linear average is made
$RSSI_i$	was the reported RSSI for lamppost microcell i in dBm.

And then comparing this value before and after each macrocell tilt change and reverting to the previous macrocell tilt if a new tilt resulted in higher interference from the downtilted macrocell onto KHS. Also if the cell's tilt was reverted then further tilt changes to that particular cell were no longer allowed.

Method 1+'s SON algorithm operated as follows:

1. *Each lamppost microcell reported the strongest measured macrocell to the SON algorithm.*
2. *The SON algorithm then generated a **Target Macrocell List** ranked by the number of reports from the microcells for each unique best serving macrocell detected.*
3. *The SON algorithm then worked through the cells of the ranked **Target Macrocell List** considering the following until a candidate macrocell to change was found*

   ***if** the current candidate macrocell's downtilt could be increased (i.e. the antenna electrical tilt was not at the maximum downtilt angle of 10^o **and** it had not had its tilt frozen by a previous iteration)*
   ***then** the macrocell's antenna was downtilted by a further tilt step size (in this case 1^o).*
   ***else if** the current candidate macrocell's transmit power could be reduced (i.e. the cell's transmit power was not at the minimum value of +37dBm)*
   ***then** the macrocell's transmit power was reduced by the power step size (in this case 0.5dB)*

   <Increased macrocell interference check>
   ***if** the current candidate macrocell's downtilt had increased the average RSSI calculated across all lamppost microcells*
   ***then** revert the current candidate macrocell's downtilt and mark the cell's antenna tilt as frozen*

4. *Steps 1-3 were repeated until no further changes could be made to the macrocells of the current **Target Macrocell List**.*

7.4.2 SON Offload Method 2 – 3D Xmap Method

The third SON offload method considered (Method 2) was based upon the analysis of 3D or multi-layered (1st best server, 2nd best server, etc.) 3G/WCDMA RF Xmaps constructed through the processing of MDT UE measurement reports or similar geo-located UE measurement reports. Each simulated UE measurement report contained the best five servers' Scrambling Code, RSCP and Ec/Io measurements. An RMS location accuracy of 25m was assumed for each UE measurement reports, since it was expected that using RF fingerprinting techniques or similar such as those presented in Chapter 5, then it would be possible to ensure that SON decisions would be based only upon a subset of UE measurement reports with very reliable location accuracy.

Using these geo-located UE measurement reports various multi-layered RF Xmaps were constructed for the entire simulation area. The 3D Xmaps generated for the MDT based methods are listed below.

Xmap1: Best Server Xmap

Xmap2: Best Server RSCP Xmap

Xmap3: Best Server Ec/Io Xmap

Xmap4: Best Server Macro within Microcell Best Server Area Xmap

Xmap5: Best Server Micro Xmap (Microcells only)

Xmap6: Best Server Macro Xmap (Macrocells only)

Values within each Xmap were overwritten with each new UE measurement report received for that location during the simulation. An averaging updating technique was also considered but was not implemented.

Since the Xmaps were constructed entirely from randomly located UE measurement reports, then there was no guarantee that values for all the pixels of the Xmap would be received during the simulations prior to the Xmap based SON algorithm making its optimisation decision. An example of a Best Server Xmap is shown in Figure 7.3, here it can be seen that for the low traffic areas, such as Kensington Gardens, very few measurement reports have been received at this moment in time within the simulation. One option, as was shown in Chapter 5, is to use interpolated values for the missing areas in order to complete the Xmap, however in reality this may also cause inaccuracies in the Xmap which may lead to incorrect optimisation decisions. Therefore the decision was taken to initially allow Methods 2 and 3 to base their optimisation decisions on partially completed Xmaps by excluding pixels without values from the calculations rather than use complete, interpolated Xmaps.

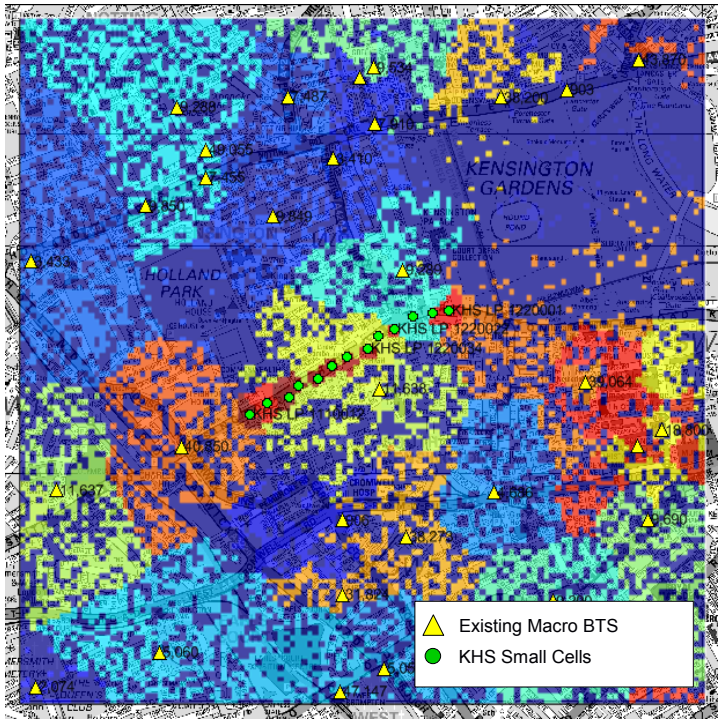

Figure 7.3 KHS Best Server Xmap example for KHS simulation area – dark blue areas are areas for which UE reports have yet to be received.

The RF Xmap based algorithm (Method 2) also considered if the proposed macrocell tilt would increase the microcell coverage area and therefore be worthwhile and if the proposed change would reduce the targeted macrocell's coverage area by more than 10% of its original value.

Method 2's SON algorithm operated as follows:

1. *The SON algorithm generated a **Target Macrocell List** by analysing the "Best Server Macrocells within Microcell Best Server Area" Xmap and ranking the interfering macrocells by the number of pixels within the Xmap that they were the strongest interferer. Only macrocells that made up greater than 5% of this Xmap were considered as change targets.*
2. *The SON algorithm then worked through the cells of **Target Macrocell List** considering the following until a change candidate was found*

   ***if** the current candidate macrocell's downtilt could be increased - (the antenna electrical tilt was not at the maximum downtilt angle of 10° **and** changes to the cell's tilt were not frozen **and** the tilt would increase the microcells' coverage **and** the tilt would not reduce the macrocell's coverage area by greater than 10% of its original value)*

   ***then** the macrocell's antenna was downtilted by a further tilt step size (in this case 1°).*

else if *the current candidate macrocell's transmit power could be reduced - (the cell's transmit power was not at the minimum value of +37dBm* ***and*** *the power reduction would not reduce the macrocell's coverage area by greater than 10% of its original value)*
then *the macrocell's transmit power was reduced by the power step size (in this case 0.5dB)*

3. *Steps 1-2 were repeated until no further changes could be made to the macrocells of the* ***Target Macrocell List****.*

7.4.3 SON Offload Method 3 – 3D Xmap Method with Change Prediction

The fourth and final SON method proposed (Method 3) was again based upon the analysis of 3D multi-layered RF Xmaps but in addition to this Method 3 also took into account the potential increase in microcell traffic each macrocell network change would provide. It did this by analysing a Traffic Density Xmap constructed from the geo-located UE measurement reports (Figure 7.4).

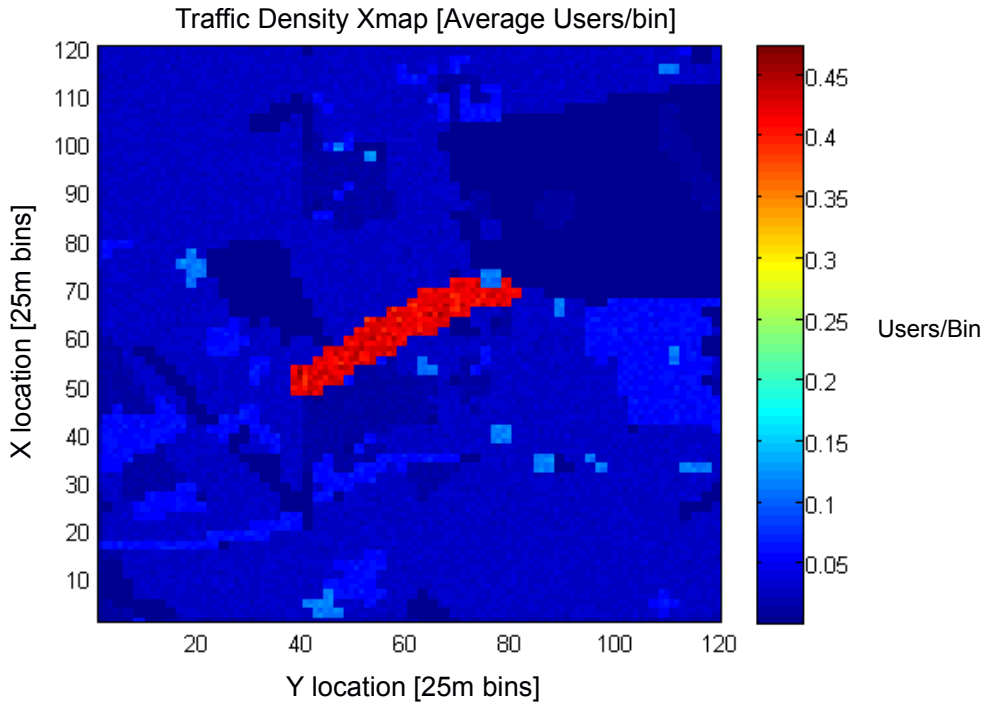

Figure 7.4 Example Traffic Density Xmap for the Kensington network simulation area

In addition since the microcell locations were already known, pseudo-post reports were also delivered to the SON algorithm simply by averaging the UE reports received for the precise microcell locations. This method delivered measurements similar to those that would have been received from the lamppost microcells, but without the added cost and complexity of having a separate downlink receiver at each microcell.

To reduce the number of steps required for Method 3 to arrive at an optimised solution, all tilt and power combinations were evaluated for each macrocell within ***Target Macrocell List*** in order to determine which change resulted in the greatest increase in microcell traffic. This was done by applying the tilt and/or power changes onto the RF Xmaps and then "predicting" the traffic offloaded from the macrocell layer onto the microcells that each potential change could deliver. The network change delivering the biggest traffic offload whilst also maintaining the overall network quality (no more than 2% of macrocell users to have an Ec/Io < -16dB) was the change that was applied to the network.

Finally once the algorithm had exhausted all possible changes in the macrocell network, if it was found that a macrocell sector in the ***Target Macrocell List*** now served fewer than five users then this macrocell sector was turned off. This removal of a dominant interferer may or may not lead to further changes being possible to the remaining macrocells of the ***Target Macrocell List***.

Method 3's SON algorithm operated as follows:

1. *The SON algorithm generated a **Target Macrocell List** by analysing the "Best Server Macro within Microcell Best Server Area" Xmap and ranking the interfering macrocells by the number of pixels within the Xmap that they were the strongest interferer. Only macrocells that made up greater than 5% of this Xmap were considered. In addition to this any additional macrocells reported from the pseudo-post reports were added to the **Target Macrocell List**.*
2. *The SON algorithm then worked through the **Target Macrocell List** considering all possible tilts (uptilts as well as downtilts) and powers for each macrocell on the **Target Macrocell List** considering which change to which cell delivered the biggest gain in microcell traffic, whilst maintaining the user outage (Ec/Io <-16dB) below the 2% threshold across the whole macrocell network.*
3. *If no changes were possible to the cells of the **Target Macrocell List** then if any of these cells now carried five or fewer users, then these cells were switched off.*
4. *Steps 1-3 were repeated until no further changes/removals could be made to the macrocells of the **Target Macrocell List** that would increase the traffic carried by the microcell layer.*

7.5 Macro to Microcell Offload SON Method Results

The proposed four SON methods were evaluated using a modified version of the Network Simulation tool described in Section 7.3. For each method, each network parameter change proposed was preceded and followed by 100 runs of the Monte Carlo simulator, with each run seeing 500 users randomly distributed across the simulation area according to clutter class. Reports from 50,000 users were therefore considered for each network change. At the end of each run the microcell reports and Xmaps were updated accordingly and at the end of each set of 100 runs the SON algorithms being evaluated then analysed the microcell reports (Methods 1 & 1+) or Xmaps (Methods 2 & 3) in order to determine the next macrocell network change. A summary of the results for each of the proposed methods is given below in Table 7.2.

Table 7.2 Microcell Coverage and Traffic Improvements for the Four Proposed SON Methods. (Original microcell coverage area = 0.08km^2 and original microcell traffic = 47 users.)

SON Method	Steps Taken	Optimised Microcell BS Area [km^2]	Microcell Area Increase [%]	Optimised Microcell Traffic [Users]	Microcell Traffic Increase [%]	Network RSCP Reduction [dB]
1	162	0.376	370%	124	164%	4.3
1+	26	0.196	145%	102	117%	0.5
2	77	0.217	171%	97	105%	1.6
3	23	0.268	235%	129	175%	1.7

7.5.1 SON Offload Method 1 Results

Method 1 resulted in 162 changes being made to the macrocell network. Whilst it significantly increased the coverage area of the microcells by some 370% and increased the offloaded traffic to the microcells by 164% (Table 7.2), it did not deliver contiguous microcell coverage along KHS (Figure 7.5) and caused an overall 4.3dB reduction in the macrocell RSCP coverage across the macrocells of the central 2x2km region of the simulation area. This reduction in macrocell coverage was due to the lack of macrocell network feedback, not possible using only microcell based measurements.

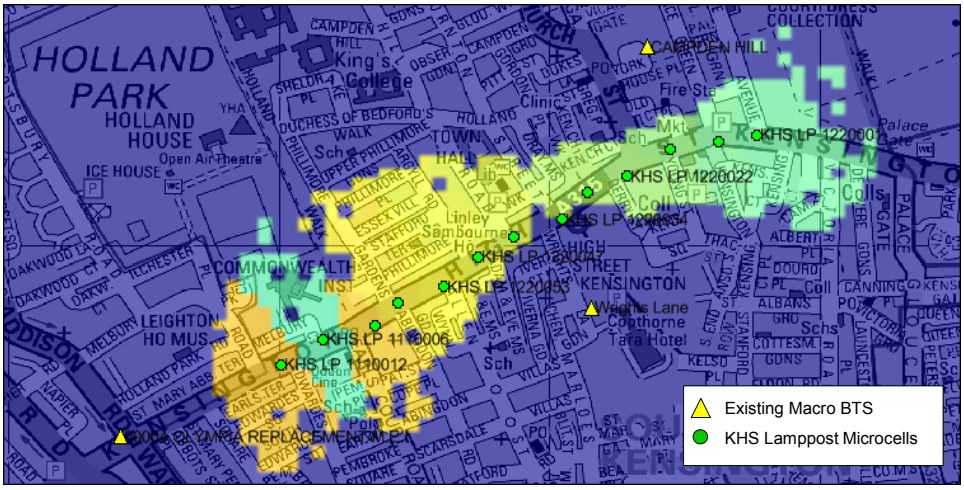

Figure 7.5 Microcell best server coverage areas delivered by Method 1.

7.5.2 SON Offload Method 1+ Results

Method 1+, however did perform much better than Method 1 because of its ability to correct any tilts that resulted in an overall increased RSSI measured at the KHS microcells. This not only avoided macrocells being tilted towards KHS that in turn increased the macrocell interference onto KHS, it also prevented extreme tilts being made to the macrocells and avoided the significant overall macrocell RSCP reduction seen in the case of Method 1. Whilst Method 1+ did not deliver as large a coverage area or as much traffic offload onto the microcell layer as Method 1 (Table 7.2), in just 26 steps it delivered contiguous microcell coverage along KHS (Figure 7.6), it increased the microcell coverage area by 145%, and delivered a reasonable increase (117%) to the traffic carried on the microcell layer. All this was achieved with just a 0.5dB reduction in the macrocell RSCP coverage across the cells of the central 2x2km region of the simulation area.

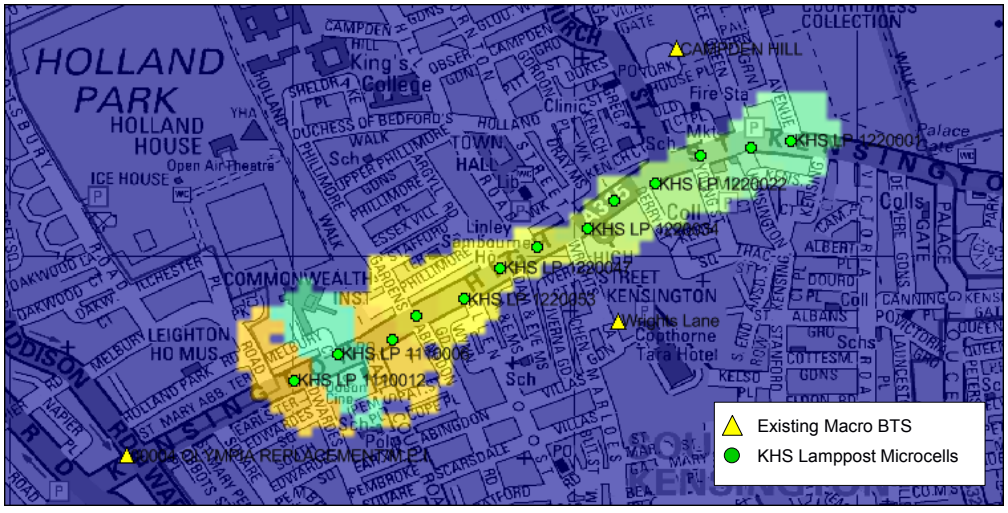

Figure 7.6 Microcell best server coverage areas delivered by Method 1+.

7.5.3 SON Offload Method 2 Results

Method 2 as expected did not deliver the kinds of gains seen by Method 1 since it cautiously optimised the network, checking that each change would increase the microcell coverage and would not decrease the macrocell's coverage area by less than 10% of their original values. That said it still provided significant coverage (171%) and traffic (105%) gains for the microcell layer (Table 7.2), but unfortunately it did not provide contiguous microcell coverage along KHS as shown in Figure 7.7 and took 77 steps to deliver its final solution. Method 2 led to a 1.6dB reduction in the macrocell RSCP coverage across the cells of the central 2x2km region of the simulation area.

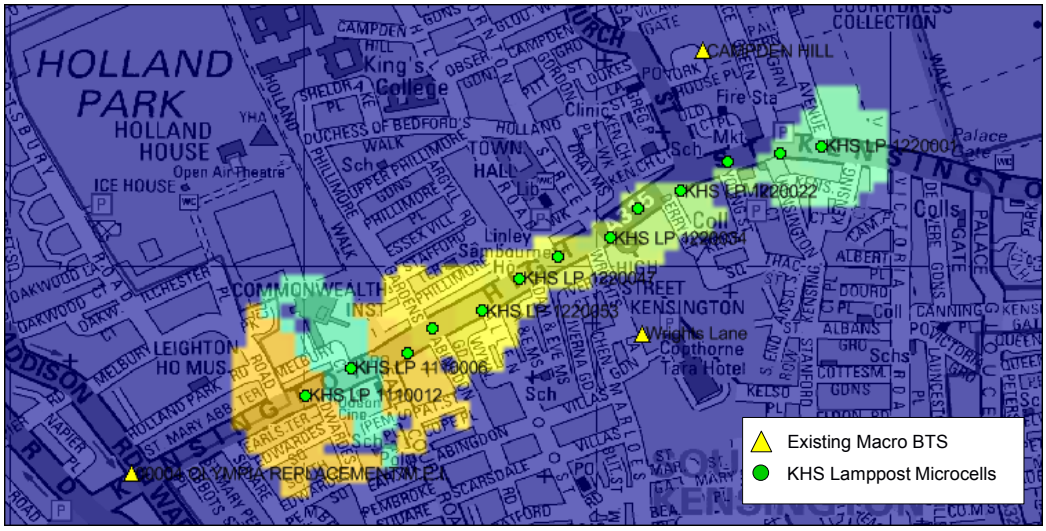

Figure 7.7 Microcell best server coverage areas delivered by Method 2.

7.5.4 SON Offload Method 3 Results

Method 3 took just 23 steps (Table 7.2) to deliver its optimised solution (Figure 7.8) and actually because of its ability to jump to the correct tilt and power setting for each change, rather than the trial and error approach adopted by the other algorithms, within its first nine steps (Figure 7.9) Method 3 had delivered more contiguous coverage to the high traffic area of KHS than any of the other algorithms did over all of their entire steps. Whilst Method 3 did not provide as great an increase in the microcell coverage areas (235%) as Method 1, the coverage increases it did provide was precisely aimed at the high traffic area of KHS, which in turn at increased traffic offload onto the microcells. For this reason Method 3 provided the greatest traffic offload (175% microcell traffic increase) onto the microcells of all the four SON methods considered. It also provided contiguous coverage along KHS whilst maintaining the users Ec/Io outage levels below the target level of 2% (Figure7.10). Method 3 led to a reasonable 1.7dB reduction in the macrocell RSCP coverage across the cells of the central 2x2km region of the simulation area.

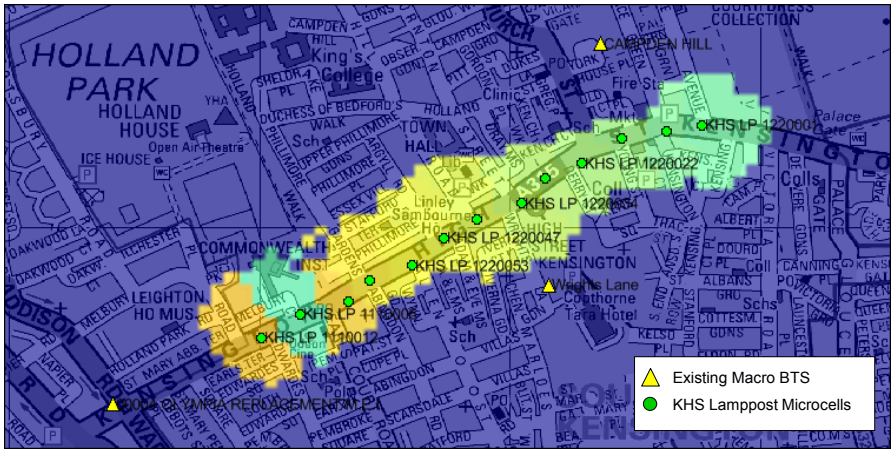

Figure 7.8 Microcell best server coverage areas delivered by Method 3.

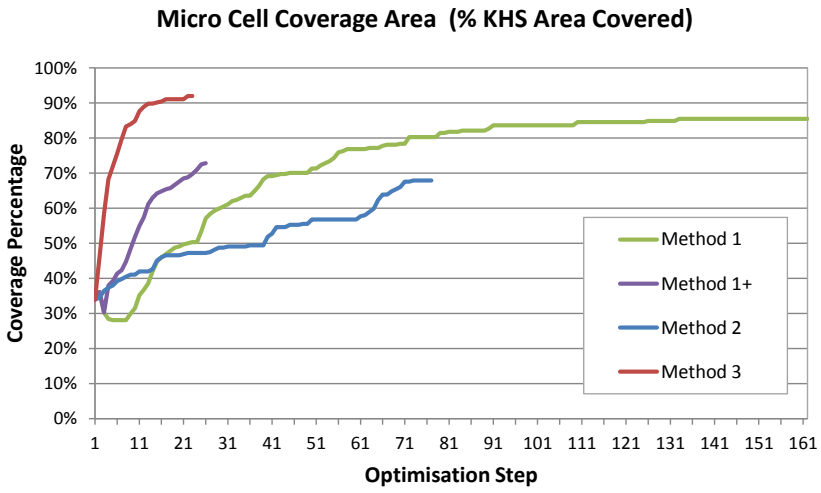

Figure 7.9 Percentage of the KHS high traffic area covered versus the optimisation steps taken to achieve these coverage levels for the four SON methods considered.

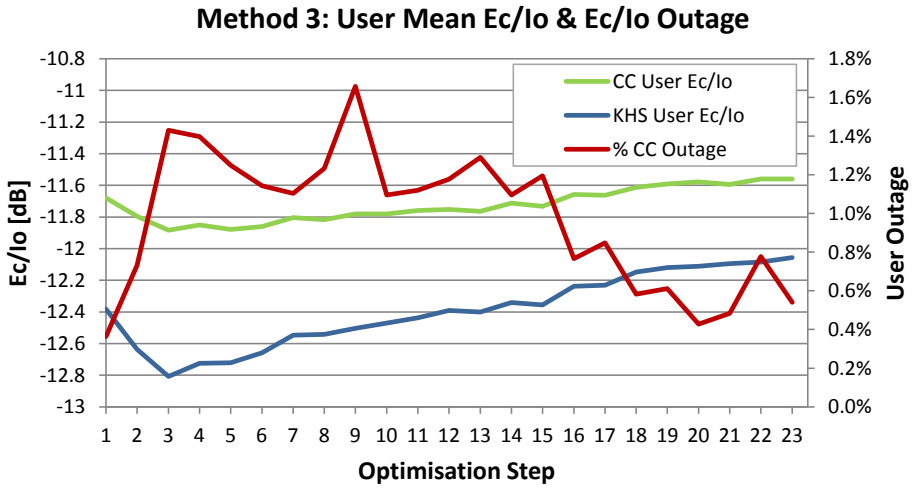

Figure 7.10 User average Ec/Io and Ec/Io outage delivered by Method 3 for the Central Area (CC) and KHS area.

7.6 Chapter Summary

This chapter has presented four proposed SON methods developed to maximise traffic offload from a 3G/WCDMA macrocell network onto low power street level 3G/WCDMA microcells deployed on a shared carrier frequency with the macrocell layer. Two out of the four algorithms use microcell based measurements only and the remaining two have been designed around the automatic collection and mapping of geo-located UE measurement reports on to a series of what has been termed here 3D Xmaps.

The first microcell based measurement method (Method 1) used a majority voting approach based upon downlink measurements at each lamppost mounted microcell to target the surrounding macrocells seen to be causing the most interference. Method 1's algorithm was then able to tilt and down power these surrounding sites without worrying about the consequences of its actions on the performance of the macrocell layer and whilst this led to a greatly increased microcell coverage area (albeit in the wrong areas), it also led to a severe RSCP coverage reduction (4.3dB) on the macrocell layer. Method 1 took 162 steps to reach its final solution and clearly as explained earlier, if each step was reliant on having a day's worth of network statistics in order to assess the effect of each change, then an algorithm taking this many steps to arrive at a solution would not be practical to deploy in a real network. Method 1 also did not achieve contiguous coverage along KHS and for this and the previous two reasons Method 1 is discounted as being a suitable SON method for microcell offload.

The second microcell based measurement method (Method 1+) again used majority voting to target the surrounding macrocells, but this time the algorithm also monitored the effect each change had on the overall macrocell interference level seen across all of the microcells on KHS. If the macrocell change increased the interference level seen by the microcells then the macrocell that had just been tilted had its tilt reverted back to its previous configuration and then that cell was excluded from any further changes. This approach certainly ensured that macrocells were not downtilted towards KHS and it also avoided the situation seen from Method 1's results where many of the surrounding macrocells were downtilted to their maximum values, resulting in significant coverage reduction on the macrocell layer. Method 1+ provided a reasonable coverage and traffic increase and did this in just 26 steps making it a practical algorithm based on the use of daily networks statistics between each change. It also provided contiguous microcell coverage along KHS.

The first of the Xmap based methods, Method 2, selected its target macrocells based upon the coverage overlap seen between the micro and macrocells and then cautiously optimised the macrocell network by ensuring each macrocell change did not result in the macrocell's coverage area being reduced by more than 10% from its original value. Whilst the algorithm aimed to maximise coverage rather than traffic carried, it still failed to provide contiguous

coverage along KHS. Method 2 took 77 steps to achieve its final solution and because of this and its failure to provide contiguous coverage Method 2 is discounted as being a suitable SON method for microcell offload.

The second of the two Xmap based methods, Method 3 was built upon on Method 2's Xmap approach but including the pseudo post reports in its decision making process. It also reduced the number of steps required to achieve its final solution by predicting the effect each proposed change would have on the macrocell and microcell networks. Method 3 operated by targeting traffic offload onto the microcells rather than purely additional microcell coverage and by doing so delivered the greatest increase in microcell traffic of all the four SON methods considered. Method 3 took just 23 steps to reach its final solution, but had provided most of its gains within the first 9 steps.

In summary two out of the four proposed methods appear to be viable SON based methods for increasing the traffic offload onto the microcell layer. The proposed post-based measurement method, Method 1+ appears from simulation to be a very simple yet effective SON method in order to increase the coverage and the traffic carried by the microcell layer without having a negative impact on the surrounding macrocells' network performance. It also lends itself to a simple implementation within the Radio Access Network (no need for an MDT server). However, the proposed Xmap based approach of Method 3 appears from simulation to be the most effective method at increasing both microcell coverage and traffic offload onto the microcell layer. The results from both these two approaches suggest that measurement based (microcell or UE) closed loop SON methods for maximising small cell offload do appear to be a realistic possibility and are worthy of further investigation.

Chapter 8
Conclusions

This thesis has presented work undertaken to study key aspects of self-organising heterogeneous networks. In particular adaptive dynamic antenna tilting and higher order sectorisation at the macrocell and cell placement, cell offload and self-organising techniques to maximise offload for small cells. An outline of the work that has been presented in this thesis, along with the main conclusions from this work are presented in Section 8.1. This is followed by Section 8.2 which highlights the main original contributions within this thesis. Finally in Section 8.3 some suggestions for future work are proposed.

8.1 Summary of Thesis

A summary of the thesis is given below:

Chapter 1 identified the main aims of the work contained within this thesis.

Chapter 2 gave an overview of the mobile broadband industry as well as an introduction and general literature review of Self-Organising Networks.

Chapter 3 proposed a dynamic macrocell antenna titling concept that could be used to facilitate a self-organising macrocell network. Simulations were undertaken to evaluate the performance of this technique on ideal hexagonal as well as real world 3G/HSPA and 4G/LTE networks. Finally results from the initial field trial of this novel antenna technique were presented and were shown to support the results of the earlier simulations.

Chapter 4 studied the capacity gains of higher order sectorisation on a 3G/WCDMA macrocell network. It began by presenting simulations undertaken to study the expected capacity gains provided by 6, 9, 12, and 15 sectored sites over the capacity of a standard three sectored 3G/WCDMA macrocell site. The simulations were undertaken on an ideal hexagonal network as well as a real world 3G/HSPA network. The chapter not only considered the predicted capacity gains but also the ideal horizontal antenna beamwidth required to maximize the downlink capacity for 3, 6, 9, 12, and 15 sector sites whilst maintaining coverage and other typical 3G/WCDMA network operator KPIs. Finally the chapter presented field trial results from live 3G/WCDMA cell sites within Telefonica UK's network upgraded from three to six sectors as well as results from the deployment of the what is believed to

be the world's first fifteen sector 3G/WCDMA site and compared these measured field results to those obtained from simulation.

Chapter 5 considered if it is possible to effectively locate small cells on a limited set of street furniture locations (in this case central London lampposts) using geo-located UE measurement reports of varying location accuracy. The chapter considered the use of RF information detailed within the UE measurement reports to better locate the traffic hotspots within the network through the use of a proposed RF fingerprinting technique. This RF information was also used to estimate the potential cell size of small cells when deployed on a common carrier frequency with the macrocell network. This cell size information was then used to choose the most effective locations for small cell deployment in order to capture the most traffic from the macrocell layer.

Chapter 6 looked at the effectiveness of low power, lamppost mounted, 3G/WCDMA microcells to capture traffic from a co-channel macrocell layer. The chapter detailed simulations that modelled the potential offload achieved by the deployment of thirteen low power, 3G/WCDMA microcells on lampposts along Kensington High Street in central London and then compared these simulation results to field measurements taken before and after the actual deployment of four lamppost mounted 3G/WCDMA microcells along the same street.

Finally Chapter 7 proposed a number of SON based methods to maximise offload from the surrounding macrocells onto the Kensington High Street lamppost mounted microcells. The first two methods proposed used only microcell based measurements on which to make macrocell network optimisation decisions. The third method proposed was based upon automatic collection of UE statistics using a 3GPP Minimisation of Drive Test approach or similar and the analysis of these geo-located UE measurements using three-dimensional Xmaps. Finally a fourth method based upon a hybrid of the first three methods was proposed and was shown to be the most effective method in terms of traffic offloaded onto the microcell layer with the fewest macrocell tilt and power changes.

The main conclusions from the work undertaken in this thesis are as follows:

As explained in Chapter 2, it is expected that until the cost of outdoor small cells reduces considerably it will always be more cost effective to maximise the capacity of existing macrocells in order to cope with growing mobile broadband data traffic volumes. Two techniques that can help improve macrocell capacity are rapid dynamic antenna tilting and higher order sectorisation.

It has been shown that rapid dynamic antenna tilting, made possible by Quintel SONWav antenna technology can deliver reasonable macrocell capacity gains for both 3G/WCDMA and 4G/LTE technologies. Ideal hexagonal network simulations undertaken predicted capacity gains of between 4 and 36% depending on the type of packet scheduler employed and the initial level of network optimisation. Simulations undertaken on an optimised central London 4G/LTE network suggested capacity gains ranging from 8 to 26% were possible, again depending on the packet scheduler employed. Initial field trials of rapid dynamic antenna tilting have confirmed capacity gains of up to 30% and showed cell edge throughput gains of up to 80%.

Chapter 4 showed that higher order sectorisation can theoretically deliver up to almost four times (15 sectors per site) the capacity of an existing 3 sectored site and that the optimum horizontal antenna beamwidths to deliver the highest capacity whilst maintaining a set of typical network operator KPIs are as follows.

- 3 sector site - optimum horizontal beamwidth = 62^{o}
- 6 sector site - optimum horizontal beamwidth = 34^{o}
- 9 sector site - optimum horizontal beamwidth = 20^{o}
- 12 sector site - optimum horizontal beamwidth = 18^{o}
- 15 sector site - optimum horizontal beamwidth = 14^{o}

Both simulation and field results have shown that higher order sectorisation gains are possible in a real network with non-ideal site placement for both a network of higher order sectored sites as well as a network containing stand-alone higher order sectored sites.

Out of the higher order sectored site configurations studied, the 15 sectored site configuration theoretically provided the highest gains, however, up until recently antenna and base station technology had not been available to validate if such a configuration was capable of providing such capacity gains. With the development of the Argus 5NPX1006F antenna and the NSN Flexi base station this technology limitation has now been overcome and this allowed the deployment and operation of what it believed to be the world's first live deployment of a 15 sectored 3G/WCDMA site. Whilst the initial trial results have not shown the capacity gains predicted by the network simulations, the trial has shown that 15 sector deployment is possible and has the potential to deliver some if not all of capacity gains predicted.

As also explained in Chapter 2 the macrocell layer's capacity is not expected to cope with the predicted future traffic demand given the traffic forecasts referenced in the chapter, and therefore a move to a network of smaller cells is inevitable. In

order to maximise the cost effectiveness of the small cell layer, Chapters 5 & 7 have also considered a number of SON techniques that can help improve the traffic offload from the macrocell layer to the small cell layer.

It has been shown in Chapter 5 that the placement of small cells, especially low powered small cells, in relation to the traffic hotspot is key to maximising the traffic capture by the small cell layer and that the use of geo-located UE measurement reports can be very effective at locating traffic hotspots so long as the accuracy of the geo-location information remains high. If the UE location information accuracy is poor, which it will be for the majority of the UEs located indoors, a simple technique based on RF fingerprinting has been shown to be effective at locating hotspot locations even at very large UE RMS location errors of 150m or greater. It has also been shown that a small cell size estimation method based upon the interpolation of geo-located UE measurement reports for the macrocell layer can be used to greatly increase the effectiveness of the locations chosen for small cell deployment when sharing a carrier frequency with the macrocell layer.

The actual effectiveness of low powered small cells to capture traffic from a co-channel macrocell layer was confirmed in Chapter 6, for a busy street in central London. Simulations have shown that thirteen low powered (+24dBm), lamppost mounted, 3G/WCDMA small cells should provide a dominant microcell layer along Kensington High Street and offload significant traffic from the surrounding macrocell layer. Results from the field trials of low powered small cells deployed on four lamppost of Kensington High Street have also confirmed this to be the case.

Finally it was shown in Chapter 7 that SON methods can be used to further enhance the traffic offload from the macrocell layer onto low power, street level small cells. Methods based on the generation of three dimensional Xmaps appear have been shown to be both practical (they can reach their optimum solutions in very few steps) and effective (235/175% microcell coverage area/traffic increase for the example chosen) whilst maintaining or improving the network performance of the surrounding macrocell network.

8.2 Statement of Originality

Both the macrocell and microcell work undertaken in this thesis have provided a number of original contributions.

The higher order sectorisation work derived for the first time the optimum horizontal antenna beamwidths for 3, 6, 9, 12 and 15 sectored 3G/WCDMA sites to maximise network capacity whilst respecting a number of network Key Performance Indicators. Higher order sectorisation field work also showed for the

first time, the gains from wide scale deployment of six-sector 3G/WCDMA sites into a live commercial network, and the potential capabilities of the world's first fifteen-sectored 3G/WCDMA site.

The rapid dynamic antenna downtilt work has shown this proposed novel SON technique to be effective from both simulation and from the results of the first trial deployment of antennas using this technique in a live 4G/LTE network.

A number of original small cell placement algorithms based upon the use of geo-located UE measurement reports and RF fingerprinting have been proposed and have been shown to be effective at capturing traffic even when using UE measurements reports with highly inaccurate location information.

The actual effectiveness of co-channel, low powered, small cells has been proven through both simulation and field results from London's first lamppost mounted 3G/WCDMA small cell network deployment.

And finally a number of original 3D Xmap based SON algorithms have been proposed and have been shown to maximise the offload from the macrocell layer onto low power, street level small cells.

8.3 Recommendations for Further Work

This section outlines some of the potential areas for future work based on the work presented within this thesis.

Whilst the horizontal sectorisation work showed significant gains, there is also now growing interest [117, 118] in vertical antenna sectorisation and it would have been interesting to have looked at the combination of both horizontal and vertical sectorisation on the ideal hexagonal and central London network models. It would also have been interesting to have compared the results of the combined horizontal and vertical sectorisation modelling to the dynamic antenna tilt results and evaluate which technique was more effective at increasing macrocell capacity for realistic and changing traffic distributions.

The dynamic antenna tilt work looked purely at localised combined cell tilt and scheduling and did not consider centralised coordinated tilt and scheduling between neighbouring cells/sites. Centralise co-ordinated scheduling and tilt therefore appears to be an attractive area for further research that should exploit the cell by cell variability of mobile data traffic in order to deliver both cell and network capacity gains.

Studies of advanced 3GPP features such as eICIC [119, 120, 121, 122] suggest there also appears to be gains to be had from co-ordinated scheduling between co-channel macro and

microcell layers in a 4G/LTE network. Therefore the combination of eICIC and dynamic antenna tilt also appears to be an area worthy of further research.

The small cell placement work produced encouraging results, especially when combined with RF fingerprinting methods. However the RF fingerprinting technique proposed only discarded UE measurement reports that were deemed to have inaccurate location information and it did not attempt to correct this location information. It is possible that through the correction of the erroneous UE location information more UE location samples would then become available on which to make small cell placement decisions and this could lead to more accurate hotspot location determination and therefore greater traffic capture per small cell.

At time of writing only four of the thirteen lampposts mounted small cells along Kensington High Street had been fully enabled for 3G/WCDMA service. Therefore whilst some initial conclusions on the effectiveness of these lamppost mounted small cells could be drawn, it would have been better to have had all thirteen lampposts fully enabled so that a direct comparison between the simulations results and the field results could have been made. Further work to analyse the performance of the full Kensington High Street small cell network will be undertaken once the network is completed Q4 2013.

Whilst the proposed macro/microcell SON algorithms appeared to provide significant offload onto the microcell layer, it would have been nice as with some of the other work presented in this thesis, to verify the simulation results with field trials. Again this further work is dependent on the completion of the full Kensington High Street small cell network and is therefore also currently scheduled to be undertaken Q4 2013.

And finally, as was seen from the small cell SON work in Chapter 7, whist SON has the ability to improve network performance, it also has the capability to significantly reduce it - if the SON technique applied does not consider the wider effect of the network changes it makes. Therefore further work considering the system stability and capacity stability delivered by SON is essential prior to real SON algorithms being allowed to optimise and manage live commercial cellular networks.

List of References

[1] GSMA, "The Mobile Economy 2013," GSMA, London, 2013.

[2] 4G Americas. (2013). *Infographic: Mobile Broadband Connected Future* [Online]. Available: http://www.4gamericas.org

[3] Cisco, "Cisco Visual Networking Index: Global Mobile Data Traffic Forecast Update, 2012–2017," Cisco, San Francisco, 2013.

[4] Informa Telecoms & Media, "Small Cell Market Status - November 2012," Informa Telecoms & Media, London, 2012.

[5] J. Ramiro and K. Hamied, *Self-Organizing Networks*. London: John Wiley & Sons, 2012.

[6] B. Spencer. (2013). *Mobile users can't leave their phone alone for six minutes and check it up to 150 times a day* [Online]. Available: http://www.dailymail.co.uk/news/article-2276752/Mobile-users-leave-phone-minutes-check-150-times-day.html

[7] European Travel Commission. (2013). *Mobile Device Market Watch: UK* [Online]. Available: http://www.newmediatrendwatch.com/markets-by-country/18-uk/154-mobile-devices

[8] R. M. Joyce, "Spectral Efficiency of Future 3GPP Technologies," Telefonica UK Internal Document, Slough, 2010.

[9] International Telecommunications Union, "Final Acts - WRC-07, Geneva," International Telecommunications Union, Geneva, 2007.

[10] Ofcom, "Digital dividend: clearing the 800 MHz band - Consultation," Ofcom, London, 2009.

[11] Ofcom, "Second consultation on assessment of future mobile competition and proposals for the award of 800 MHz and 2.6 GHz spectrum and related issues," Ofcom, London, 2012.

[12] Ofcom. (2013) *Ofcom announces winners of the 4G mobile auction* [Online]. Available: http://media.ofcom.org.uk/2013/02/20/ofcom-announces-winners-of-the-4g-mobile-auction/

[13] L. Kelion. (2013) *O2 4G mobile network launch date announced for the UK* [Online]. Available: http://www.bbc.co.uk/news/technology-23521211

[14] Radiocommunications Agency. (2000) *Byers Announces 3G Mobile Licence Winners* [Online]. Available: http://www.ofcom.org.uk/static/archive/spectrumauctions/auction/auction_index.htm

[15] W. C. Jakes, *Microwave Mobile Communications*. New York: John Wiley & Sons, 1974.

[16] K. S. Gilhousen *et. al.*, "On the Capacity of a Cellular CDMA System," *IEEE Trans.Vehicual Technology,* vol. 40, pp. 303-312, May 1991.

[17] 4G Americas. (2013). *MIMO and Smart Antenna Systems for Mobile Broadband Systems* [Online]. Available: http://www.4gamericas.org/index.cfm?fuseaction=page&sectionid=428

[18] *3GPP Technical Specification Group Radio Access Network; Coordinated multi-point operation for LTE physical layer aspects (Release 11)*, 3GPP 36.819, v11.1.0, 2011.

[19] R. M. Joyce *et. al.*, "Orange UK WCDMA Field Trials Overview," *Proc. IEE 3G2003 Inernational Conference on Mobile Communication Technologies*, London, 2003, pp. 68-73.

[20] R. Coombs and R. Steele, "Introducing microcells into macrocellular networks: A case study," *IEEE Trans. Communications,* vol. 47, pp. 568-576, Apr 1999.

[21] S. Dehghan and R. Steele, "Small cell city," *IEEE Communications Magazine,* vol. 35, pp. 52-59, Aug 1997.

[22] Motorola. (2009) *LTE Operations and Maintenance Strategy Using Self-Organizing Networks to Reduce OPEX* [Online]. Available: http://www.motorolasolutions.com/web/Business/Solutions/Industry%20Solutions/Service%20Providers/Network%20Operators/LTE/_Document/Static%20Files/LTE%20Operability%20SON%20White%20Paper.pdf.

[23] H. Olofsson *et. al.*, "A concept for dynamic neighbor cell list planning in a cellular system," *Proc. The Seventh IEEE International Symposium on Personal, Indoor and Mobile Radio Communications*, Taipei, 1996, pp. 138-142.

[24] R. T. Love *et. al.*, "A pilot optimization technique for CDMA cellular systems," *Proc.IEEE Vehicular Technology Conference*, Amsterdam, 1999, pp. 2238-2242.

[25] K. Raivio *et. al.*, "Analysis of mobile radio access network using the self-organizing map," *Proc. IFIP/IEEE Eighth International Symposium on Integrated Network Management*, Colorado Springs, 2003, pp. 439-451.

[26] C. J. Debono and J. K. Buhagiar, "Cellular network coverage optimization through the application of self-organizing neural networks," *Proc.IEEE Vehicular Technology Conference - Fall*, Dallas, 2005, pp. 2158-2162.

[27] C. Shen *et. al.*, "A framework for self-management of hybrid wireless networks using autonomic computing principles," *Proc. 3rd Annual Communication Networks and Services Research Conference*, Halifax N.S., 2005, pp. 261-266.

[28] G. Hampel *et. al.*, "The tradeoff between coverage and capacity in dynamic optimization of 3G cellular networks," *Proc. IEEE Vehicular Technology Conference - Fall*, Orlando, 2003, pp. 927-932.

[29] L. Du *et. al.*, "Intelligent cellular network load balancing using a cooperative negotiation approach," *Proc. IEEE Wireless Communications and Networking Conference*, New Orleans, 2003, pp. 1675-1679.

[30] S. Sharma *et. al.*, "Situation-aware wireless networks," *IEEE Communications Magazine,* vol. 41, pp. 44-50, Jul 2003.

[31] A. G. Spilling *et. al.*, "Self-organisation in future mobile communications," *IEE Electronics & Communication Engineering Journal,* vol. 12, pp. 133-147, Jun 2000.

[32] NGMN Alliance. (2006) *Next Generation Mobile Networks Beyond HSPA & EVDO* [Online]. Available: http://www.ngmn.org/uploads/media/Next_Generation_Mobile_Networks_Beyond_HSPA_EVDO_web.pdf

[33] *3GPP Technical Specification Group Radio Access Network; Study on Minimization of drive-tests in Next Generation Networks; (Release 9)*, 3GPP 36.805, v9.0.0, 2009.

[34] *3GPP Universal Terrestrial Radio Access (UTRA) and Evolved Universal Terrestrial Radio Access (E-UTRA); Radio measurement collection for Minimization of Drive Tests (MDT); Overall description; Stage 2 (Release 10)*, 3GPP 37.320, v10.4.0, 2012.

[35] *3GPP Technical Specification Group Services and System Aspects; Telecommunication Management; Self-Organizing Networks (SON); Concepts and requirements (Release 8)*, 3GPP 32.500, v8.0.0, 2009.

[36] *3GPP Technical Specification Group Services and System Aspects; Telecommunication management; Self-configuration of network elements; Concepts and requirements (Release 11)*, 3GPP 32.501, v11.0.0, 2012.

[37] *3GPP Technical Specification Group Services and System Aspects; Telecommunication management; Automatic Neighbour Relation (ANR) management; Concepts and requirements (Release 11)*, 3GPP 32.511 v11.0.0, 2012.

[38] *3GPP Technical Specification Group Services and System Aspects; Telecommunication Management; Self-Organizing Networks (SON) Policy Network Resource Model (NRM) Integration Reference Point (IRP); Requirements (Release 11)*, 3GPP 32.521 v11.1.0, 2012.

[39] *3GPP Technical Specification Group Services and System Aspects; Telecommunication management; Self-Organizing Networks (SON); Self-healing concepts and requirements (Release 11)*, 3GPP 32.541, v11.0.0, 2012.

[40] J. Niemela *et. al.*, "Sensitivity of optimum downtilt angle for geographical traffic load distribution in WCDMA," *Proc. IEEE Vehicular Technology Conference - Fall*, Dallas, 2005, pp. 1202-1206.

[41] O. N. C. Yilmaz *et. al.*, "Self-optimization of Remote Electrical Tilt," *Proc. IEEE 21st International Symposium on Personal Indoor and Mobile Radio Communications,* Istanbul, 2010, pp. 1128-1132.

[42] N. Zheng *et. al.*, "Antenna Tilt and Interaction with Open Loop Power Control in Homogeneous Uplink LTE Networks," *Proc. IEEE International Symposium on Wireless Communication Systems*, Reykjavik, 2008, pp. 634-638.

[43] Q. H. Li *et. al.*, "MIMO Techniques in WiMAX and LTE: A Feature Overview," *IEEE Communications Magazine,* vol. 48, pp. 86-92, May 2010.

[44] *3GPP Technical Specification Group Radio Access Network; Evolved Universal Terrestrial Radio Access (E-UTRA); Physical layer procedures (Release 9)*, 3GPP 36.213, v9.3.0, 2010.

[45] *Kathrein 800 10647 CLA 2X 790–960 MHz Antenna Specification*, Kathrein, 2012.

[46] R. M. Joyce, "NextGen Wireless Quotation to Model Adaptive Dynamic Tilting Antennas," Next Generation Wireless Ltd., August 2008.

[47] P. Song and D. Barker, "Antennas, how many do we need?," *IEEE Antennas and Propagation Soc. Website, Invited paper*. [Online], Available: http://www.ieeeaps.org/pdfs/Peter_Song_Feature_Article.pdf

[48] R. Miura *et. al.*, "Maximal-Radio-Combining Array Beamformer Assisted by a Training Sequence for Space Division Multiple Access in Power-Limited Channels," *IEICE Trans. on Communications,* vol. E83-B, pp. 394-405, February 2000.

[49] J. Lamanse *et. al.* (2002*). Innovation: Assisted GPS: A Low-Infrastructure Approach. GPS World* [Online]. Available: http://www.gpsworld.com/wp-content/uploads/2012/09/gpsworld_Innovation_0302.pdf

[50] B. Ludden and L. Lopes, "Cellular based location technologies for UMTS: A comparison between IPDL and TA-IPDL," *Proc. IEEE Vehicular Technology Conference*, Boston, 2000, pp. 1348-1353.

[51] *3GPP Physical layer aspects for evolved Universal Terrestrial Radio Access (UTRA) (Release 7)*, 3GPP 25.814, v7.1.0, 2006.

[52] *3GPP Evolved Universal Terrestrial Radio Access (E-UTRA); Further advancements for E-UTRA physical layer aspects (Release 9)*, 3GPP 36.814, v9.0.0, 2010.

[53] *3GPP Technical Specification Group Radio Access Network; Base Station (BS) radio transmission and reception (FDD) (Release 12)*," 3GPP 25.104, v12.0.0, 2013.

[54] European Union, "COST 231 final report: digital mobile radio towards future generation systems", chapter 4 propagation prediction models, 1996.

[55] *3GPP Technical Specification Group Radio Access Network; Evolved Universal Terrestrial Radio Access (E-UTRA); Base Station (BS) radio transmission and reception (Release 12)*, 3GPP 36.104, v12.0.0, 2013.

[56] MSI (2000). *MSI Planet Antenna File Format* [Online]. Available: http://www.comsitesoftware.com/resources/MSI%20Planet%20Antenna%20File%20Format.pdf

[57] Aircom, "Aircom ASSET User Reference Guide, Version 4.2, Appendix A – Algorithms, Antenna Tilt and Masking Calculations," pp. 223-224, 2004.

[58] C. E. Shannon, "A mathematical theory of communication," *Bell System Technical Journal,* vol. 27, pp. 379-423, Jul-Oct 1948.

[59] H. Holma and A. Taskala, *HSDPA/HSUPA for UMTS.* London: John Wiley & Sons, 2006.

[60] Ericsson, "Simulation assumption for the block of flats scenario," 3GPP TSG-RAN Working Group 4 (Radio)February 2008.

[61] J. D. Parsons, *The Mobile Radio Propagation Channel*. 2nd ed. London: John Wiley & Sons, 2000.

[62] E. Dahlman *et. al.*, *3G Evolution - HSPA and LTE for Mobile Broadband*, 2nd ed. Oxford: Academic Press, 2008.

[63] R.M. Joyce *et. al.*, "Coordinated Dynamic Antenna Tilt & Scheduling in a Central London LTE Network," presented at the LTE 2013 World Summit, Amsterdam, The Netherlands, 2013.

[64] A. Wacker *et. al.,* "The impact of the base station sectorisation on WCDMA radio network performance," *Proc. IEEE Vehicular Technology Conference*, Amsterdam, 1999, pp. 2611-2615.

[65] P. Zetterberg, "Performance of three, six, nine and twelve sector sites in CDMA - based on measurements," *Proc. IEEE Eighth International Symp. on Spread Spectrum Techniques and Applications*, Sydney, 2004, pp. 394- 399.

[66] J. Niemela and J. Lempiainen, "Impact of the base station antenna beamwidth on capacity in WCDMA cellular networks," *Proc. IEEE Vehicular Technology Conference-Spring*, Jeju, 2003 pp. 80-84.

[67] A. Osseiran and A. Logothetis, "Impact of Angular Spread on Higher Order Sectorization in WCDMA Systems," *Proc. International Symposium on Personal, Indoor and Mobile Radio Communications*, Berlin, 2005, pp. .301-305.

[68] A. Osseiran and A. Logothetis, "Smart Antennas in a WCDMA Radio Network System: Modeling and Evaluations," *IEEE Trans. on Antennas and Propagation,* vol. 54, pp. 3302-3316, November 2006.

[69] B. Hagerman *et. al.*, "WCDMA 6-sector Deployment - Case Study of a Real Installed UMTS-FDD Network," *Proc. IEEE Vehicular Technology Conference-Spring*, Melbourne, 2006, pp. 703-707.

[70] S. Kumar *et. al.*, "Performance Evaluation of 6-Sector-Site Deployment for Downlink UTRAN Long Term Evolution," *Proc. IEEE Vehicular Technology Conference-Fall*, Calgary, 2008, pp. 1837-1841.

[71] R. M. Joyce and S. Brown, "Delivering Small Cells into the Heart of London," presented at the Small Cells World Summit 2012, London, 2012.

[72] L. J. Ibbetson and L. B. Lopes, "An automatic base site placement algorithm," *Proc. IEEE Vehicular Technology Conference Proceedings*, Phoenix, 1997, pp. 760-764.

[73] X. M. Huang *et. al.*, "Automatic base station placement and dimensioning for mobile network planning," *Proc. IEEE Vehicular Technology Conference-Fall*, Boston, 2000, pp. 1544-1549.

[74] J. Cardeiro and L. M. Correia, "Optimisation of Base Station Location in UMTS-FDD for Realistic Traffic Distributions," *Proc. International Symposium on Personal, Indoor and Mobile Radio Communications*, Helsinki, 2006, pp. 1-5.

[75] I. Kocsis *et. al.*, "3G base station positioning using simulated annealing," *Proc. International Symposium on Personal, Indoor and Mobile Radio Communications*, Lisbon, 2002, pp. 330-334.

[76] M. Unbehaun and M. Kamenetsky, "On the deployment of picocellular wireless infrastructure," *IEEE Communications Magazine,* vol. 10, pp. 70-80, Dec 2003.

[77] H. Liang *et. al.*, "Optimal New Site Deployment Algorithm for Heterogeneous Cellular Networks," *Proc. IEEE Vehicular Technology Conference-Fall*, San Francisco, 2011, pp. 1-5.

[78] I. Jami and H. Tao, "Micro-cell planning within macro-cells in UMTS: Downlink analysis," *Proc. Third International Conference on 3G Mobile Communication Technologies,* London, 2002, pp. 211-215.

[79] *3GPP Technical Specification Group Radio Access Network; Physical layer; Measurements (FDD) (Release 11)*," 3GPP 25.215, v11.0.0, 2011.

[80] Arieso. (2013). [Online]. Available: www.arieso.com

[81] Astellia. (2013). [Online]. Available: www.astellia.com

[82] J. Winter and C. Wengerter, "High resolution estimation of the time of arrival for GSM location," *Proc. Vehicular Technology Conference-Spring*, Tokyo, 2000, pp. 1343-1347.

[83] Metricell. (2013). [Online] Available: www.metricell.co.uk/netcare.php

[84] E. Trevisani and A. Vitaletti, "Cell-ID location technique, limits and benefits: an experimental study.," *Proc. Sixth IEEE Workshop on Mobile Computing Systems and Applications*, Lake District National Park, 2004, pp. 51-60,.

[85] L. Zimmermann *et. al.*, "GSM mobile phone localization using time difference of arrival and angle of arrival estimation," *Proc. International Multi-Conference on Systems, Signals and Devices*, Chemnitz, 2012, pp. 1-7.

[86] Z. Yilin, "Mobile phone location determination and its impact on intelligent transportation systems," *IEEE Trans. on Intelligent Transportation Systems*, vol. 1, pp. 55-64, 2000.

[87] *3GPP Evolved Universal Terrestrial Radio Access Network (E-UTRAN); Stage 2 functional specification of User Equipment (UE) positioning in E-UTRAN (Release 10)*, 3GPP 36.305, v10.5.0, 2013.

[88] S. Bohanudin *et. al.*, "Simulation model and location accuracy for observed time difference of arrival (OTDOA) positioning technique in Third Generation system," *Proc. IEEE Student Conference on Research and Development*, Putrajaya, 2010, pp. 63-66.

[89] J. Medbo *et. al.*, "Propagation Channel Impact on LTE Positioning Accuracy - A Study Based on Real Measurements of Observed Time Difference of Arrival," *Proc. IEEE International Symposium on Personal, Indoor and Mobile Radio Communications*, Tokyo, 2009, pp. 2213-2217.

[90] N. M. Drawil *et. al.*, "GPS Localization Accuracy Classification: A Context-Based Approach," *IEEE Trans. on Intelligent Transportation Systems*, vol. 14, pp. 262-273, 2013.

[91] Informa Telecoms & Media, "Mobile Broadband Access at Home," Informa Telecoms & Media, London, 2008.

[92] U. Birkel and M. Weber, "Indoor localization with UMTS compared to WLAN," *Proc. 2012 International Conference on Indoor Positioning and Indoor Navigation*, Montbeliard, 2012, pp. 1-6.

[93] T. Wigren *et. al.*, "Enhanced WCDMA Fingerprinting Localization Using OTDOA Positioning Measurements from LTE," *Proc. IEEE Vehicular Technology Conference-Fall*, Québec City, 2012, pp. 1-5.

[94] T. Wigren, "Adaptive enhanced cell-ID fingerprinting localization by clustering of precise position measurements," *IEEE Trans. on Vehicular Technology,* vol. 56, pp. 3199-3209, Sep 2007.

[95] Unknown. *GPS Horizontal Position Accuracy* [Online]. Available: http://www.leb.esalq.usp.br/disciplinas/Molin/leb447/Arquivos/GNSS/ArtigoAcuraciaGPSsemAutor.pdf

[96] *3GPP Requirements for support of radio resource management (FDD) (Release 10)*, 3GPP 25.133, v 10.9.0, 2013.

[97] Mathworks. *Griddata: Interpolate scattered data* [Online]. Available: http://www.mathworks.co.uk/help/matlab/ref/griddata.html

[98] *3GPP 3rd Generation Partnership Project; Technical Specification Group Radio Access Network; User Equipment (UE) procedures in idle mode and procedures for cell reselection in connected mode(Release 10)*, 3GPP 25.304, v 10.7.0, 2012.

[99] C. Y. Kim, "The evaluation of HCS scenarios included in HSDPA," *Proc. IEEE Vehicular Technology Conference-Fall*, Los Angeles 2004, pp. 4772-4776.

[100] V. Erceg and J. F. Whitehead, "Microcell Size and Architecture Analysis from the Propagation and Capacity Points-of-View," *Proc. IEEE Vehicular Technology Conference*, Stockholm, 1994, pp. 215-219.

[101] W. R. Young, "Advanced Mobile Phone Service - Introduction, Background, and Objectives," *Bell System Technical Journal,* vol. 58, pp. 1-14, 1979.

[102] M. Bezler *et. al.*, "Comparison of Spectrum Efficiency in Digital Cellular-Systems - GSM and Amps-D," *Proc. IEEE Vehicular Technology Conference*, Denver, 1992, pp. 1008-1011.

[103] H. Claussen and D. Calin, "Macrocell Offloading Benefits in Joint Macro- and Femtocell Deployments," *Proc. IEEE 20th International Symposium on Personal, Indoor and Mobile Radio Communications*, Tokyo, 2009, pp. 350-354.

[104] D. Calin *et. al.*, "On Femto Deployment Architectures and Macrocell Offloading Benefits in Joint Macro-Femto Deployments," *IEEE Communications Magazine,* vol. 48, pp. 26-32, Jan 2010.

[105] P. Fuxjager *et. al.*, "Measurement-Based Small-Cell Coverage Analysis for Urban Macro-Offload Scenarios," *Proc. IEEE Vehicular Technology Conference-Spring*, Budapest, 2011, pp. 1-5.

[106] *3GPP Technical Specification Group Radio Access Network; User Equipment (UE) radio transmission and reception (FDD) (Release 12)*, 3GPP 25.101, v12.0.0, 2013.

[107] European Union 7th Framework Program, "SOCRATES Project: Final Report on Self-Organisation and its Implications in Wireless Access Networks,", 2010.

[108] C. Brunner and D. Flore, "Generation of Pathloss and Interference Maps as SON Enabler in Deployed UMTS Networks," *Proc IEEE Vehicular Technology Conference-Spring*, Barcelona, 2009, pp. 2928-2932.

[109] M. Garcia-Lozano *et. al.*, "UMTS optimum cell load balancing for inhomogeneous traffic patterns," *Proc. IEEE Vehicular Technology Conference-Fall*, Los Angeles, 2004, pp. 909-913.

[110] O. Sallent *et. al.*, "A Roadmap from UMTS Optimization to LTE Self-Optimization," *IEEE Communications Magazine,* vol. 49, pp. 172-182, Jun 2011.

[111] J. Seokyun *et. al.*, "Self-optimization of single femto-cell coverage using handover events in LTE systems," *Proc. IEEE 17th Asia-Pacific Conference on Communications*, Kota Kinabalu, 2011, pp. 28-32.

[112] K. Han *et. al.*, "Optimization of Femtocell Network Configuration under Interference Constraints," *Proc. Seventh International Symposium on Modeling and Optimization in Mobile, Ad Hoc, and Wireless*, Seoul, 2009, pp. 90-96.

[113] H. Claussen *et. al.*, "Self-optimization of coverage for femtocell deployments," *Proc Seventh Wireless Telecommunications Symposium*, Pomona, 2008, pp. 278-285.

[114] F. Meshkati *et. al.*, "Mobility and Capacity Offload for 3G UMTS Femtocells," *Proc. IEEE Global Telecommunications Conference*, Honolulu, 2009, pp. 5306-5312.

[115] A. Barbieri *et. al.*, "LTE Femtocells: System Design and Performance Analysis," *IEEE Journal on Selected Areas in Communications,* vol. 30, pp. 586-594, Apr 2012.

[116] D. Lopez-Perez *et. al.*, "Enhanced Intercell Interference Coordination Challenges in Heterogeneous Networks," *IEEE Wireless Communications Magazine,* vol. 18, pp. 22-30, Jun 2011.

[117] O. Yilmaz *et. al.*, "System Level Analysis of Vertical Sectorization for 3GPP LTE," *Sixth International Symposium on Wireless Communication Systems*, Siena, 2009, pp. 453-457.

[118] Y. Fu *et. al.*, "Analysis of Vertical Sectorization for HSPA on a System Level: Capacity and Coverage," *Proc. IEEE Vehicular Technology Conference-Fall*, Québec City, 2012, pp. 1-5.

[119] Y. Wang *et. al.*, "Sensitivity Study of Optimal eICIC Configurations in Different Heterogeneous Network Scenarios," *Proc. IEEE International Conference on Communications*, Ottowa, 2012, pp. 6792 - 6796.

[120] L. Jiang and M. Lei, "Resource Allocation for eICIC Scheme in Heterogeneous Networks," *Proc. IEEE 23rd International Symposium on Personal Indoor and Mobile Radio Communications*, Sydney, 2012, pp. 448-453.

[121] K. I. Pedersen *et. al.*, "eICIC Functionality and Performance for LTE HetNet Co-Channel Deployments," *Proc. IEEE Vehicular Technology Conference-Fall*, Québec City, 2012. pp. 1-5.

[122] A. Weber and O. Stanze, "Scheduling Strategies for HeTNets using eICIC," *Proc. IEEE International Conference on Communications*, Ottowa, 2012, pp. 6787 - 6791.

Appendix A - Nominal User Densities per Clutter Category

Table A.1 Assumed nominal traffic density (users/km^2) for each clutter category.

Clutter Category	Description	Users/km^2
0	Unclassified	0
1	Industrial	100
2	Dense Urban	300
3	Urban	200
4	Dense Suburban	100
5	Suburban	50
6	Rural Urban/Village Centre	10
7	Agricultural Land	10
8	Non Agricultural Land	10
9	Semi Natural Vegetation	10
10	Coastal Water Features	10
11	Wetlands	10
12	Deciduous Woodlands/Forests	10
13	Coniferous Woodlands/Forests	10
14	Mixed Woodlands/Forests	10
15	High Rise Buildings	400
16	Road/Motorway Junction	200
17	Origin/Special Category	1500
18	Inland Water Features	50

Appendix B - Example of an Antenna Beam Pattern in PLANET Format

Shown below is an example of a PLANET beam pattern for a 3G antenna with a bore sight gain of 17.35dBi. As can be seen from the beam pattern the maximum gain occurs in the horizontal plane at Azimuth = 0^o and in the vertical plane at downtilt = 2^o.

NAME Example Antenna

FREQUENCY 2110

GAIN 17.35 dBi

TILT ELECTRICAL

COMMENT DATE 21.03.2001 -45 degrees polarized system Lever position 2 deg

HORIZONTAL 360

Azimuth (Degs.)	Rel. Gain [dB]	Azimuth (Degs.)	Rel. Gain [dB]	Azimuth (Degs.)	Rel. Gain [dB]	Azimuth (Degs.)	Rel. Gain [dB]	Azimuth (Degs.)	Rel. Gain [dB]	Azimuth (Degs.)	Rel. Gain [dB]
0	0.0	60	10.4	120	32.8	180	39.6	240	37.9	300	10.8
1	0.0	61	10.7	121	32.8	181	39.5	241	38.2	301	10.5
2	0.0	62	11.0	122	32.9	182	39.4	242	38.4	302	10.2
3	0.0	63	11.4	123	32.9	183	39.2	243	38.7	303	9.8
4	0.1	64	11.7	124	32.8	184	39.0	244	38.8	304	9.5
5	0.1	65	12.1	125	32.8	185	38.8	245	38.8	305	9.2
6	0.1	66	12.4	126	32.8	186	38.5	246	38.7	306	8.9
7	0.2	67	12.8	127	32.7	187	38.3	247	38.3	307	8.6
8	0.2	68	13.2	128	32.7	188	38.1	248	37.8	308	8.3
9	0.3	69	13.5	129	32.6	189	38.0	249	37.1	309	8.0
10	0.3	70	13.9	130	32.5	190	37.8	250	36.4	310	7.7
11	0.4	71	14.3	131	32.4	191	37.7	251	35.5	311	7.4
12	0.5	72	14.7	132	32.4	192	37.6	252	34.7	312	7.1
13	0.6	73	15.1	133	32.3	193	37.5	253	33.8	313	6.8
14	0.6	74	15.5	134	32.2	194	37.4	254	33.0	314	6.5
15	0.7	75	16.0	135	32.2	195	37.3	255	32.2	315	6.3
16	0.8	76	16.4	136	32.2	196	37.2	256	31.4	316	6.0
17	1.0	77	16.9	137	32.1	197	37.1	257	30.6	317	5.7
18	1.1	78	17.3	138	32.1	198	37.1	258	29.8	318	5.5
19	1.2	79	17.8	139	32.2	199	37.0	259	29.1	319	5.2
20	1.3	80	18.3	140	32.2	200	37.0	260	28.4	320	5.0
21	1.4	81	18.8	141	32.2	201	37.0	261	27.8	321	4.7
22	1.6	82	19.3	142	32.3	202	37.0	262	27.1	322	4.5
23	1.7	83	19.8	143	32.4	203	37.0	263	26.5	323	4.3
24	1.9	84	20.3	144	32.5	204	37.0	264	25.9	324	4.0
25	2.0	85	20.9	145	32.6	205	37.0	265	25.3	325	3.8
26	2.2	86	21.4	146	32.8	206	37.1	266	24.8	326	3.6
27	2.4	87	22.0	147	33.0	207	37.1	267	24.2	327	3.4
28	2.5	88	22.6	148	33.2	208	37.2	268	23.7	328	3.2
29	2.7	89	23.2	149	33.4	209	37.2	269	23.2	329	3.0
30	2.9	90	23.8	150	33.7	210	37.2	270	22.7	330	2.8
31	3.1	91	24.4	151	33.9	211	37.3	271	22.2	331	2.6
32	3.3	92	25.0	152	34.2	212	37.3	272	21.7	332	2.5
33	3.5	93	25.6	153	34.5	213	37.2	273	21.3	333	2.3
34	3.7	94	26.2	154	34.8	214	37.2	274	20.8	334	2.1
35	3.9	95	26.8	155	35.1	215	37.1	275	20.4	335	2.0
36	4.1	96	27.4	156	35.4	216	37.1	276	19.9	336	1.8
37	4.3	97	28.0	157	35.7	217	37.0	277	19.5	337	1.7
38	4.5	98	28.5	158	36.1	218	36.9	278	19.1	338	1.5
39	4.7	99	29.0	159	36.4	219	36.9	279	18.7	339	1.4
40	5.0	100	29.5	160	36.8	220	36.8	280	18.3	340	1.3
41	5.2	101	30.0	161	37.2	221	36.6	281	17.9	341	1.1
42	5.4	102	30.4	162	37.6	222	36.5	282	17.5	342	1.0
43	5.7	103	30.7	163	38.0	223	36.4	283	17.1	343	0.9
44	5.9	104	31.0	164	38.3	224	36.2	284	16.7	344	0.8
45	6.2	105	31.3	165	38.7	225	36.1	285	16.3	345	0.7
46	6.4	106	31.5	166	39.0	226	36.0	286	15.9	346	0.6
47	6.7	107	31.7	167	39.3	227	36.0	287	15.5	347	0.5
48	6.9	108	31.8	168	39.5	228	36.0	288	15.1	348	0.5
49	7.2	109	32.0	169	39.7	229	35.9	289	14.7	349	0.4
50	7.5	110	32.1	170	39.9	230	36.0	290	14.4	350	0.3
51	7.7	111	32.2	171	40.1	231	36.0	291	14.0	351	0.2
52	8.0	112	32.3	172	40.2	232	36.1	292	13.6	352	0.2
53	8.3	113	32.4	173	40.2	233	36.2	293	13.3	353	0.1
54	8.6	114	32.5	174	40.2	234	36.3	294	12.9	354	0.1
55	8.9	115	32.6	175	40.2	235	36.5	295	12.6	355	0.1
56	9.2	116	32.6	176	40.1	236	36.8	296	12.2	356	0.0
57	9.5	117	32.7	177	40.0	237	37.0	297	11.9	357	0.0
58	9.8	118	32.7	178	39.9	238	37.3	298	11.5	358	0.0
59	10.1	119	32.8	179	39.8	239	37.6	299	11.2	359	0.0

VERTICAL 360

Elevation (Degs.)	Rel. Gain [dB]	Elevation (Degs.)	Rel. Gain [dB]	Elevation (Degs.)	Rel. Gain [dB]	Elevation (Degs.)	Rel. Gain [dB]	Elevation (Degs.)	Rel. Gain [dB]	Elevation (Degs.)	Rel. Gain [dB]
0	1.6	60	30.3	120	39.5	180	40.8	240	32.6	300	26.0
1	0.5	61	30.6	121	37.9	181	41.3	241	35.5	301	28.4
2	0.0	62	32.1	122	36.0	182	41.3	242	40.8	302	30.6
3	0.1	63	35.0	123	34.5	183	40.6	243	38.8	303	32.7
4	0.9	64	40.1	124	33.6	184	39.3	244	34.1	304	35.5
5	2.4	65	40.5	125	33.3	185	37.9	245	31.9	305	36.4
6	4.8	66	35.4	126	33.6	186	36.6	246	31.1	306	32.1
7	8.5	67	32.4	127	34.6	187	35.2	247	31.3	307	28.1
8	14.1	68	30.9	128	36.5	188	33.7	248	32.2	308	25.7
9	21.4	69	30.2	129	39.0	189	32.4	249	33.2	309	24.4
10	18.0	70	29.8	130	41.9	190	31.7	250	34.0	310	24.1
11	15.2	71	29.3	131	44.5	191	31.8	251	34.2	311	24.8
12	14.9	72	28.6	132	46.8	192	32.5	252	33.7	312	26.1
13	16.6	73	28.0	133	49.8	193	33.8	253	33.0	313	27.4
14	20.9	74	27.6	134	53.9	194	34.6	254	32.3	314	27.6
15	29.7	75	27.8	135	57.8	195	34.3	255	31.5	315	27.0
16	26.1	76	28.6	136	56.3	196	33.5	256	30.8	316	26.6
17	21.0	77	30.0	137	51.7	197	33.0	257	30.3	317	27.2
18	19.3	78	31.8	138	48.1	198	33.3	258	30.0	318	29.2
19	19.6	79	33.4	139	46.0	199	34.7	259	29.9	319	34.0
20	21.7	80	34.1	140	45.5	200	37.6	260	30.1	320	37.1
21	26.3	81	33.9	141	46.7	201	42.3	261	30.3	321	29.1
22	33.2	82	33.8	142	50.3	202	46.8	262	30.5	322	24.2
23	28.6	83	34.0	143	60.2	203	44.0	263	30.4	323	21.0
24	24.6	84	34.7	144	52.9	204	41.3	264	30.0	324	18.9
25	23.3	85	35.5	145	45.5	205	40.4	265	29.6	325	17.5
26	23.5	86	35.4	146	41.5	206	40.3	266	29.1	326	16.8
27	24.5	87	34.5	147	39.0	207	40.2	267	28.5	327	16.8
28	24.5	88	33.4	148	37.5	208	39.4	268	27.8	328	17.5
29	22.6	89	32.8	149	36.9	209	38.1	269	27.0	329	18.8
30	20.4	90	36.7	150	37.3	210	36.8	270	26.3	330	21.1
31	18.8	91	33.8	151	38.9	211	35.9	271	25.8	331	24.5
32	18.0	92	35.5	152	42.4	212	35.6	272	25.6	332	29.4
33	17.9	93	37.1	153	50.3	213	36.0	273	25.6	333	35.6
34	18.5	94	38.2	154	49.6	214	37.5	274	25.9	334	37.9
35	19.7	95	38.4	155	42.1	215	40.3	275	26.3	335	34.9
36	21.5	96	38.8	156	38.7	216	45.4	276	26.8	336	30.4
37	23.7	97	40.3	157	36.7	217	56.1	277	27.2	337	26.3
38	26.2	98	43.5	158	35.4	218	55.0	278	27.7	338	23.5
39	28.5	99	47.1	159	34.1	219	49.5	279	28.4	339	21.8
40	29.8	100	48.0	160	32.9	220	47.9	280	29.4	340	21.5
41	29.5	101	50.1	161	31.9	221	46.7	281	30.9	341	22.5
42	27.8	102	68.6	162	31.2	222	44.1	282	33.1	342	25.8
43	25.8	103	48.3	163	31.1	223	40.7	283	36.1	343	32.1
44	24.0	104	41.8	164	31.4	224	37.7	284	40.2	344	27.5
45	22.4	105	39.1	165	32.2	225	35.4	285	48.1	345	21.7
46	21.3	106	38.5	166	33.5	226	33.7	286	53.0	346	18.7
47	20.4	107	39.4	167	35.0	227	32.6	287	41.0	347	17.5
48	19.9	108	41.5	168	36.5	228	32.1	288	35.5	348	17.7
49	19.8	109	42.7	169	37.2	229	32.1	289	31.5	349	19.4
50	20.1	110	40.3	170	37.2	230	32.5	290	28.4	350	23.1
51	20.8	111	37.0	171	36.7	231	33.4	291	26.0	351	27.5
52	22.1	112	34.8	172	36.3	232	34.2	292	24.1	352	25.5
53	23.9	113	33.6	173	36.3	233	34.8	293	22.5	353	23.4
54	26.3	114	33.6	174	36.8	234	35.7	294	21.4	354	24.0
55	29.1	115	34.4	175	37.7	235	37.5	295	20.7	355	21.8
56	31.6	116	36.0	176	38.6	236	38.6	296	20.5	356	15.1
57	32.3	117	37.6	177	39.3	237	35.9	297	20.9	357	9.8
58	31.5	118	39.0	178	39.8	238	33.1	298	22.0	358	6.1
59	30.6	119	39.7	179	40.3	239	31.9	299	23.7	359	3.4

Appendix C – 15 Sector Site Antenna Specification: Argus 5NPX1006F

PRODUCT SPECIFICATIONS PRELIMINARY

5NPX1006F

1710 - 2170 MHz Multi-Beam Panel Antenna

RF SPECIFICATIONS

Frequency	1710-2170 MHz	
	1710-1880 MHz	1920-2170 MHz
Gain	22 dBi	23 dBi
Return Loss	> 15 dB	
Polarization	Dual Slant ± 45°	
Horizontal Beamwidth	11°- 14°	10° -12°
Vertical Beamwidth	12°	11°
Electrical Downtilt	Fixed 6°	
Beam Crossover	- 10 dB typical	
Upper Sidelobe Level	< -18 dB	
Front to Back Ratio	> 30 dB	
Isolation Port to Port - Polarization	> 25 dB	
Isolation Port to Port - Beam	> 16 dB	
Power Rating	300W per port	
Intermodulation	< -150 dBc (2 x 43 dBm)	
Impedance	50 ohm	
Lightning Protection	DC grounded	
Connector Type	7-16 DIN female, 10 ports	

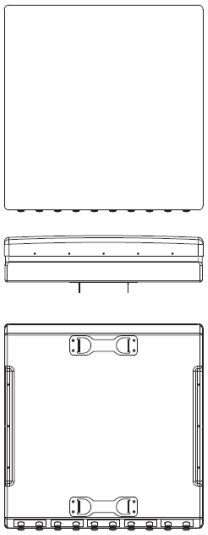

MECHANICAL DATA

Antenna Dimensions	890 x 865 x 250 mm
Packed Dimensions	1015 x 950 x 300 mm
Antenna Weight	30 kg
Radome Material	ABS

MOUNTING OPTIONS

T-045-GL-E	
F-042-GL-E	

MAXIMUM ENVIRONMENTAL RATINGS

Humidity	95% RH @ +30°C
Lateral Loading (Front)	1.06 kN @160km/h
Lateral Loading (Rear)	1.06 kN @160km/h
Rain	140 mm per hour
Rated Wind Velocity	Limited by mounting pole
Temperature	-40°C to +70°C

BASE VIEW CONNECTOR LAYOUT

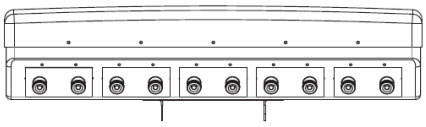

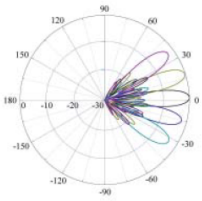

Azimuth Superimposed

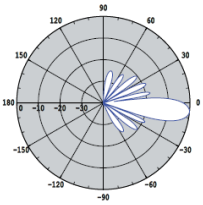

Elevation

Last Modified: 04/03/2011
W: www.argusantennas.com E: info@argusantennas.com
Argus Technologies is continually improving products. Specifications may change at any time without notice.

Appendix D - Ruckus Wireless 8800 Access Point Datasheet

Ruckus
Simply Better Wireless.

data sheet

BENEFITS

Integrated support for Wi-Fi and small cell radios
Enables a more complete macro cellular underlay in dense urban areas

Compact form factor for ease of deployment on light poles
Ability to integrate a Wi-Fi AP and a small cell into one compact node makes site acquisition much easier

SmartMesh for wireless backhaul
Is essential in backhauling traffic from light poles and other types of street furniture

Integrated GPS receiver
Enables location-based services

Spectrum analysis
Automatically scans all available channels for RF activity. Can be used for dynamic frequency selection (DFS) and for reporting purposes

AC power and power-over-Ethernet
AC power is required on most light pole deployments and power-over-Ethernet on most stadium/arena deployments

Adaptive antenna technology
BeamFlex technology increases gain by up to 6 dB and interference mitigation by up to 15 dB which greatly improves the user experience in high-density environments

Polarization diversity with maximal ratio combining
Enables a superior user experience regardless of the physical orientation of the mobile device

SmartCell™ 8800

SMART WI-FI DUAL-BAND OUTDOOR AP WITH INTEGRATED SMALL CELL OPTION

The First Multi-Function Small Cell Node Purpose Built to Meet Deployment Challenges of Real-World Urban HetNets

The Ruckus SmartCell 8800 Series represents a completely new class of outdoor access point (AP) technology designed specifically to address the capacity and siting challenges mobile operators face in deploying heterogeneous networks in dense urban environments. It is the first high-performance dual-band 802.11n outdoor AP with integrated LTE (or 3G) small cell support. By integrating this capability into the SC 8800, the mobile operator can provide both a Wi-Fi and LTE (or 3G) underlay to offload heavily congested macro cellular networks in dense urban environments.

Site acquisition is always an issue when deploying small cells, and this is made much easier by integrating a small cell into a Wi-Fi access point as the latter is an operator neutral solution that is preferred by most site owners. The SC 8800 can also provide wireless backhaul using Wi-Fi technology in the 5 GHz band. Other capabilities include support for AC power, power-over-Ethernet, integrated GPS receiver, integrated spectrum analysis, BeamFlex adaptive antenna technology, and much more.

A key part of the Ruckus value proposition is our BeamFlex technology with integrated antennas, which steers RF energy toward the user that it is communicating with and away from all other AP's in close proximity. This increases the gain by as much as 6 dB and the interference mitigation by as much as 15 dB. The latter is essential in most high-density deployments where interference is almost always the limiting factor.

The SmartCell 8800 AP can be centrally managed from the mobile packet core using the SmartCell Gateway 200, the industry's most scalable and versatile 3GPP compatible WLAN Gateway. The SCG 200 also supports capabilities like Hotspot 2.0 which will be essential in the rollout of carrier-class Wi-Fi solutions.

SmartCell™ 8800

MODULAR, DUAL-BAND 802.11N OUTDOOR AP WITH INTEGRATED SMALL CELL OPTION

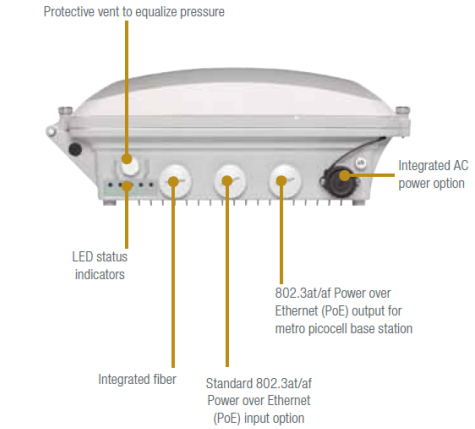

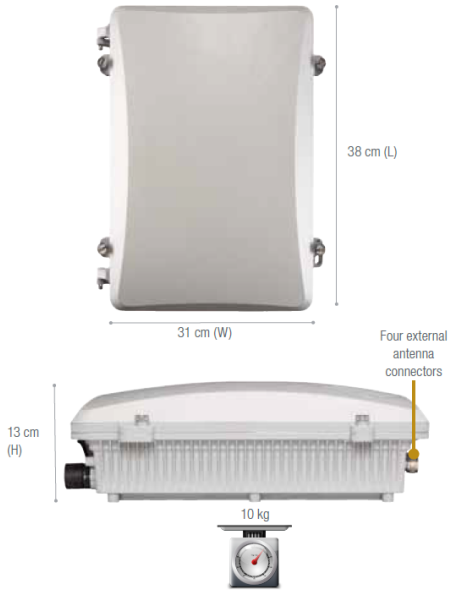

FEATURES

- Concurrent dual-band (2.4/5 GHz) support
- Adaptive antenna technology and advanced RF management
- Up to 6 dB signal gain / 15 dB interference mitigation
- Chip based transmit beamforming increasing signal gain up to 3 dB when used with supported clients
- Automatic interference mitigation, optimized for high-density environments
- PoE output supports up to 25 Watts to power small cells and surveillance cameras
- Polarization diversity for optimal mobile device performance
- Integrated AC power
- IP-67 rated, -40°C to +65°C
- Integrated GPS for location-based services
- Wall or pole mountable
- Small, lightweight, and sleek form factor
- 2 to 4 times extended range and coverage
- Multicast IP video streaming
- 900 Mbps of user throughput (450 Mbps/radio)
- 3x3:3 radio support with a 120° beam width
- 32 BSSIDs with unique QoS and security policies
- Auto packet classification and priority for latency-sensitive traffic
- Standalone or centrally managed by ZoneDirector, SCG 200, or FlexMaster
- Spectrum analysis
- Dynamic, per-user rate-limiting for hotspot WLANs
- WEP, WPA-PSK (AES), 802.1X support for RADIUS and Active Directory*
- SmartMesh Networking*
- Zero-IT and Dynamic PSK*
- Admission control/load balancing*
- Band steering and airtime fairness support
- Captive portal and guest accounts *

*When used with Ruckus ZoneDirector controller

SmartCell™ 8800

MODULAR, DUAL-BAND 802.11N OUTDOOR AP WITH INTEGRATED SMALL CELL OPTION

ESSENTIAL INGREDIENT FOR DENSE URBAN SMALL-CELL NETWORKS

SmartCell 8800 enables a new class of easy-to-deploy truly heterogeneous networks with unprecedented capacity density from multiple technologies

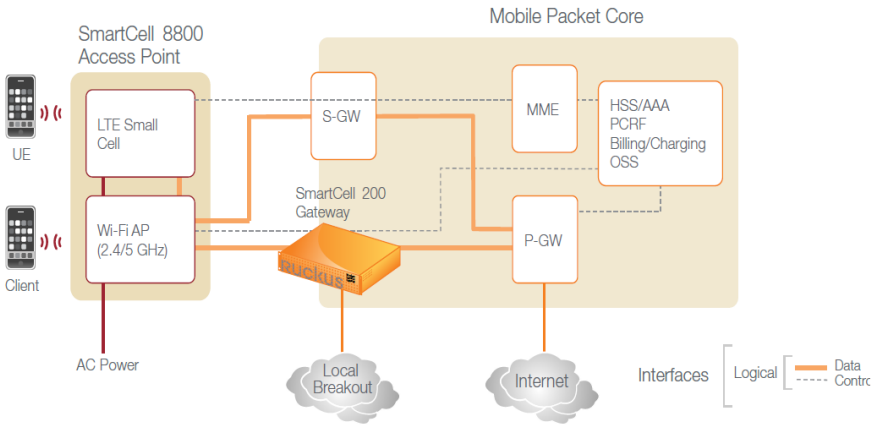

Specifications

PHYSICAL CHARACTERISTICS	
POWER	**AC Input** • Idle: 8W • Typical: 10W • Peak: 18W (PoE output off) • Peak: 50W (PoE output 25W) **PoE Input** • Idle: 6W • Typical: 8W • IEEE 802.3af/at
PHYSICAL SIZE	• 38 cm (L), 31 cm (W), 13 cm (H)
WEIGHT	• 10 Kg (22 Lbs.)
ETHERNET PORTS	**PoE Input** • 10/100/1000Base-T 802.3, 802.3u, 802.3ab, 802.3at/af PoE PD Input up to 44W with high power PoE injector • Jumbo frame support* (2000 byte MTU) **PoE Output:** • 10/100/1000Base-T 802.3,802.3u, 802.3ab, 802.3at/af PoE PSE Output up to 25W • Jumbo frame support (2000 byte MTU) • PoE power out powered with AC in or 60W PoE injector

RF	
ANTENNA	• >16 patterns
MAXIMUM EIRP**	• 41 dBm (2.4 GHz); 43 dBm (5 GHz)
PHYSICAL ANTENNA GAIN	• 11 dBi (2.4 GHz); 13 dBi (5 GHz)
BEAMFLEX* SINR TX GAIN	• Up to 6 dB
BEAMFLEX* SINR RX GAIN	• Up to 4 dB
INTERFERENCE MITIGATION	• 15 dB
MINIMUM RX SENSITIVITY	• -101 dBm (2.4GHz); -97 dBm (5 GHz)

NOTE: BeamFlex gains are statistical system level effects translated to enhanced SINR based on observations over time in real-world conditions with multiple APs and many clients

PERFORMANCE AND CAPACITY	
MAX THROUGHPUT	• 900 Mbps
CONCURRENT STATIONS	• 500
SIMULTANEOUS VoIP CLIENTS	• Up to 30

MANAGEMENT	
DEPLOYMENT OPTIONS	• Standalone (individually managed) • Managed by ZoneDirector • Managed by FlexMaster • Managed by SmartCell™ Gateway (SCG 200)
CONFIGURATION	• Web User Interface (HTTP/S) • CLI (Telnet/SSH), SNMP v1, 2, 3 • TR-069 vis FlexMaster

WI-FI	
STANDARDS	• IEEE 802.11a/b/g/n • 2.4GHz and 5GHz concurrent operation
DATA RATES	• 802.11n: 802.11n: 6.5 Mbps – 216.7 Mbps (20MHz); 13.5 Mbps – 450 Mbps (40MHz) • 802.11a: 54, 48, 36, 24, 18, 12, 9 and 6 Mbps • 802.11g: 54, 48, 36, 24, 18, 12, 9 and 6 Mbps
RADIO CHAINS	• 3x3:3
FREQUENCY BAND	• IEEE 802.11n: 2.4 – 2.484 GHz and 5.15 – 5.85 GHz • IEEE 802.11a: 5.15 – 5.875 GHz • IEEE 802.11g: 2.4 – 2.484 GHz
BSSID	• 32 per radio (64 per AP)
ADVANCED RADIO FEATURES	• BeamFlex Adaptive Antenna Technology • TxBF, LDPC, and ML receiver • GPS • Spectrum Analysis
WIRELESS SECURITY	• WEP, WPA-PSK, WPA-TKIP, WPA2 AES, 802.11i • Authentication via 802.1X, local authentication database, support for RADIUS and ActiveDirectory
CERTIFICATIONS	• U.S., Canada , Europe, Argentina, Australia, Brazil, Chili, China, Columbia, Costa Rica, Hong Kong, India, Indonesia, Israel, Japan, Korea, Malaysia, Mexico, New Zealand, Philippines, Peru, Singapore, South Africa, Taiwan, Thailand, UAE, Vietnam • WEEE/RoHS compliance • Wi-Fi Alliance Certification (Wi-Fi Certified™)

** Maximum power varies by country

Product Ordering Information

MODEL	DESCRIPTION
SmartCell™ Outdoor Access Point	
901-8800-XX01	SmartCell™ 802.11n Outdoor Wireless Access Point, 2.4 GHz/5 GHz antenna. Includes mounting kit, 1 year warranty. Does not include PoE Injector. Does not include AC Power Cord.
Optional Accessories	
902-0180-XX00	60W Power over Ethernet (PoE) Injector (10/100/1000 Mbps) quantity of 1 unit US Plug
902-0113-0000	SC 8800 Fiber interface kit. (SPF optics not included)
902-0183-0000	Spare Data Connector for contains 1 weatherizing data cable gland
902-0185-0000	Spare Weatherized AC Connector ; 4-pin AC connector

PLEASE NOTE: When ordering you must specify the destination region by indicating -US, -WW, -IL instead of -XX.

Ruckus
Simply Better Wireless.

Ruckus Wireless, Inc.
350 West Java Drive
Sunnyvale, CA 94089 USA
(650) 265-4200 Ph \ (408) 738-2065 Fx

www.ruckuswireless.com

Appendix E - Alcatel Lucent Metro v2 3G Microcell Datasheet

ALCATEL-LUCENT 9364 METRO CELL OUTDOOR V2

2100 MHZ FOR THE EUROPEAN MARKET RELEASE BCR 2.4.1 AND BCR 3.0

The Alcatel-Lucent 9364 Metro Cell Outdoor (MC OD) V2 is a low power, high capacity device that cost-effectively extends Wideband Code Division Multiple Access (W-CDMA) coverage and high-speed packet access (HSPA) capacity to public outdoor places, delivering fast, responsive data service and crystal-clear voice. It is well suited for providing dedicated coverage in high-use hotspots such as train stations, bus stops, and busy outdoor shopping and entertainment centers, for extending coverage to remote rural locations, and for filling in coverage holes within the larger macro network.

Front

Back

Bottom with cover removed

The Alcatel-Lucent 9364 MC OD is a rapidly installed device that is easily deployed without the complexity associated with macro cell site installation, and with its unique capability to form autonomous self-organizing groups, it makes covering large areas as easy as covering smaller ones. With the Alcatel-Lucent 9364 MC OD application enablement application programming interfaces (APIs), mobile service providers can leverage unique network capabilities, such as location and presence, for the creation of revenue-generating, public localized services.

The Alcatel-Lucent 9364 MC OD uses a flat IP architecture and secured access through an existing broadband internet connection to substantially reduce Capital Expenditures (CAPEX) and Operating Expenditures (OPEX), while simultaneously offloading voice and data traffic from the macro network. Bell Lab's Self-Organizing/ Self Optimizing Network (SON) technology ensure minimal-touch configuration and self-optimization to deliver outstanding performance with reduced operational expenses. The Alcatel-Lucent 9364 MC OD is part of the carrier-grade, end-to-end Alcatel-Lucent 9360 Small Cell solution that easily integrates into any operator's existing Third Generation (3G) network.

FEATURES

- Small, lightweight unit, designed to withstand extreme outdoor conditions, that is mountable on a pole or wall
- High capacity, supporting up to 32 users
- Extended coverage with a maximum transmit power of 250 mW
- Supports cell range of up to 2 KM and metro cell users traveling at speeds up to 120 km/hr
- Service segmentation enables the operator to deploy Metro Cell Outdoor access points only for a specific service type, such as HSPA data traffic
- Rx space diversity for improved signal quality and greater capacity
- 64 QAM for higher throughput
- Real-time operational status and service monitoring
- SON capabilities
- Handovers to and from the macro network
- Small Cell net capability to form autonomous self-organizing groups of extended coverage
- Applications enablement with presence API, network local routing, and internet traffic breakout
- Secure, tamper-resistant outer casing
- Supports shared secret and certificate-based authentication

Alcatel·Lucent

AT THE SPEED OF IDEAS™

BENEFITS

- Easily deployed almost anywhere without the complexity associated with macro cell site installation
- Network deployment flexibility – ideal for both urban and rural coverage
- Fast, reliable data connections and high data throughput
- Offers extended W-CDMA coverage and high-speed downlink packet access (HSDPA)/high-speed uplink packet access (HSUPA) capacity to public outdoor locations with a low total cost of ownership (TCO)
- Enhanced performance and fault management for public, operator-owned small cells
- Seamless mobility with simultaneous voice and data service continuity within metro cell group and with macro network
- Enables the development of value-added, innovative services based on location, presence, QoS, and trusted security
- Provides secure access to the MSP's network

TECHNICAL SPECIFICATIONS

Dimensions (HxWxD)

- 241x241x53 mm
- 9.48x9.48x2.08 in

Weight

- <2 kg
- <4.4 lb

Mount

- Pole or wall mountable
- Vertical position

Power

- Supply: Power over Ethernet (PoE+)
- Supply option: External PoE+ injector
- Consumption:
  - ¬ Typical: 20 W
  - ¬ Maximum: 25 W

Interface

- Transmission and PoE+: 10/100Base T RJ45

Certification

- EC

Compliance

- RoHS
- WEEE
- Basic requirements of Directive R&TTE 1999/5/EC on telecommunications terminal equipment, pertaining to electromagnetic interference, safety and health
- Ingress Protection Rating of the Metro Cell Outdoor enclosure conforms to IP65 (according to IEC 60529)

Operating temperature

- -33°C to +45°C
- -27.4°F to +113°F
- Optional solar shield recommended for locations with temperature above +33°C (91.4°F)

Electromagnetic compatibility (EMC)

- EN 301 489-1
- EN 301 489-23
- EN 301 908-1
- EN 301 908-3
- EMC Directive 2004/108/EC
- EN-55022 Class B/CISPR22 Class B
- EN-55024/CISPR 24
- 3GPP TS 25.113

Electrical safety

- EN 60950-1

Health safety

- 1999/519/EC including EN 50383 and EN 50385

Radio characteristics

- Operating band: 2100 MHz
- Listening bands:
  - ¬ 2100 MHz UMTS
  - ¬ 900/1800 MHz GSM sniffing bands
- Rx diversity
- Capacity
  - ¬ 16 active users
  - ¬ Option to increase capacity in steps of 8 users, up to a maximum of 32 active users, with the purchase of additional licensing keys (with SW release BCR 3.0)
- Maximum bearers
  - ¬ BCR 2.4.1
    - 14.4 Mb/s HSDPA
    - 2 Mb/s HSUPA
  - ¬ BCR 3.0
    - 21 Mb/s HSDPA (with 64 QAM optional feature)
    - 5.7 Mb/s HSUPA
- Maximum transmission power: 250 mW
- Sensitivity: -107 dBm

Alcatel·Lucent